IOWA STATE UNIVERSITY
Digital Repository

Graduate Theses and Dissertations

Iowa State University Capstones, Theses and Dissertations

2013

Understanding the physics of degradation of polymer solar cells

Joydeep Bhattacharya
Iowa State University

Follow this and additional works at: https://lib.dr.iastate.edu/etd

 Part of the Electrical and Electronics Commons

Recommended Citation
Bhattacharya, Joydeep, "Understanding the physics of degradation of polymer solar cells" (2013). *Graduate Theses and Dissertations*. 13475.
https://lib.dr.iastate.edu/etd/13475

This Dissertation is brought to you for free and open access by the Iowa State University Capstones, Theses and Dissertations at Iowa State University Digital Repository. It has been accepted for inclusion in Graduate Theses and Dissertations by an authorized administrator of Iowa State University Digital Repository. For more information, please contact digirep@iastate.edu.

www.manaraa.com

Understanding the physics of degradation of polymer solar cells

by

JOYDEEP BHATTACHARYA

A dissertation submitted to the graduate faculty

In partial fulfillment of the requirements for the degree of

DOCTOR OF PHILOSOPHY

Major: ELECTRICAL ENGINEERING

Program of Study Committee:
Rana Biswas, Co-major Professor
Vikram Dalal, Co-major Professor
Sumit Chaudhury
Ruth Shinar
Mani Mina

Iowa State University
Ames, Iowa
2013

Copyright © Joydeep Bhattacharya, 2013. All rights reserved.

www.manaraa.com

DEDICATION

to my mother……

www.manaraa.com

TABLE OF CONTENTS

www.manaraa.com

www.manaraa.com

www.manaraa.com

LIST OF FIGURES

www.manaraa.com

www.manaraa.com

www.manaraa.com

www.manaraa.com

LIST OF TABLES

www.manaraa.com

NOMENCLATURE

1.	MALDI	Matrix-assisted laser desorption/ionization time-of-flight mass spectroscopy
2.	MDMO-PPV	Poly[2-methoxy-5-(3′,7′-dimethyloctyloxy)-1,4-phenylenevinylene]
3.	P3HT	Poly(3-hexylthiophene-2,5-diyl)
4.	PCBM	Phenyl-C61-butyric acid methyl ester
5.	HOMO	Highest occupied molecular orbital
6.	LUMO	Lowest unoccupied molecular orbital
7.	PL	Photo Luminescence
8.	EQE	External Quantum Efficiency
9.	NORM	Normalized
10.	DOS	Density of States
11.	PEDOT:PSS	Poly(3,4-ethylenedioxythiophene) poly(styrenesulfonate)
12.	MoOx	Molibdenum Oxide
13.	HTL/ETL	Hole/electron Transport Layer
14.	BHJ	Bulk Hetero Junction
15.	PPA	Post Production Annealing
16.	GIXRD	Grazing Incidence X-ray Diffraction
17.	XPS	X-ray Photo electron Spectroscopy

www.manaraa.com

ACKNOWLEDGEMENT

It was my privilege to work under the guidance of Dr Rana Biswas and Dr Vikram Dalal, who gave me the opportunity to learn the diverse field of semiconductors and optics. It is their continuous support that helped me to gather the wonderful experience of learning. I am grateful to them for their continuous support and encouragement throughout my graduate study. I also want to thank Dr Sumit Chaudhury, Dr Ruth Shinar & Dr Mani Mina for their time for serving as my committee member.

During my entire tenure, I met numerous people who enriched my experience of working and learning here at *Microelectronics Research Center*. I thank Max Noack for his technical help, discussion, and special comments. Special thanks to Kay Hun and Wai Leung for their help in different experiments. Thanks also go to Bob Mayer for his support in making the experimental data acquisition automatic. Without that taking every piece of data manually would have become cumbersome.

Being from a different professional field, I took some time to get accustomed to this field. Initially it was hard to understand the basic physics of solar cells. The person who helped me in that is no other than Dr. Nayan Chakravarty. Thanks to Nayan for all his help. A special thanks to my team-mates Pranav, Ron & Balaji with whom I had many thought provoking technical and historical discourse. The finishing of this work would have been impossible without their active support. Thanks to my colleagues specially Bryan Lewis. Sambit , Ashutosh, Shantan, Dan, Siva, Bryan Motland , Preston, Spencer, Andrew & Janel. I enjoyed working with all of you.

www.manaraa.com

Thanks to Rakesh, Kanwar, John, Aaron, Yuchin, Moneim for numerous event full discussion in understanding the organics. Thanks to Teng Xiao and Yifen Liu for both discussion and fabrication of some earlier solar cells for degradation study.

Thanks to my friends here at Ames who encouraged me continuously throughout my stay for my accomplishment. Thanks to Gunjan, Sambarta, Shabhavi, Praveen, Srishti, Sabya Da, Sarmishtha Di, Ganesh, Parth and many others. Watching Suresh Oberoy, Jeevan classics with Gunjan, Praveen & Sambarta were unforgettable and most enjoying part of my PhD life. My friend Sudarshan, Goutam and Ritika back home were always my inspiration in my PhD life and will be forever. Their tenacity and fighting spirit always kept my morale high. Special thanks to my sister Gauri for her cheerful advice.

No words are enough for the support of my family. It was their persistent mental support and encouragement, that I reached the end line. My pranam to my mother Smt Geeta Bhattacharya and my Father Mr Pinaki Kumar Bhattacharya. My elder brother Mr Pratip Bhattacharyya and My Sister in Law Smt Sutapa Bhattacharyya were always my great support throughout. My niece Titli was my source of happiness.

Finally my gratitude to Mother Bhawani and my Motherland for their grace on me.

www.manaraa.com

This work is supported & funded by
National Science Foundation
&
Iowa Power Fund

www.manaraa.com

ABSTRACT

Polymer solar cell has been an active field of research in recent years. Thin film inorganic and organic solar cells are gaining significant momentum to outperform the already commercialized high efficiency crystalline counterpart. However the fundamental limitation of inorganic solar cell is limited number of active layer material. Organic conjugated polymer presents huge prospect in providing flexibility in designing photo active organic molecules which allows us to have tunable optical as well as electrical properties. Recent use of lower band gap polymer such as PCDTBT(6-7)%, PDTSTPD(6.7%), p-DTS(FBTTh$_2$)$_2$(7%), PTB7(9.2%-9.6%) has shown promising future for reaching highly efficient single junction solar cell. By using two different polymer or small molecule in two different tandem structure namely parallel tandem and series tandem were shown to enhance the efficiency in excess of 10.5% - 12%.

However degradation is the fundamental drawback that has limited the widespread commercialization of organic photovoltaic. Both in ambient atmosphere as well as under light, organic photovoltaic tend to degrade rapidly with time. In this work we report on the measurement of fundamental properties such as deep defects and hole mobility in poly-3-hexyl-thiophene (P3HT)/[6,6]-phenyl-C60-butyric acid methyl ester(PCBM) solar cells when exposed to solar radiation without any atmospheric exposure. It was observed that light itself can contribute significantly to the degradation of organic photovoltaic. It was found that the mid-gap defect densities in P3HT and the interface density between P3HT and PCBM increase upon light soaking. Such increase in defect density leads to an increase in reverse saturation current of the diode which can be correlated with the decrease in basic parameters of OPV that determine the final power conversion efficiency of solar cells. It was also found that thermal treatment after photo degradation can recover the solar cell performance completely. Some simultaneous processes consisting of metal cathode diffusion into active layers were found to influence the post production annealing of organic solar cells with regular architecture. Photo degradation study on inverted organic solar cells were performed and found that similar degradation behavior observed irrespective of the cell architecture which corroborated the fact that photo induced degradation in organic solar cells are an active layer phenomena which is intrinsic to the blend properties and does not depend on any interface layers.

www.manaraa.com

"If we knew what it was we were doing, it would not be called research, would it?"

- Dr Albert Einstein

www.manaraa.com

CHAPTER 1: INTRODUCTION

The development of polymer solar cells has become an active field of research in recent years. Inorganic thin film silicon solar cells using nano-crystalline and amorphous silicon have already achieved reasonable power conversion efficiency of 12-15%[1] which are somewhat lower than that of thick crystalline silicon solar cells(22-24%)[1]. Both periodic photonic –plasmonic and random textured back reflectors have enhanced the conversion efficiencies and photo-current by increasing the photon path length and utilizing advanced photon management scheme.[2-10]

Alternate inorganic solar cell materials are cadmium telluride (CdTe) and copper indium gallium selenide(CIGS) which have achieved 15-20% power conversion efficiency. However, fundamental limitation of such inorganic solar cells is the limited availability of the active layer material. Also toxicity is a major concern for materials like CdTe[11].

Organic conjugated polymers have an advantage over its inorganic counterparts in its flexibility in material properties. By carefully changing certain elements and side groups in the polymer,[12] it is possible to change the fundamental property of the polymer namely the band gap, electron density, electron affinity and ionization potential. The change in the position of HOMO (highest occupied molecular orbital) and LUMO (lowest unoccupied molecular orbital) can have tremendous influence on the efficient charge generation and charge separation at the bulk hetero junction interface.[13] The use of bulk industrial production techniques such as roll to roll fabrication, doctor's blading, spray coating, inkjet printing have made it possible to produce organic solar cells in automated manufacturing unit.[14-30]

Approximately in the mid 2000's conjugated polymer solar cells have reached 4-5% efficiency using the high band gap polymer such as Poly(3-hexylthiophene-2,5-diyl)[*P3HT*][31,32]. Recent use of lower band gap polymer such as poly[N - 9′-hepta-decanyl-2,7-carbazole- alt-5,5-

www.manaraa.com

(4′,7′-di-2-thienyl-2′,1′,3′-benzothiadiazole)] (*PCDTBT*) led to the solar efficiencies in the range of 6-7% ,[33-37] followed by Thieno3,4-cpyrrole-4,6-dione and Dithieno3,2-b:2',3'-dsilole (*PDTSTPD*)(6.7%)[38], 7,7′-[4,4-Bis(2-ethylhexyl)-4H-silolo[3,2-b:4,5-b′]dithiophene-2,6-diyl] bis[6-fluoro-4-(5′-hexyl-[2,2′-bithiophen]-5-yl)benzo[c][1,2,5]thiadiazole](*p-DTS(FBTTh$_2$)$_2$*) (7%) [39], Poly[[4,8-bis[(2-ethylhexyl)oxy]benzo[1,2-b:4,5-b']dithiophene-2,6-diyl][3-fluoro-2-[(2-ethylhexyl)carbonyl]thieno[3,4-b]thiophenediyl]] (*PTB7*) (9.2%)[40]. These low band gap polymers have shown promise of reaching highly efficient single junction solar cells. By using two different polymers or small molecules in two different tandem structure namely parallel tandem and series tandem were shown to enhance the efficiency further to 10.5%.[41-44] Very recently Heliatech (Germany) had reported a 12% record efficiency for organic photo-voltaic.[45] The performance of organic solar cells has become comparable with thin film inorganic silicon based solar cells with significant promise for future solar energy harvesting. However one fundamental disadvantage of the polymer based solar cell is their short life time and instability when exposed to the ambient atmosphere as well as solar illumination. That creates serious problems for outdoor use which is the primary requirement for the photovoltaic operation. It was observed that the typical power conversion efficiency of these solar cells decreases rapidly with exposure to oxygen and moisture. [46-50]

It was experimentally observed that prolonged light exposure can create defect states (sub-band gap states) inside the polymer[36,51], which can increase the rate of mono-molecular(Shockley-Read-Hall) SRH recombination because those states can act as a recombination centers. Some work suggested possible evolution of trap states in the electron acceptor phase may induce loss in photo current.[52] In a very recent work Street et al had also proved that light induced creation of recombination centers is a dominant source of loss mechanism in photo-

www.manaraa.com

degradation dynamics.[53,54] Further, authors have argued that cession of C-H bond present in alkyl side chain of polymer and subsequent migration of H atom along the backbone could be a probable cause of x-ray/white light induced creation of energetic defect states at the mid-gap in the interface of bulk hetero-junction.[53] The role of electron acceptor was investigated in the photo-oxidation behavior of organic solar cells in another study.[55]

In this work we have studied extensively the photo-degradation pathways for P3HT:$PC_{60}BM$ based bulk hetero-junction solar cells and tried to address some fundamental questions, such as which particular parameters of the solar cell are most affected by photo degradation and why? What fabrication condition can lead to better photo-stability? Is it possible to obtain completely photo-stable organic solar cells? Fundamentals of basic device physics of bulk hetero junction solar cells were also studied in parallel to the understanding of photo-degradation mechanism. We studied the effect of photo degradation on different electrical parameters that govern the power conversion efficiency of the polymer based solar cell. It was found that solar cell's open circuit voltage (V_{oc}) as well as short circuit current (I_{sc}) are directly affected by prolonged light soaking. The loss in photovoltaic performances can be directly attributed to the increased amount of trap assisted (SRH) recombination through the mid gap states at donor-acceptor interface.

We have studied systematically the effect of different inter-layers on the photo-degradation of the organic solar cell. We briefly discuss the literature in chapter 2, which is followed by basic device physics and discussion on experimental setup and theory in chapter 3 and chapter 4 respectively. In chapter 5, we discuss in general, the experimental results related to the photo-degradation of regular P3HT:$PC_{60}BM$ based bulk hetero-junction solar cells. We have also mentioned several aspects of photo-degradation of regular cell including exposure with different spectra of light and varying light intensity. We identified functional relationships of induced de-

www.manaraa.com

fect density with various doses of exposure of full spectrum white light. The DOS (density of states) of BHJ solar cell were measured in-situ, as a function of exposure time to study the dynamics of change in defects in the device with exposure time. In chapter 6, we investigated the effect of post-production annealing as a method of complete device performance recovery and its implication on the device performance as well as change in fundamental properties. We showed that it is difficult to see the changes in the induced defect states by post degradation annealing because of diffusion of metal contacts into the active layer and subsequent formation of recombination centers. We showed that by obtaining a thermally stable anode, we can see the complete recovery of device performance by post production annealing.

In the remaining part of the thesis, numerous experiments related to organic as well as in-organic solar cells were reported. The photonic/ plasmonic back reflector based light trapping in in-organic nano-crystalline silicon based n-i-p solar cell is discussed in Appendix A. The estimation of mobility-life time and the influence of interface states are discussed in Appendix B. In Appendix C, numerous methods of estimation of flat band voltage is discussed. Study of photo-induced changes in organic solar cells are discussed in Appendix D-F where we varied different fabrication parameters including HTL, active layer annealing, active layer concentration and ETL etc. In Appendix G, ZnO:Al based inverted solar cells are discussed with special attention to photo-stability. There is some confusion about the exact nature of trap states measured by capacitance –frequency measurement. Appendix H is dedicated solely to understand the nature of trap states estimated by capacitance measurement. Finally we discussed briefly about the irreversible nature of photo-oxidation in Appendix I.

www.manaraa.com

CHAPTER 2: PREVIEW ON OPV DEGRADATION

2.1 Moisture induced degradation

Moisture is one of the most important degradation constituents that reduces PCE of un-encapsulated polymer based solar cells. Krebs et al[46] in their paper suggested that the water molecule diffuses through the Al cathode. It was suggested that the water molecules are absorbed into the Al cathode and it then diffuses further towards the ITO layer and through all other interfacial layer leading to the degradation of all interfacial layers.[46] Water induced degradation was termed as homogeneous degradation compared to inhomogeneous degradation through oxygen. It was further suggested that the presence of molecular oxygen and light accelerates the water induced degradation. Under illumination, the active layer of the solar cell undergoes different photo chemical reaction between constituent of the device and the atmospheric agents.[46,48,49]

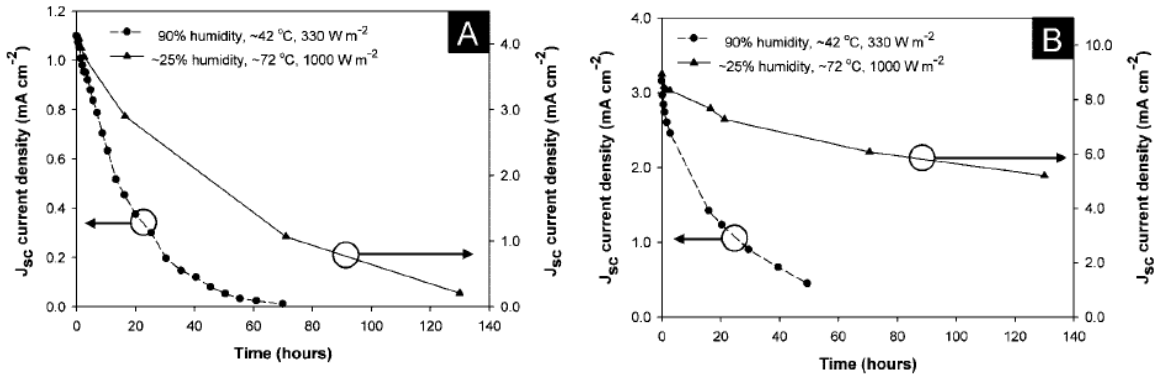

Figure 2.1(a): Drop in Jsc under different humidity and different light intensity exposure to MDMOPPV-PCBM cell (b): Drop in Jsc under different humidity and different light intensity exposure to P3HT: PCBM cell[56]

Two polymers – P3HT and MEH-PPV were used as an active layer and exposed to two different environmental conditions. It was found that firstly that the MEH PPV based solar cell degraded faster compared to the P3HT based devices.[56] However by carefully looking at the experimental condition it can be observed that the comparison was made based on two completely different experimental conditions. [56] Two different humidity levels were accompanied by two dif-

www.manaraa.com

ferent light intensities that had complicated the understanding further. The same authors approached the problem of degradation from both chemical and mechanical aspect. [48]

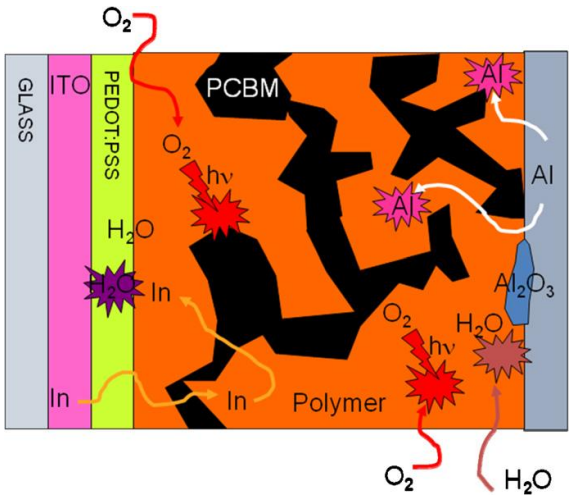

Figure 2.2: Different degradation pathways depicted –attacking different parts of solar cell [48]

The figure shows different degradation pathways. In the process of chemical degradation the diffusion of both molecular oxygen and water are the important source of degradation. It also suggested that there can be different pathways of diffusion of oxygen, water, aluminum or indium into the active layer which can initiate degradation in OPV. It was further emphasized that oxygen can be activated by UV illumination in the presence of some organic molecules,[47,48,52,57,58] which lead to the formation of peroxide or superoxide compounds that further aggressively attack and degrade the active layers.[46,48] Different polymer are prone to such chemical degradation at different rates. For example, the PPV based polymer such as MDMO-PPV is susceptible to such active layer degradation. [48]

Diffusion of molecular oxygen and moisture were thought to be initiated through the microscopic pinholes formed on the aluminum cathode. The following high resolution secondary electron microscope(SEM) image of the aluminum cathode shows big crater like structure which substantiates the possibility of having microscopic pinholes.[46] Another entrance route for these molecules could be the aluminum grain boundaries at the surface of the aluminum cathode.

www.manaraa.com

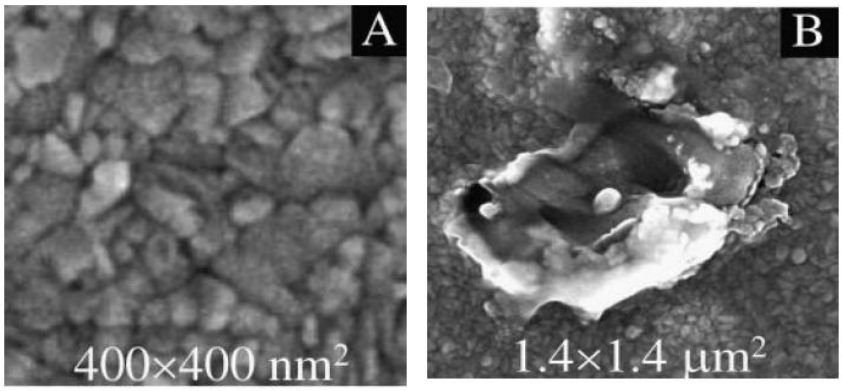

Figure 2.3(a): SEM images of P3HT:PCBM coated with Al showing the presence of crater like pinhole.[46]

It was further suggested that, the organic active layer after being oxidized in the presence of diffused oxygen and moisture, resulted in the material expanding in all directions and thus lead to the formation of protrusions on the outer electrode surface. [46] Irrespective of the presence of light illumination, this process continues to affect the solar cell performances. The thermal evaporation was singled out as a method of aluminum evaporation that induces microscopic pinholes during the aluminum evaporation. As an alternative, DC magnetron sputtering of aluminum cathode was recommended as a solution with proper precautionary measures.[46]

Kawano et[49] al in their paper tried to address the problem from mostly basic electrical characterization and concluded that the hole transporting layer PEDOT:PSS is the source of air induced degradation. In their experiment they used a controlled atmosphere and measured light IV at different time. Their experiment indicated that the increase in series resistance[49] with exposure time indicates the presence of barriers at one electrode interface which hinders the efficient charge collection, resulting in the rapid drop of short circuit current and fill factor. They used the MDMO-PPV polymer in place of P3HT for their air degradation study. It was also pointed out that air exposure did not change the hole mobility. They concluded that there was an increase in the injection barrier at the PEDOT: PSS and active layer interface due to the formation of some insulating domains.[49] It was concluded that the light independent degradation under ambient at-

www.manaraa.com

mosphere is due to the moisture absorption by the PEDOT: PSS layer. The moisture induced changes only increases the injection barrier and does not affect the intrinsic charge carrier such as the mobility. In addition the degradation of PEDOT: PSS layer is spatially inhomogeneous. They emphasized it was necessary to find a suitable alternative of PEDOT: PSS which could be less reactive to moisture. [49]

There is significant research done on the degradation of polymer based solar cell by groups at NREL. In the paper by MO Reese at el[59], the author had experimented with different materials for cathode. They concluded that the organo-metallic interface is the main source of degradation of polymer based solar cell.[59] By using different types of electrode materials and studying the degradation for several days author concluded that –there is indeed a "non-photo activated" pathway of degradation at the organo-metallic interface -in the case of "thiophene" based devices with silver in the contacts.[46,48,59] It appears that most of the electrode materials except silver are fairly stable. In their experiment they used also different set of encapsulation strategies to mitigate the problem of air induced degradation. [25]

In another study by M .Wang et al [60] the degradation of polymer solar cell exposed to ambient atmosphere was discussed. They argued that the presence of aluminum oxide(Al_2O_3) at the cathode organic interface creates a barrier that reduces the injection current in the dark as well as the photo current during illumination. [60]

www.manaraa.com

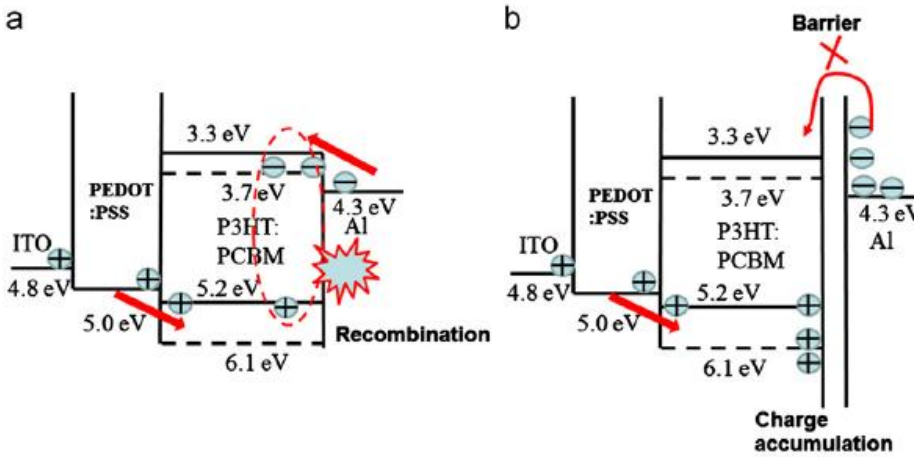

Figure 2.4: Effect of moisture attacking the organic –metal interface creating barrier for both charge injection and collection-(a) Before degradation, (b) After degradation[60]

2.2 Oxygen doping and related degradation

Oxygen is considered to be an important element that was considered responsible for the degradation in polymer based solar cells.[47,48,57,61] In this section we will review the degradation pathways initiated by oxygen. Significant research was already done on assessing how oxygen took an active part in degrading the polymer active material and hence reducing the power conversion efficiency (PCE) of polymer based solar cells.[46-48,57,61-64] One of the pioneering researcher in the field of degradation study of organic polymer based solar cells is Dr F Krebs who published a large amount of research on studying the effect of oxygen exposure on the different polymer based solar cells and their subsequent degradation pathways. [46,48,62-65]

In the figure 2.5(a) it was described how the electronically excited triplet oxygen reacts with the PPV polymer.[48] The polymer first reaches an excited state S1 followed by a transition to a triplet state T1. In the T1 state the polymer can transfer the excitation to the adsorbed oxygen. This results in the formation of singlet excited state. The electron donation from polymer excited state to the oxygen results in the reaction of the polymer chain with the singlet oxygen and form-

www.manaraa.com

ing an intermediate di-oxytane and finally a rapture of the polymer chain. The final product can further react with oxygen. Dam et al found that oxygen initiated reactions with polymer depends on nature of reactive groups[48]. Electron donating groups enhance the rate of reaction while the electron withdrawing groups retard the reaction rate.[48]

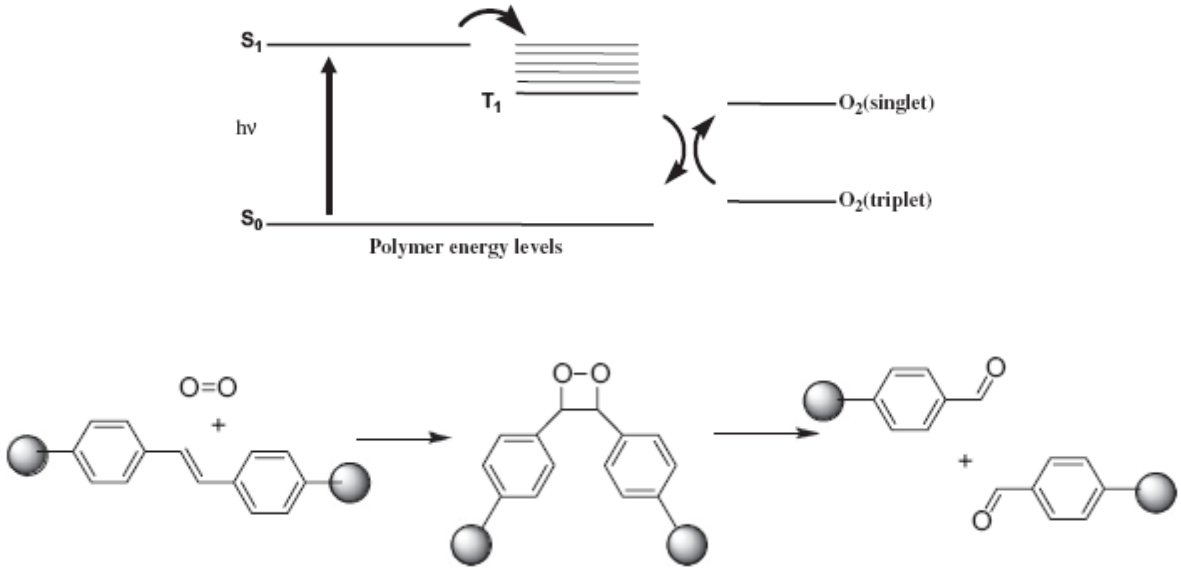

Figure 2.5.(a) Formation of triplette state due to the presence of oxygen. (b) Breaking of backbone in the presence of light and oxygen.[48]

The polymer P3HT does react with oxygen at the temperature as low as -50 C. It was observed that thiophene based polymer such as poly(3-alkylthiophenes) form charge transfer complexes with oxygen.[48] The resulting negative and positive radical species can be detected by electron spin resonance. [48]

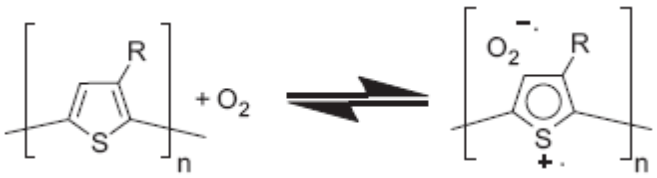

Figure 2.6 Poly-thiophene forming charge complex with oxygen[48]

www.manaraa.com

With oxygen exposure the density of electron spin increases by an order of magnitude. This leads to an increase in the film mobility and conductivity which is understandable. Oxygen after accepting an electron from the polymer, leads to a vacant hole in the polymer. The reversible formation of complexes between oxygen and P3HT was investigated by oxygen-induced fluorescence quenching by Lu et al.[48,66] Oxygen not only attacks the polymer active layer but can also attack the polystyrene sulfonic acid(PSS) of PEDOT:PSS bottom hole transport layer (HTL).[48] In the previous section while describing the moisture induced degradation, we mentioned the work of Kawano et al[49] where they considered the PEDOT:PSS responsible for absorbing atmospheric moisture and subsequent increase in the PEDOT:PSS layers sheet resistance. It was also mentioned that under light illumination, the degradation rate in PEDOT:PSS layer has increased. Norman at al[67] had observed the formation of agglomerated PSS derivative in the form of particle in the PEDOT:PSS layer due to the oxygen exposure observed by the fluorescence microscopy imaging. Further secondary mass spectroscopy was used to characterize the molecular structure and proposed a scheme for the formation of the fluorescent particle (likely to be made of PSS) in the PEDOT: PSS layer. [48]

It was also hypothesized that, PSS is present in excess in the PEDOT :PSS solution in comparison to PEDOT. That PSS may diffuse through the active layer and hence react with the active layer material such as the polymer or fullerene based acceptor molecule.[48] The PSS may undergo a oxido-de-sulfonato-substitution forming the phenolate which can then react with PSS forming two PSS chains linked together via a sulfonic ester group.[48] Oxidation of the carbon indicated by an asterisk in the figure 2.7 will then consequently form the proposed molecular structure of the PSS particles observed. [48]

www.manaraa.com

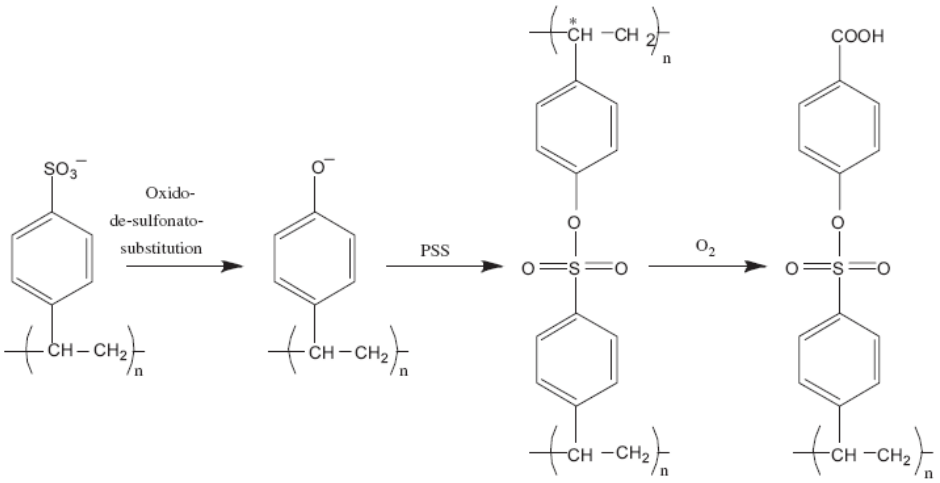

Figure 2.7: PEDOT:PSS reacting with oxygen [48]

In a recent paper by A. Guerrero et al, [61] the degradation of P3HT and P3HT: PCBM BHJ cell due to the deliberate oxygen treatment of the solar cells during fabrication was discussed in detail. The authors observed that, upon exposure to molecular oxygen, formation of P3HT:O_2^- complex and metal oxide formation at the interface between the active layer and metallic contact occur simultaneously.[61] A loss in photocurrent is associated with formation of P3HT:O_2^- complex, which reduces the concentration of neutral P3HT present in the film. It was also mentioned that this type of degradation by oxygen doping is reversible by nature. This polymer-oxygen complex is responsible for the drop in photocurrent of OPV. Loss in photo-voltage for cells doped with molecular oxygen is in agreement with the reduced light absorption that generates less charge carriers, inhibiting the Fermi level splitting to some extent.[61]

www.manaraa.com

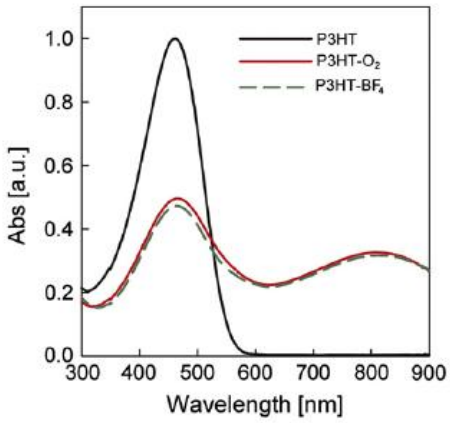

Figure: 2.8 Effecting Absorbance due to oxygen exposure [61]

The above figure 2.8 shows how both molecular oxygen and an oxidant can react with P3HT polymer. When the absorbance spectra was measured in the solution of P3HT in ODCB(ortho-dichloro benzene) both treated with molecular oxygen and Nitrosonium tetrafluoroborate ($NOBF_4$) , the absorbance spectra tends to drop with an extra peak at higher wavelength near 800nm. [61]

In order to analyze the effect of oxygen doping on the photocurrent, the steady-state absorption of films processed under the same conditions was measured. Author argued that, increase in the concentration of $NOBF_4$ as well as with oxygen treated solution, the absorption decreases along with developing a significant absorption peak at higher near IR wavelength.[61] They also measured quantum efficiency (EQE) and showed that the short circuit current density decreased with the treatment of molecular oxygen or any oxidant. With increasing amount of oxidant, short circuit current density decreased further without increasing the quantum efficiency at higher wavelength. This shows that the exposure of oxygen on P3HT solution reduces the cell performance.[61] However carefully looking at the EQE curve we can see that the absorption enhancement was noticed in the infrared region of the spectrum which lies within the band gap of P3HT.

www.manaraa.com

So the absorption peak might be reflected in the sub band gap EQE measurement which does not contribute to the integrated short circuit current density. [61]

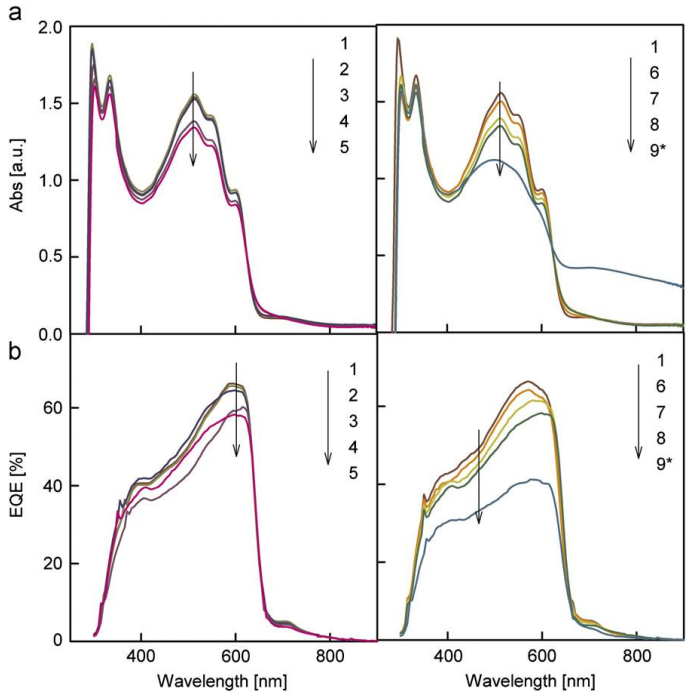

Figure: 2.9(a) Effect of oxygen on P3HT:PCBM ABSORBANCE(in dark) ;(b) Effect of oxygen on P3HT:PCBM under(light); (c) Effct of Oxygen on P3HT (in dark) on EQE ; (d) Effect of Oxygen on P3HT (under light)EQE [61]

These authors concluded from their finding that[61], oxidation of P3HT results in the loss of absorption in the P3HT absorption band and lead to the further reduction in both short-circuit current and open circuit voltage. In the same paper by Jorgensen et al, the authors argued that the oxygen exposure not only degrades the polymer intrinsically but also reacts with the calcium used for making cathode contact.[48] It forms Calcium oxide at the cathode –polymer interface resulting in higher series resistance and lowering of the fill factor. It was suggested that further thermal annealing steps can be applied to heal the degradation in the active material but formation of the CaO interfacial oxide is irreversible.[48]

www.manaraa.com

2.3 Light induced degradation-photo oxidation

In the previous sections 2.1 and 2.2 we briefly surveyed that molecular oxygen species can diffuse and react with the active layer. However it was further emphasized[48,68,69] that the oxygen reactivity with different polymer systems become accelerated in the presence of light. Most of the scientific community termed it as a photo oxidation effect.[36,51,52,55] In this section we will discuss in detail, the effect of photo induced changes in different polymer system.

Photo induced degradation of both inorganic as well as organic material is a widely studied phenomenon. Many groups have already studied these phenomena in great detail. In a-Si: H the effect of light soaking was first demonstrated by David L Staebler and C. R. Wronski in 1976.[70-84] They showed that both dark and photo conductivity[70] of the hydrogenated amorphous silicon tend to decrease by prolonged light soaking[82]. However it is possible to reverse the Staebler-Wronski effect by thermally treating the solar cell devices by 160^{o}C-200^{o}C.[71,72,80,82] Physically prolonged light soaking creates dangling bonds, resulting in mid-gap defect states which were considered responsible for performance drop in amorphous silicon solar cells. In one of the earliest models, light soaking breaks the weak Si-Si bond and then a neighboring H atom moves to make a bond with of the Si atoms resulting dangling bonds that have mid energy defect states.[85] Other models describe the rupture of Si-H bonds and formation of Si-dangling bond accompanied by Si:H complexes[86]. Some other theory suggests that the rupture of Si-Si bonds are followed by the diffusion of strained species in the network and which lead to the formation of dangling bonds.[87]

www.manaraa.com

Similarly several groups in last decade had investigated the mechanism of photo induced changes in the polymer based solar cells. A Rivaton et al[58] conducted studies on the photo degradation of several polymer system based solar cells. They conducted studies on MDMO –PPV films as well as P3HT film with their corresponding bulk hetero-junction with $PC_{60}BM$ fullerene.[57,58]

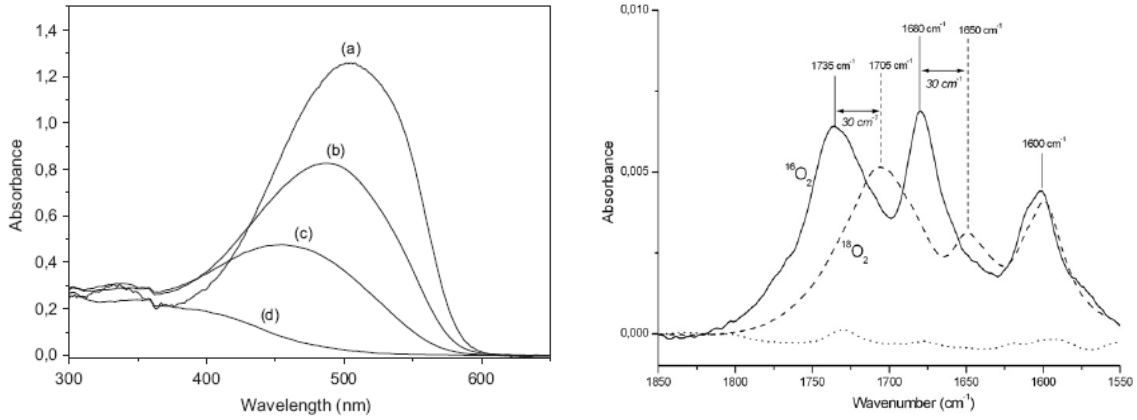

Figure 2.10(a): UV-VIS Absorbance evolution(photo bleaching) (b) IR spectroscopy of Light soaked sample in Oxygen[57]

In the figure 2.10, pristine MDMO-PPV before exposure to light was shown to have a broad absorption band centered at 500 nm that results from conjugated structure. During irradiation, a decrease of the intensity of the absorption band accompanied by a blue shift was observed.[57] This suggests a reduction of the conjugation length, which leads to the "photo-bleaching" of the polymer.[57,58] By the infusion of two different isotopic forms of oxygen- O^{16} and O^{18}, author studied how the IR spectra had changed under illumination.[57] It shows that Using infrared spectroscopy, irradiation under the oxygen 18 atmosphere allowed discrimination between compounds formed via fixation of oxygen from the atmosphere and those formed by reorganization of the matrix. Exposure of MDMO-PPV carried out in $^{18}O_2$ atmosphere was compared to experiments carried out at ambient air.[58] The IR spectra drawn in fig. 2.10(b) first showed that the products at 1735 cm^{-1} and 1680 cm^{-1} formed under conditions of irradiation in $^{16}O_2$ were respectively the products

www.manaraa.com

at 1705 cm^{-1} and 1650 cm^{-1} when irradiations was carried out under $^{18}O_2$, the photo-products at 1735 and 1680 cm^{-1} resulted from an oxidation of the polymer by fixation of oxygen from the atmosphere. In the figure 2.11, authors attempted to explain the photo-oxidation reaction process. In the two step photo oxidation process, the oxidation of the either substituent happens as shown in the reaction 1 followed by the oxidation of the double bonds as shown in the second reaction.[58]

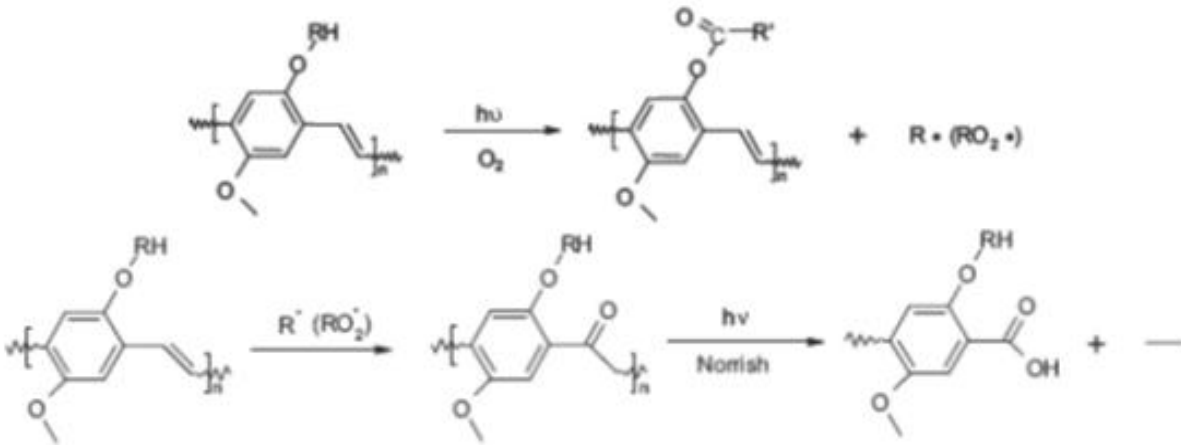

Figure 2.11: Oxygen reaction pathways[57,58]

In the similar way like MDMO-PPV, the authors also comprehensively studied the illumination effect on P3HT only and on P3HT:PCBM BHJ films.[58]

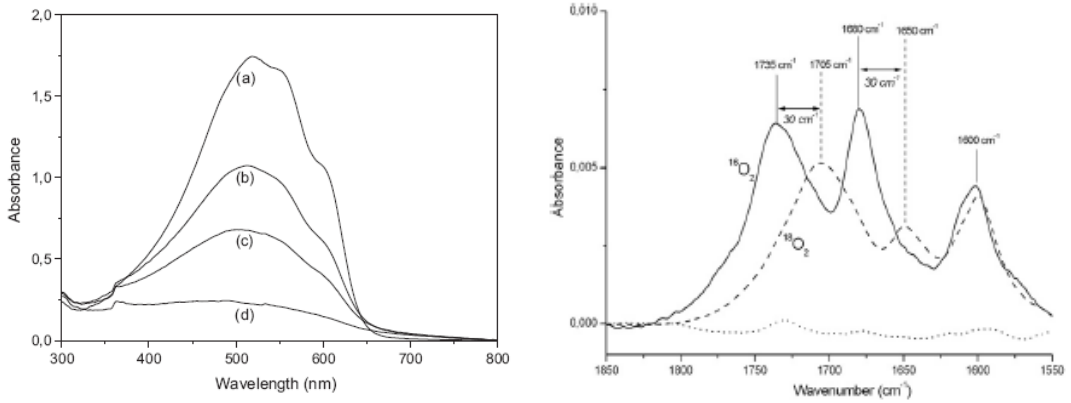

Figure 2.12(a): UV-VIS Absorbance evolution(photo bleaching) (b) IR spectroscopy of Light soaked sample in Oxygen[57]

www.manaraa.com

The authors used both XPS and IR spectroscopy to determine the new functional groups that might be generated in response to the photo-oxidation reaction process. The observation from the absorbance plot shown above is that, light soaking a P3HT film in the presence of oxygen is drastically degrades the polymer absorption. They observed several noticeable changes in the IR spectrum of P3HT dynamically after certain times of light exposure[57]. It shows that both carbonyl and hydroxyl groups were developing their fingerprints in IR spectrum. On the other way – the characteristics peaks observed for P3HT thiophene ring, aromatic group and alkyle group are continuously decreasing with time of exposure. [57]

The authors proposed a reaction scheme in accordance with the observed changes in the UV-Vis absorbance and the changes observed in IR spectroscopy.[57] The authors argued that oxidation was shown to involve the radical oxidation of the n-hexyl side chains and the subsequent stepwise oxidation of the sulfur atom of the thiophene ring. This lead to the breaking of the molecular backbone resulted in a loss of pi-conjugation, and the bleaching of the sample. It was further found that P3HT exposed under inert conditions tend to retain its pristine absorbance spectra as well as IR spectra. That leads to the conclusion that P3HT is photo chemically stable under light in the absence of oxygen.[57]

In a similar experiment[57] they exposed a P3HT: PCBM blend film coated on PEDOT: PSS coated substrate and found a minor drop in the UV-VIS absorbance by a nominal 7% after 3000 hours of exposure. This concludes that both P3HT as well as P3HT: PCBM blends are photochemically stable under inert atmosphere but might undergo slight morphological changes.[57]

In another work by A Kumar et al, from the Yang Yang group[88] it was observed that some changes in the electrical properties in P3HT”PCBM blend were identified when exposed to x-ray irradiation. They found that open circuit voltage is getting effected by the irradiation. It was also

www.manaraa.com

observed that samples with higher PCBM ratio (1:2) tend to have higher loss in V_{oc} compared to the higher P3HT ratio sample (10:1).[88,89] The drop in V_{oc} in devices with high PCBM concentration is 30% of its initial value, while it is only 1% in the low PCBM device. They also observed that the presence of higher PCBM ratio leads to better susceptibility of fill factor from the drop after x-ray irradiation. Further study showed no change in absorbance spectra was observed after x-ray irradiation which is a contrasting observation to the earlier work[57] . In their experiment they observed that the drop in J_{sc} was mostly independent of x-ray dose. [88]

These authors[86] conducted dark current voltage measurement on three different sample with three different P3HT:PCBM ratios and found that the sample with the lower PCBM ratio tends to have reduced dark current after x-ray irradiation.[88,89] For 1:2 P3HT:PCBM ratio, dark current increased after irradiation. They concluded that, the drop in the injection current which is causing the drop in the built in potential is the main reason behind the drop in V_{oc}. The accumulation of the opposite charge at the interface of the P3HT and PCBM reduces the built-in potential and that reduces both the open circuit voltage and short circuit current. [88]

These authors explained the drop in dark current in two low PCBM concentration devices with charge accumulation theory.[88] However their conclusion on the increase in reverse saturation current in the third device in which P3HT:PCBM ratio is 1:2 is that, the increase in the number of minority carrier at the interface resulting in higher reverse saturation current. In the authors[86] own word-"Following the photovoltaic (PV) theory, the physics of a solar cell, namely the separation of the photo-generated charges, lies in two parameters, I_o and n. The saturation current density I_o determines the absolute size of the diode current around zero bias, while the exponential behavior is dominated by the diode's ideality factor n. A microscopic model of I_o and n in bulk hetero-junction PSC is missing and hence we follow a qualitative discussion to un-

www.manaraa.com

derstand the findings. For bulk hetero-junction devices, I_o represents the minority charge density in the vicinity of the barrier, which is at the donor/acceptor interface for bulk hetero-junction solar cells. We do not expect any change in morphology of the films here. Increase of I_o can however be explained by increased doping or a source of additional minority carries created near the interface."[88,89] They concluded that the charge carrier accumulation at the interface due to the x-ray irradiation caused the open circuit voltage and short circuit current to decrease. [88]

M.O Resse et al [52] from NREL also conducted detail experiments on the photo induced degradation of P3HT:PCBM bulk hetero-junction solar cell. Under inert atmosphere, both the polymer and the blend were observed to be stable for at least 1000 hours of illumination at one sun intensity.[52] It was found that the active layers by themselves are intrinsically stable in an inert atmosphere, at least over the experimental time period, and the photo induced degradation observed in complete devices under illumination in inert atmospheres can be solely attributed to effects caused by charge collection layers and interfaces.[52] While under exposure to air and light simultaneously, pristine P3HT bleaches quite fast with a complete loss of absorbance after 700 h (as already mentioned in the literature as photo bleaching). The presence of the acceptor in the P3HT: PCBM film slows the bleaching kinetics of the polymer under illumination in air, presumably by quenching the polymer excited state. The photo-conductance of the blend decreases during degradation under light in air faster than the pure polymer, indicating the involvement of PCBM in the degradation process.[52]

The drop in absorbance spectra were measured for several different experimental conditions in figure 2.13(a/b).[52] The top two spectra correspond to the P3HT UV-VIS spectra. P3HT kept in dark shows a lower decrease in absorption compared to the drop in the P3HT film illuminated under one-sun intensity. The bottom graphs show the change in the blend both under dark, as

www.manaraa.com

well as under light soaking. Light soaking shows a higher drop in absorbance. It seems that blend is more stable compared the only P3HT polymer. There is an interesting point is that all the samples with UV-VIS spectra of figure 2.13a (A-D) were kept in air. However the spectra of figure 2.13b (A-D) were of those samples which were kept in a nitrogen atmosphere. It can be observed further that there is hardly any change in the absorbance spectra for blend under nitrogen even under light exposure. This lead author to conclude that P3HT:PCBM blend is inherently stable under inert atmosphere.[52]

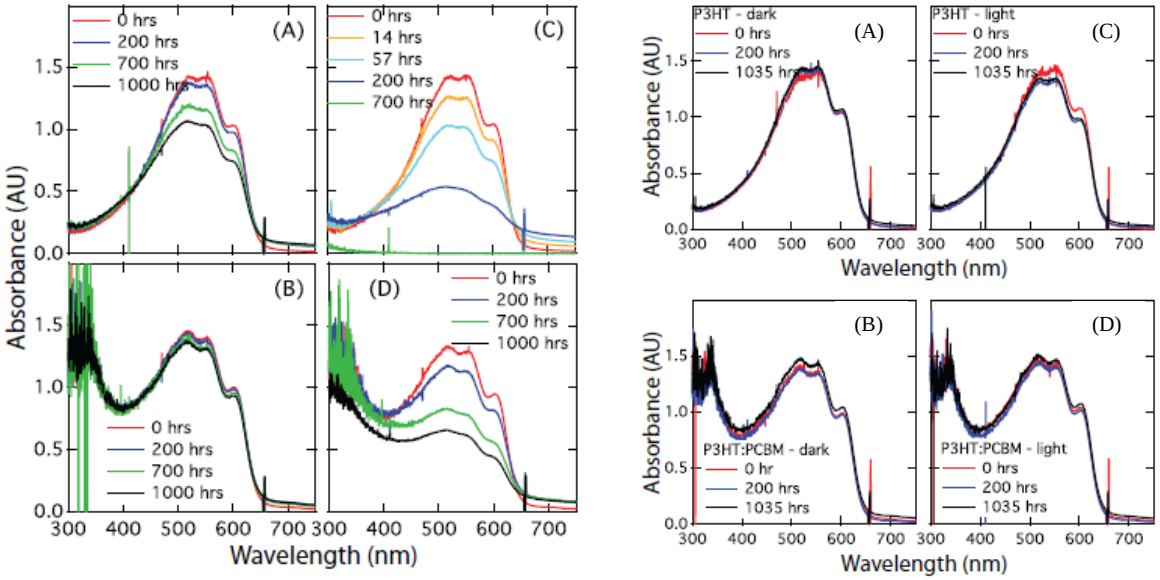

Figure 2.13(a): (A)Change in Absorbance of P3HT in the presence of oxygen(in dark), (C) Change in Absorbance of P3HT in the presence of oxygen(in Light), (B) Change in Absorbance of P3HT:PCBM in the presence of oxygen(in dark), (D) Change in Absorbance of P3HT:PCBM in the presence of oxygen(in Light),

Figure 2.13 (b) (A) Change in Absorbance of P3HT in the absence of oxygen(in dark), (C) Change in Absorbance of P3HT in the absence of oxygen(in Light),(B) Change in Absorbance of P3HT:PCBM in the absence of oxygen(in dark), (D) Change in Absorbance of P3HT:PCBM in the absence of oxygen(in Light),[52]

The new aspect of this paper is that[52], unlike the previous hypothesis in which polymers were found to be mostly responsible for the oxidation by molecular oxygen, the authors argued that PCBM fullerene cages are reacting with oxygen in air and creating deeper trap states within PCBM.[52] These trap states reduce the mobility of electrons after the separation of excitons at the

www.manaraa.com

P3HT: PCBM interface. According to the authors, that is a fast degradation mechanism which can be attributed to the photo-induced oxidation of PCBM following the photo-excitation of the P3HT in a blend film. The creation of the deeper traps in fullerene cage prevents electrons from contributing to the photo-conductance signal of the blend and subsequently the photo-current of the solar cell. They measured the photo conductivity of film in air using TMRC (Time Resolved microwave Conductivity) technique which show that drop in photo conductivity of blend under light soaking (in air) is faster than that of P3HT film, from which they concluded that the faster drop in photo-conductivity in the blend is due to the lower electron mobility in PCBM. To understand further the root cause of such lower electron mobility in PCBM they used matrix-assisted laser desorption/ionization time-of-flight mass spectroscopy (MALDI-TOF) measurement to enumerate the oxygen content present in the PCBM molecule. Without going into the further details of the experiment and its analysis, the main conclusion is that PCBM photo-oxidation is another pathway that can lead to the degradation of the polymer solar cell.[52]

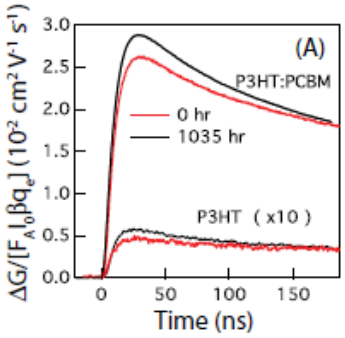

Figure 2.14*:* matrix-assisted laser desorption/ionization time-of-flight mass spectroscopy (MALDI-TOF) on Oxygen exposed sample[52]

In conclusion author had proposed an entirely new degradation pathway where PCBM is oxidized when it is exposed to light in ambient atmosphere- a conclusion that is in agreement with finding by Hoke et al [55].

www.manaraa.com

In 2012 both Street et al[53,54] from PARC(Paolo Alto research Center) and C.H. Peters[36,51] et al from Stanford showed the role of sub-band gap defect states in the active layer that can be created due to white light illumination or x-ray illumination. Street et al[53] discussed in detail with supporting numerical calculations to show that prolonged photo exposure results in the cession of C-H bonds resulting in the formation of mid-gap defect states. They [53] concluded that light in the absence of oxygen and moisture can cause significant damage to the solar cell performance due to increased trap assisted recombination which is essentially a pathway that does not require the participation of oxygen. The microscopic atomistic changes in the active organic material is an issue of much research.

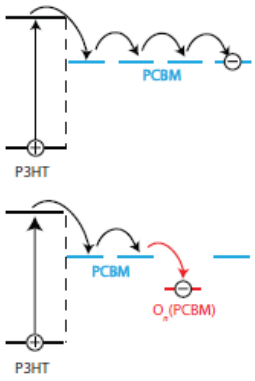

Figure 2.15: Presence of trap states in PCBM cage reducing electron mobility.[52]

2.4: Other stability related issues

Metal electrode

This reactivity between the aluminum metal and the organic material has been recognized for a long time in organic chemistry, where such reactions have been used for reduction via electron transfer to organic compounds.[90] Lo¨gdlund et al proposed the direct interaction between the aluminum metal and polymer (PPV based materials) resulting in direct formation of Al-C bond.[48,90] Aluminum is attractive metal to utilize because of its low work function which makes

www.manaraa.com

it useful as the negative electrode material in solar cells. The organo-aluminum compounds are highly reactive species that will react with any proton donors present like oxygen in the atmosphere. One such proton donor could have traces of water introduced in the production of the device e.g. from PEDOT:PSS. The end result would be the reduction of the vinylene groups with a loss of conjugation in the polymer. [48]

The calcium electrode can react with water under room temperature. However calcium can't react with molecular oxygen under inert atmosphere. It was argued that calcium can also react with the organic compound and thus form C-Ca bond that can further react with oxygen in a similar way that oxygen reacts with the organic- aluminum compound.[48]

Different fullerene molecules also have the tendency to react with aluminum metal because of the high electron affinity of aluminum. C60 reacts with alkali metals to form compounds such as K_3C_{60} where the alkali atom resides within the fullerene cage. A similar reaction could be envisaged at the interface between PCBM and the aluminum electrode though this has not yet been demonstrated.[48]

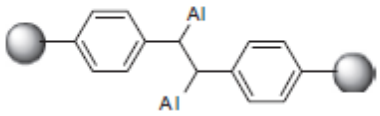

Figure 2.16 Reaction of Polymer with Aluminum[48]

ITO has also a significant role to play under air exposure in the degradation of the polymer solar cell.[31,36] A faster erosion of the ITO film occurred when devices were exposed to ambient air. A film stored at 81C in air had 1.2% indium in the PEDOT layer after 10 days. It was concluded that the ITO/PEDOT interface is very sensitive to air and that the hygroscopic nature of PSS allows absorption of water that facilitates etching of the ITO layer. ITO etching was indirectly by observing indium diffusion into the organic layers in an OPV device with the composi-

www.manaraa.com

tion Al/C60/P3CT/ITO, where P3CT is poly (3-carboxythiophene-co-thiophene).[31,36] The authors concluded that indium diffuses through all layers in the device and ends up on the outer surface of the counter-electrode. It is uncertain as to what extent indium is involved in degradation processes when it diffuses through the organic layers of the device.[48,91,92]

Thermal stability:

The thermal stability is not a conventional degradation pathway but an important parameter that has significant influence on device performances. The impact of the different thermal treatments on the active layer of bulk hetero junctions was proposed by Bertho et al.[93,94]

In their paper they showed that the active layers based on MDMO-PPV show a rapid formation of PCBM-clusters upon annealing. The smaller interfacial area between the electron acceptor and the electron donor results in a lower photocurrent output. The blend shows a dual crystallization behavior. On the one hand, P3HT crystallizes, which leads to improved charge conduction and a higher photocurrent output; on the other hand, PCBM forms clusters, again reducing the interfacial area between electron acceptor and donor regions, which results in a decrease in photocurrent.[93,94] These two effects oppose each other.

The authors argued that morphology changes are strongly related to the molecular weight of the polymer as well as to the glass transition temperature. For example they showed that 'high T_g -PPV' active layers leads to the higher thermal stability of the device characteristics in comparison to P3HT and MDMO-PPV. As a possible explanation, the authors suggested that due to the higher glass transition temperature, the 'High Tg PPV', the matrix is more rigid. The firmer matrix of polymer reduces the further chance of possible migration and segregation of the PCBM

www.manaraa.com

molecules leading to a more stable active layer and consequently a more stable photovoltaic behavior.

As we will see later in chapter 6 that thermal stability may be an inherent necessity before making a photo-stable organic solar cell. Especially post production thermal treatment can deteriorate the solar cell performance significantly as reported elsewhere.[95] Conflicting results on the effect of post-production annealing was published which suggested that post production annealing actually improves[96] the photovoltaic performance of solar cell which is contrary to our experimental observation.

www.manaraa.com

CHAPTER 3
FUNDAMENTAL OF DEVICE PHYSICS OF POLYMER SOLAR CELL

3.1.1 Basic physics of different solar cell architecture

In the previous chapter we reviewed several different pathways for the polymer solar cell degradation and found that oxygen, moisture and light all play vital role in the degradation kinetics of polymer based solar cells. Before going further into the study of light induced degradation we must understand the device physics of solar cell in general and specifically the device physics of polymer based bulk hetero junction solar cell. In the present chapter we briefly cover the device physics and fundamentals of solar cells by the excitation of electrons from the Fermi level to the vacuum level.

In 1905 Dr Albert Einstein[97] explained the famous photo electric effect in a metal. In a semiconductor material due to its lower energy band gap compared to dielectric[98], it can absorb UV, visible and infrared photons which can subsequently produce an electron hole pair. However that does not contribute to external current until they are separated by some way and collected at the opposite electrode. Hence a PN junction diode is the best choice for photo current generation, which can both generate and separate the charge carriers.

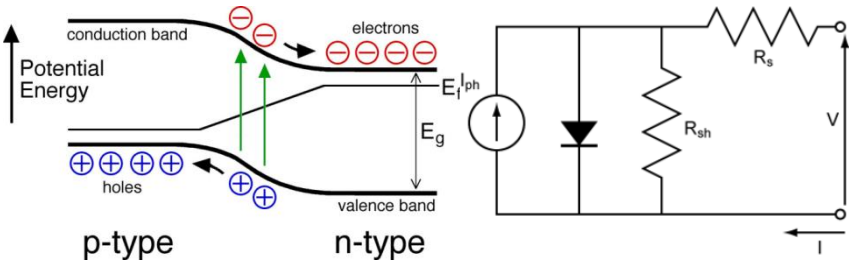

Figure: 3.1 Energy band diagram of p-n junction with equivalent circuit[85,99]

www.manaraa.com

A solar cell can be modeled by a simple P-N junction diode with special characteristics. The device physics of a solar cell can be best understood by understanding the device physics of P-N junction diode. In figure 3.1(a), the energy band diagram of a simple P-N junction diode is illustrated. The green upward arrow shows the generation of electron and hole pair at the space charge region. Subsequently, the photo-generated charges were separated by the built in electric field at the junction resulting in the charge separation. That was further followed by the charge transport to the respective electrode. The whole process contributes current to the external circuit. So to observe a photovoltaic effect in any material in general, we need to have the following sequence of physical phenomena inside the material. Firstly there is charge generation by the absorption of the incident photon followed by the separation of the charge carrier. In the next step electrons transport in the acceptor material and holes transport in the donor material. The carriers transport to their respective electrodes.

In an ideal situation, we assume that all the generated charge carriers are separated at the interface and finally collected at the electrodes. This neglects several inherent loss mechanism of the device. Later in further subsections we will discuss, what are the different loss mechanisms that govern the continuity equation of the solar cell.[98,100]

The solar cell operation can be best described by the equivalent circuit as depicted in the figure 3.1(b). The solar cell junctions that produce and separate the charge carrier are denoted as a current source. This was accompanied by a forward biased diode and shunt resistance in parallel indicating the opposite direction of photo generated current and forward biased current. The shunt resistance represents all the low resistive paths that produce leakage path for the current to flow avoiding the junction. Finally a series resistance was employed to include the effect of re-

www.manaraa.com

sistive loss in the quasi-neutral region of the p-n junction diode. The model can be further modified to include another current loss mechanism which is also known as double diode model.

In the organic material based solar cells, one significant limitation is the lower dielectric constant resulting in the formation of the exciton[37,101,102] (bound pair of electron and hole). Excitons are typically hole –electron pair coupled by columbic attraction force. This formation of exciton led to extremely low diffusion length of the bound photo generated charge pair. For dissociation of such bound photo-generated charge pair and their subsequent collection at the respective electrode, some efficient strategies must be employed. Both the thermal energy of the order of K_BT as well as the built-in electric field generated due to the equilibration of the Fermi level of cathode and active layer is insufficient to break the exciton.

In a simple organic p-n hetero-junction diode, at first a photon is absorbed close to the junction leading to the generation of a e-h pair. The exciton then diffuses to the junction and dissociates at the interface (due to energy band offset which produces huge electric field) into electron that moves to the n regions and a hole that stays in the p region. Later that electron moves toward n-side of the junction due to the built in electric field of the junction and hole moves towards p side. Since the light illumination creates extra electron and hole – they disturb the thermal equilibrium and tend to shift the Fermi level of the n side closer to the conduction band and in p side closer to the valence band. They are known as a quasi-Fermi level. In the case of light illumination the direction of current flow is exactly opposite to the direction of current flow in the forward bias. By increasing the forward bias voltage reduces the barrier potential and thus tends to cancels out the photo-generated current. The particular forward bias voltage at which the photocurrent is exactly equal to the forward current is called the open circuit voltage. At that voltage

www.manaraa.com

no external current flows through the solar cell (p-n) junction. At the zero external bias condition, the current that flows through the circuit is termed as the short circuit current.[103]

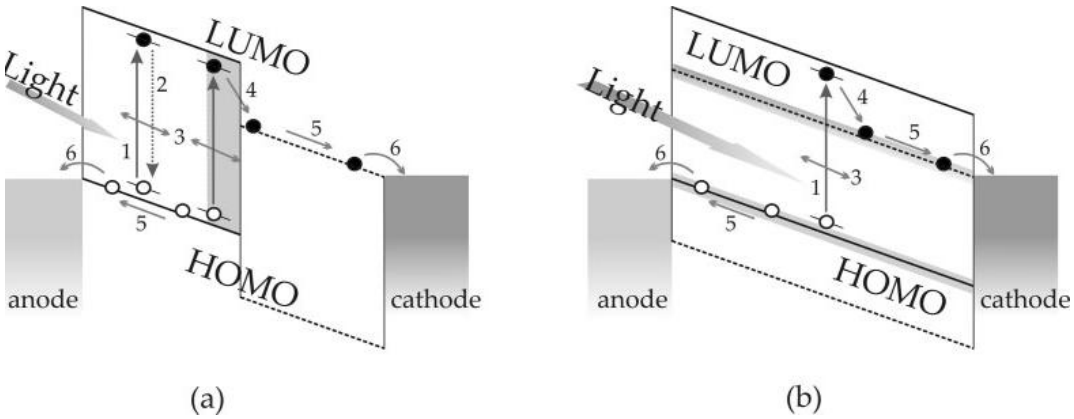

Figure 3.2(a) energy band diagram of bi-layer structure/(b) energy band diagram of bi-layer structure

The first attempt to extract current from organic anthracene [104] was unsuccessful because of inefficient charge separation. As shown in the figure 3.2(a) only those carriers can be collected which are created very close to the electrode-semiconductor junction because the rest of the generated carriers would eventually recombine in a process called geminate recombination which will be discussed in detail in later subsection.

In 1986 C.W. Tang[105] discovered that it is indeed possible to separate the bound charge carrier by using two different organic materials. The electron donor material has smaller electron affinity and lower ionization potential while an acceptor type material has higher electron affinity and higher ionization potential. As shown in the figure 3.2(b)- resulting difference in the potential between donor and acceptor will help in separating the bound excitons provided the difference in potential energy is greater than excitons binding energy. This kind of interfacing strategy of using two different materials and forming a hetero junction structure enhanced the charge separation greatly.[13]

As discussed previously, in order to observe the photo voltaic effect in the organic polymer based system, we need some basic criterion to be filled. Firstly, we need significant charge gen-

www.manaraa.com

eration with low active layer thickness. The generation process is followed by separation (quenching) of the generated exciton. Finally this is followed by charge transport and collection at the opposite electrode. The following figure 3.3(a) describes the different process of carrier collection.

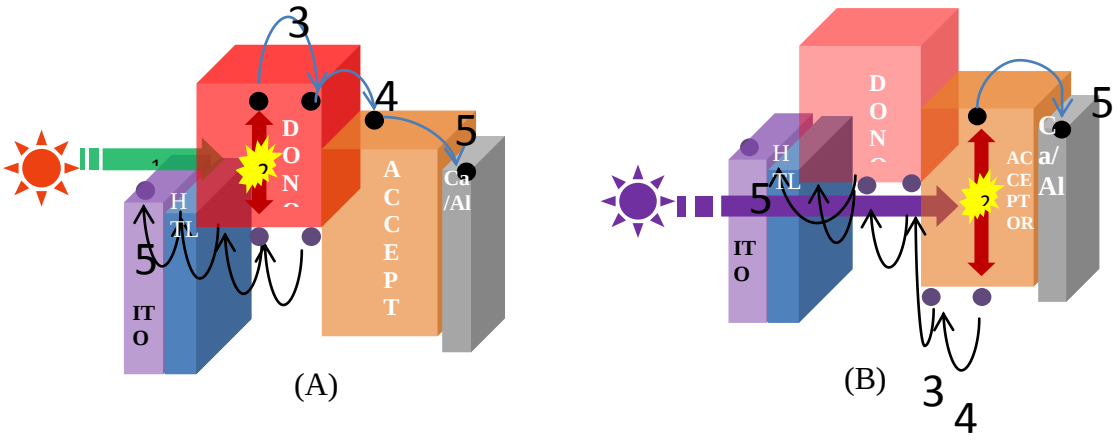

Figure 3.3(a-b) Schematic showing different charge transport mechanism[70]

The figure 3.3(a)and (b) describe different process involved in current generation. A photon absorbed by the polymer in in the step 1 produces one bound electron hole pair in step 2. This exciton can diffuse to the nearest interface junction between an acceptor fullerene and donor polymer in the third step. Once they reach the interface, electrons finds an empty state lower in energy and dissociates from the hole and create a CT (charge transfer) state depicted as step 4. Once the electron reaches LUMO of acceptor, it acts like a free charge carrier and diffuses to the nearest cathode. The hole alternatively transports through the acceptor to the anode, as depicted in step 5. The similar process of charge separation and transport occur when an exciton is generated in the acceptor molecule. Because of the higher band-gap of of acceptor molecule the probable absorption band is around the blue and UV region where the AM 1.5 photon flux decreases rapidly. Part of the optical absorption in the blue region of the solar spectrum is because of the

www.manaraa.com

PCBM. For fullerene-same process of charge generation, dissociation, separation and collection are followed.[12]

As described by Gang Li et al in 2012[12] each successive step is associated with an efficiency that collectively defines the efficiency of the solar cell. The external quantum efficiency (EQE) is the product of the efficiencies in each of the four processes.

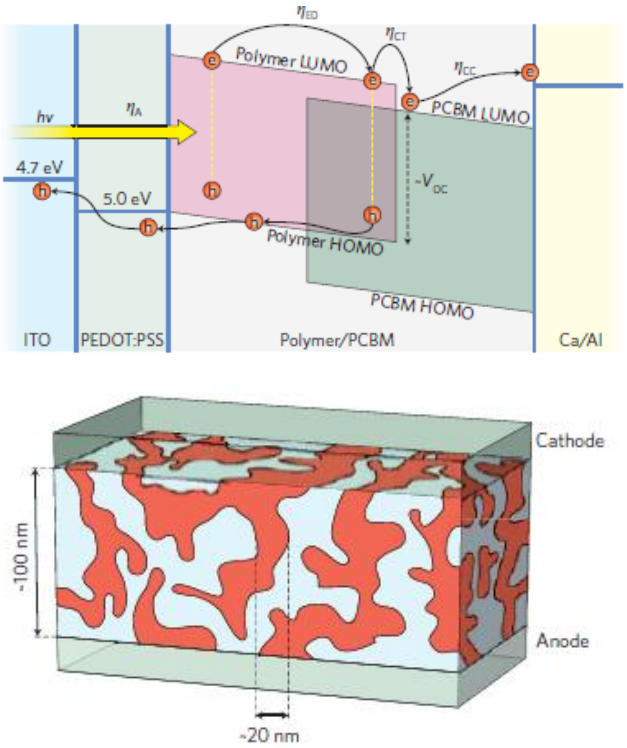

Figure 3.4: Schematic showing BHJ charge transport[12]

$$EQE(\lambda) = \eta_A(\lambda) \times \eta_{ED} \times \eta_{CS} \times \eta_{CC} \quad \ldots\ldots(1)$$

$\eta_A(\lambda)$ is the probability of absorption a photon which is the function of wavelength and the density of filled states in the valence band (HOMO) and the empty states in the conduction band(LUMO). This is associated with the steps 1 and 2 as depicted in the figure 3.2(a) and (b). In the step 3 (η_{ED})the geminate pair of exciton might recombine after travelling the mean exciton diffusion length if they could not reach any donor acceptor interface before that. Step 4 is associ-

www.manaraa.com

ated with the factor η_{CS} (corresponding to the charge separation where the charge carrier may recombine geminately before successful separation). Finally after the separation and formation of charge transfer states there is also a possibility of either monomolecular or bimolecular recombination of the separated charge carrier either at the interface or in the bulk which may further reduce the number of the successfully collected charge carrier. Thus, all these steps collectively contribute to the amount of short circuit current, a cell can generate. η_{CC} also include the effect of any barrier at either of the electrode interface that might inhibit the efficient charge collection due to barrier. [12]

3.1.2 Factors effecting the short circuit current (Isc)

The photo-current that is extracted from the solar cell under short circuit condition can be affected by several factors. Foremost of them is the absorption of the active layer and hence the thickness of the film. So the absorption of the entire film comes into picture to determine the short circuit current. However an optimization is necessary because with a thicker film, the electric field reduces (which is important for charge transport in disordered materials), resulting in lower charge collection, hence lower short circuit current. The next factor is morphology – the interpenetrating network of polymer donor and fullerene acceptor which determines how easily the exciton gets separated before geminate recombination takes place. The next factor is the geminate as well as non-geminate recombination of charge transfer states or free charge respectively, at the interface of donor-acceptor or before reaching the interface. Finally the mobility of the individual charge carrier(eg. hole mobility in polymer and electron mobility in acceptor determine, how easily the carriers after separation can be collected. Altogether the absorption, de-

www.manaraa.com

gree of interpenetration of donor acceptor network, non-geminate recombination at the interface and mobility in the individual donor acceptor determine the final short circuit current.

3.1.3 Factors affecting the open circuit voltage (Voc)

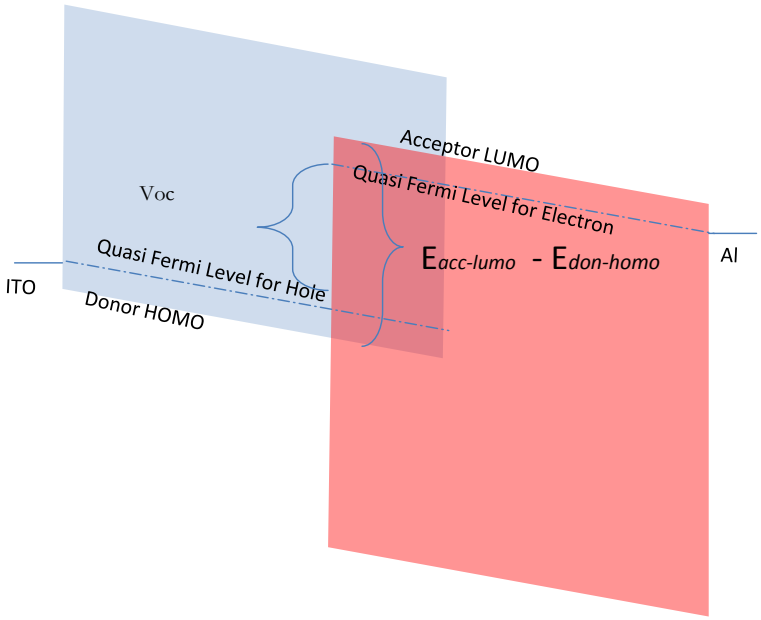

Figure 3.5 Origin of open circuit voltage (Voc)

As explained in numerous literature review the difference between the LUMO of acceptor and the HOMO of donor was considered the main reason for the open circuit voltage.[33,106-119] The value of V_{OC} for a organic solar cell can be expressed by the empirical equation

$$V_{OC} = [|E_{HOMO\ donor}| - |E_{LUMO\ acceptor}|]/q - 0.3\ eV, \quad (2)$$

[120-123]

where q is the elementary charge and 0.3 V results from the temperature dependence of the quasi-Fermi-levels in the polymer and fullerene domains as discussed in more detail elsewhere.[121]

www.manaraa.com

However the Voc can generally be defined as the difference between the two quasi Fermi level in both the polymer and fullerene as shown in the Figure 3.5. Further the Voc is chiefly governed by the non-geminate recombination term as well as absorption of light by the solar cell. The complete equation of Voc was proposed by Koster et al (by solving the continuity equation) in 1994 as described elsewhere.[122,124]

$$Voc = \left(\frac{Eg}{q}\right) + \left(\frac{KT}{q}\right) * Ln\left(\frac{P \times G}{(1-P) \times \vartheta \times Nc^2}\right) \quad \text{.....(3)}$$

$$\vartheta = \gamma + \left(\frac{1}{\tau p \times n + \tau n \times p}\right) \quad \text{.....(4)}$$

The equation of V_{oc} is modified vertion of the equation proposed by Koster et al[74]. This equation predicts the maximum open circuit voltage to be the Eg the effective band-gap which is $[|E_{\text{HOMO donor}}| - |E_{\text{LUMO acceptor}}|]$ as shown in the figure 3.5. V_{oc} can be affected by several terms, included in the main equation. P is the probability of the dissociation of exciton. G is the generation rate. ϑ is the term that contains both the recombination coefficient for monomolecular SRH recombination as well as bimolecular (γ) band to band recombination.

In addition the morphology (i.e. the packing of polymer domains) changes the band-gap of polymer as shown by Jenny Nelson group. Depending on the processing condition the crystallinity of the polymer changes those results in the change in band-gap.[125-128] Depending on the crystallinity, the position of the HOMO level shifts upward for a polymer like P3HT as shown by the same group. This change in crystallinity and subsequent change in the band-gap of the polymer results in the change in the effective band-gap for the polymer-fullerene interface. That also changes the effective open circuit voltage of the solar cell which can be obtained from external quantum efficiency measurement as well as optical absorbance study. Finally the shunt

www.manaraa.com

resistance can also affect the open circuit voltage of any solar cell. If the photo generated charge carrier finds an alternate low resistive path bypassing the junction of the bulk hetero junction, then it can reduce the amount of separation of both quasi Fermi level resulting in lower Voc.

3.1.3 Factors affecting the fill factor (FF)

Fill factor is another important parameter that needs to be optimized to obtain an highly efficient solar cell. Fill Factor is the measure of the square-ness of the IV curve of the solar cell under light. The FF is the ratio between the maximum obtainable power and the product of J_{SC} and V_{OC}. The FF is affected by several factors,[129] mostly by charge carrier mobility (hole and electron) and mismatching in carrier mobility, charge collection due to interface state recombination, series and shunt resistances etc. The following figure 3.6(a-d) shows different factors affecting the fill factor. The mobility mismatch of electron and hole can result in the accumulation of one carrier in either polymer or fullerene domain which can lead to the lowering of built-in electric field thus affecting the charge collection. So both mobility mis-match and trap assisted recombination are responsible for the inefficient charge collection and hence poor FF.

www.manaraa.com

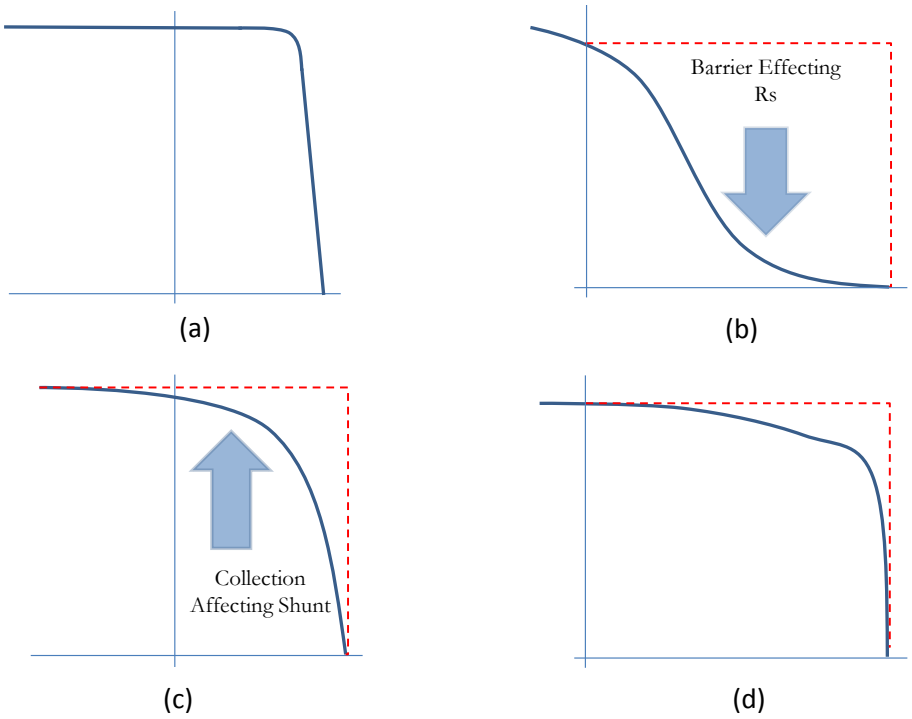

Figure 3.6(a-d) Light IV showing various reason of FF drop

3.2 Different loss mechanism in solar cell

To maintain the principle of detail balance all the generated charge carrier must recombine at the open circuit condition. Recombination is considered to be the source of loss of photo generated charge carriers in all solar cells. In this subsection we will review different possible recombination mechanisms and their possibility of occurring in realistic physical situation.

In general in all semiconductor material, recombination of the free carrier is a natural phenomenon. Different recombination mechanisms have different rate of occurrence. For example, band to band recombination also known as radiative recombination is more likely to occur in the direct band gap semiconductors resulting in radiation.[100] Unlike band to band recombination, trap assisted recombination is more likely to occur in in-direct band gap semiconductors where the

www.manaraa.com

probability of direct transition of electron from conduction band to valence band is very small. For an electron in conduction band to recombine with a hole directly in valence band, K-value (momentum) of an electron in conduction band and hole in valence band must match.[98,100] But for in-direct band-gap semiconductor, mismatch in momentum leads to trap assisted transition of electron from valence band to conduction band. There is another type of recombination called Auger recombination. In this type of recombination, the excess energy given off by an electron recombining with a hole is given to a second electron (in either band) instead of just emitting the energy as a photon. The newly excited electron then gives up its additional energy in a series of collisions with the lattice, relaxing back to the edge of the band. All the recombination process can occur simultaneously.[100] The recombination process with higher rate dominates the other type of recombination and dictates the minority carrier life time of the solar cell.

Band to band, trap assisted and Auger recombination, all are the recombination mechanism in the bulk of the material. There are some other recombination's that can take place at the surface of the material where the material has an interface with air resulting in discontinuity in the molecular/ atomic structure. This results in several surface states or interface states between the active materials. Sometime the active materials itself contains several crystalline grains with a grain boundary between the two grains. This grain boundary can have interface states which can take part in recombination. This type of recombination is prevalent in the poly/nano crystalline silicon based solar cell. Different recombination mechanisms are depicted in the following figure 23(a-e).[100]

www.manaraa.com

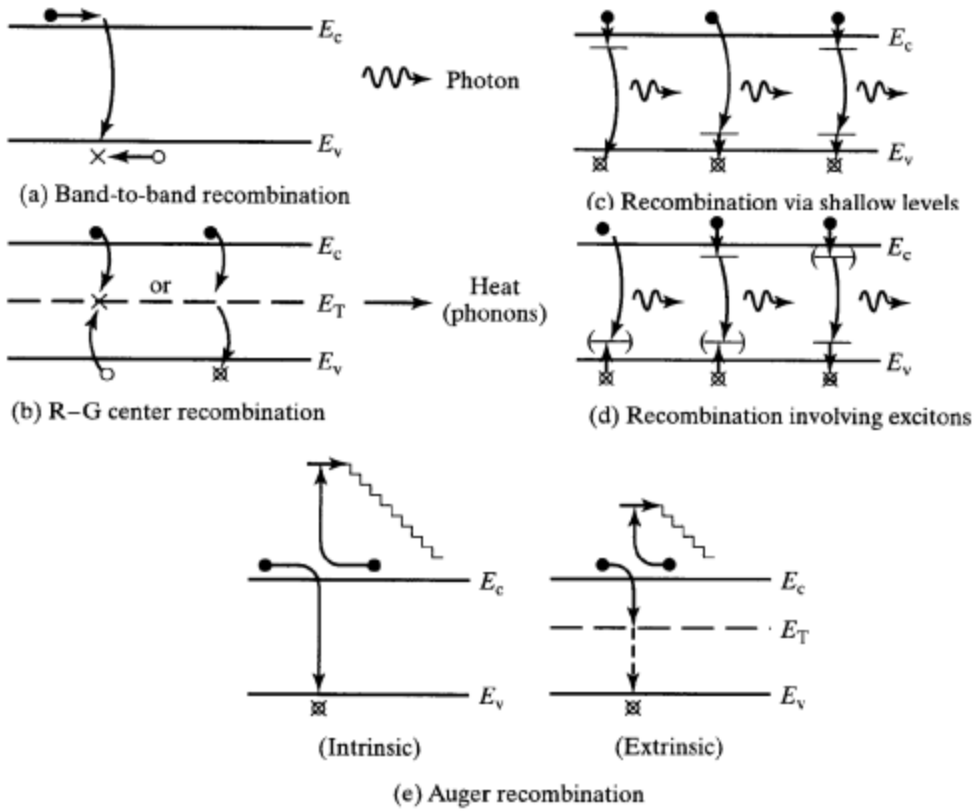

Figure 3.7 (a-e) - Schematic showing different recombination mechanism[100]

In addition to this general recombination, we have exciton recombination which occurs both in organic as well as inorganic semiconductors. For example in GaAs exciton formation occurs at very low temperature. In organic semiconductor exciton formation occurs at room temperature because of its lower dielectric constant resulting in higher excition binding energy in organic semiconductors. In the exciton recombination, electron- hole pairs recombine after being generated from the photon absorption and diffusion of exciton for some small distance called exciton diffusion length.[102] The recombination can be broadly classified into two distinct families. geminate recombination and non-geminate recombination.[129,130]

The term geminate recombination stands for the recombination of the geminate electron – hole pair which are created from a same photon. This type of electron hole pair recombination results in the radiative recombination which emits light out of the material.[131] The term non-

www.manaraa.com

geminate recombination refers to all other recombination that includes band to band recombination, trap assisted SRH recombination, auger recombination etc. In several literatures recombination can be broadly classified into two distinct families, mono-molecular recombination and bi-molecular recombination.[71,120,121,123,131-146]. In our work we will define the term monomolecular and bimolecular precisely based on the rates (R) and their dependence on the electron or hole density (n). For example monomolecular =$R \propto n^1$ and bimolecular = $R \propto n^2$. [100] Following figure 3.8 depict different recombination mechenism.

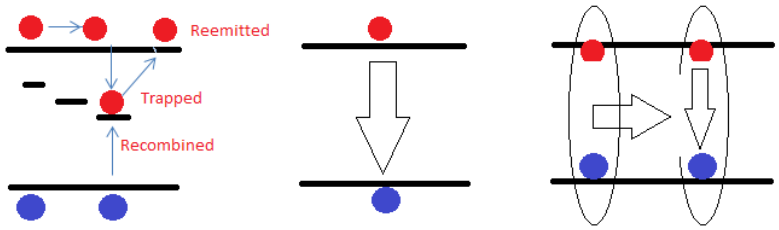

(a) (b) (c)

Figure 3.8 (a-c) Different recombination mechanisms in organic solar cell

3.3 Discussion on recombination in OPV

The issue of which recombination process dominates, is an issue of long debate. Whether the recombination is at the bulk or at the interface is also a matter of discussion. Several researchers have proposed different recombination mechanisms and research groups have not agreed on the specific dominant recombination processes in the bulk hetero-junction based polymer solar cells. A leading researcher in this area Dr Robert Street in his several papers had argued that it's the trap assisted recombination (at the interface) that dominates the other recombination.[54,135,147,148] In contrast several groups from Europe had argued that band to band recombination[132,133,136,137,149] is dominating over the trap assisted recombination at the interface. Jenny

www.manaraa.com

Nelson et al[131] in their paper argued that it is the tail state which is dominant mechanism of recombination at the interface.

3.3.1 Different proposed recombination schemes

Briefly several possible recombination mechanisms were discussed in the literature consisting of, A) Recombination of the exciton before it reaches the interface (geminate recombination),[130] B) Recombination of geminate charge pair before separation at the interface,[147] C) Band to Band recombination of one electron from acceptor conduction band and hole in donor valence band(strictly non-geminate in nature),[122,132,133] D) Non-geminate trap assisted recombination via the traps present near the middle of the effective band gap at the interface of polymer and fullerene,[147] E) The reverse diffusive recombination at the metallic contact.[147]

In reverse diffusive recombination, the carrier must diffuse against the built in electric field towards the metallic contact. That is only possible when the carriers are absorbed too close to the contact. However it is argued that free charge carriers in the organic solar cell are generated near the interface. In such a scenario, a carrier can only diffuse against the built in electric field if the cells flat band voltage is few times K_BT. So that recombination might dominate near the flat band condition of the solar cell. However the signature of such recombination was not visible in the experiment reported by Street et al. So this type of recombination is neglected thereafter.[147]

To understand further the process of recombination via field ionization of charge transfer excitons we need to gather more in depth understanding about the concept of the charge transfer state of exciton. [150-152]

www.manaraa.com

3.3.2 Geminate ct recombination[147]

A charge-transfer complex (CT complex) is an association of two or more molecules, or of different parts of one very large molecule, in which a fraction of electronic charge is transferred between the molecular entities. The resulting electrostatic attraction provides a stabilizing force for the molecular complex. The nature of the attraction in a charge-transfer complex is not a stable chemical bond, and is much weaker compared to the covalent forces. The attraction is created by an electronic transition into an excited electronic state, and is best characterized as a weak electron resonance.[147,153,154]

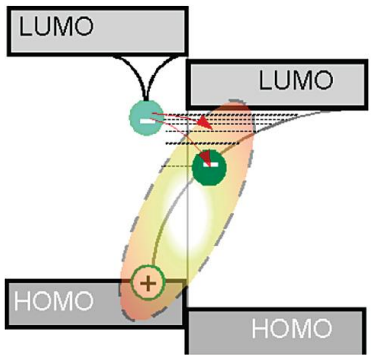

Figure 3.9 Formation of charge transfer states[155]

For a CT state to exist across the interface the electron and hole must be spatially close and must possess a dipole moment. According to Zhu et al the CT exciton is formed after the separation of the geminate electron hole pair.[155-157] The geminate pair has its own exciton binding energy. When they separate and form CT exciton, they are also bound by a weak Columbic force. From numerical simulation author[153] found that the CT binding energy of the lowest lying CT exciton is one order of magnitude higher than the thermal energy (K_BT) at room temperature.

www.manaraa.com

The details of the calculations can be found elsewhere.[147,153] As we know that, in the CT state- electron and holes are placed further apart, It is thus logical to presume that the binding energy of the CT exciton must be less than 0.25 eV.[153] Further ionization of CT exciton was addressed by three separate models, The Onsagar[158], Broun[159] and Pool frenkel Model as mentioned elsewhere[147]. While Onsager model did not include the bound state (CT) of exciton, The Braun model predicts that it is not necessary to apply electric field to separate the CT pair or in other words there is a significant probability of zero field ionization of bound CT exciton. The Pool –Frenkel model explains the classical picture of bound electron hole pair by the barrier lowering with applied electric field. Street et al[147] used the Poole-Frenkel model to calculate the photo current for different CT binding energy and found that the experimental photo current matches with the model using 0.23 eV binding energy. It was shown that when binding energy is high , a high electric field is required to separate the bound CT pair. While for lower binding energy less than 0.25 eV the probability of CT ionization is very large and photo current becomes less dependent of external electric field. [155]

The above discussion about the probability of CT state ionization was done to understand whether the ionization is field dependent or not. It was found that the rate of ionization of CT states with binding energy less than or equal to 0.25 ev have high probability of ionization. This conclusion may eliminate the possibility of such CT recombination at the interface. [147]

3.3.3 Non-geminate ct recombination

It was argued by Street et[147] all that even though the probability of the geminate CT recombination is lower because of lower CT binding energy and lesser field dependent ionization, It is still possible two non-geminate charge carriers at the interface can form a CT exciton and can recombine further in the process. However it was suggested that this type of recombination can

www.manaraa.com

occur at higher intensity of light where the presence of both type of charge carrier near the interface is high. It was further mathematically proposed that the rate of this recombination process is rather small in the open circuit condition.[147]

3.3.4 Recombination via interface states

When the probability of ionization of charge transfer exciton at zero electric field is high and also the probability of non-geminate CT recombination is low under open circuit condition, the only channel left for free carrier to recombine is recombination via trap states that are present within the energy gap at the interface. Recombination can happen when a charge carrier (eg. electron) is trapped by states inside the band gap and become a trap for a free hole. If it captures a hole, then two free carriers can recombine. For this type of recombination to occur the recombination rate depends on the concentration of one carrier and the density of trap states. This type of recombination usually occurs in amorphous material such as amorphous silicon. In the paper by J G Simmons and G W Taylor[160], author explained the presence of multiple trap levels energetically distributed across the entire energy band gap. However only those trap that lie roughly between the two quasi Fermi levels will act as an effective recombination center for hole and electron.[160]

3.4 Conclusion

In this chapter we tried to understand the basics of solar cell and its operating principles. We also discussed the figure of merits of solar cells and the origination of short circuit current, open circuit voltage and fill factor. We also discussed about different types of recombination and their effect on the electrical properties of solar cell. Finally we explained different dominant recombination mechanism in the literature for organic solar cells.

www.manaraa.com

CHAPTER 4
EXPERIMENTAL SETUP AND CHARACTERIZATION TECHNIQUES

4.1 Introduction

This chapter will briefly discuss about the experimental setup used for studying photo degradation of organic solar cell. In addition we will also discuss about different characterization technique used to probe the changes in different fundamental properties of organic solar cells.

4.2 Environmental chamber

The environmental chamber is accompanied by one backing and one turbo-molecular pump to pump out the chamber prior to measurement. The front of the chamber has a quart glass with higher transmittance of visible spectrum of the light. For light soaking we used ABET solar simulator with xenon arc lamp. We can change the intensity of the lamp by either changing the position of the lamp or by using the combination of Lens and neutral density filter. The chamber is connected to a dry nitrogen gas cylinder that helps to flow nitrogen at a continuous rate set by a flow meter. We also have a fan inside the chamber to dissipate the temperature accumulated on the exposed contact. Both the nitrogen and fan helps to keep the sample at normal room temperature (~25^{o}C).

Since all the organic solar cells are bottom illuminated cell where light enters from the back of the solar cell through glass substrate as shown in the following figure. The sample is mounted on a stage with for passing light. We also cover the entire device except the exposed contact to keep the unexposed contact in dark. A light guiding mirror inside is used to change the direction

www.manaraa.com

of the light beam from horizontal to vertical direction. Two electrical probes are used for all electrical in-situ measurement.

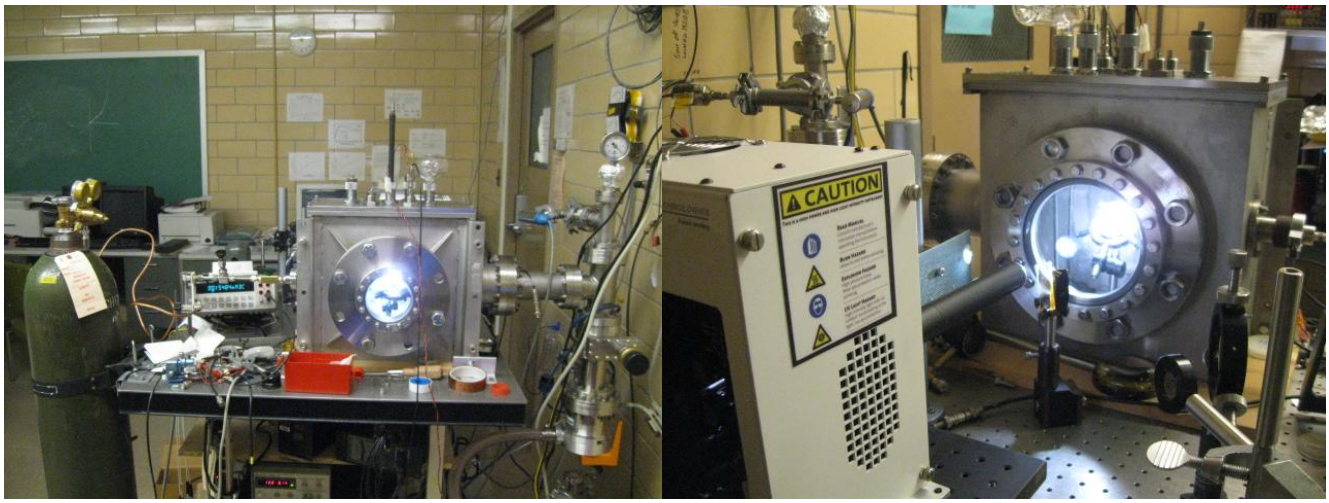

Figure 4.1 Degradation Chamber

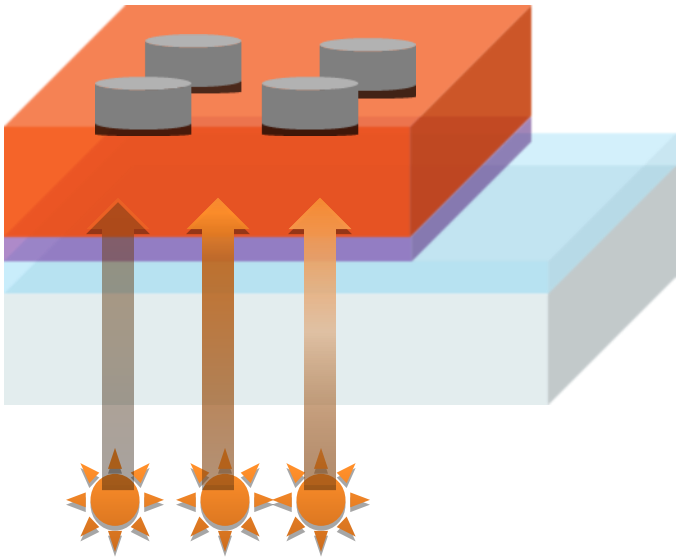

Figure 4.2 Schematic diagram of the solar cell prepared

We follow a standard operating procedure for loading, exposing and unloading a sample. The standard operating procedure is mentioned as follow.

www.manaraa.com

1. The light source is calibrated by a known working standard crystalline silicon (Hammamatsu-0.05 cm^2) solar cell to set the intensity.
2. The sample is loaded after covering with aluminum foil except the dot to be exposed.
3. Except during the exposure the front quartz window is covered with aluminum foil.
4. Before closing the top lid of the chamber we need to make sure that the electrical contact to the cell is working. So we measure light IV and Dark IV using Keithley 236 connected to the chamber top lid by a BNC connector.
5. We close the lid after making sure all the electrical contact to the cell.
6. We start the roughing pump with back flowing nitrogen to set the chamber pressure to (700-800) m-torr. This process helps to get rid of all the moisture stuck to chamber wall while the chamber was open due to loading and unloading. This step continues for 4-5 Hrs.
7. Then we start close the nitrogen valve to chamber and set the flow at lowest to make sure no burst of nitrogen can enter inside the chamber while the turbo is on.
8. Then we start turbo pump while the backing pump is still on.
9. After the turbo pump is active, we can open the nitrogen valve slowly and adjust the pin-valve to set the backing pressure 30-50 micron.
10. The step 9 can continue until pressure at the chamber reaches around 5E-5 torr. This usually takes 3-4 hours. This is a faster process of drying chamber and getting rid of the moisture inside the chamber.
11. It was found that we have a continuous outgassing from the different component put inside the chamber that includes electrical probe, wires connecting them to BNC plug, Fan, Metal stage, Mirror assembly. We have experimental results which suggests that

www.manaraa.com

without these entire components inside the chamber can reach 1E-6 torr pressure very soon (within 30 minutes) of starting turbo.

12. Once we reached the desired pressure, (5E-5 torr), we stop the pump assembly and start backfilling the chamber with nitrogen. Once the chamber is at atmospheric pressure, we start the fan to cool the environment inside the chamber. After setting the flow of nitrogen we start the exposure.

4.2 Characterization techniques

4.2.1 Light current voltage measurement

This is the most basic measurement to check the overall performance of a solar cell. The light IV measurement consist of shining light to the DUT(device under test) and then sweeping the external voltage to measure current at each measurement point. As we already know that for a simple P-N junction diode shining of light creates excess hole-electron pair and they are subsequently separated by the built in electric field. They build up excess charge carrier (electron in the n-side and hole in the p-side. This results in the split up of quasi Fermi level as shown in the figure. However as the excess carrier starts building up, the built-in potential of the diode drops resulting in the forward diffusion of charge carrier resulting in the dark current in the direction as shown in the figure. In the short circuit condition Fermi level do not split as all the excess carriers are collected at the output circuit. However at the open circuit condition the forward voltage become such that the forward bias dark diode current is exactly equal to the photo generated current in the opposite direction. This results in the cancellation and subsequently zeros current at the output circuit. This leads to the open circuit condition. Both open circuit voltage and short circuit current plays significant role in estimating the efficiency of any solar cell. In addition to

www.manaraa.com

them Fill factor can be calculated from the ratio of the maximum power delivered to the output circuit to the product of Voc and Isc.

The efficiency of any solar cell can be calculated in the following way.

$$\eta = (V_{oc} \times I_{sc} \times FF) / P_{in}$$

P_{in} is the input optical power taken to be 100 mW/cm2 for AM 1.5 solar spectrum.

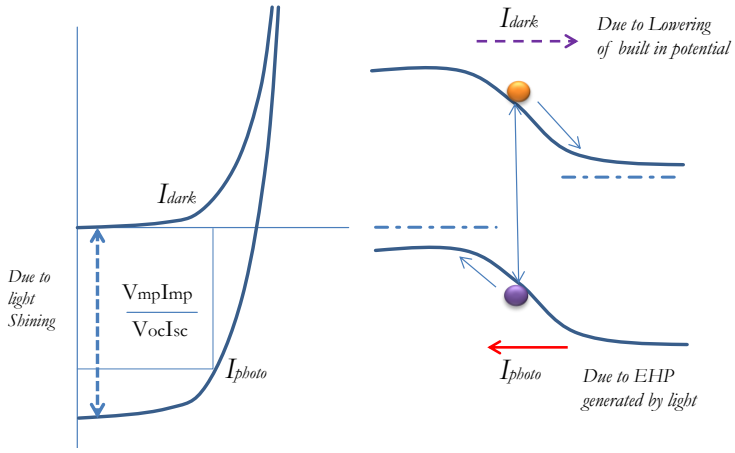

Figure 4.3 Typical light IV curve of solar cell

This method of basic characterization was used extensively throughout in our work to check the performance of our solar cells. This measurement were made both in-situ(inside the degradation chamber) using a Keithley 236 precision current meter as well as using same instrument outside chamber in IV measurement test bench. We used a calibrated crystalline silicon solar cell to set the intensity of the ELH as well as Xenon Arc lamp to 1X sun intensity. For higher intensity degradation experiment we used lens to concentrate the light beam to increase the intensity.

www.manaraa.com

4.2 Dark iv measurement

Dark current voltage measurement is a simple and effective tool in measuring different fundamental parameters of a solar cell. The linear plot of current and voltage do not provide much information. However when plotting them in the semi log, they carry valuable information about different current transport mechanism inside the diode. They also provide us the estimation of density of recombination center.

Recombination is a source of diode forward current under dark, a well-known phenomenon as described by William Shockley.[161] Dark current under forward bias can be an efficient and simple tool to estimate the nature of current and different recombination mechanism.

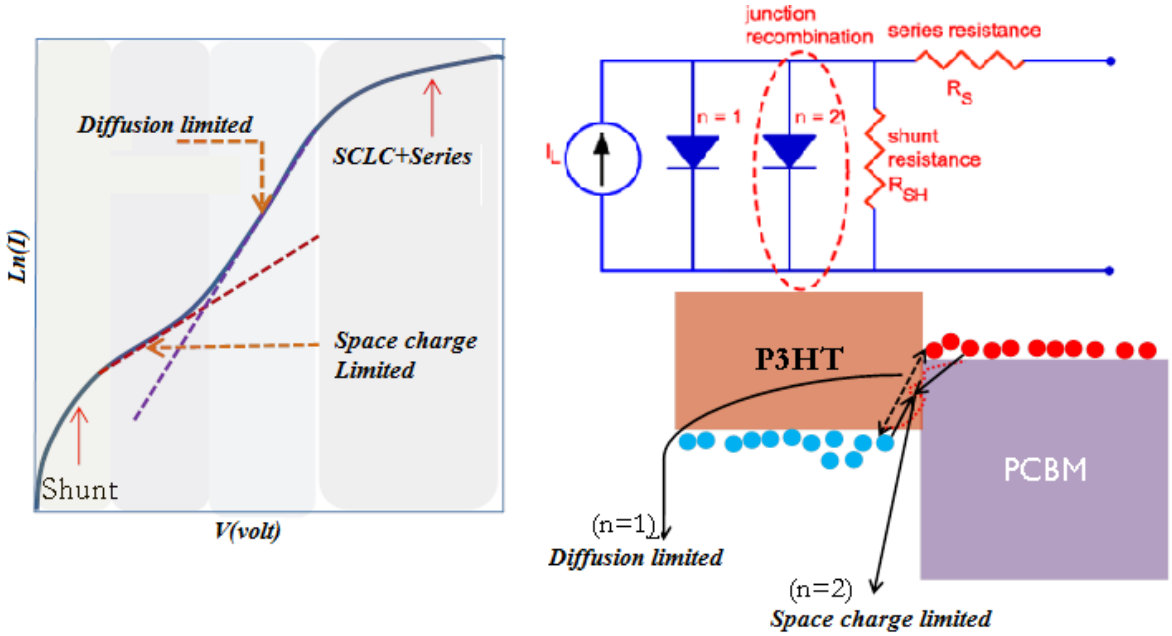

Figure 4.4 : (a)Typical dark current voltage characteristic's of a solar cell.(b) Equivalent circuit of solar cell , (c) Schematic showing recombination mechanism at interface of organic solar cell.

As shown in the above figure 4.4, a solar cell can be modeled as a current source in parallel to a diode and a shunt resistance and a resistance connected in series to take into account differ-

www.manaraa.com

ent resistive element such as resistance of contacts and quasi neutral region of diode. The left hand side figure shows atypical dark I-V curve with potentially different regions.

Under dark we can remove the current source from the circuit and we are left with two diode and a very high resistance in parallel and a small resistance in series with the load. The entire forward bias dark current voltage plot can be distinguished into five distinct region or voltage regime. The low voltage regime (V<0.1 Volt) is named as shunt region which is essentially linear. That is followed by an exponential region (0.2<V<0.4) where current is proportional to $\exp(qV/n_{1\times}KT)$. Here q is the electronic charge and K is Boltzmann constant and T is the temperature in kelvin and V is the applied voltage. The term n1 refers to the diode ideality factor of the corresponding region. In ideal case for a single level trap distribution around mid of the energy band gap , n1 will be 2. However we see often this number to be lower than two implying multiple level of trap distribution inside the band-gap. At higher voltage we notice the third region where current is proportional to $\exp(qv/n_{2\times}KT)$ where n_2 refers to the diode ideality factor of that region. In ideal condition the value of n_2 will be close to 1 because in that region the current is dominated by the diffusion of majority charge carrier. With higher voltage the current tends to saturate from its exponential increase because of dominance of series resistance. [98,147]

$$Vj=Vapp- IRs$$

This simple equation says as the current increases further, the IR drop(where Rs is the collective resistive drop in neutral region and cathode and anode all together) become significant and starts to reduce the voltage drop across the junction. So the current in this region is mostly linear. However it is also possible to notice a small voltage regime before this series region which is termed as high level injection region where the current is mostly dominated by space charge limited current. Depending on the nature of recombination mechanism dominating the current

www.manaraa.com

transport in a solar cell, we can either see all the voltage regimes or some of the regimes. The exponential regime is the center of importance as from this regime we can extract the density of recombination center which can be related to the loss mechanism of a solar cell.

$$I = I_0 \left[\exp\left(\frac{qV}{nkT}\right) - 1 \right]$$

We can extract Io (reverse saturation current) and n (diode ideality factor) by fitting the exponential regime to the above equation. Typical value of Io varies from 1E-12 Amps to 1E-9 Amps. The value of n varies from 1-2. The current in the first exponential regime can be described by the following equation in the simplest form.[147]

$$J_{SHR} = \frac{qn_i x'}{2\tau}(e^{V_a/2V_t} - 1)$$

The above equation clearly correlates reverse saturation current to n_i and τ. The τ is particularly important because it's inversely proportional to the total density of recombination center. So from the measurement of Io we can estimate the total density of recombination center (not total density of trap states) which are responsible for the forward bias dark current at the specific voltage regime. The following figure4.5 shows the presence of traps in the depletion region of a p-n junction. All the traps above electron quasi Fermi level are trap sites for electrons but not a recombination center. Similarly all the traps located below the hole quasi Fermi level are good trap sites for hole but not recombination center. So only those traps that are present inside the two quasi Fermi level are the effective recombination center for both hole and electron. The arguments are applicable to the hetero junction architecture of solar cell as well as to homo junction.

www.manaraa.com

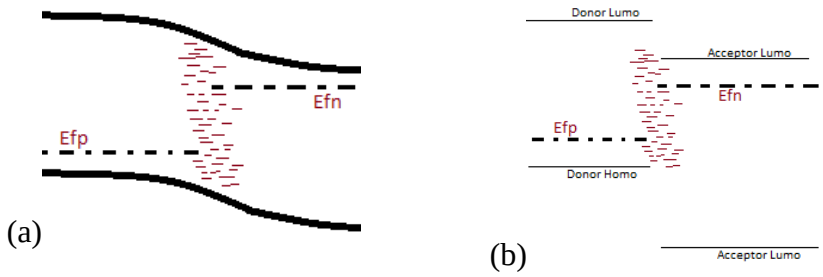

Figure 4.5: (a) Presence of traps at the p-n junction depletion region.(b) Schematic of traps at BHJ interface.

The dark current measurement can also be used to estimate the flatband voltage as well as mobility of minority carrier. This analysis is further discussed in APPENDIX C.

4.2.3 Quantum efficiency:

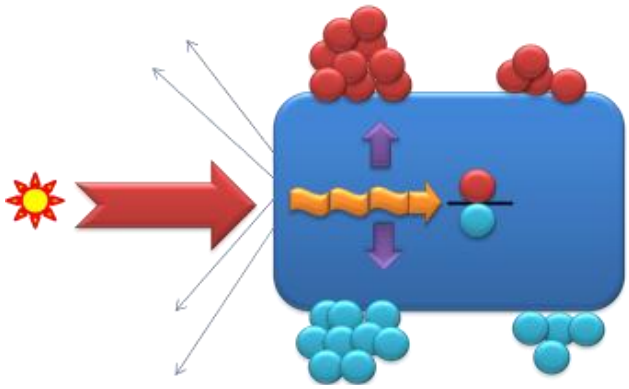

Figure 4.6:Schematic showing photo generation process in any semiconducting materials.

$$EQE = \left(\frac{NO\ OF\ CHARGE\ CARRIER\ COLLECTED}{NO\ OF\ INCIDENT\ PHOTON}\right)$$

In very simple word quantum efficiency (QE) is defined as the ratio of charge carrier collected to the number of incident photon. The above figure depicts several loss mechanisms in a solar cell. A percentage of light gets reflected at the entry because of refractive index mismatch

www.manaraa.com

between air and semiconductor. The inclusion of transparent conducting oxide can help reducing the loss but can never remove this phenomenon completely. Rest of the photon enters the active layer of semiconductor and gets absorbed depending on the band gap and absorption coefficient of the active layer material. Assuming one photon generates one electron hole pair(EHP) we can correspond the number of absorbed photons to the number of generated electron hole pairs. However from the point of generation to the point of collection at the respective cathode, there are several loss mechanism that can reduce the number of generated electron hole pair. These loss mechanisms include band to band recombination, SRH recombination etc.

IQE= Number of Carrier Collected /Number of Absorbed Photon

The internal quantum efficiency (IQE) is defined as the ratio of number of charge carrier to the number of absorbed photon taking into account of the reflection.

In all cases the internal quantum efficiency will always be higher than the external quantum efficiency (EQE).

$$\text{ABS EQE}(\lambda) = \frac{\frac{Sample\ Signal}{Area}}{\frac{Reference\ Signal}{Area}} * \text{Ref EQE}(\lambda)$$

The EQE is measured as follow.

Following are the details of measuring external quantum efficiency of a solar cell .Depending on the architecture, superstrate or substrate the solar cell can be bottom illuminated or top illuminated. The above figure is for the measurement of organic solar cell.(which are mostly bottom illuminated)

www.manaraa.com

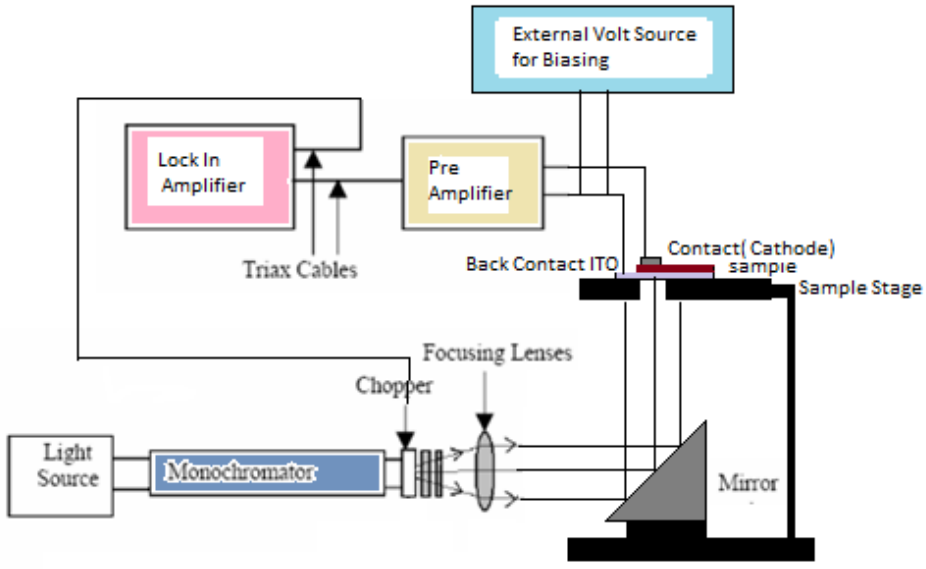

Figure 4.7:Schematic showing EQE measurement procedure.

1) A mono-chromator is used to generate photon of a particular wavelength by using internal grating structure. The wavelength of the incident light can be changed by changing the grating spacing by mechanical switching.

2) A chopper of low frequency is used to transform the light source into a suitable AC signal so that we can get rid of the entire dc noise component from the solar cell current and can only measure photo generated charge carrier. Generally the frequency of the chopper is set to a frequency away from 60 Hz , commercial electrical frequency to reduce the interference noise. In our experiment we have used 13 Hz as a chopper frequency.

3) Filters at 580nm, 700nm, 900nm and 1200nm are used to isolate harmonics. The monochromator grating structure produces higher order harmonics of the monochromator lamp signal which monochromator grating structure fails to remove. These filters are used to cut-out the noise from the longer wavelength harmonics. For wavelength below 580 nm a low pass filter is used. While for wavelength between 580 nm and 700 nm no filters are inserted. For wave-

www.manaraa.com

length above 700nm up to 900 nm another filter(High pass) is inserted. Finally wavelength above 900 nm to 1200 nm another filter is added.

4) DC bias light is an extremely important component of a QE measurement system. DC bias light is used to fix the position of quasi Fermi level. In the absence of dc bias light there will be separate position of quasi Fermi level for different wavelength leading to the generation of more carriers from the trap levels. The intensity of the DC bias light should have sufficiently high intensity as compared to the AC monochromator signal to fix the position of quasi Fermi level. The high intensity dc bias light will help in saturating the trap states, providing a equal environment for the measurement of low level ac photo carrier at different wavelength of incident photon.

5) Lock-in amplifier helps in latching the input ac light signal to the out put electrical signal. By this we can make sure that the current output from the lock in amplifier has a direct correspondence to the input photon of different wavelength.

6) Lens and Mirrors are the essential optical component in the EQE measurement system specially used to guide the light from the monochromator to the sample. Minor stains or finger prints causes huge change in the reflectivity as well as transmission of the mirrors and lens respectively. It has also been observed that metal used on the back side of the mirror also affects the spectrum intensity. For Aluminum we use a factor of 0.9 to account for its absorption of the light at the lower wavelength of the spectrum.

7) Pre amplifier helps in enhancing the low signal obtained from the DUT. Since the number of photon are very less in the monochromator output, generally the amount of charge carrier generate from the sample are very less which is leading to the out put photo current in the order of nano to pico amps. Pre amplifier helps to enhance the signal level by the multiple order of mag-

www.manaraa.com

nitude to make the signal visible. However this comes at the cost of noise enhancement too. So for very low signal during subgap quantum efficiency measurement, the noise due to scattered light , and other measurement system inherent noise become so significant that it becomes almost impossible to detect and measure the photo current. In our measurement we used a crystalline silicon solar cell of known are (50 mm^2) from Hamamatsu as a reference solar cell whose quantum efficiency is well known.

8) External DC bias is also an important part of the measurement system. Measurement of EQE under external bias shows the collection problem of a specific carrier (either hole / electron). This is a quite useful detection technique for specific collection problem in inorganic solar cell. However for organic solar cell, due to the specific nature of bulk hetero-junction architecture same conclusion cannot be made. However an overall idea about the trap assisted recombination can be obtained from the specific shape of EQE vs Bias plot which will be discussed in the subsequent section,

4.2.4 Sub-gap quantum efficiency

Sub-gap quantum efficiency is basically an extension of the external quantum efficiency measurement which gives us invaluable information about the nature of traps states and their energetic location. The measurement of the external quantum efficiency was limited only to those wavelengths which is equivalent to or slightly more than the band gap of the solar cell active material. In sub-gap measurement we reduce the photon energy further in order to track the optical absorption between the states which are locating deeper into the energy band of the active material. The discussion of the sub-gap measurement will be limited specifically to the organic bulk hetero junction architecture. However the basic physics is applied to any architecture.

From the Sub-gap photo current measurement we derive essentially the

www.manaraa.com

1. Quantitative estimation of effective interface band-gap between (Donor HOMO to Acceptor LUMO).
2. The Urbach energy (Eu) slope of the tail state which defines how defective the material is.
3. Location of mid-gap states and their nature (whether they are interface or bulk).
4. There are several works[80-83] that suggest the quantitative analysis of mid-gap defect states for organic solar cell. However in the further discussion we will see that the mid-gap absorption comes around 1ev to 0.8 ev where the signal from photo current is extremely low resulting in higher noise and fluctuation. Any quantitative conclusion from the photo current in this range may be erroneous. Though there are some solutions suggested to get around the problem of noise at low every regime by using the red bias light which we did not use in our experiment.

Referring to fig 4.8(A) in the left hand side shows a typical sub-gap photo current of a bulk hetero junction solar cell made of P3HT(Donor polymer) and $PC_{60}BM$ Acceptor fullerene material. Different numbers are used to signify different region of importance.

1. The region 1 corresponds to the absorption in the polymer (P3HT) domain or fullerene domain corresponding to the inter band absorption as depicted in the figure 4.8(D).
2. The region 2 shows direct absorption from polymer valence band(HOMO) to Acceptor conduction band(LUMO).
3. The region 3 corresponds to the absorption between valence band tail state of donor to the conduction band of acceptor or valence band of donor to the tail state of conduction band of acceptor of acceptor as depicted in the figure 4.8(D). The region in the 3 is essentially exponential implying the fact that the tail states are exponentially distributed and they are going

www.manaraa.com

down towards the mid-gap. The slope of this exponential region is called Urbach energy which is a direct measurement of material quality. For amorphous material the typical Urbach energy varies between 38 meV to 55 meV.

4 The little bump in the final region shows the transition of charge carrier via mid-gap energy states which are essentially Gaussian in nature (for amorphous silicon and many organic semiconductors). Though it is undoubtedly seen that the absorption in the fourth region is due to the mid energy states, the exact location of these states in the spatial dimension is not yet understood very well. [78-81]

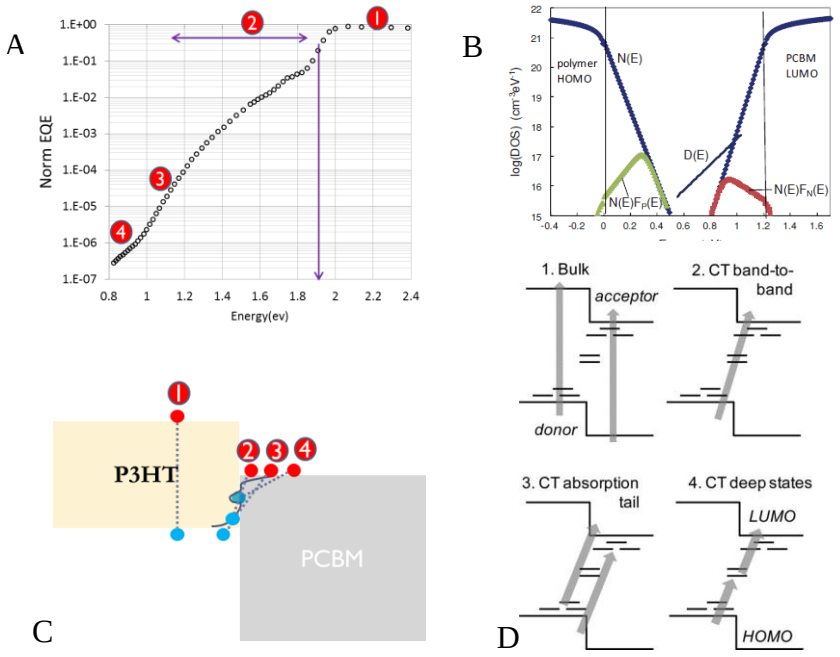

Figure 4.8: (A) Typical sub-gap EQE plot, (B) Tail and mid-gap states, (C) Different photo-excitation region, (D)[82] Different photo transition process [53,146,148,162]

4.2.5 Capacitance voltage measurement

Capacitance measurement is a very powerful tool for a quantitative estimation of total defect density in and a widely used and proven measurement technique used for inorganic solar characterization. The basic theory of the capacitance –voltage measurement is based on the depletion

www.manaraa.com

capacitance of a normal p-n junction diode.[98] In the thermal equilibrium depletion layer of a p-n junction behaves like a parallel plate capacitor having two sheet of opposite charge with a separation between them. The capacitance can be represented by the following equation, where w stands for depletion width and ε_r is the relative permittivity of the material.

$$C = \frac{\varepsilon_0 \varepsilon_r A}{w} \qquad w = \sqrt{\frac{2\varepsilon(V_{bi} - V)}{qN_A}} \qquad \text{..... (1/2)}$$

,

$$\left(\frac{A}{C}\right)^2 = \left(\frac{2\,(Vbi - V)}{q \in 0 \in r\, Na}\right) \qquad \text{..... (3)}$$

Now applying DC bias can change the capacitance by changing the depletion width because depletion width can be described by the equation 2, where Na is doping density, V_{bi} is flat band voltage and V is applied DC bias. The only assumption is that the device is a metal semiconductor junction with semiconductor is p-type doped. By plotting the equation 3 with respect to voltage we can estimate the dopant density of an metal semiconductor schottkey junction.

Measuring dopant density

Typical Mott-Schottky curve is depicted in the following figure. The intercept of the forward bias straight line with the voltage axis gives the estimation of built in potential (flat band voltage). By fitting the equation 3 in the forward bias region we can estimate the value of dopant density Na(the semiconductor was assumed to be p-type doped). As it approaches farther to the reverse bias , the capacitance and in turn $(1/C)^2$ tends to saturate because the depletion width has been extended all across the active layer.

www.manaraa.com

The frequency at which we perform this measurement is also another point of concern. Generally the dopant states are shallower than the deeper states. So at lower frequency of input small ac signal will allow both shallow as well as deeper states to respond. However as we increase the frequency, deeper states stop responding to the input perturbation because deeper states need longer time to re-emit the trapped charge carrier. This gives us the freedom to select particular frequency at which we want to measure capacitance. Generally we follow a thumb rule which says that , the frequency above which solar cell stops showing Mott-Schottkey[163,164] behavior is the intended frequency of choice. Generally above this frequency the measured parallel capacitance is only the geometrical capacitance of the device. In our experiment we have used 100KHz as a probe frequency to calculate the dopant density.[165]

To probe deeper states we need to use lower frequency. Lower the frequency, steeper the forward bias region will be. The voltage above which the capacitance starts dropping and

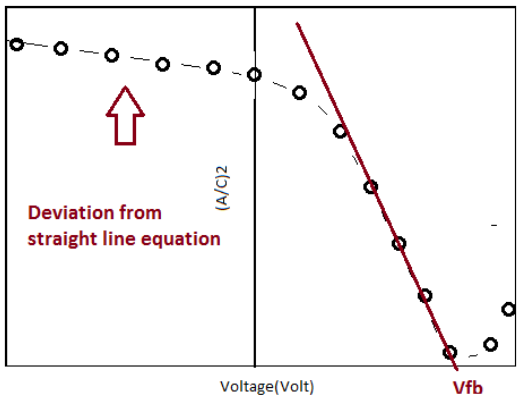

Figure 4.9: Typical capacitance –voltage plot of a solar cell.

conversely (1/C)2 starts shooting up is the region where diffusion (chemical) capacitance dominates.[163,166-168]

www.manaraa.com

4.2.6 Capacitance spectroscopy measurement:

In addition to the capacitance voltage measurement, capacitance –frequency spectrum of a solar cell can also be measured to obtain the energetic location and approximate density of defect states. As in the case of capacitance –voltage technique, this method is also widely used in inorganic semiconductors. This was first proposed by Walter Harberholtz.[169] Later in 2009 P Boix et al[170] and KS Nalwa et al[171] applied the model to describe the defect states distribution in organic semiconductor based solar cell.

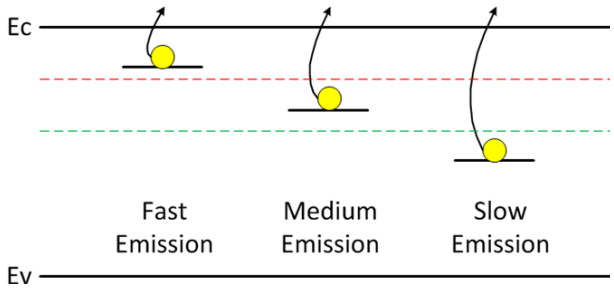

Figure 4.10: Trap response to input small signal excitation for capacitance-frequency measurement

The measurement technique is based on the theory of trapping and de-trapping of defect states inside the energy band gap. The speed of re-emission depends on the energetic location of the traps in the forbidden energy gap. The traps which are closer to either valence/conduction band would have faster emission rate, while deeper states takes larger time to re-emit a carrier. As we know capacitance is the measure of change in the fraction of charge over the change in the fraction of input ac voltage. For a given input ac drive voltage we can measure capacitance (parallel) for different frequency ranging from 1Hz to 1 MHz. Lower frequency response include the contribution of all the states including the deeper states, while the higher frequency signal is only contributed by the shallow trap states. Taking the differential of this capacitance spectrum will eventually give us the estimation of the defect states as per following equation which was derived by Walter and Harberholtz[169].

www.manaraa.com

$$g_t(E_\omega) = -\frac{V_{fb}}{qwk_BT}\frac{dC(\omega)}{d\ln\omega}$$

Demarcation energy level **(Eω) =KT Ln (ωo/ω)**

w_o – attempt to escape frequency

. . . . . (4)

Here E_ω , The demarcation energy level is defined as the hypothetical energy level as defined above , All the traps above which will not respond while , all the traps below this level will contribute to the parallel capacitance. ω_o is the attempt to escape frequency while ω is the frequency of the input signal. By changing the frequency of the input ac signal, we basically change the position of demarcation energy level. V_{fb} is the flat band voltage and w is the depletion layer width. th the value of V_{fb} and ω will shift the entire DOS curve in y-axis while selection of correct ω_o will shift the DOS curve in x-axis. In our experiment we have used 5E10 /sec as a value for ω_0.[167]

4.2.7 Space charge limited current for hole mobility measurement

There are numerous ways by which we can measure charge carrier mobility in any semiconductor. The simplest of all is space charge limited current technique.[91]Following schematic (fig 4.11) shows the working principle behind the space charge limited current proposed by M Lampart[172,173]. The objective of this technique is to sandwich a semiconductor layer between two metal electrodes. In addition we need to make sure that the current transport is dominated by a single charge carrier. This can be achieved by depositing a particular layer with proper matching work function which will produce a barrier one particular carrier. With the proper choice of electrode we can measure mobility of both electron and hole. The above schematic is particularly for hole mobility measurement, both side of the semiconductor has a huge barrier for the electron

www.manaraa.com

injection to the conduction band of semiconductor. The current transport in this architecture is driven by hole only. The device behaves identically under both biases.

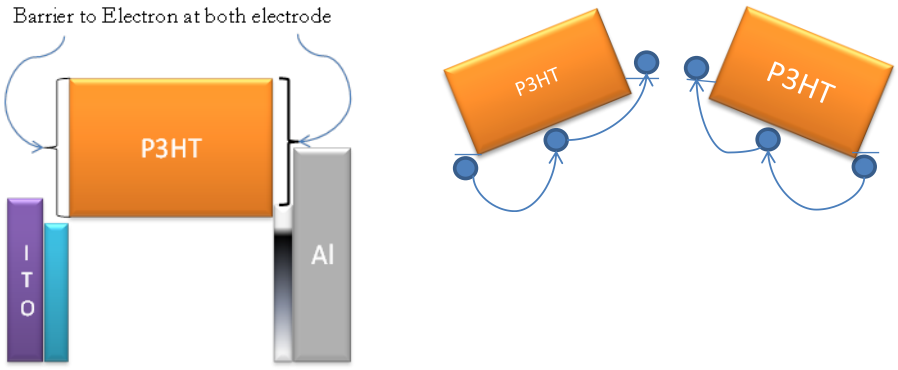

Figure 4.11: Schematic showing basic of SCLC transport in semiconductor.

In the low voltage regime it shows a linearly increasing current. When the number of injected charge carrier is smaller than the number of resident charge carrier, the current follows Ohms law. However at a voltage (V_{sclc}), injected number of charge carrier become equals to the number of resident charge carrier and from that point current starts to deviate from its original linear path. This happens because of non-uniform field and non-uniform charge accumulation in the material. Thus current will eventually vary qudratically with voltage. The mobility can be extracted from the following formulae. Here L is the thickness of the semiconductor slab and ε is the dielectric constant. Following two figure shows the typical IV curve for a hole only P3HT based device whose mobility is estimated to be around 1-4E-4 cm2/V-sec.

$$J = \frac{9}{8}\varepsilon\mu_0\frac{V^2}{L^3} \qquad \text{.....(5)}$$

www.manaraa.com

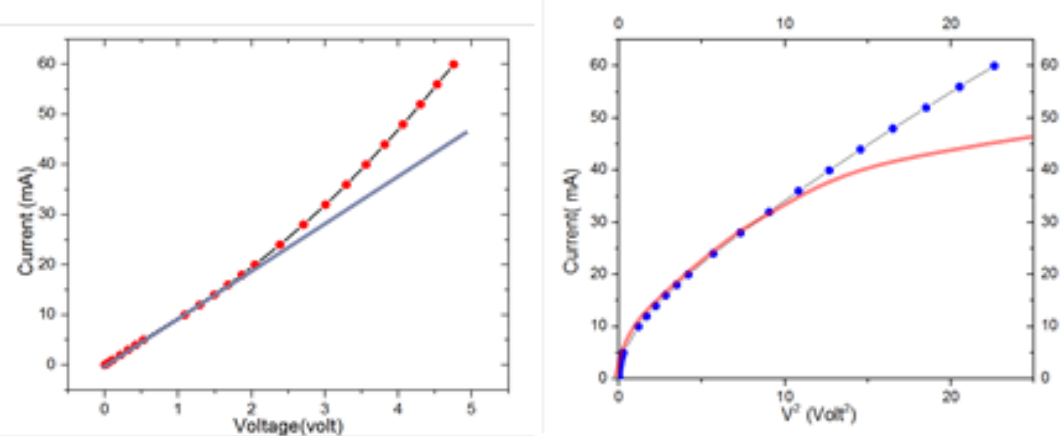

Figure 4.12: Typical SCLC measurement data for P3HT based polymer film.

4.2.8 Optical measurement

The optical measurement of organic thin film includes the absorbance measurement and reflectance measurement. We know that A+R+T=1, where A is the % of absorption, R is the % of reflection and T is the % of transmission. This measurement gives us the idea about the percentage of the total light absorbed by the thin film. The absorption study also gives us the qualitative information about the crystalline vibration as well as the band gap energy of polymer. A typical curve of optical absorbance of a P3HT polymer is shown in fig 4.13. The vibronic peaks are indicating the dominant optical absorption and their corresponding transition. These peaks depend on the crystalline property of the polymer. With amorphous phase, these signature vibronic peaks will disappear from the absorption spectrum.

The absorption is measured by Varian Carry 5000 spectrometer as shown by the following schematics (fig 4.14).

www.manaraa.com

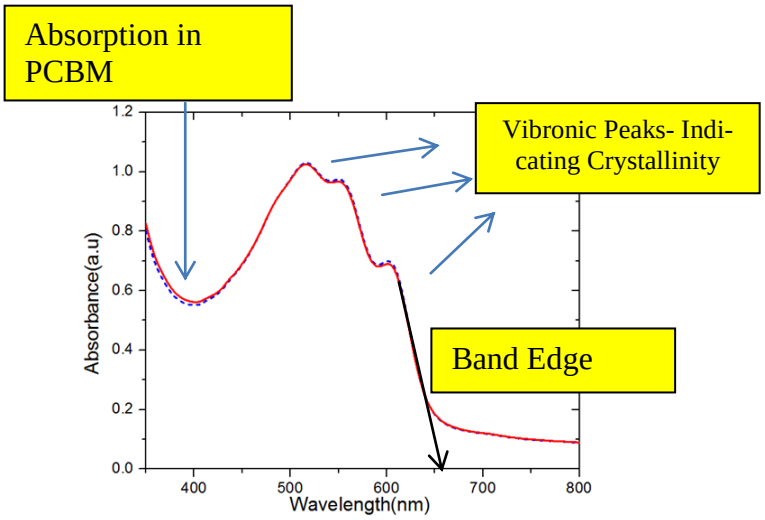

Figure 4.13: Typical optical absorbance data for P3HT:PCBM blend solar cell with different feature

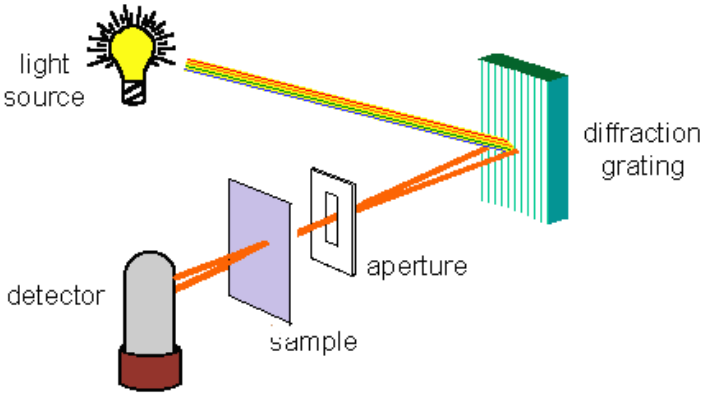

Figure 4.14: UV-VIS spectrometer principle in block diagram

The diffraction grating is used to change the wavelength of spectrometer light source. The detector measures the percentage of photon transmitted through the film . The point here to remind is that the measured spectrum is absorbance not absorption which some ti me confusingly used in the literature.

$$A = Log_{10}(1/T)$$

www.manaraa.com

Absorbance is only a quantity (without any unit) that represents transmission of a film in slightly different form.

4.2.9 Thickness measurement

The thickness of the polymer as well as bulk hetero junction film can be measured very precisely by atomic force microscopy(AFM) or precision step profilometer, The film is first scratched by a needle head to remove the active layer and to form a step. Later either a profilometer or an AFM is used to measure the step height. Both measurement are accurate and match in the step height. However for thin film with thickness less than 50 nm, AFM proves more delicate and precise compared to its counterpart. The present and following paragraph will describe the detail of AFM operation and the steps to measure thickness. A typical example of the thickness measured from AFM is shown fig 4.15.

The AFM measurement is also used to measure the surface roughness of the bulk heterojunction film. Some report suggests[12] that roughness of the polymer surface can be correlated to the crystallinity of the polymer domain. However our observation reveals that instead it might be the indication of polymer aggregation. One interesting point to note that the figure 4.15 is the height image of the polymer surface which shows only the height contrast of the surface feature by the color map. It does not say anything about the mix of two different phases namely polymer and acceptor. 3-d image of the surface do not reveal any quantitative information about the polymer: acceptor morphology.

www.manaraa.com

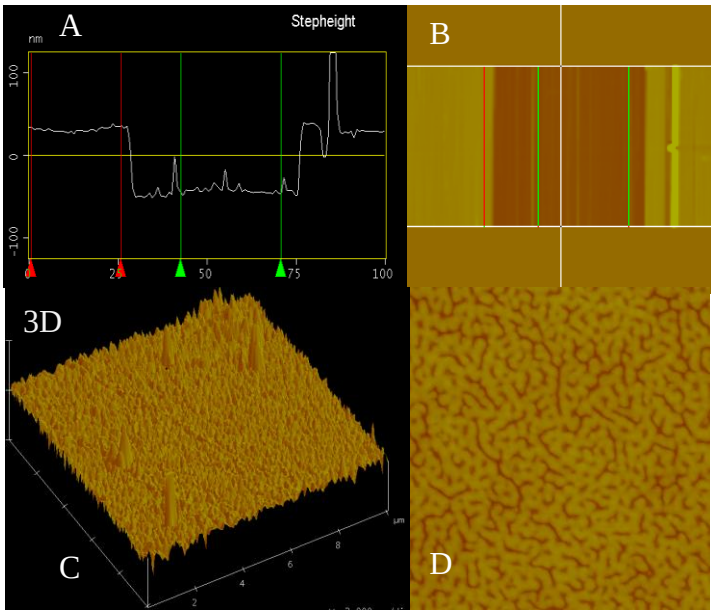

Figure 4.15: (A) Thickness measurement using AFM(step image), (B) height image (C) surface roughness measurement (3D image) (D) 2-d height image

4.2.10 Photo luminescence measurement

Photoluminescence emission spectra are determined by exciting at a fixed wavelength and varying the wavelength at which emission is observed. The schematic in the figure 4.16 shows typical excitation and fluorescence and phosphorescence emission spectra for a molecule in any chemical solution of solid semiconducting film. Between excitation and emission, electronically excited molecules normally lose some of their energy because of relaxation processes. As a consequence, the emission spectrum is at longer wavelengths, that is, at lower energy, than the excitation spectrum. Because the magnitude of the energy loss due to relaxation processes is greater for phosphorescence than for fluorescence, phosphorescence occurs at longer wavelengths than fluorescence. The spectra extend over a range of wavelengths, because in solution, molecules exist in a continuous distribution of vibrational and rotational energy levels.

www.manaraa.com

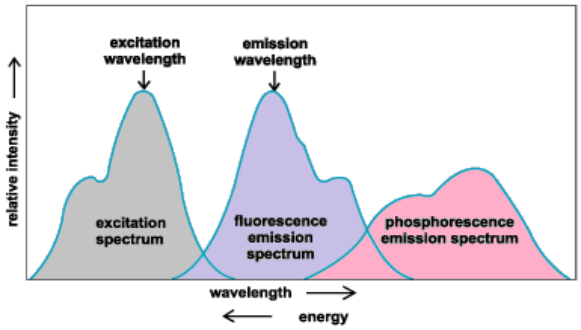

Figure 4.16: Schematic diagram of typical absorption, fluorescence emission and phosphorescence emission.

Observed luminescence intensities depend on three factors: (1) the number of electronically excited molecules or atoms produced by the excitation process; (2) the fraction of electronically excited molecules that emit light as they relax to a lower energy state; and (3) the fraction of the emitted luminescence that impinges on the detector and is measured. In the case of photoluminescence, the number of excited molecules is proportional to incident excitation intensity, the concentration of the luminescent species, and the efficiency with which the luminescence species absorbs the incident radiation.

The following figure 4.17 shows different transition and relaxation of singlet and triplet exciton in different energy states. The lowest and darkest horizontal line represents the ground-state electronic energy of the molecule which is the singlet state labeled as So. At room temperature, majority of the species are in this state. The upper lines represent the energy state of the three excited electronic states: S_1 and S_2 represent the electronic singlet state (left) and T_1 represents the first electronic triplet state (right). The upper darkest line represents the ground vibrational state of the three excited electronic state. The energy of the triplet state is lower than the energy of the corresponding singlet state.[174]

www.manaraa.com

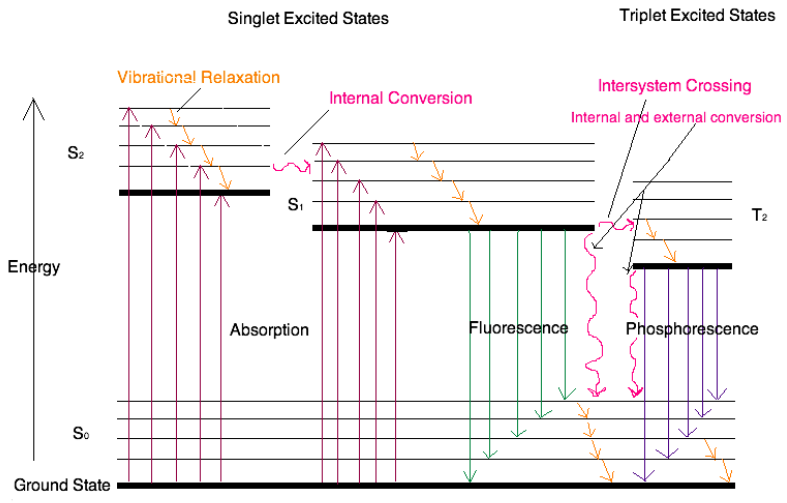

Figure 4.17: Different transition and relaxation of excited species during photo –luminescence [174]

There are numerous vibrational levels that can be associated with each electronic state as denoted by the thinner lines. Absorption transitions (red lines in Figure 4.17) can occur from the ground singlet electronic state (S_o) to various vibrational levels in the singlet excited vibrational state. Molecules also go through vibration relaxation to lose any excess vibrational energy that remains when excited to the electronic states (S_1 and S_2) as demonstrated in orange in Figure 4.17. The knowledge of forbidden transition is used to explain and compare the peaks of absorption and emission.

There can be several relaxation processes as shown in figure 4.17 including vibrational relaxation where molecule maybe promoted to several vibrational levels during the electronic excitation process. Collision of molecules with the excited species leads to rapid energy transfer. Vibrational relaxation is so rapid that the lifetime of a vibrational excited molecule (<10-12) is less than the lifetime of the electronically excited state. For this reason, fluorescence always produces a red shifted spectrum compared to absorption spectrum.[92] Apart from vibrational relaxation, there can also be some internal conversion, external conversion, inter system crossing and phos-

www.manaraa.com

phorescence which are discussed in detail in following literature. In our experiment we wanted to see how light exposure changes the luminescence spectrum of organic bulk hetero junction thin film. This can give a rough idea about the process of exciton dissociation and grain size in polymer.

4.2.11 QE vs bias- μτ estimation

This is an extension of quantum efficiency measurement where we measure photo current of a solar cell at any particular wavelength as a function of different applied external bias. This experiment shows how charge collection is depending on the external bias. Normally for P3HT:PCBM based bulk hetero junction solar cells we used 600 nm as fixed wavelength and varied the external voltage from -1 V to 0.6 volt. A typical photo current vs bias plot can be seen in figure 4.21. This plot give us accurate estimation of flat band voltage as well as mobility life time product. Mobility life time is a basic parameter of any semiconductor which helps in understanding the charge transport. [135,147,148,175]

Higher μτ indicates better charge transport while lower μτ can be related to higher recombination losses and lower photovoltaic performances. The value of μτ can be estimated by curve fitting the following equation to the photo current vs bias.

$$\frac{Q}{Q_0} = \frac{\mu\tau(V_S - V)}{dd'}\left\{1 - \exp\left[-\frac{dd'}{\mu\tau(V_S - V)}\right]\right\}, \quad F = \frac{V_S - V}{d} \qquad \text{.....(6)}^{145}$$

www.manaraa.com

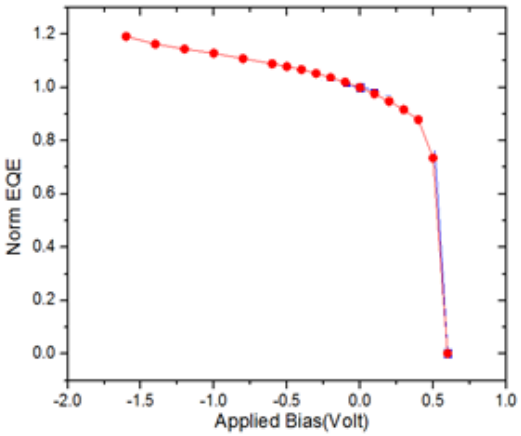

Figure 4.18: Typical EQE vs Bias plot for an organic BHJ solar cell.

Where Q is the total charge collected at the electrode which contribute to the photo current while Qo is the total number of free charge generated. Vs is the flat band voltage while d and d' is total thickness and charge collection distance respectively. V is the external applied bias. For simplicity d' is assumed to be d/2. [147]

www.manaraa.com

CHAPTER 5
ORGANIC SOLAR CELL-PHOTO DEGRADATION

5.1 Introduction

What causes the solar cell to degrade over time- especially the organic solar cell? In chapter 2 we have seen many degradation mechanisms. In this chapter we will attempt to understand the root cause of photo degradation in organic solar cells. Light is an in-separable entity in photovoltaic industry. From the commercial perspective it will be highly disadvantageous to have a photo-active material unstable under the light itself. In order to find a solution, we need to know the main causes that can lay down the roadway for solution of the problem. Some very recent work has stressed[36,51,53,55,57,59,88,89,176-178] on the photo degradation in inert atmosphere. In this chapter we will show with the help of simple electrical characterization technique, that light indeed degrades efficiency of non-encapsulated solar cell. Here in this work we have conducted a careful investigation of the influence of light exposure on fundamental material properties of P3HT/[6,6]-phenyl-C60-butyric acid methyl ester (PCBM) solar cells, which shows that there are significant changes in mid-gap defects in P3HT and at the P3HT/ PCBM interface, which in turn change both the dark I-V characteristics and the open circuit voltage.

5.2 Experimental summary and discussion

The P3HT/PCBM device samples were prepared using standard spin coating techniques on ITO coated glass as discussed in Appendix D, device fabrication section. The thickness of the P3HT/PCBM layer was 150-180 nm. The initial conversion efficiency of the cell was 3.6%. After fabrication, the device was immediately measured for its light I-V characteristics and then rapidly transferred to a vacuum system capable of pumping down to a pressure <1E-6 Torr. After

www.manaraa.com

evacuation, high purity nitrogen gas was introduced into the light testing chamber. A xenon source solar simulator with appropriate filters to simulate AM1.5 sunlight was used as the source for studying the degradation of the solar cells. During degradation, high purity nitrogen was continuously flowing in the light testing chamber. The chamber was provided with appropriate instrumentation to measure dark I-V, light I-V, and defect densities in-situ without exposing the sample to air. Absolute quantum efficiency (QE) was measured before and after degradation. The intensity of light could be changed by using a lens. For the results reported here, we used an intensity of 200 mW/cm2 (2_sun) for 96 h from a full spectrum solar simulator.

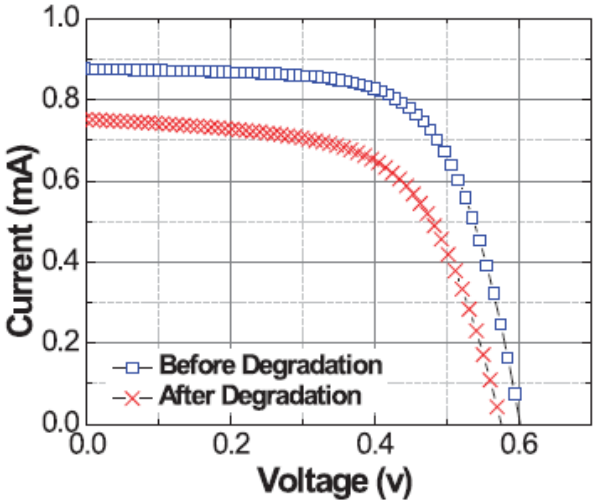

Figure 5.1 Light IV of P3HT:PCBM blend cell measured under 100 mW/cm^2 ELH lamp –before and after the photo exposure for 96 hrs under Xenon Arc lamp (200mw/cm^2) intensity. (contact are -0.106 cm^2)

In Fig. 5.1, we show the light I-V curve for a cell before and after photo-induced degradation. We also measured sub-gap quantum efficiency before and after degradation so as to determine changes in Urbach energies of tail states near HOMO levels and changes in mid-gap defects. A representative data for the sample before and after degradation is shown in Fig. 5.2.

The sharp tail in quantum efficiency corresponds to excitation from tail states near the HOMO level, and the shallow portion at very low photon energies (0.8-0.9 eV) corresponds to exci-

www.manaraa.com

tation from mid-gap states in P3HT. From Fig. 5.2, we can observe that the mid-gap defect density in P3HT has increased significantly after degradation, whereas there is virtually no change in tail state densities. We also measured the mid-gap defect density using the capacitance-frequency-technique described in Ref.[167,169-171,179] In this technique, one measures capacitance (C) vs. frequency (f), and then calculates the defect density as a function of energy from a measurement of dC/df.[57,58]In Fig. 5.3, we plot the measured defect density vs. defect energy above the HOMO level of P3HT for our sample at two different times, original, and after degradation for 96 hours. The data of Fig. 5.3 show that the defect density keeps increasing as a function of light soaking time and has increased by a factor of 2 at 0.3 eV above the valence band after 96 h of light soaking, but by a factor of 5 in the 0.5 eV–0.6 eV region after photon exposure. This is a different energy region than the mid-gap of P3HT (0.8-1.0 eV) and corresponds to an energy region which is about half the energy between the LUMO level of PCBM and the HOMO level of P3HT. This fact strongly suggests that these states are located at the interface between P3HT and PCBM.

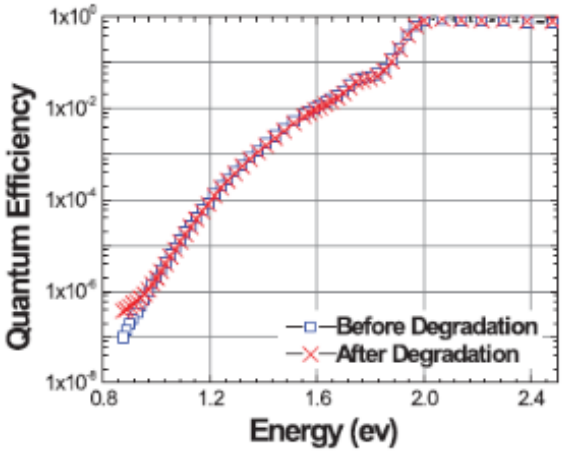

Figure 5.2 Sub-gap photo-current (normalized to maximum value) was compared for both pristine and after exposure of P3HT:PCBM based BHJ cell.

www.manaraa.com

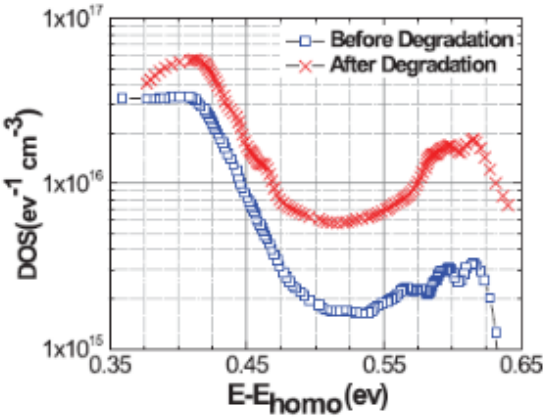

Figure 5.3 DOS measured and compared for both pristine and after exposure cells of P3HT:PCBM using capacitance spectroscopy.

A necessary consequence of the increase in interface defect density is that the dark I-V curve must change as a result of degradation, with an increase in reverse saturation current Io.[59] In Fig. 5.5, we show the dark I-V curve before and after degradation. The dark I-V curves show a very interesting development, namely, that the I-V curve after degradation not only shows a higher value for dark current, but actually has an inflection point, clearly showing two distinct regions of dark I-V, one at low forward voltages (<0.3 V) and one at higher voltages, in addition to the usual shunt and series resistance regions. The two regions in the I-V curve after degradation strongly suggest that the current at low voltages corresponding to the generation-recombination factor, which is closely related to increases in defect density in the midgap region including changes at the interface between the two materials, has increased significantly after degradation Since recombination due to mid-level interfacial states leads to an I-V curve with a diode factor close to 2, whereas the band-to-band recombination leads to a diode factor of 1, an increase in the midgap recombination must increase the average diode factor of the I-V curve. Data analysis shows that the average diode factor of the curve increased from 1.26 before degradation to 1.35 after degradation. The I_{o1} (reverse saturation) current corresponding to this early voltage part of the curve after degradation increased to 6.0×10^{-11} A, from 1.2×10^{-11}A prior to

www.manaraa.com

degradation, a factor of 5 increase. This increase in I_{o1} is directly due to the increase in mid-gap defect density at the interface.[59 135] Note that the increase in midgap densities, measured using C-f method, was also a factor of 5, showing very good agreement between the two independent measurements of the increase in defect density upon light soaking. The change in open circuit voltage upon degradation can be calculated from the dark current values and the effective diode factor before and after degradation. The effective diode factor changed to 1.35 after degradation from 1.26 before, with the average Io increasing from 9.7×10^{-12} Amp to 4.5×10^{-11} Amp. Using the standard voltage equation, $Voc = \left(\frac{nKT}{q}\right) \times Ln(\frac{Isc}{Io})$, gives an initial calculated voltage of 600mV and voltage after degradation 583 mV, in good agreement with the measured values in Fig. 5.1. It is useful to note that these results are not a single sample result. Many similar devices were measured in a similar fashion, and all devices showed very similar behavior, with an increase in dark current and in midgap and interfacial defects, with a strong correlation between the two measurements. The change in short-circuit current upon degradation cannot be explained by changes in optical absorption.[52,61]

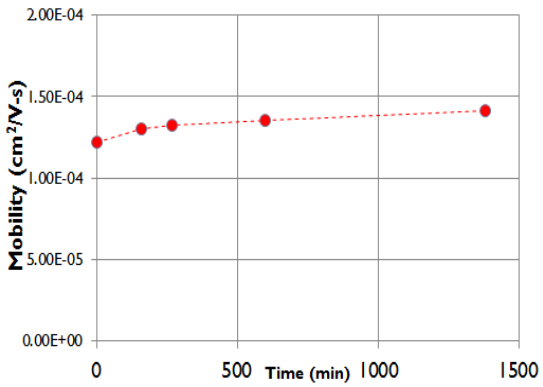

Figure 5.4 Hole mobility measured using space charge limited current as a function of exposure time (In-Situ)

We also measured hole mobility using space charge limited current, which shows little change in hole mobility during photo exposure. One reason for the loss in photo current could be

www.manaraa.com

the unsuccessful dissociation of exciton at the interface which could lead to less free charge carrier at either side of the interface. Another reason for the decrease in current may be increased recombination and indeed, the change in slope in I-V curve near short circuit conditions strongly suggests a voltage-dependent current collection, a classical signature of increased recombination. The change in fill factor can be easily be explained by noting the change in resistance due to either drop in electron mobility in acceptor side(as we have already seen the hole mobility to remain unchanged) resulting in inefficient charge carrier collection, and increased recombination. Our results convincingly demonstrate that fundamental properties of the active photovoltaic material are changing upon exposure to photons, and that it is inaccurate to ascribe changes in device properties to changes in just the contact layers, or to the influence of oxygen and moisture alone. The significant changes in the midgap densities occur both in the P3HT material (0.8–1.0 eV above the HOMO level of P3HT) and at the interface between P3HT and PCBM (0.5–0.6 eV above the HOMO level).

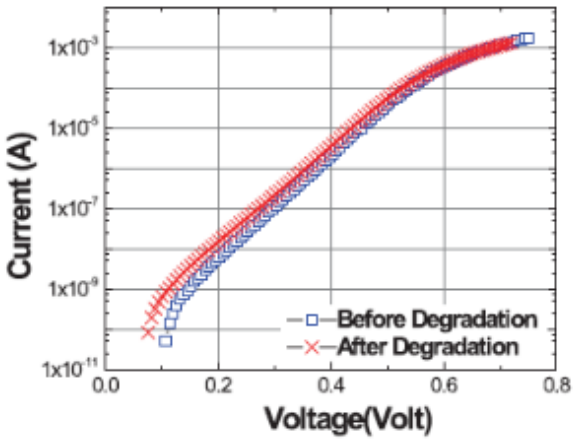

Figure 5.5 Dark current –voltage characteristics was measured and compared for both pristine and after exposure

We also measured mobility lifetime product from the photocurrent vs external bias experiment. In that experiment we measured photo current using a mono-chromator and lock-in ampli-

www.manaraa.com

fier. Further we fitted the photo current with the hetch expression[135] as given below. This expression helps us to estimate the mobility-lifetime product which can be a good indicator of the transport property of the active layer of solar cell.

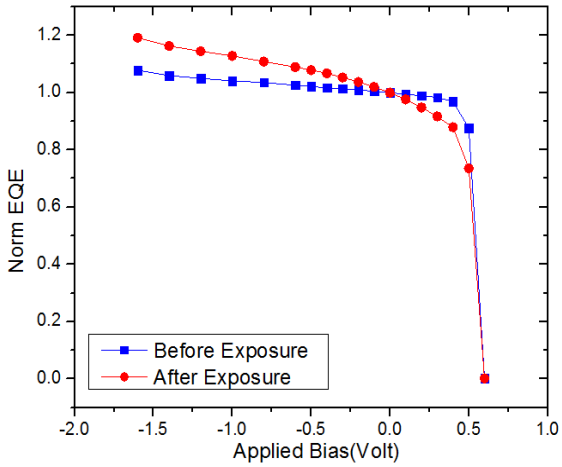

Figure 5.6 Photo-current (normalized to maximum value) was measured as a function of external applied voltage to check the bias dependence of photo current.

In the experiment, first point to notice is that there is no change in flat band voltage for both conditions (before/after). This eliminate the argument of drop in flat band voltage as a possible reason of photo-instability proposed by A Kumar et al. Secondly the photo current becomes highly bias dependent after light exposure which is an indication of possible trap assisted recombination. The following expression relates mobility lifetime product to the amount of charge collected as a photo current.[135]

$$\frac{Q}{Q_0} = \frac{\mu\tau(V_S - V)}{dd'}\left\{1 - \exp\left[-\frac{dd'}{\mu\tau(V_S - V)}\right]\right\}, \quad F = \frac{V_S - V}{d}$$

Where Q_o is the total charge generated(free charge carrier at the interface, Q is the number of charge collected, Vs is the flat band voltage, V is the external applied bias and d and $d^{/}$ is the average charge collection distance which was assumed to be the distance from interface of donor

www.manaraa.com

and acceptor to respective electrode. We fitted the experimental data obtained for the device before and after the prolonged photo exposure and found that- prolonged exposure reduces the mobility lifetime product from a pristine value of 7.5E-10 cm2/V to 1.5E-10 cm2/V. This apparent drop (5 times) is quite well matching with earlier observation of increase in Io (extracted from dark IV) by roughly 4-5 times. The self-corroborating data reveals the fact that recombination (mainly trap assisted) is the dominant source of loss mechanism that accelerates the degradation of organic solar cell under light exposure.

Thus using our simple electrical characterization technique we were able to find that there are electrically measurable increases in mid-gap defects states in P3HT/PCBM solar cells when exposed to light alone, and that the decrease in current and voltage upon light exposure, as well as changes in dark diode I-V curves, can be explained using these changes. There may also be additional changes in the materials when exposed to atmosphere which will be the topic of further investigations.

5.3 Photo degradation of standard P3HT and P3HT:PCBM BHJ film

In this experiment we performed the same intensity exposure to two film 1-P3HT (17mg/ml) spin coated at 500 rpm for 60 sec on PEDOT:PSS coated (ITO) glass substrate. We kept the internal atmospheric condition same to see if there is any change in the optical property of P3HT alone and when mixed with PC61BM in(1:1) ratio. The following figure shows that even after 96 hours of degradation under same condition as of device as mentioned before. We observe very little or no change in the absorbance spectra of the film as shown. This further substantiate that the degradation kinetics observed in the device degradation is not similar to the degradation kinetics of photo oxidation.[52,61] Eliminating the presence of oxygen during light exposure, can remove the possibility of photo oxidation. Because backbone of the polymer chain remain intact

www.manaraa.com

after 96 hours of 2x intensity exposure, the conjugation length remains unchanged as observed from the absorbance spectra, a result in good agreement with Reese et al.[52]

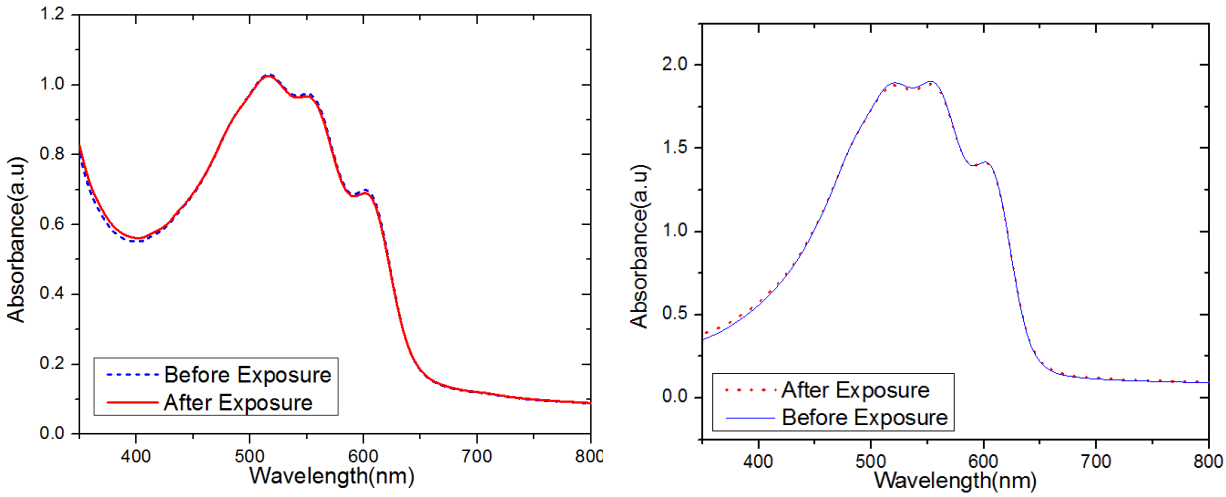

Figure 5.7(a) Absorbance of P3HT:PCBM film measured before and after light soaking, Figure 5.7(b) Absorbance of P3HT film measured before and after light soaking

5.4 In-*situ* measurement results (light iv)

In our experiment we used several in-situ measurements to tap the dynamics of photo-degradation in-situ while the degradation is underway. The light IV and Dark IV were measured numerous times, before degradation, during degradation and after degradation using Keithley 236 meter. The drops recorded in the solar cell performances as measured in-situ were found to be in good agreement with the drop measured under 1x sun outside the chamber.

www.manaraa.com

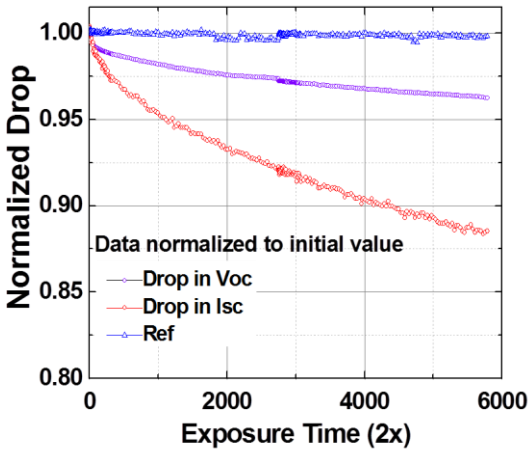

Figure 5.8 Short circuit current and open circuit voltage measured under (200 mw/cm ^{2}) in-situ during exposure.

As we can see, both Isc and Voc are dropping non-linearly with time. The efficiency drop of solar cell follows the drop of Isc as it is the most significant drop among Voc/Isc and FF. We have also measured capacitance as a function of frequency in-situ to see the change in DOS with time of exposure as well as for different dose of exposure. It was observed that the states lying closer to the mid-gap increases non-linearly with the time of exposure co-relating directly to the drop in Voc over time as recorded and shown in the previous figure. During measurement, the exposure was temporarily stopped by covering the front quartz window of environmental chamber by metallic foil to produce dark environment inside the chamber. It can be seen from the figure that the increase in the defects around mid-gap are faster during the first few hours (which is proposed as burn-in time by Peters et al)[51] of light exposure. Later it tends to saturate with time. This observation on one hand substantiates the saturation in the drop of open circuit voltage, but on the other hand raises a serious question. If the dynamics of defects creation around mid-gap is well saturating, then why short circuit current is continuing to go down (as can be seen in fig 5.8).

www.manaraa.com

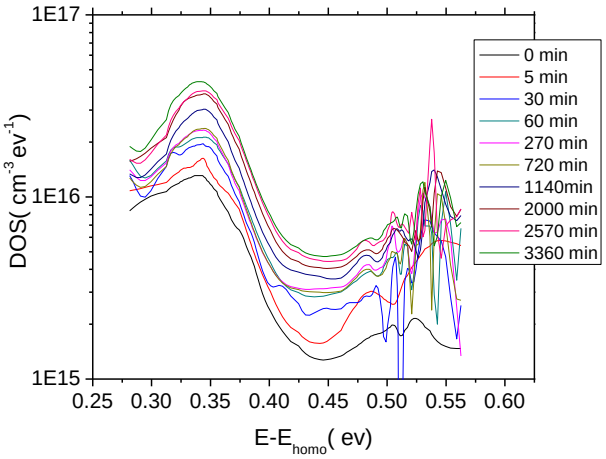

Figure 5.9 DOS measured in-situ during prolonged exposure (Front window of the exposure chamber covered to obtain dark condition. Measurement performed after 30 min of stabilization of capacitance value in dark.

We will try to address this question partly in this chapter with the help of photo luminescence experiment.

5.5 Photo luminescence measurement on exposed blend film

Photoluminescence is the process to track the radiative recombination s going on inside the active material of the solar cell. Both photo current and voltage depends on the successful dissociation of the optically excited bound electron-hole pair. The EHP that fails to reach interface undergoes both type of radiative as well as non-radiative recombination. Any increase in radiative recombination is a possible indication of the fact that some of the photo-generated exciton are not able to reach the interface leading to successful charge dissociation. That means significant portions of the absorbed photon are actually lost in that failed process of charge separation. We already know that out of total exciton that undergoes recombination before getting separated, only one third recombine radiatively (which is called singlet exciton). Rest of them recombine non-radiatively (called triplet exciton).

www.manaraa.com

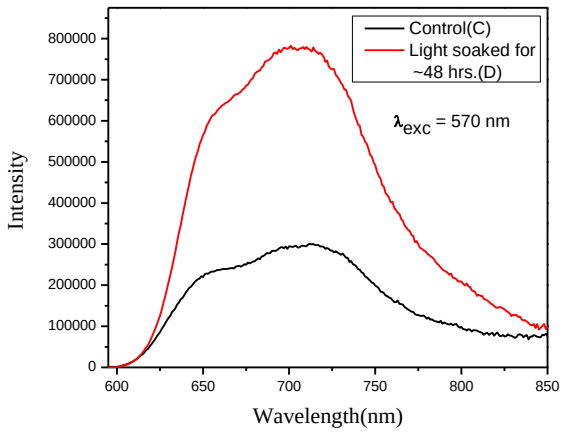

Figure 5.10 PL measurement done before and after light exposure of P3HT:PCBM blend film

Such increase in the quantum yield of photo coming out of the active layer (after photo degradation) is indicating to a process of growth in polymer domain. Exact nature of this dynamics is not yet understood properly.

5.6 Induced defect states vs intensity of exposure

In addition to the light IV measurement, we also measured DOS in-situ to see, how the defect state evolves with exposure time as well as intensity. The following figures show how the states from 0.4 ev to 0.55 ev changes with exposure time for different intensity. In addition to the raw data of DOS we have also plotted integrated density of defect states in various ranges of energy. The plot (see figure 5.11) of integrated DOS shows the non-linearity in the increase of DOS with exposure time.

www.manaraa.com

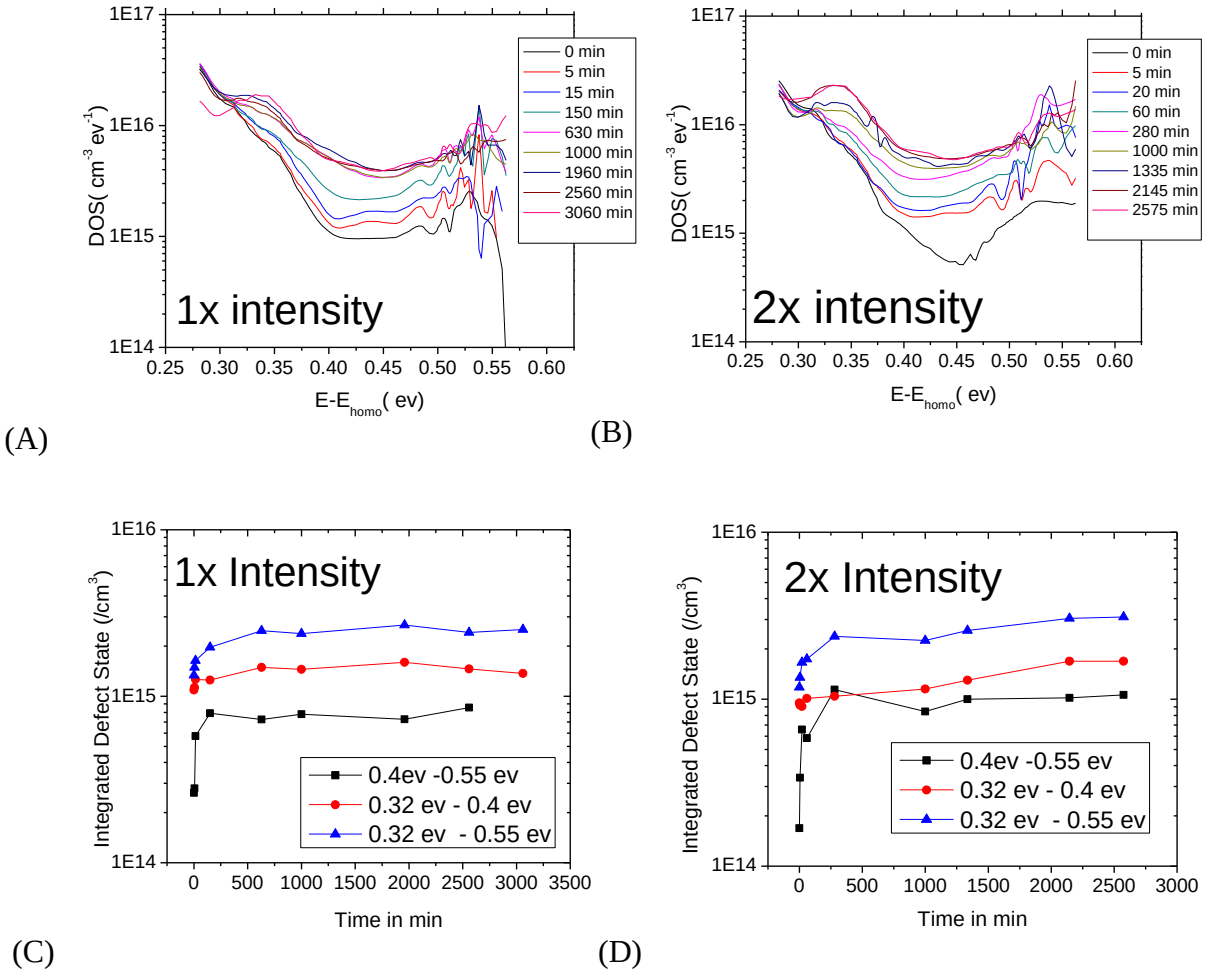

Figure 5.11 (A) In-DOS plotted at 100 mW/cm^2 intensity exposure , (B) In-DOS plotted at 200 mW/cm^2 intensity exposure,(C) Integrated DOS plotted for various energy range as a function of time(1X) (D) Integrated DOS(2X)

Such non linearity is an intrinsic characteristic's which remain unchanged for all different exposure intensity. This again raises the question, if increase in defect states saturates with time, then why current continues to drop further. We have also compared the evolution of defect states over time for various intensity and found that –defect creation is a faster for higher intensity. The following figure compares increase in total defect states with exposure time for various intensities.

www.manaraa.com

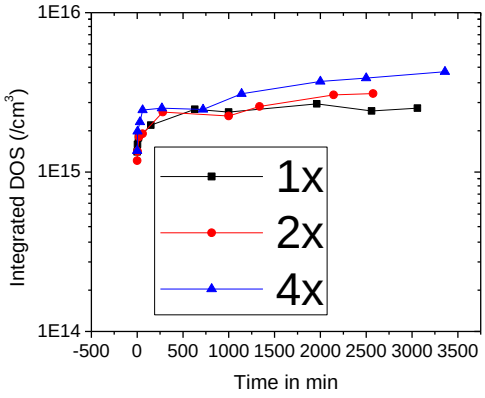

Figure 5.12 (a) Total integrated -DOS plotted for different intensity exposure

The above experiments are performed on regular cell architecture with P3HT: PCBM blend active layer. The same experiments were carried out on inverted architecture to check if the functional relationship between induced defect states and intensity of light exposure are same?

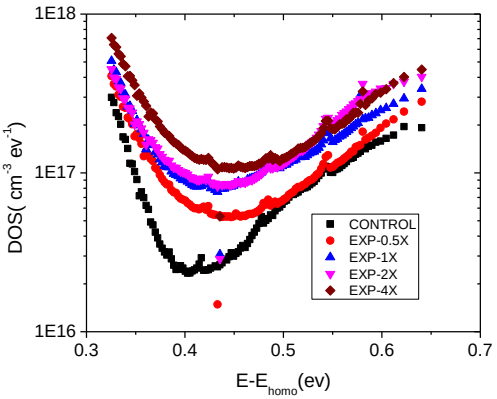

Figure 5.13 (a) DOS plotted for different intensity exposure for 48 hours to see the increase in mid-gap density

It can be easily observed that with different intensity of exposure, tail states (between <0.4 ev) do not change significantly. However we notice a change in mid-gap Gaussian distribution with different intensity. To understand it better, we integrated the Gaussian mid-gap between 0.45ev-0.65ev and plotted as a function of intensity of exposure.

www.manaraa.com

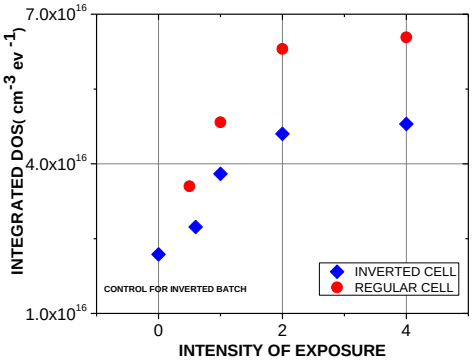

Figure 5.14 (a) Integrated DOS (0.45ev-0.65ev) plotted as a function of intensity of exposure for same time

It is observed that the density of induced defect states upon prolonged light illumination follows a non-linear behavior with intensity of exposure. It first increases with intensity of exposure followed by saturation at higher intensity. Interestingly the non-linearity was observed for both type of architecture (inverted and regular). This again validates the idea that photo-degradation of organic solar cells are an intrinsic property of active layer blend independent of contact layers such as HTL and ETL's. Same functional relationship with light intensity was observed for amorphous silicon based solar cells long back. There can be two possible reasons for that. Firstly the species that creates defects might be limited in number (Si-H bond for amorphous silicon/ C-H bond in the side chain of polymer back bone). Secondly this saturation can be due to the self-annealing process occurring at higher intensity. Higher intensity can lead to increased blend temperature which can anneal out defect states created by light exposure. This explains why induced defect state density seems to saturate at higher intensity.

To substantiate the defect measurement by capacitance spectroscopy, we performed dark current measurement after exposure, for various intensity. We de-convoluted the measured forward bias dark current into two exponential region and extracted reverse saturation current and

www.manaraa.com

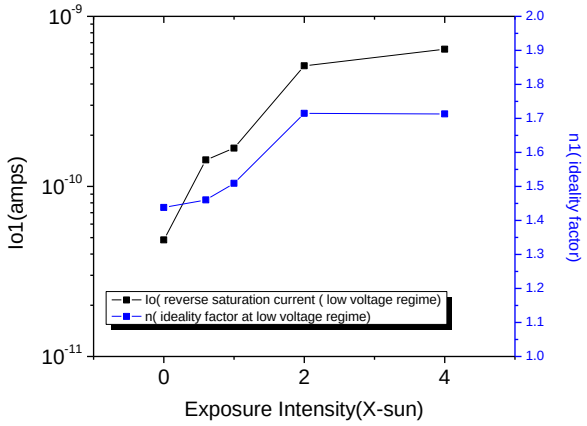

Figure 5.15 Estimated I_{o1} and n_1 for various intensity of exposure for solar cells with inverted architecture.

diode ideality factor. As we already know, Io extracted at the lower voltage region is related to trap assisted recombination via traps located closer to mid-gap of the energy band, while Io extracted at the higher voltage regime is significant because of diffusion. In organic bulk-hetero junction solar cells these trap assisted recombination and band to band recombination take place at the interface of donor and acceptor. As we can see in the fig 5.17, reverse saturation current increases first with intensity of exposure and then saturate at higher intensity. Interestingly Io (extracted from the higher voltage regime- originating from diffusion limited recombination) does not seem to change much as can be seen in the figure-5.18. I_{o2} varied between 4E-13 amps to 3E-12 amps. At higher intensity I_{o2} increased compared to the control sample probably because of some increased diffusion limited current. The exact mechanism is not yet understood properly. However in section 5.5 we have seen the increase in photo-luminescence upon prolonged light soaking which can only occur due to enhanced band to band recombination. Band to band recombination depends on the density of opposite charge carrier. We do not know yet why band to band recombination increases upon illumination? Further work needed to be done in this direction.

www.manaraa.com

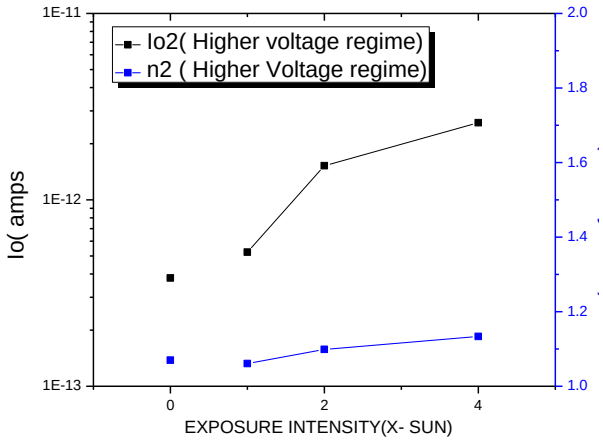

Figure 5.16 Estimated I_{o2} and n_2 for various intensity of exposure for solar cells with inverted architecture.

Diode ideality factor remained almost unchanged for all the illumination intensity showing good agreement with the change in experimental I_{o2}. Finally we observed the same functional relationship between induced defect states and light intensity as we have observed during stabler-wronski effect in amorphous silicon based solar cells.

5.8 Which wavelength is most damaging?

In this subsection we are interested to see which particular photon wavelengths are detrimental to the organic solar cells. For this reason we planned a separate experiment to explore the effect of prolonged illumination using stop band filter. We used a-Si:C filter in front of the light source to cut mostly the blue photon from the spectrum. It's well-known[180,181] that high band gap a-Si-C absorbs mostly blue photon and become transparent to all higher wavelength. Following figure shows the result of one such experiment where we exposed two identical samples (made in the same batch of fabrication) with and without a-Si-C filter in front.

www.manaraa.com

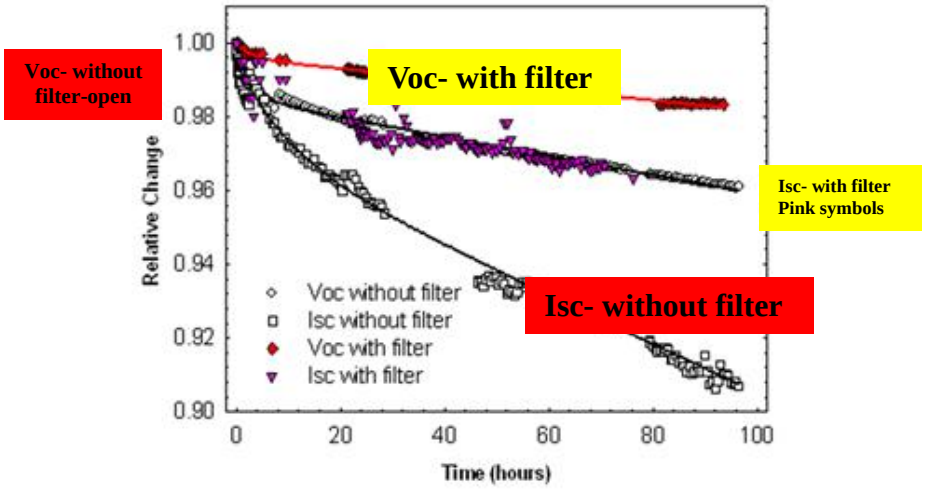

Figure 5.17 (a) Change in Isc and Voc (Measured In-Situ) plotted for same device under with filter exposure and without filter (standard) exposure to show the effect of blue photon damage to solar cell performance.

The result shows that solar cell performance decay faster in the case without filter. That decay slows down once we put a-Si-C film in front of chamber window. This shows immense promise to reduce the effect of photo degradation. However in the process of improving the stability by a-Si-C filter we are losing some efficiency because of losing blue photon which contributes to the photo current. New strategies must be developed to address this problem so that we can make more photo stable solar cells without compromising its efficiency.[42]

5.9 Conclusion

In the present work we concentrated on several questions related to the stability of polymer based solar cell under certain environmental condition. We wanted to see if the solar cell is itself stable under light illumination or not. If not then how do they degrade. Is there any patter in the degradation of cell performance? If the cell is found unstable under light soaking, then what is the main reason for such instability? As we continued our investigation, several other questions and different parameters deemed further attention. In this work we found that the polymer is un-

www.manaraa.com

stable under light exposure and the evolution of new defect states around the mid-level energy at the interface are the cause of mono-molecular Shockley –Reed –Hall (SRH) recombination that further affect the performance of the solar cell.

However our investigation raises more questions that needed further investigation. For example, increase in defect state saturates over time when short circuit current is still reducing. If SRH recombination mechanism is the only source of loss, then drop in photo current should also saturate with time. We have yet to figure out what fabrication parameter affect the photo-degradation of organic solar cell so that we can make more photo stable solar cell without compromising the solar cell efficiency.

www.manaraa.com

CHAPTER 6
POST PRODUCTION THERMAL ANNEALING and PERFORMANCE RECOVERY

6.1 Introduction

Till now we have investigated diverse architecture of standard (P3HT:$PC_{60}BM$ based) bulk hetero junction solar cell. For now we would like to concentrate on recovering the solar cell performances by post photo-degradation treatment. Recently in 2012 Street et al reported[53] the reduction in photo- induced states by the thermal annealing treatment after the prolonged photo-exposure. In the hope of complete curing of solar cell performances, we did some initial experiment on non-degraded sample and later tried different temperature as well as different time for same temperature. What we found is somehow contrasting to the result reported earlier by street et al[53]. This chapter will discuss various aspect of thermal treatment on completed solar cells.

6.2 Temperature treatment on a non-degraded cell

Before using the temperature treatment on the degraded cell, we thought of using that treatment on a non-degraded cell to see what affect it has on a plain solar cell. How its performance changes with post production annealing (PPA) treatment. This would help us at first to distinguish between any inherent change to the standard cell compared to the changes occurred in a photo-degraded cell.

www.manaraa.com

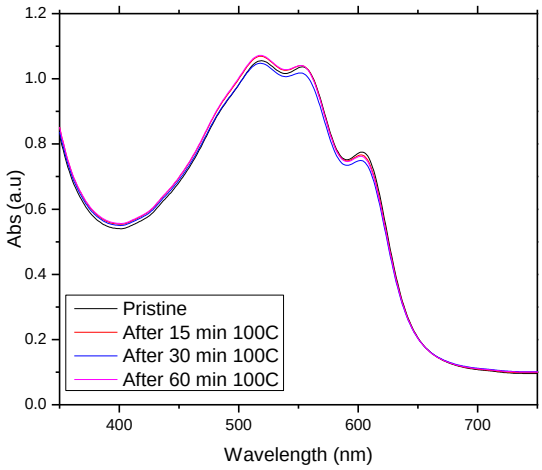

Figure 6.1 Absorbance comparison of same BHJ (P3HT: PCBM) based film after several stages of post-production annealing (PPA)

Firstly we checked if there is any change in absorption property due to PPA for longer time. It can be seen in the fig 6.1 that for the first step, absorbance dropped slightly. However, with longer time annealing, absorption is actually increasing. This shows the bulk active layer do not seem to have much changes in their conjugation length or crystallinity with longer temperature treatment.

We further checked the electrical properties of solar cell fabricated with standard recipe as mentioned in the chapter 5 as well as Appendix D. As can be seen in figure 6.2, light IV and EQE shows efficiency of the solar cell drops with temperature annealing. But why is that?

The initial observation is that we are losing Voc /Isc and FF with subsequent annealing. Absolute quantum efficiency is also agreeing with the drop in short circuit current with longer PPA. Further electrical measurements were carried out on the samples with subsequent thermal annealed sample. It was found that the dark current increases over the pristine sample after temper-

www.manaraa.com

ature treatment. At the same time Io also increases as can be seen from the figure 6.3. This increase in Io might explain the drop in both open circuit voltage as well as short circuit current.

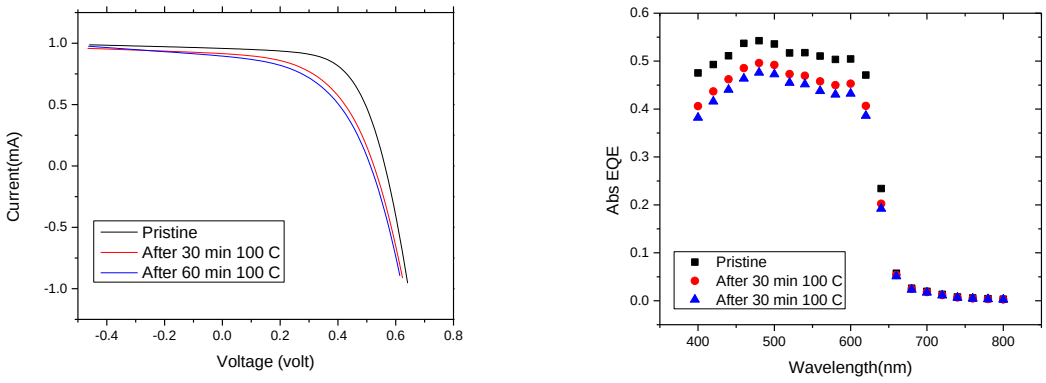

Figure 6.2 Change in light IV and EQE of a standard P3HT: PCBM BHJ device after several stages of post-production annealing (PPA)

Defect density was calculated from the capacitance spectra measured at various stages of annealing treatment. It was observed with every thermal annealing treatment; defect distribution is not only increasing but also drifting to the right (towards mid-gap). This was observed repeatedly in our further studies later. In addition a shoulder is also appearing in the first Gaussian band. For the time being we observed post production thermal annealing is actually detrimental to the regular organic solar cell in terms of new distribution of defect states which might have enhanced the effective recombination in the cells leading to a degraded cell performances. This initial observation is certainly counter intuitive in one sense because in the earlier chapter we have seen that thermal annealing (pre –production baking) actually helps to not only get rid of the trapped solvents, but also helps in getting proper enhanced crystallization and optimized morphology that might actually results in better charge separation and transport. There were two conflicting report in the previous literature, one claiming[103] to enhance the performance while other had reported same effect of performance reduction.[102] The Io was found to get changed

www.manaraa.com

from 1.52E-10 amps to 1E-9 , a change of roughly 6 times. Similar changes were observed in DOS from the energy between 0.4 to 0.6 ev. This indicates a possible increase in defect states as a result of thermal annealing.

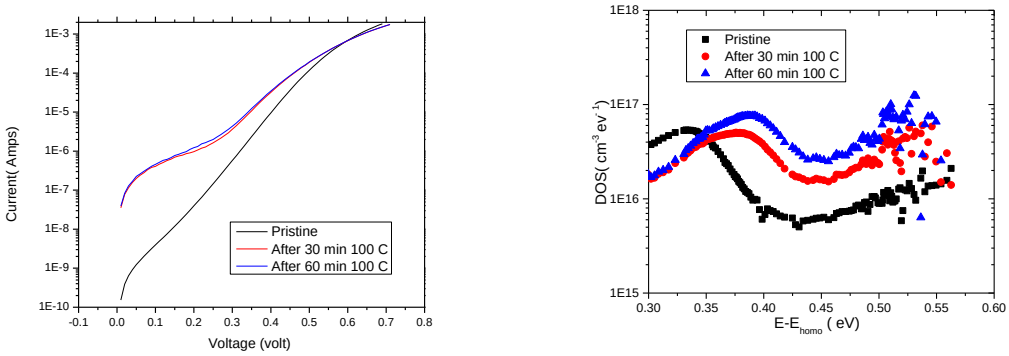

Figure 6.3 Comparison in dark IV and DOS measured of BHJ solar cell (P3HT: PCBM) after several stages of post-production annealing (PPA)

6.3 Temperature treatment on a photo-degraded cell

In this section we will present the result of different annealing treatment performed on the photo-degraded samples. We did not perform all of the measurement at every stages of the experiment in order to reduce the air exposure time. This batch of experiment were performed during summer time with high humidity point. Also all the device used in this work are non-encapsulated which increases the chance of air exposure and might result in a moisture induced degradation. However there is a technique by which we can separate both type of degradation. Ambient air exposure generally attacks the metal –organic interface resulting in a barrier formation and subsequent drop in short circuit current. However open circuit voltage remains same which serves as an symbol to differentiate between two type of degradation. In this single an-

www.manaraa.com

nealing step experiment we first exposed our sample to 2x intensity illumination produced by ABET solar simulator. After that we took out the sample from environmental chamber and took it inside the glove box for thermal annealing in nitrogen atmosphere. Thermal annealing was performed on a hot-plate at 100^{o}C for 15 minutes.

For this single step annealing experiment we measured light IV /EQE and dark IV to see what changes it has for the degraded cell upon annealing. The light IV shows enhancement in the short-circuit current from the photo degraded state. However open circuit voltage actually slightly dropped. To understand it better, we performed absolute quantum efficiency and found that photo-current is actually going up after post production annealing at 100C.

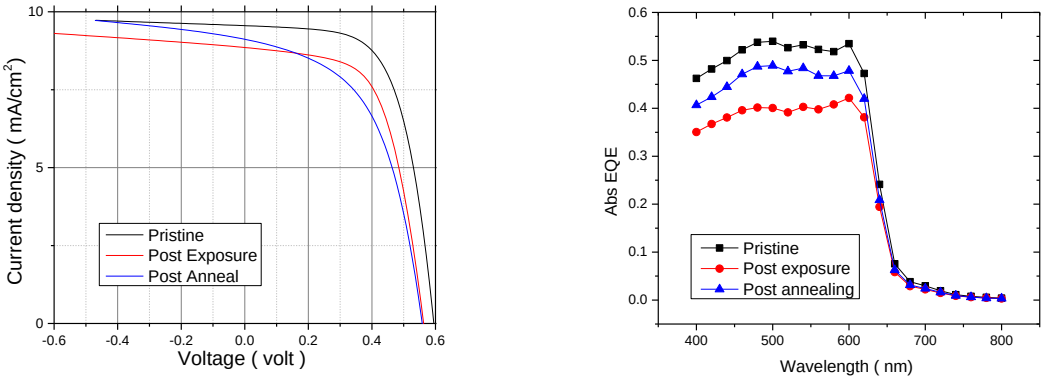

Figure 6.4 Change in light IV and EQE of a standard P3HT: PCBM BHJ device after post-production annealing (PPA) on an exposed dot(2x- 48 hrs)

Dark IV and DOS were measured after photo exposure and post degradation annealing as can be seen in figure 6.5. It shows some interesting trend as well. Firstly Io estimated from dark current increased as usual after light exposure. However Io decreased after post degradation annealing step as can be seen from the following figure. In the similar way DOS also decreased at the lower energy however remained same at the higher energy. In the earlier section we have seen DOS has not only increased in the mid-gap region but also shifted toward mid-gap and also

www.manaraa.com

showed some evolution of shoulder[possibly a second Gaussian (with shifted center) and with lower amplitude]. Here we can see that the first observed Gaussian band is actually shifting toward right with a broader shoulder to it. However mid-gap density of states remains same of slightly lower than the photo-exposed state.

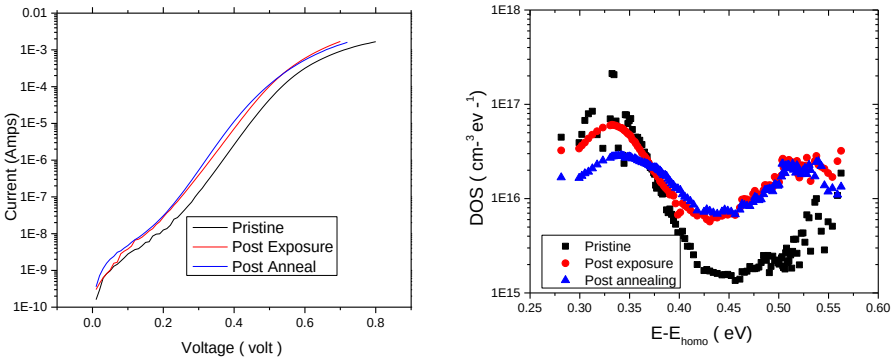

Figure 6.5 Change in dark IV and DOS of a standard P3HT: PCBM BHJ device after post-production annealing (PPA) on an exposed dot(2x- 48 hrs)

Both Io and n (ideality factor) were observed to first increase due to photo exposure and then reduced because of thermal annealing treatment. This shows a promise for us to recover our solar cell performance back to the pristine performance by the thermal treatment.

6.4 Multi-step temperature treatment on a photo-degraded cell

In the previous section we have investigated the effect of single step post production annealing on a photo degraded cell. This experiment was indication of the fact that partial recovery of photo degradation is indeed possible by post production temperature treatment. However we wanted to see what happens when we do extended annealing steps on photo degraded as well as non-degraded cells. In this experiment we exposed a standard bulk-hetero-junction solar cell and

www.manaraa.com

tracked changes in defect density as well as EQE at various stages of exposure and post degradation thermal treatment. See figure 6.6 for reference.

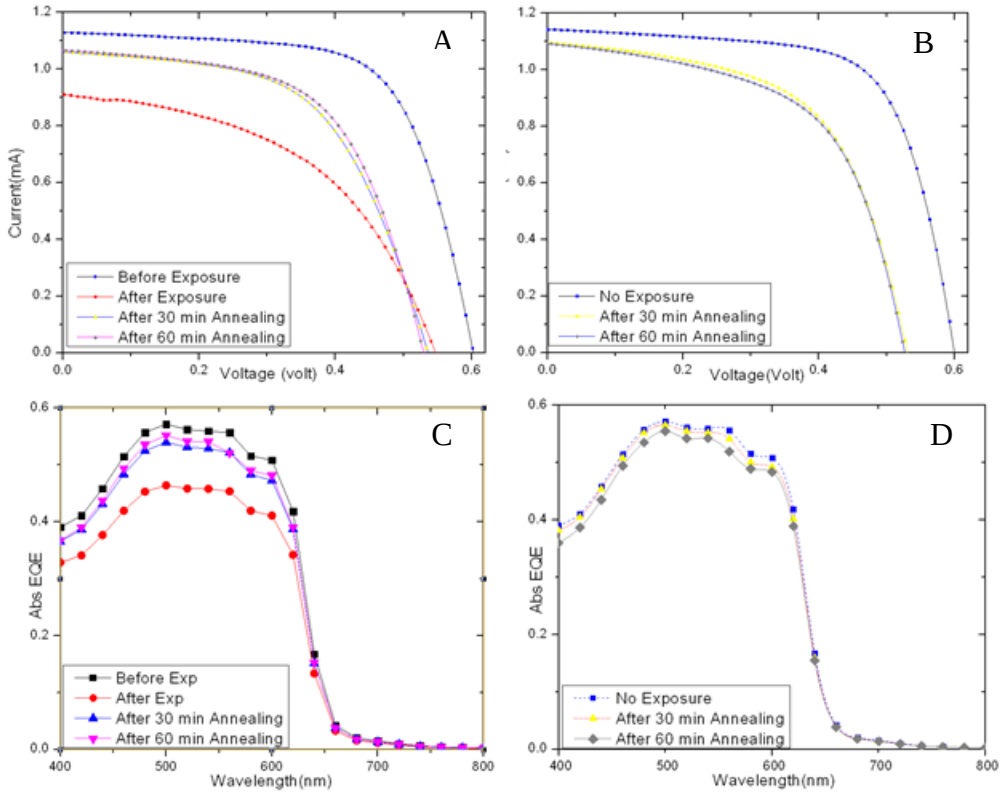

Figure 6.6 (A) Light IV of the exposed sample after different treatment.(B) Light IV of the unexposed sample after different treatmen.(C) EQE of the exposed sample after different treatment.(D) EQE of the unexposed sample after different treatment.

The figure 6.6 substantiates our initial findings that photo-current can be partially recovered. Figure a, c represents the change in the photo degraded cell while figure b,d track the changes occurred in non-degraded cell. There was an interesting observation that was made during that present experiment and which was consistent with the previous experiments observations discussed in previous sections. After first thermal annealing step on complete cell, open circuit voltage decreased by around 40-50 mv roughly and the drop in Voc is consistent for all experiment. However that is not the case for the photo degraded cell where we didn't see any changes in Voc.

www.manaraa.com

Again as observed before, short circuit current increased by approximately 10 % from its degraded state which is in stark contrast to the drop recorded after thermal treatment on a non-degraded cell.

The change in quantum efficiency is consistent with the change in the light IV measured. FF is slightly improved after the first thermal annealing while Voc continues to drop further with further annealing steps. It was also observed that first thermal annealing step reduces defect states closer mid-gap which were actively participating in the trap- assisted recombination as can be seen in the following figure.

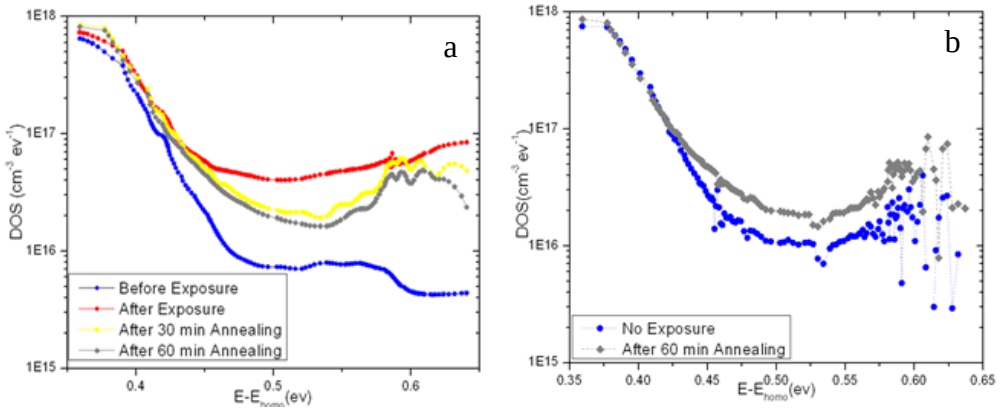

Figure 6.7: (a) DOS of the exposed sample after different treatment. (b) DOS of the unexposed sample after different treatment.

The drop in defect states can be used as an explanation why short circuit current increases after first thermal annealing. However it is well understood that with reduced recombination, Voc is supposed to increase again. But on the contrary, it remains same or decreased slightly. This pointed out to the fact that there might be two different dynamics going on simultaneously. As we have already seen in section 6.2 that post production thermal annealing is inherently damaging to the solar cell performance. So during PPA one dynamics (better to say – a process) cures some of the defect states closer to mid-gap leading to the increase in short circuit current

www.manaraa.com

while the other one actually increases the defect states as can be seen in the DOS figure which shows that for non-degraded cell DOS near mid-gap is actually increasing after 60 min of PPA treatment, So the result we are seeing from our multi-step annealing experiment is basically an cumulative effect of two counter process of curing and damaging. The experiment also shows that first thermal annealing step is the step that recovers most of the photo-current. Further annealing do not help much in recovery. To understand the change in Voc/Isc and FF with different stages of experiment the data are summarized in the figure 6.8(a-c).

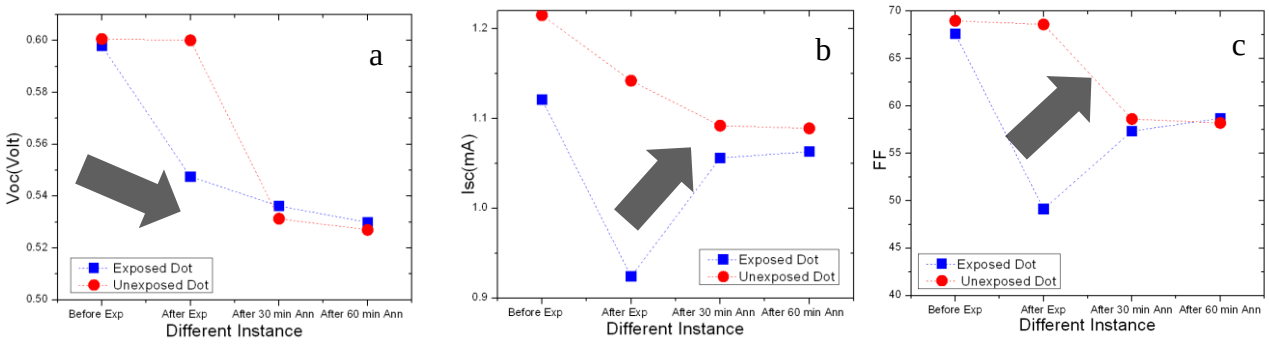

Figure 6.8: (a) Summary of change in Voc after different treatment .(b) Summary of change in Isc after different treatment .(c) Summary of change in FF after different treatment .

6.5 Post production annealing – change in morphology

We initially suspected the morphological change in photo-active layer upon post production annealing. To understand the morphological change in active layer, we made a film of standard bulk hetero junction following the complete recipe except depositing the cathode layer(metal and inter layer). We did the same heat treatment as PPA on one half of substrate with photo-active blend and left the other half un-treated. We measured AFM to detect the change in surface morphology as well as photo-luminescence quantum yield for both heat treated as well as untreated sample. See figure 6.9 for reference.

www.manaraa.com

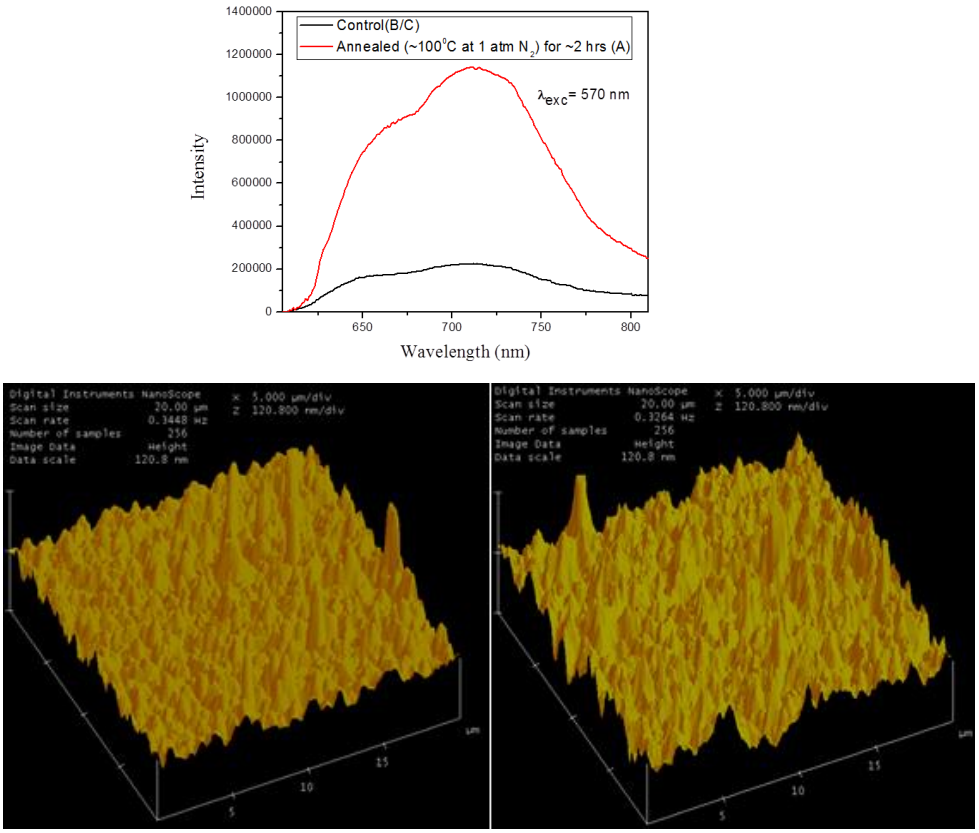

Figure 6.9 : (a) PL quantum yield of the normal control film (P3HT:PCBM) and same after annealing at 100 C for 120 min at nitrogen atmosphere. (b)AFM 3d surface image of control sample, (c) AFM 3d surface image of sample annealed at 100C for 2Hrs.

Some important observations can be made from the above two experiments. Firstly the quantum yield enhancement can indicate a possible growth of polymer domain which lead to in-efficient quenching of some of the photo-generated excitons. The PL lifetime is also increasing from 0,12ns to 0.31 ns for exciton which is also a direct quantitative indication of broadening of P3HT crystallites leading to less free separated charge carrier. Initially this argument seemed befitting to explain the initial drop in both open circuit voltage and short circuit current with thermal treatment. If less number of exciton is separating at the interface, then the number of free separated charge carrier is also less. This will reduce the separation in quasi Fermi level. That will further reduce the open circuit voltage as well as Isc subsequently. Secondly AFM shows

www.manaraa.com

increase in surface roughness upon thermal annealing of the film over its untreated counterpart. This again corroborates the results of PL measurement earlier reported.

6.6 Post production annealing at different temperature

Previously we have seen how we can recover short circuit current partly by post exposure annealing. However the temperature of the thermal annealing is not yet optimized. Also we have seen in the previous chapter that only first annealing step recover most of the photo current. Subsequent steps tend to saturate and do not help much in increasing short circuit current. Here in this experiment we used different annealing temperature ranging from 50 C to 125 C. Also for each temperature we did four subsequent annealing steps to get a general idea about how the performance of the exposed dot changes as a function of temperature and annealing time. See figure 6.10 for reference.

The numbers in the x-axis of the above figure is the enumerated steps as mentioned in the above table. The observation can be made is about the changes in device performance is a strong function of temperature. As expected at step 2(after photo exposure) all devices recorded drop in Voc/Isc/FF. One interesting phenomena occurs at step 4 in Figure 2. Except 50C all for all temperature treatment, Isc increased by certain percentage. However interestingly Voc shows reducing trend. Further thermal annealing do not help in recovering the solar cell performance. In-fact on the contrary it is degrading the solar cell performance.

www.manaraa.com

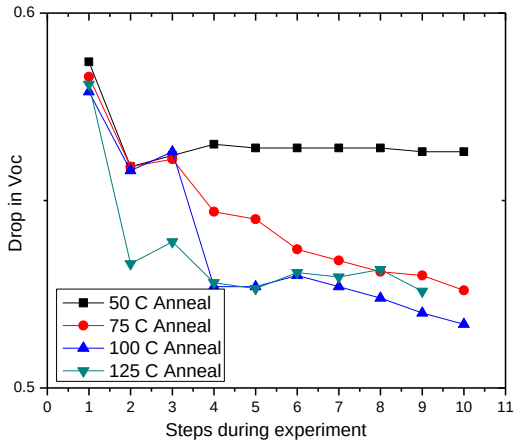

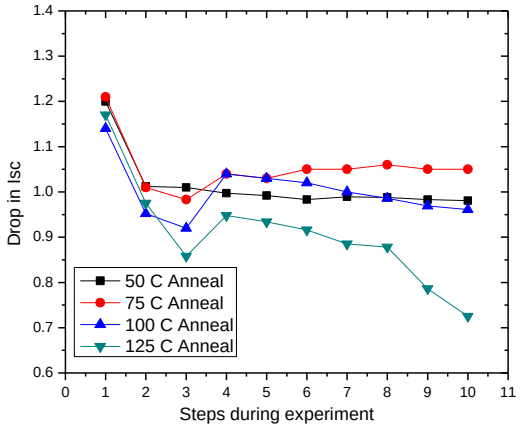

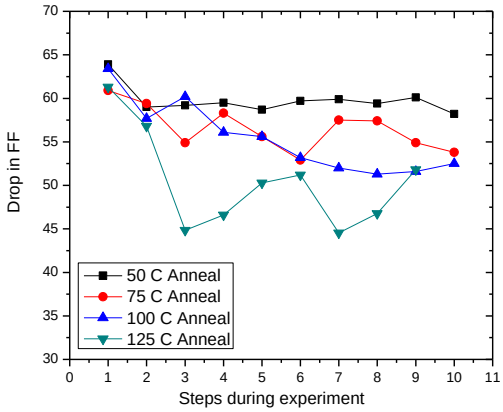

1	BEFORE EXP
2	After Exp
3	Before 5 Min Anneal
4	After 5 Min Anneal
5	Before 15 Min Anneal
6	After 15 Min Anneal
7	Before 30 Min Anneal
8	After 30 Min Anneal
9	Before 60 Min Anneal
10	After 60 Min Anneal

Figure 6.10 (A) Change in Voc over different steps of annealing(PPA) for different annealing temperature (B) Change in Isc over different steps of annealing (PPA) for different annealing temperature (C) Change in FF over different steps of annealing (PPA) for different annealing temperature,(D) Legend for different annealing steps

One lesson that we learnt from this experiment that regular organic solar cells, when treated thermally, even at a lower temperature like 75C can induce changes in device performance. It can not only be morphological change in blend as we have shown already. Because for P3HT:PCBM cell, such blend structure is stable upto 100C-110 C[47]. We have also measured DOS for different temperature and at different instance.

www.manaraa.com

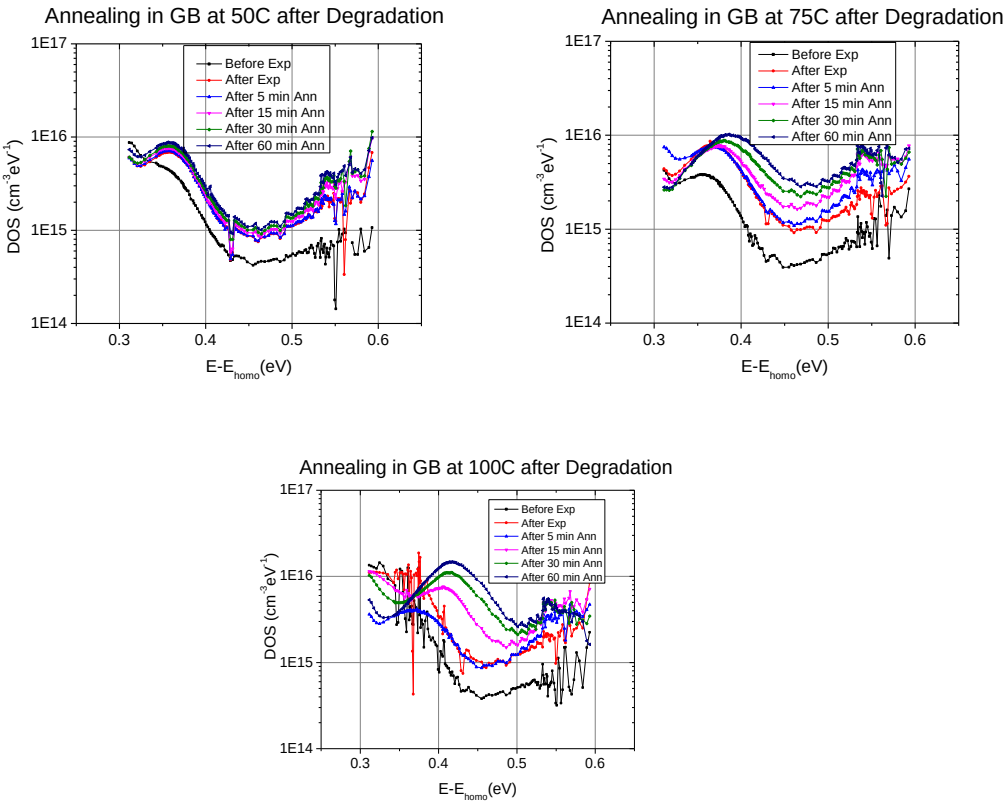

Figure 6.11 (A) Change in DOS over different steps of annealing(PPA) for 50C PPA temperature (B) Change in DOS over different steps of annealing(PPA) for 75C PPA temperature (C) Change in DOS over different steps of annealing(PPA) for 100C PPA temperature

Measured DOS shows a clear trend that with increasing annealing temperature, amounts of defects that are evolving at interface are increasing. Also the Gaussian band is drifting toward the middle of the band gap which is consistent with the earlier observation. Only conclusion we can make from this set of experiment that, we found experimentally 100C is the best temperature that can recover maximum current possible in comparison to other annealing temperature. Very low temperature (like 50C)do not show much change in device performance which very high temperature (125C) is degrading the cell rapidly.

www.manaraa.com

Further we repeated the same experiment at 100 C in the nitrogen atmosphere which was found to be optimized annealing temperature for device performance recovery. This time we have also measured dark IV and extracted Io and ideality factor to see if that follows the trend in DOS change.

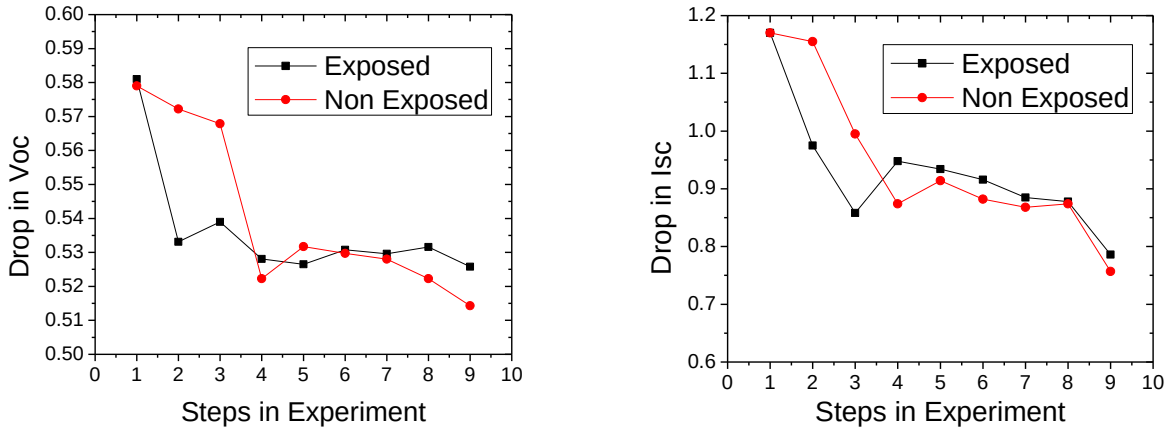

Figure 6.12 (A) Change in Voc over different steps of annealing (PPA) at 100C PPA temperature for both exposed (2x-96 hrs) and non-exposed contact of same device. (B) Change in Isc over different steps of annealing (PPA) at 100C PPA temperature for both exposed (2x-96 hrs) and non-exposed contact of same device.

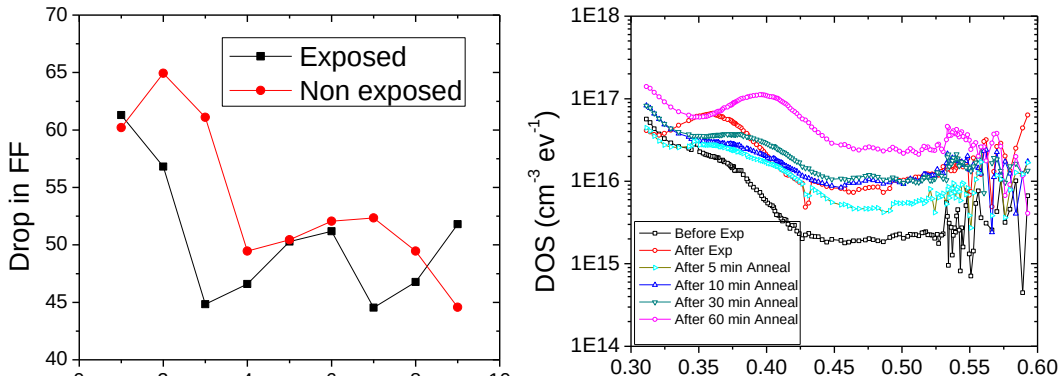

Figure 6.13 (A) Change in FF over different steps of annealing (PPA) at 100C PPA temperature for both exposed (2x-96 hrs) and non-exposed contact of same device. (B) Change in DOS over different steps of annealing (PPA) at 100C PPA temperature

www.manaraa.com

The data above repeatedly shows that subsequent annealing degrades the cell. Only first annealing step reduces the defect density which can be directly correlated to the increase in short circuit current. The right ward shift in DOS is a consistent observation throughout the post production annealing experiment. The following figure shows the change in dark current parameters (Io/n) with different annealing time. It follows the trend of the change in defect states.

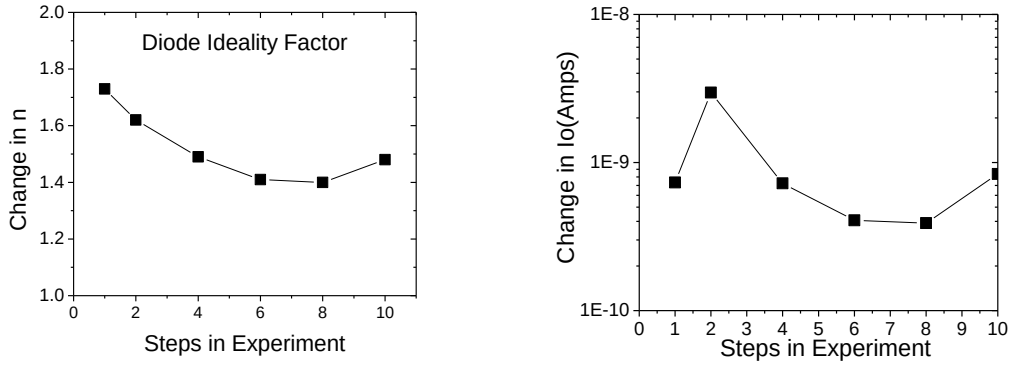

Figure 6.14 (A) Change in n(ideality factor) over different steps of annealing (PPA) at 100C PPA temperature (B) Change in Io(Reverse saturation current) over different steps of annealing (PPA) at 100C PPA

It was now well understood that there are two process going on simultaneously. One cures the defect while other induces defect that increases trap assisted recombination. But question that arises is we already know that organic solar cells are found to show some morphological changes and also changes in crystallinity as a function of temperature but at a temperature higher than 100-110 C. What makes the performances degrading? What makes the non-degraded cell to get degraded after repeated thermal treatment? These questions lead to a pool of experiments that we are going to discuss in the next section.

www.manaraa.com

6.7 Are device thermally stable?

What make us think that, organic solar cells are not thermally stable? Figure 6.15(A-C) summarize the fact that organic solar cell are thermally unstable even they are not exposed to light. What makes them unstable? It's quite clear from the figure 6.15 that at 50C the device performance remain almost same even after subsequent annealing steps for longer time. However as we are going further in temperature, we see a drastic drop in device performances.

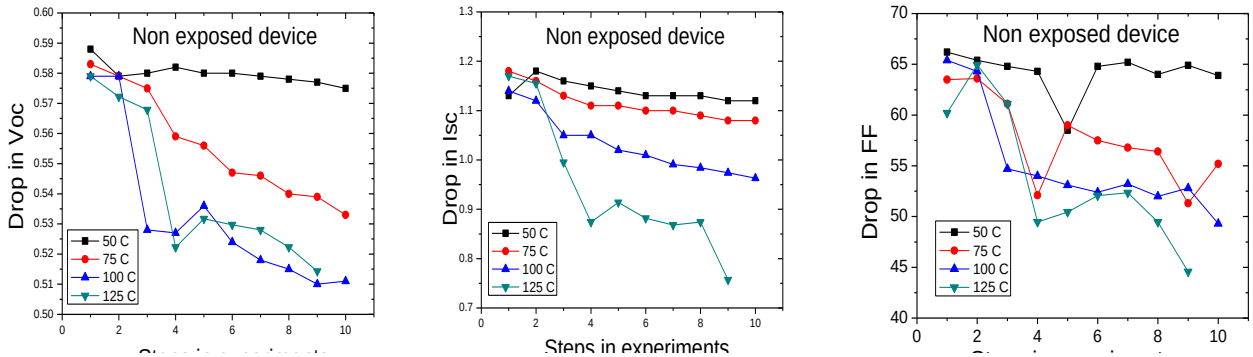

Figure 6.15 Change in different parameters over different steps of annealing (PPA) at 100C PPA temperature for non-exposed -(A) Voc , (B) Isc, (C) FF

We found it worthy to investigate. We wanted to check if any of the interlayer is causing problem to the thermal degradation process during post production annealing. We designed a set of experiment to see the effect of inter-layer as well as active layer change during PPA. The following flow chart in figure 6.16 shows different process involved in the fabrication of solar cell and different thermal treatment involved every steps. Our first temperature treatment is done during the deposition of HTL (at 150C). Second thermal treatment (which is also called pre-production annealing) is done to optimize the active layer. And finally the post production annealing is performed after making the complete device (after metallization). We chose our PPA temperature to be 100 C and time of annealing to be 15 minutes. The entire process of PPA was

www.manaraa.com

done inside the glove box to make sure the removal of any other variable like atmospheric oxygen and moisture out of the experiment.

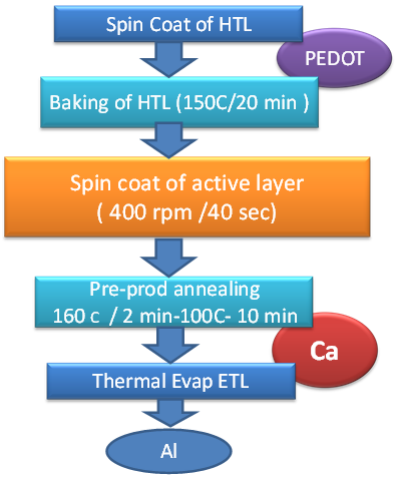

Figure 6.16 Schematic block diagram showing different fabrication steps with respective annealing

Firstly we wanted to check if hole transport layer is causing the problem. So we made a two solar cell on separate substrate and used PEDOT:PSS in one and MoO_x in other. We kept the HTL baking recipe same for both the device. All other subsequent recipe was kept same. The results are shown in figure 6.17.

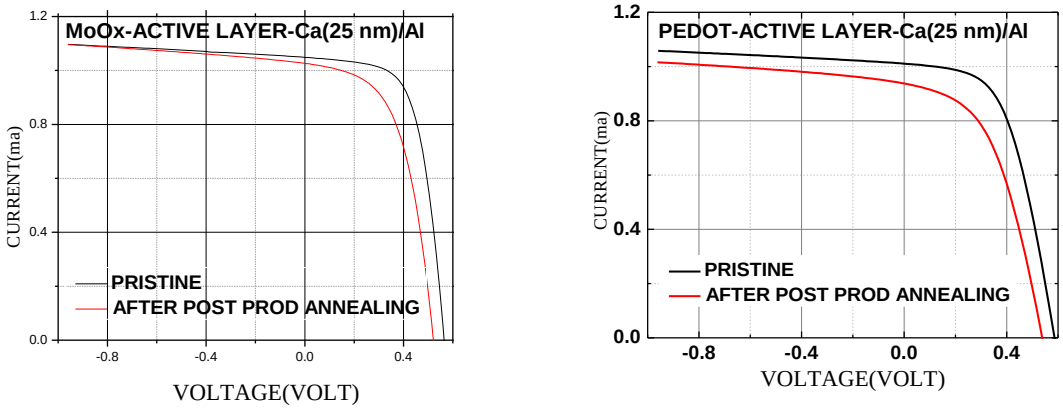

Figure 6.17 (A) Comparison of Light IV's of MoOx based Standard cell before and after PPA, (B) Comparison of Light IV's of PEDOT based Standard cell before and after PPA

www.manaraa.com

There are two observations that can be made. First In both the devices open circuit voltage is decreasing by roughly 7%. Secondly for MoO_x based device shows smaller change in short circuit current compared to PEDOT based device. This phenomenon is possible to explain by the argument given in Appendix D, where we have shown thermal treatment of MoO_x film under nitrogen atmosphere increases the MoO_2 content of the film resulting in better electrical transport and less series resistance. It is possible that during post production annealing (PPA) MoO_x is becoming more conductive resulting in increase in short circuit current, while at the same time due to PPA the device is losing some amount of current. Over all, the loss in short circuit current is small compared to PEDOT based device. It seems that HTL has nothing to do with the performance drop during PPA as both type of HTL recorded almost similar amount of drop in Voc. So we can rule out the possibility of HTL to play any part in the thermal instability during PPA.

Next we took active layer as our object of investigation. In this experiment we used standard PEDOT:PSS as a HTL and kept the baking recipe same. We made two devices. In one device we did as usual thermal annealing as mentioned in the flow chart previously at 160C for 2 min followed by 110 C for 10 min. We deposited Ca(25 nm) and Al(120 nm) as usual. In the other device we did maintain the same pre-production annealing step as the first one. But we did an extended annealing step at 100 C for 15 min before putting Ca(25nm) cathode to simulate the same environment during post production annealing. We wanted to see if the solar cell performance drops because of this extended thermal annealing step.

www.manaraa.com

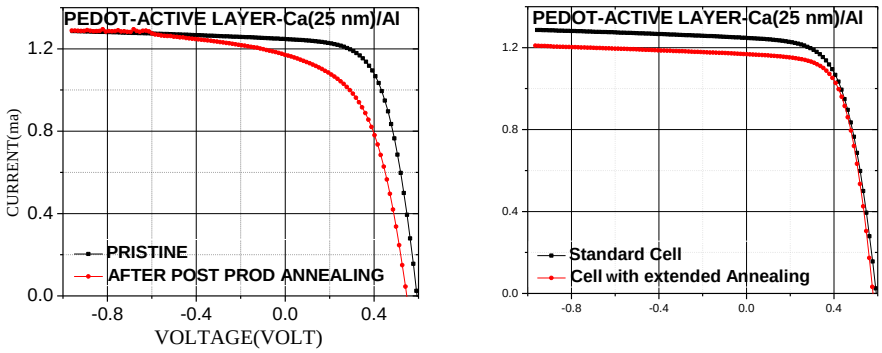

Figure 6.18 (A) Comparison of Light IV's of PEDOT:PSS based Standard cell before and after PPA, (B) Comparison of Light IV's of PEDOT based Standard cell with extended annealing (without PPA)

Firstly the thermal annealing shows almost same change in device light iv curve as we have observed before. But when we did same thermal annealing before depositing calcium on top of active layer, we saw a slight drop in current along with even slighter drop in Voc. That is well explained by the morphological change in active layer as discussed before. For the extended annealing step FF did not suffer any drop (See figure 6.18(B) for reference), while for standard post production annealing it degraded significantly. This fact shows that the drop in device performance is not in any way related to the change in active layer. So finally we did an experiment we used the variation in cathode inter-layer. All the recipe remained same in active layer as mentioned in the flow chart. In one device we put Ca(25 nm) before depositing aluminum, while in the other device we deposit only aluminum of same thickness by thermal evaporation. The objective is to see, what happens to the device performance when we perform post production annealing on both the sample. See figure 6.19 for reference. It can be seen that device with Ca/Al shows same drop in Isc and Voc while device with only Aluminum shows greater degree of drop in Voc.

www.manaraa.com

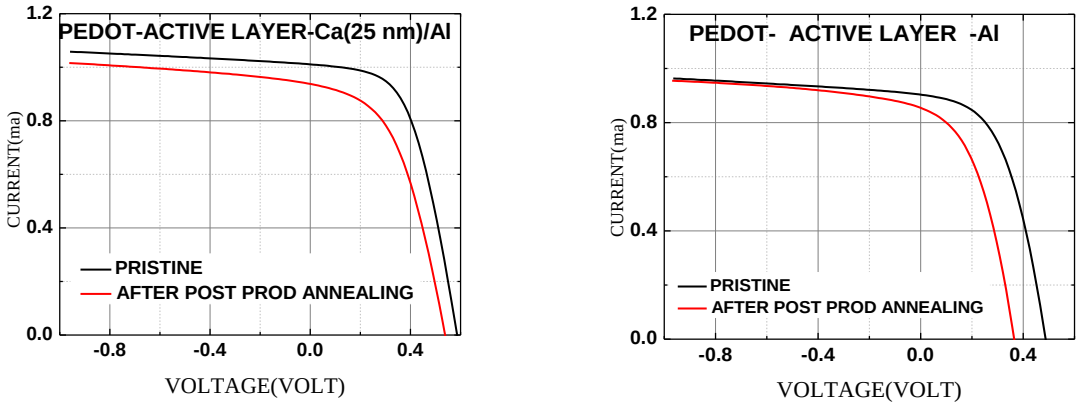

Figure 6.19(A) Comparison of Light IV's of PEDOT:PSS based Standard cell before and after PPA of standard Ca/Al device, (B) Comparison of Light IV's of PEDOT:PSS based Standard cell before and after PPA of only Al device.

It can be concluded that cathode interlayer play a major role in the degradation during PPA. Both Calcium and Aluminum are causing the damage. Aluminum is actually aggravating the problem. So we asked our self whether it has anything to do with calcium thickness, Is it possible for aluminum to diffuse through calcium. The results are shown in figure 6.20.

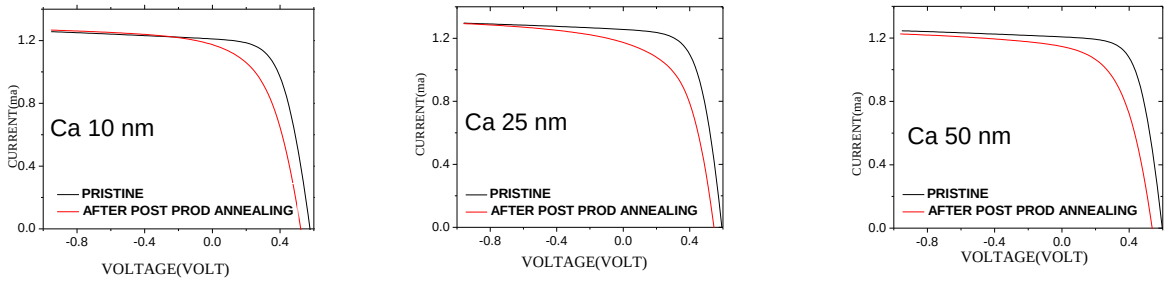

Figure 6.20 Comparison of Light IV's of PEDOT:PSS based Standard cell before and after PPA of standard Ca/Al device for different calcium thickness.

It was found from the above experiment that thermal degradation of cells during PPA is not a function of calcium thickness as devices with different thickness of calcium recorded almost same drop in solar cell performance.

So up-to this point we already knew why solar cell performance drops during PPA even though this result is contrasting to the result published by W Ma et al[94] which suggested that PPA improves the solar cell efficiency. So in order to see the full recovery of photo-degraded

www.manaraa.com

sample we must first make our solar cell architecture thermally stable. But there are no know materials that can help us to stop thermal degradation of our solar cell because of metal diffusion into active layer.

So we turned to Inverted solar cell to see if we can make any device which can give us better thermal stability. We kept the recipe same for the entire batch of experiment. Instead of using PEDOT:PSS as a hole transport layer we used Cs_2Co_3 as an electron transport layer. The electron transport layer was baked at 170C for 25 min. Further active layer was spin coated in the same rpm (400 for 40 sec) and dried thereafter. Now as a hole transport layer we used both MoOx as well as V_2O_5 . However unlike the standard architecture device, MoOx layer is not annealed.

Firstly we make a standard sample as mentioned. Then we tested the post production annealing inside glove-box under nitrogen atmosphere. It recorded a dramatic drop in both voltage and current which is in the range of 20%. Later we followed the same recipe and made three different inverted solar cell with three different thickness of MoOx to see if at all drop in performance is related to the thickness of MoOx. See figure 6.21 for reference. For a thin layer pf 10 nm it is highly probable that some metal can diffuse into the active layer creating defects either at metal organic or D-A interface resulting in loss due to trao assisted recombination as seen in standard cell. The following figure describes the light IV of inverted solar cells with different thickness of MoOx film. It records almost equal amount of drop in Isc/Voc and FF.

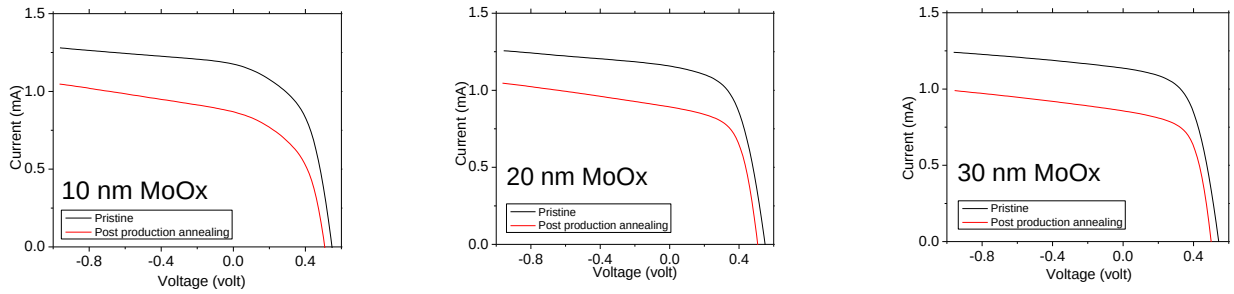

Figure 6.21 (A) Comparison of Light IV's of MoO_x based inverted cell before and after PPA of standard Ca/Al device for different MoO_x thickness.

www.manaraa.com

Next we tried to see if thermal annealing after deposition of MoO_x does have any impact on the device performance of the solar cell as well as on their thermal stability during post production annealing. See figure 6.22 and 6.23 for reference. It shows that as we anneal our solar cell after the deposition of MoO_x (10) nm, the device performances went down. The drop is in-fact higher for the higher annealing temperature. Next step was to see the effect of post-production annealing on this thermally annealed MoO_x cells. The following figures show the effect of post-production annealing on 100nm MoO_x cells. In the device with un-annealed MoO_x, performance dropped significantly upon PPA. While for thermally annealed MoO_x sample, the change in device performance is insignificant. This shows a great promise for the first time for a possibly thermal stable architecture. This is not yet known(could be another direction of study in the future), why cells with annealed thick MoO_x behave as a thermally stable architecture for certain temperature and time of annealing.

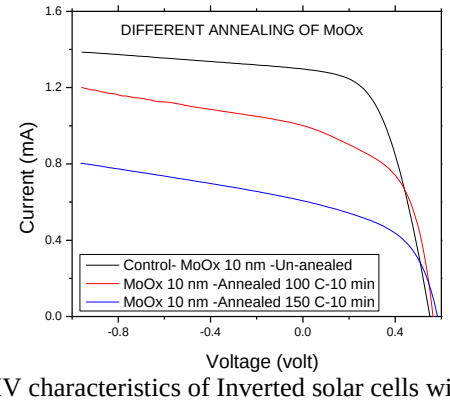

Figure 6.22(A) Comparison of Light IV characteristics of Inverted solar cells with MoO_x as HTL annealed at different temperature.

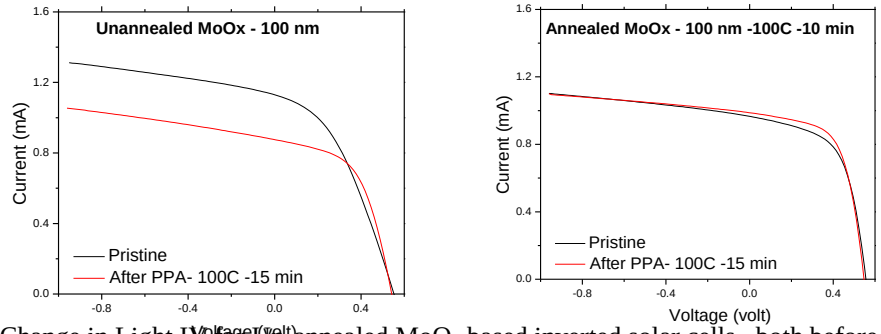

Figure 6.23(A) Change in Light IV for Un-annealed MoO_x based inverted solar cells –both before and after PPA, (B) Change in Light IV for annealed (110C for 15 min) MoO_x based inverted solar cells –both before and after PPA.

www.manaraa.com

To eliminate the idea of active layer change during PPA we have also repeated the experiment of extended annealing (same temperature and time as that used during PPA) before the deposition of MoO_x layer. It was found that such extended annealing do not change the device performance significantly. The change is mostly with within 1% of experimental error limit.

In a separate experiment we tried to see if we can reduce the drop in device performance upon PPA by reducing the PPA temperature. We used two different temperature of 100C as control and 85 C for PPA on an un-annealed control device. See figure 6.24and 6.25 for reference.

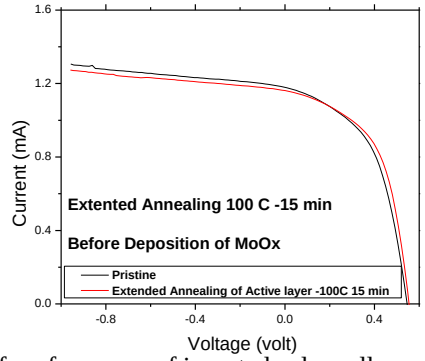

Figure 6.24(A) Comparison of performance of inverted solar cell upon extended annealing

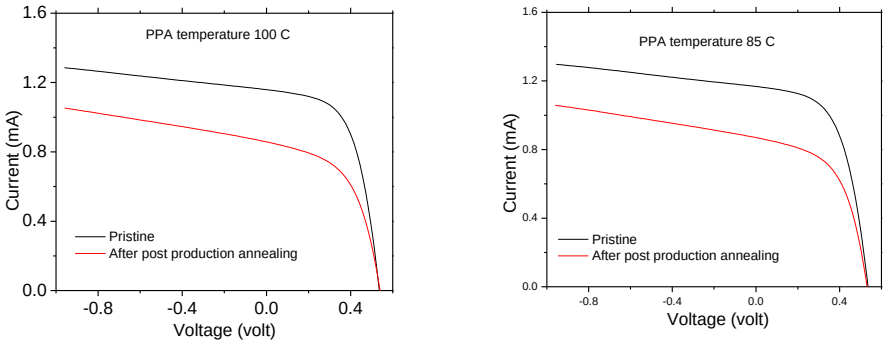

Figure 6.25(A) Comparison of Light IV for un-annealed MoO_x based inverted solar cells –both before and after PPA(100C). (B) Comparison of Light IV for un-annealed MoO_x based inverted solar cells –both before and after PPA(85C)

It was found that both the temperature seems to make same effect on the device so far the thermal degradation is concerned.

www.manaraa.com

6.8 Degradation and post production anneal on inverted cells

Until now, it was found that prolonged light exposure creates some defect states which can be annealed out by post production thermal annealing. However that annealing occurs simultaneously with metal diffusion into active layer resulting in the formation of recombination center, mostly closer to interface resulting in excess recombination and extra loss mechanism. So we observed partial recovery of solar cell performance upon annealing and drop in performance upon further thermal treatment. It was rather difficult to distinguish between two different processes occurring at the same time. At that time making the device (metal contact) thermally stable was of utmost importance. In the last section we observed that, it is indeed possible to make thermally stable metal contact for certain inverted cell architecture as described in Appendix G. We decided now to do the same experiment of post-production annealing on inverted solar cells with top MoO_x layer annealed at 100C for 10 min.

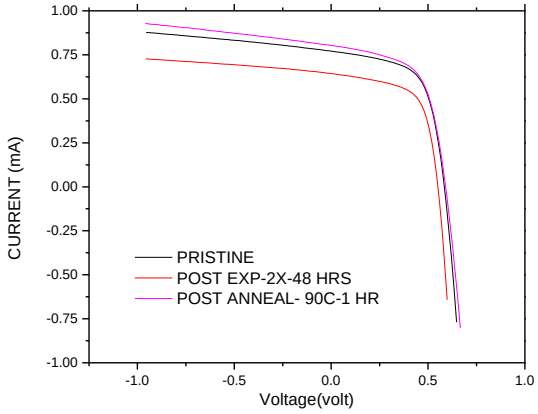

Figure 6.26: Light IV measured before /after exposure and after post production annealing at 90C for 1 hour

The cells with inverted architecture were exposed to 2x intensity for 48 hours and then annealed at different temperature for 1 hour. The entire experiment was conducted inside glove box under nitrogen atmosphere. The black line shows the IV measured before exposure while red line shows the light IV measured after exposure. The purple line shows after PPA. It's quite interest-

www.manaraa.com

ing to notice that after thermal annealing, it's possible to recover the complete solar cell performance including short circuit current and open circuit voltage. In-fact the short circuit current actually increased slightly more than the current recorded during pristine condition. It could be because of some experimental error or the device could be under-annealed during its fabrication stage. Fig 6.27 shows how the quantum efficiency changed upon annealing at two different temperatures (90C/110C).

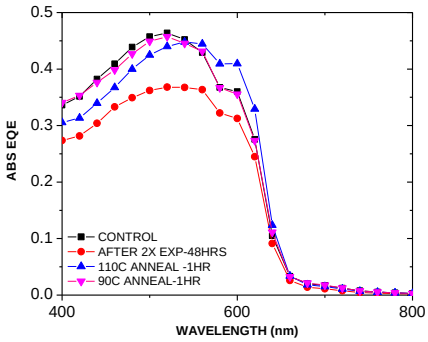

Figure 6.27: Change in EQE measured before /after exposure and after post production annealing at 90C/110c for 1 hour

It can be seen that, the short circuit current can be recovered completely by thermal annealing at 90c for 1 hours. However when annealed at 110C, the morphology of the cell changes and become more crystalline with a red-shift and more photo current at 600nm which essentially the spectral location of vibronic peaks in the blend absorption band. This agrees with the observation in light IV and also suggest to the possibility of under-annealing of the device itself during fabrication. Further we measured DOS by capacitance measurement and found that after 90c anneal, DOS dropped in the mid-gap region (0.5ev-0.65ev) and almost got back to the pristine measured DOS as can be seen in the fig 6.28. When the degraded device annealed at 110C, the DOS dropped way below the pristine DOS.

In the figure 6.29(A) we plotted integrated DOS (0.5ev-0.64ev) for different temperature of annealing. It can be seen that, annealing reduces the defects created by light exposure. We obtain

www.manaraa.com

a similar agreement between the estimated density of states (total) from low frequency CV measurement. The lowering of total estimated states upon annealing indicates to the possibility of under-annealing of the device during fabrication.

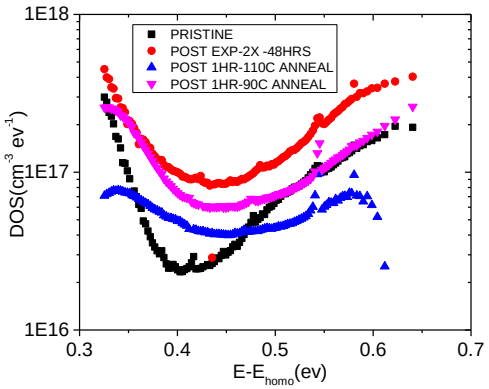

Figure 6.28: Change in DOS measured before /after exposure and after post production annealing at 90C/110c for 1 hour

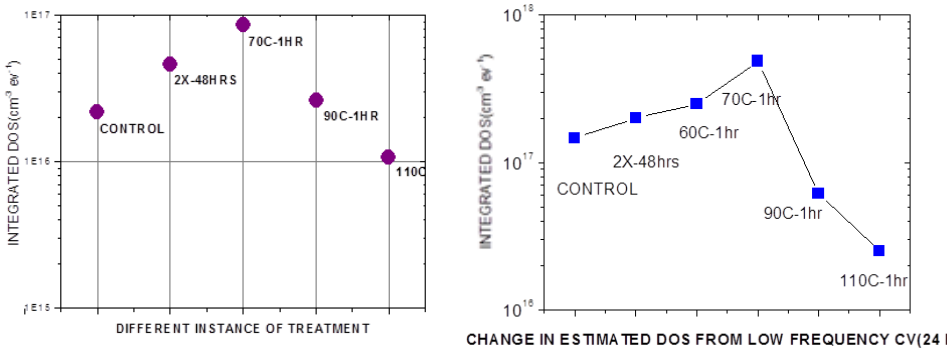

Figure 6.29(A) Change in DOS (integrated at mid-gap from DOS spectrum) upon different annealing temperature. Change in total defect states estimated from low frequency (24 Hz) Mott-Schottky technique upon different annealing temperature

We measured dark current at reverse bias for all the samples for both before and after degradation and after post production annealing. Fig 6.30 shows how the reverse bias dark current drops after annealing at different temperature. It follows a similar trend observed in the change in mid-gap DOS upon annealing as seen in fig 6.29. Since at reverse bias, dark current is contributed mainly by thermal generation and recombination of charge carrier via traps, it's highly possible that any change in trap density should be directly reflected in the careful measurement of re-

www.manaraa.com

verse bias dark current. However it was observed many times during the experiments that, if the device develops a shunt path across diode during any treatment, the reverse bias generation recombination current will be surpassed by the higher shunt current which makes it difficult to identify and observe any change in thermal generation-recombination current which can lead to confusion.

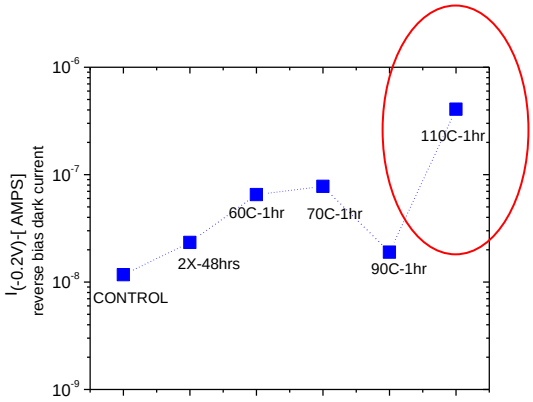

Figure 6.30 Change in reverse bias dark current at -0.3V for different annealed cell after 2x degradation for 48 hours

Finally we observed the change in induced defect states upon thermal annealing and found that the defect states (created by prolonged light illumination) can be annealed out by proper thermal treatment after photo degradation. We found the reason of an apparent anomaly described in section 6.4 where we observed that thermal annealing recovers short circuit current partly but lost open circuit voltage in the process. In this section (all the experiment done on inverted cells) show in-fact, thermal treatment can recover both short circuit current and open circuit voltage upon annealing. However we must make sure that the device are thermally stable for the annealing temperature and time we are going to perform on the degraded cell.

To make sure the device are thermally stable for long post production annealing steps, we annealed our DUT for 1hour at 110C for both during active layer annealing (pre-production annealing) and during HTL annealing(soon after the deposition of MoOx layer). It was found that the device become thermally stable for the intended post production annealing (for 1 hour). We measured DOS and dark current at reverse bias following post degradation annealing steps. Fig-

www.manaraa.com

ure 6.31 shows the drop in DOS (integrated) as well as change in I(-0.3V)- seems to saturate for higher temperature. It's quite evident from the fact that thermal stability of the solar cell is an absolute necessary for complete recovery by post degradation thermal treatment.

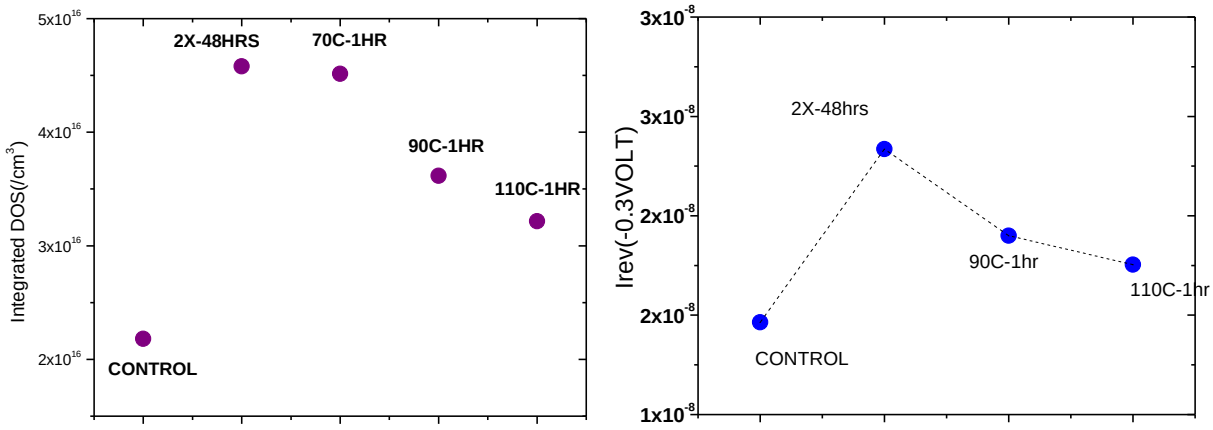

Figure 6.31(A) Change in Integrated DOS for different annealed cell after 2x degradation for 48 hours, (B) Change in reverse bias dark current at -0.3V for different annealed cell after 2x degradation for 48 hours

6.8 Conclusion

In summary we investigated in detail the performance recovery of organic solar cell after photo-degradation by post production annealing. It can be concluded that PPA can effectively recover some of the short circuit current for regular cell only for first annealing step. For successive annealing the performance tends to go down which could be due to the diffusion of metal cathode (for standard cell) and metal oxide anode (for inverted cell) into the photo active layer. We also found that it's more important to find a thermally stable solar cell before doing further experiments on performance recovery of photo-degraded cell. We finally conducted experiment on the thermally stable INVERTED architecture and found that it is indeed possible to recover the efficiency of solar cell after light induced degradation by temperature treatment. The main reason of performance recovery is the reduction in the interface defect states(at D-A interface)

www.manaraa.com

that leads to lesser trap assisted recombination and improved performance as a result. The conclusion, then, is that for cells which are thermally stable, increase in defects and decrease in PV device performance can be totally reversed by thermal annealing after prolonged photo-degradation.

www.manaraa.com

CHAPTER 7
CONCLUSIONS AND FUTURE WORK

The work was concentrated mostly on the experimental study of different photo degradation dynamics present in a P3HT: PCBM based solar cells. Our study concluded that prolonged light exposure created mid-gap defect states at the donor acceptor interface. Further such creation of defect states saturates over time of exposure indicating a second degradation dynamics which is yet to be explained. The continuous drop in photo current with exposure time is a good indication of the second photo-degradation dynamics. Photo degradation is also a function of blend film morphology, thickness and type of anode and cathode contact. When studying the effect of cathode interlayer, we discovered that aluminum cathode can enhance the amount of photo degradation quite significantly compared to calcium which led to the conclusion that Al plays a vital role in photo degradation. It seems aluminum diffusion inside the active layer could be a major source of charged defect states that can act as a recombination center for SRH recombination.

Thermal annealing is a good way of performance recovery. However, again cathode contact seems to present problem during such annealing steps. It was found that such thermal annealing helps in annealing out the extra defect states being created by prolonged light exposure. However as we have seen in chapter 9, subsequent annealing step increases the defect state density and reduces Isc and Voc further which is consistent with the dark current(Io) measurement. This result again is pointing to the fact that aluminum and calcium cathode plays a vital role in device performance in a macro scale.

The work on organic solar cell –especially understanding of device physics is widely open with many points to be closely investigated. In our work we tried to investigate few perspectives

www.manaraa.com

with many work to be done in future. This section will guide to some future unexplored road-ways.

Structural study

We have already observed the change in mid-level defect states under light soaking. But we have yet to figure out the main reason behind the origination of defect states. In amorphous silicon the prolonged light exposure creates dangling bonds which is considered as a source of mid-level defect states. However we are yet to figure out which particular bonds in the polymer system are causing the change in defect states. Is it the C-H bond of side chain, or C-C bond/C=C bond/ C-S (thiophene-ring)? Further study into the structural analysis might lead us to the better understanding of the source cause of photo-degradation.

Crystallinity of polymer and fullerene blend is an important factor that affects the efficiency of solar cell. During the device fabrication it was found that there are several fabrication parameters that can lead to higher crystallinity of polymers. In order to understand how crystallinity is impacted by the photo-degradation, we need a direct one to one comparison between the photo degradation and variation in crystallinity. Some careful plan of experiments need to be made in order to understand the behavior of crystalline orientation of P3HT domain with prolonged photo exposure.

Which morphology is more photo-stable?

In appendix D and E we did a study of change in morphology on photo-stability by changing the hole transport layer followed by variation in pre-production temperature and finally by changing the concentration. But there are other parameters which can be changed in order to obtain different other morphology. It would be an interesting study to have a detail comparison of

www.manaraa.com

electrical and structural property of different morphology by varying the molecular weight. With higher molecular weight leading to higher conjugation length –presumably bigger domain size.

Morphology can also be changed by changing the spin rate. It is very well known that by changing the spin rate, we change the evaporation rate of solvent from the solutions that are spread on top of substrate. With lower spin rate, solvent gets more time before they can be evaporate. This leads to growing chance of crystallization in P3HT domain and PCBM to agglomerate together. However with higher spin rate solution evaporates faster resulting in freezing the spatial distribution of PCBM molecule and intermixed P3HT resulting in bigger active interface area between donor and acceptor.

Modulated intensity dependent photo-degradation

We have already demonstrated that the light intensity is a factor to play with the rate of photo to degradation. Higher intensity leads to faster degradation while lower intensity has slower rate. As we know, during the day time there is only a small window of time when the solar cell are actually exposed to 1x(AM 1.5) intensity. If the panels are not accompanied by some solar tracker, large amount of solar flux may be lost due to the angular reflection from the front surface and thus the solar illumination will not be the same throughout. We want to understand the degradation dynamics for solar intensity less than 1x sun. For that we can use simple neutral density filter to reduce the intensity of our solar simulator. By doing this we expect to get an quantitative information about the decay rate for different intensity. Once we have the idea about the decay rate, we can try to explain the decay rate in efficiency by some mathematical formulation and try to predict what will be amount of degradation of a solar cell exposed to certain intensity for certain time. This will enable us to give us a brief idea about the percentage change in cell efficiency over a day of normal sun illumination.

www.manaraa.com

O_2 Induced photo-degradation

This is one of the topics widely studied in organic solar cell degradation that must be revisited once again. It was proposed by various previous groups that oxygen is behind the process of photo-degradation in P3HT:PCBM based bulk hetero junction cell. It was observed that oxygen is believed to dope the polymer and can create deep states that can work as a recombination center.

All the experiments performed in this work are conducted under nitrogen atmosphere, We anticipate the need of controlled injection of oxygen in addition to nitrogen atmosphere to see the changes in defects states by our capacitance spectroscopy measurement. This will also be an good experiment to identify the activation energy of the trap states created by oxygen. Light Iv comparison can tell us about possible correlation between recombination losses with the trap states created only due to oxygen.

Change in regio-regularity in polymer

It was already known that amorphous (disordered) P3HT helps in separation of charges while crystalline phases helps in transporting the hole from interface to electrode. It is understandable that PCBM makes interface with amorphous region of P3HT. The trap density measured in the DOS measurement could be the signature of amorphous polymer phase. It could be ascertained if we can change the amount of amorphous phase in the polymer blend and measure the corresponding defect density. One way of varying the amorphous phase is to vary the region-regularity in the polymer. So by introducing regio0randomness in polymer we can find out a nice correlation between defect density and recombination dynamics in organic photovoltaic.

www.manaraa.com

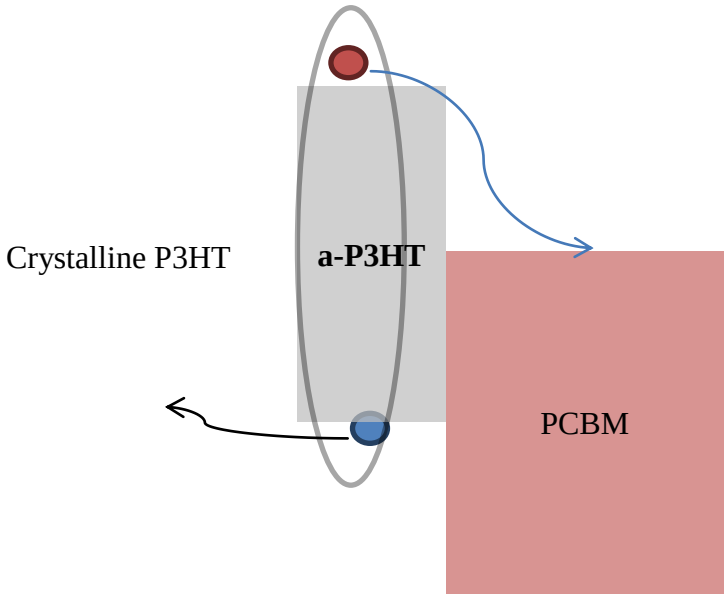

Another important study could be to see the effect of photo-induced degradation on devices made from different region-regularity of P3HT. This could give us more insight into different recombination dynamics occurring in an organic solar cells.

Measurement of trap density in bilayer- solar cells

It's a difficult problem for all the device engineer to visualize the energy band diagram in a bulk hetero junction solar cell because of its complex nature and intermixing of different phases altogether. In order to have a better understanding of alignment of Fermi level, we need to make perfect bilayer structure. However its difficult in reality to make a perfect bilayer structure because of un-avoidable intermixing in a quasi-bilayer. A detail study is required to study the defect distribution in a perfect bilayer. There are some initial results which suggest there can be capacitance response to bilayer structure which is not expected to appear. In a perfect bilayer, PCBM is in contact with aluminum cathode while P3HT is in contact with PEDOT:PSS anode. This remove the possibility of having any Scotty barrier and eliminates the chance of seeing any Mott-Scotty behavior (if theory of Mott-Scotty based CV are to be believed). However presence

www.manaraa.com

of any Mott-Scotty behavior in a bilayer would emphasize the need for remodeling the capacitance response in a bulk hetero junction solar cell. In addition it would be nice study to compare the photo-stability of bulk he5tero junction and bilayer. This would prove without any doubt, the nature and location of trap states evolving in organic solar cells that are found to be main force behind the recombination loss in the cells.

Solution to photo-degradation

This work mostly concentrated on the investigation in detail to find out the cause of photo degradation of bulk hetero junction solar cells. As we identified some possible path ways of photo-degradation in organic solar cells. We need a detail work on the possible solution of photo-degradation. One simple way of reducing the effect of photo-degradation is the formation of tandem architecture. This will not only ensure better photo-stability but also enhance improve the solar cell performance. Our initial work on parallel and series hybrid tandem cell with amorphous silicon solar cell showed huge promise for further study.

We can try different polymer-polymer tandem solar cells which can make the process more suitable for all solution processing. Comparing the photo-stability of different tandem cell could be a potential study in the future.

Auger electron microscopy-depth profiling

In the following Appendix E and F, we have experimental evidence that suggested the possible diffusion of metal inside the photo-active layer. It will be difficult to say affirmatively unless we have further experimental proof. Auger electron microscopy is the best option for the elemental detection inside the active layer. For that we can make a solar cell with very thin cathode layer (Ca- 5 nm and Al(5-10 nm)). Further the device should be exposed and treated (post production anneal). Finally a depth profiling of different composition needs to be plotted as a func-

www.manaraa.com

tion of etching time where etching will be performed from to surface towards bottom layer. Even SIMS (Secondary ion mass spectroscopy) can also be a very good tool to determine the elemental presence inside the active layer.

Photo-degradation of low band gap polymer based pv

Next generation solar cells with lower band gap donor are excellent candidate for high performance solar cells. Some literature reported ~9% single junction solar cell using novel PTB7polymer. One interesting feature of such solar cells are their extremely low thickness, 70-90 nm. Also such new high performance polymer based devices are mixed in 1:3 ratio with acceptor which changes the conventional ratio of 1:1 for P3HT based system. This will be an nice study to compare the photo induced drop in solar cell performances and may help in developing the understanding in better way.

www.manaraa.com

APPENDIX-A

PERIODIC TEXTURED BACK REFLECTOR FOR INORGANIC SOLAR CELLS

Introduction

Thin film silicon solar cells utilize a micro-morph solar architecture Composed of a top cell of high band gap amorphous silicon (a-Si:H) followed by a bottom-cell of nano-crystalline silicon (nc-Si) [182,183]. The longer wavelength red and near-infrared photons are absorbed in the bottom cell, whereas the top cell absorbs the shorter wavelengths. A ubiquitous problem in all silicon based solar cells is the poor absorption of long-wavelength red and near-infrared photons as shown in figure 11.1[8,10,183-185] . The absorption length of these photons exceeds the thickness of the nc-Si layer (~1 μm), and the quantum efficiency of these solar cells decreases rapidly at wavelengths near the band edge (1.1 μm in nc-Si) [184].

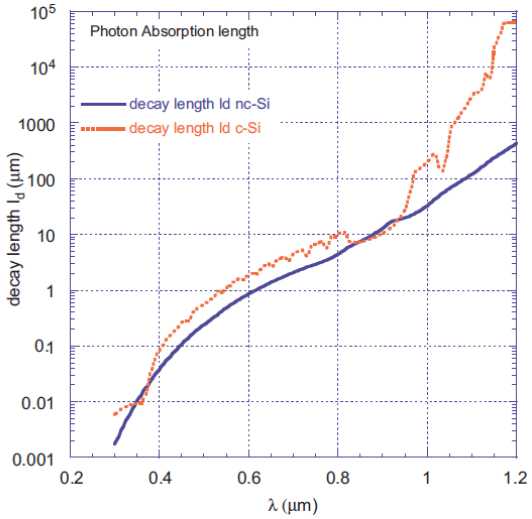

Figure A.1 Decay Length vs. Wavelength (□m)

www.manaraa.com

The common strategy to harvest photons is to use light trapping approaches. Two competing approaches have emerged. The first and traditional approach uses a randomly roughened back reflector (BR)[10,183] as opposed to the second and more recent approach involving periodic photonic–plasmonic back reflectors[8,184,186,187] . Randomly textured BRs scatter light randomly at the back reflector, through all angles, and increase the path length of photons within the absorber layer. Each scattering event is an independent process. If the incident angle at the top interface is greater than the critical angle, light is trapped, otherwise the light escapes. For an ideal loss-less Lambertian scattering surface, which reflects incoming light uniformly into all angles, the enhancement factor of the path length inside the absorber layer has the limiting value of $4n^2$[188,189]. This factor can be derived by comparing the probability of escape with that of trapping. It is a current challenge to develop BRs that approach and exceed the $4n^2$ limit[4,190].

Light trapping by photonic structure in nc-si:h solar cell

The recent approach is to use a periodically textured back reflector that i) diffracts light intowave-guided modes and ii) concentrates light within the unit cell. Wave-guided modes are phase matched standing waves (Fig. 1) in a planar layer that occur when the phase difference of rays from the top and bottom surface of the layer is a multiple of π. At each interface the reflected waves are in phase with each other. Waveguide modes traverse in the plane of the structure parallel to the interfaces. On the other hand, surface plasmons are longitudinal modes that occur at metal–semiconductor interfaces with wave propagation parallel to the interface. The concentrated electric fields extend a short distance in the metal and a more significant distance in the semiconductor absorber layer—thus causing absorption of light.[3,4] Plasmons and waveguide modes are in general coupled in the periodic BRs. Propagating plasmons are not expected in random structures which may instead support localized plasmons[9,191,192] at the location of the nano-

www.manaraa.com

particles. These plasmons can lead to optical losses, unless localized plasmons re-radiate into photon modes[193]. Hence it is of great interest to compare the optical properties and performance of these two different classes of back reflectors to assess which family may be more suitable for solar cell applications. We present in this paper a systematic experimental comparison of the optical performance of these two families of back reflectors.

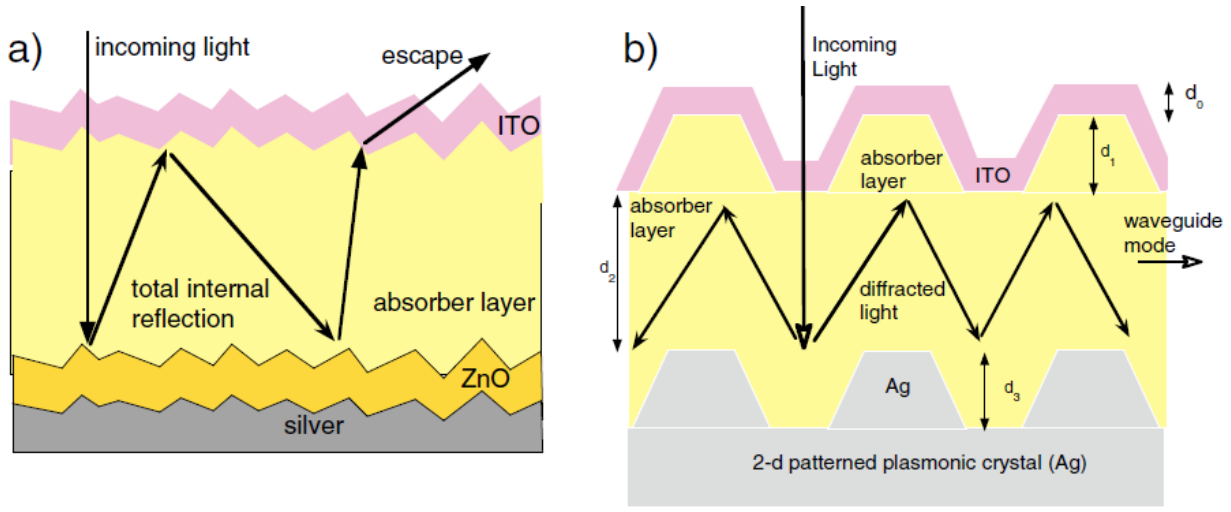

Figure A.2(a) Schematic diagram of random textured back reflectors, (b) periodically patterned back reflectors, showing trapped waveguide modes propagating parallel to the layers.

Experimental procedure

All back reflectors were fabricated on stainless steel substrates. The first randomized back reflector was annealed silver fabricated by thermal evaporation of 5 nm Cr on stainless steel, followed by evaporation of a 200 nm Ag layer. This was annealed at 400 °C for 60 minutes to obtain a random distribution of features (Fig. 2). An 80 nm ZnO capping layer was then deposited. he second random back- reflector was fabricated by sputter depositing 2000 nm ZnO on stainless steel and then etching ZnO in a solution of dilute hydrochloric acid (0.0189%) for 35 s. A 5 nm Cr layer, followed by a 200 nmAg layer and an 80 nmZnO layerwas then deposited, resulting in

www.manaraa.com

randomized surface structures (Fig. 2). The SEM images (Fig. 2) show a randomized corrugated structure for the annealed Ag/ZnO with broad feature sizes from ~0.3 to 1.5 μm. The etched ZnO shows randomized corrugations and pits with feature sizes ranging also from ~0.3 to 1.0 μm. There are some filamentary structures. The diffuse and total reflectance (Fig. 2), measured with an integrating sphere, is an important measure of the ability of the random microstructure to scatter light. The annealed Ag/ZnO has a diffuse reflectance exceeding 60% over the entire range of solar wavelengths (Fig. 2a) and a still higher total reflectance. The specular reflectance (the difference between total and diffuse) is small, since the reflectance is dominated by the diffuse component. The etched ZnO has diffuse reflectance exceeding 70%. The high diffuse reflectance of these samples indicates high scattering efficiency comparable to stateof- the-art randomly textured substrates. Thus these randomized back reflectors are ideal for characterizing the difference between random and periodic back-reflectors.

The first dip (~320 nm) in the reflectance (Fig. 2) is an intrinsic property of Ag, resulting from well-known inter-band electronic transitions at the L-point [194]of the Ag-band structure. The intrinsic inter-band absorption in Ag remains almost unaffected by the ZnO deposition. The second dip between 400 and 500 nm is due to the red-shifted plasmons mode in small silver nanoparticles on the Ag surface in the presence of a ZnO (ε~4) dielectric background[194]. The coating of ZnO results in reduction of both diffuse and total reflectance due to the antireflection property of the layer as observed in previous studies[183,195,196]. It is well known that silver BRs are insufficient for wavelengths below 400 nm, although the solar intensity is also very low in this regime. The errors in reflectance measurements were estimated by performing the reflectance measurements on different portions of the sample. We then estimated the reflectance to have errors that are less than 2%, caused by random structural variations of the sample.

www.manaraa.com

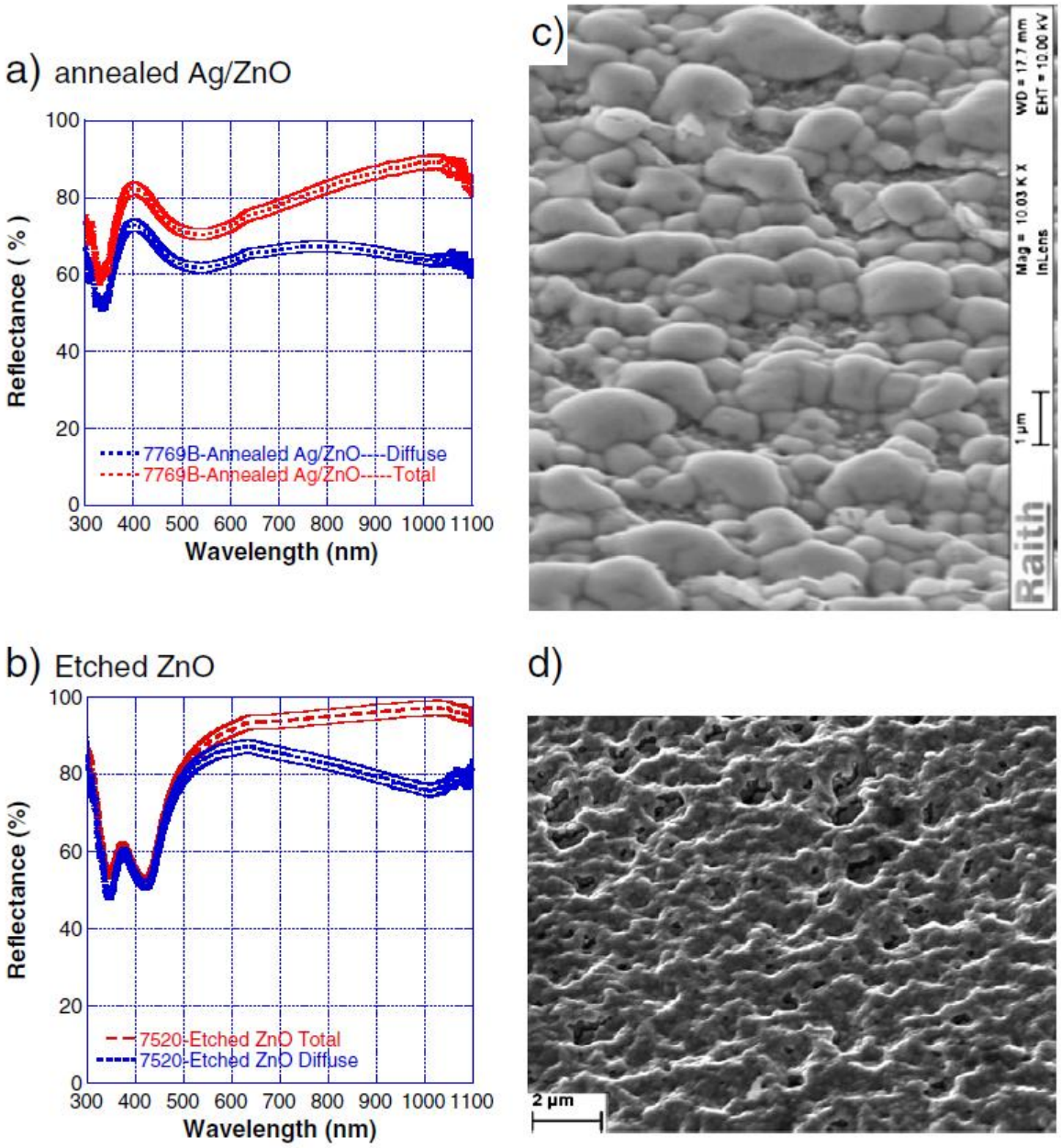

Figure A.3: (a) Total and diffuse reflectance measured for the annealed Ag/ZnO substrate, using an integrating sphere. (b) Total and diffuse reflectance measured for the etched ZnOsubstrate. (c) SEM image of the annealed Ag/ZnO substrate. (d) SEM image of the etched ZnO substrate.

The wavelengths in both the reflectance measurement and the external quantum efficiency measurement are accurate to within 0.1 nm i.e. an error of less than 0.02%. Consequently we only show the error in the reflectance measurement in Fig. 2.The major source of error in the exter-

www.manaraa.com

nal quantum efficiency (EQE) measurement is the intensity of the lamp which can lead to different ratios for the source current and reference current. In addition the slight variation in chopper frequency (~13 Hz) could possibly lead to some random error in the measurement. Similar random variations of the lamp intensities lead to errors in the photo-current. The error in EQE and photo-current measurements were determined by taking measurements on different illuminated spots and measurements at different times on the same spot. This has yielded an error in EQE and photo-current of less than 1%, which is shown on all the measurements in this paper. Systematic errors were avoided by allowing the entire measurement system to come to a steady state. We note that the photo-current measured from current voltage measurements and that inferred from EQE can differ by up to 5%, due to calibration procedures.

Nano-pillar/bump arrays and nano-hole arrays were fabricated at Lightwave Power using nano-imprint lithography. The pitch of these arrays was ~750 nm for nc-Si. We show both SEM and AFM images for the structures showing excellent order over large areas in Fig. 3. As designed through simulations, the nano-pillars are tapered at the top surface which is evident in the AFM shown in Fig. 3(d). We have grown n-i-p nc-Si devices on 1) stainless steel, 2) flat Ag on stainless steel, 3) the random Ag/ZnO substrate, 4) etched Ag/ZnO and the 5) photonic plasmonic nano-array. We utilize a conventional 70 nm thick ITO layer at the top of the cell as an anti-reflection coating. The identical device architecture and similar thickness (0.95 μm) was used so that the devices on different substrates could be meaningfully compared. All solar cells grow conformally with the top surface of the cell displaying the pattern of the substrate. Optimization of the pitch (a) of the periodic back-reflectors is an important consideration. We have performed rigorous scattering matrix simulations[3,190] where Maxwell's equations are solved in Fourier space for both incident polarizations of incoming light. We simulate the absorption and cur-

www.manaraa.com

rent Jsc for a conformal nc-Si solar cell, with the periodic back reflector, assuming no losses in the back reflector. We find (Fig. 4) that the optimized pitch does vary somewhat with the thickness of the nc-Si absorber layer. For a thin 500 nm nc-Si absorber layer we find an optimized pitch of ~700 nm, whereas for a thicker 1000 nm nc-Si absorber layer, we find an optimized pitch of ~900 nm (Fig. 4). An enhancement exceeding 60% is predicted for the 1000 nm thick nc-Si. Optimized currents from the simulation have approached the classical 4n2 limit for Lambertian scattering from a randomly textured back-reflector (Fig. 4). We have chosen the optimized pitch nearer to result for the 500 nm nc-Si thickness, rather than the 1000 nm thickness. It would be interesting in future work to evaluate a longer pitch of ~900 nm, appropriate for thicker nc-Si cells.

The optimized pitch of 900 nm for 1000 nm thick nc-Si is in good agreement with previous simulations[197] for inverted three-dimensional pyramids in the front ZnO layer, for a n-i-p solar cell which predict an optimized pitch near 850 nm for 300 nm high pyramids. Differences are expected between the patterned front surface reflector of ZnO and the present back-surface reflector of Ag. An analogous Al back-reflector consisting of a periodic array of dimples i.e. conical depressions was fabricated[198] by anodic oxidation, and was found to considerably enhance the current, with an optimum pitch of 1000 nm, for 1000 nm thick nc-Si. Although the back-reflector of dimples[198] has a different structure from the array of nano-pillars investigated here, the agreement with our simulations for 1000 nm thick nc-Si (Fig. 4) is reasonable.

Results

We measured the external quantum efficiency (EQE) for the various solar cells as a function of wavelength (Fig. 5), and show the comparison in two separate panels (Fig. 5a, b) for clarity.

www.manaraa.com

Clearly the nano-bump photonic–plasmonic has the highest EQE over most of the wavelength range. For wavelengths below~900 nm the nano-bump array BR has higher EQE than the randomly roughened annealed Ag/ZnO, both of which show considerable enhancements over the flat Ag/ZnO substrate (Fig. 5a). Above 900 nm the annealed Ag/ZnO has slightly higher EQE than the nano-bump BR (Fig. 5b). We observed that the nano bump substrate has higher EQE than both the nano-hole and etched Ag/ZnO BR for wavelengths below 900 nm, but slightly lower EQE above 900 nm. It is likely that this wavelength of 900 nm can be adjusted by changing the lattice pitch. The oscillations of the EQE as a function of wavelength in the periodic back reflectors (nano bump and nano-hole array), arise from the diffractive resonances or wave guided modes generated by the periodic Back-reflector [7,10], where the light propagation is parallel to the layers, generating maxima in the absorption as discussed in our previous theoretical work[3,4,187]. The table 1 includes the respective short circuit current and their enhancement with respect to the flat silver and normal stainless steel back reflector based solar cell.

Type of back reflector	J (at −1.0 V) (mA/cm^2)	% Enhancement over flat Ag/over bare SS
Bare stainless steel substrate	14.2	—
SS + Ag	16.1	—/13
Annealed Ag/ZnO	20.4	27/43
Etched ZnO	19.9	18/39
Nano hole/Ag/ZnO	20.4	27/43
Photonic plasmonic BR/Ag/ZnO	21.5	34/51

Table A.1: Photo-currents (J) obtained from the EQE under AM1.5 illumination for a sequence of nc-Si solar cells, grown under identical device architectures on the different types of periodic, random, and flat reference BRs. The photo-current enhancement over the reference flat Ag/ZnO and bare SS substrates are shown.

www.manaraa.com

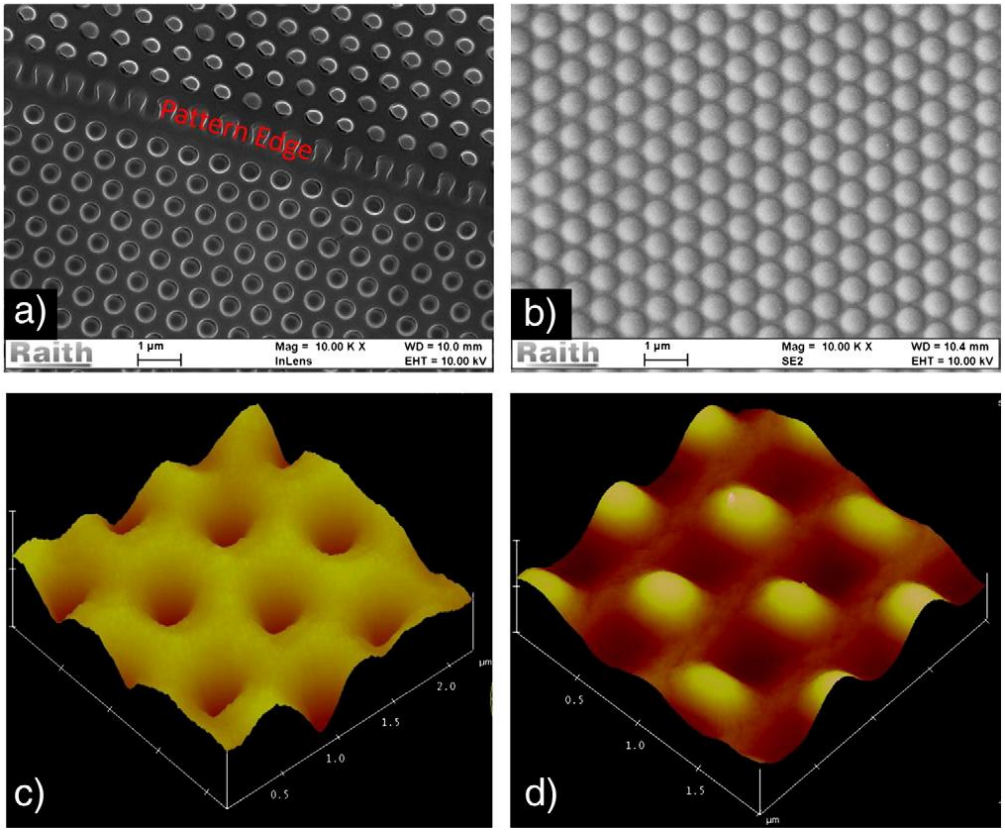

Figure A.4: Photonic–plasmonic nano-array substrate (a) SEM images for the nano-hole array, (b) SEM images for the nano-bump array , (c) AFM image for the nano-hole array , (d) AFM image for the nano bump array.

The EQE ratio of the different substrates to that of the flat silver substrate (Fig. 6a) as a function of wavelength was determined from the measured EQE (Fig. 5). The highest EQE is for the periodic back reflector of nano-pillars/bumps over the entire spectral range. The measured current density is also therefore the highest in the nano-pillar case as compared to the rest of the substrates as shown in Fig. 6(b). Both randomly textured substrates have lower EQE than the nano-pillar back-reflector. The nano-pillars have higher EQE throughout the 600–900 nm range. Although the annealed Ag has higher EQE above 900 nm, the EQE is very small at such long wavelengths. Since the EQE ratio involves dividing two separate EQE measurements the error in the EQE ratio are compounded to ~2% and indicated in Fig. 6a. The error bars in current are nearly 5% and are shown in Fig. 6b.

www.manaraa.com

We further validated these results by calculating the apparent optical absorption coefficient αa(λ) for the solar cells (Fig. 7) on the different substrates, factoring out slight variations in the thickness (t) of the absorber layers with.

$$EQE(\lambda) = (1-R(\lambda))(1-\exp(-\alpha_a(\lambda)\bullet t))$$

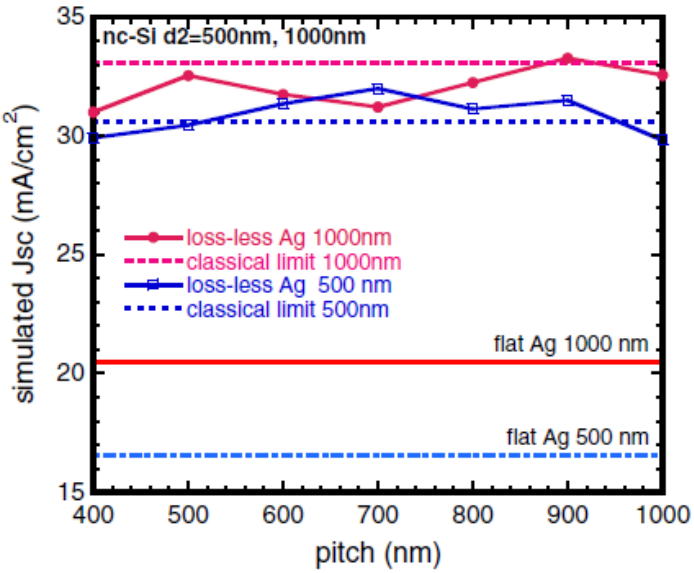

Figure A.5: Simulated current as a function of pitch (a) for a triangular photonic–plasmonic lattice of tapered nano-cones as a back reflector for a nc-Si cell. No losses in the Ag back reflector are assumed. Results are shown for two thicknesses of 500 nm and 1000 nm of the nc-Si. The back-reflector consisted of tapered cones of height 240 nm and base radius R=0.4a, where a is the lattice pitch. Both the Lambertian classical 4n2 limit and the flat Ag case is shown.

Here R is the measured reflectance. This yields highest optical absorption αa for the periodic back-reflector of nano pillars/bumps, averaged over the entire range of solar wavelengths (400–1100 nm). The corresponding current–voltage measurements (Fig. 6b) show the highest current (21.5 mA/cm2) for the nano-pillar/bump back reflector which is significantly higher than the next value of 20.4 mA/cm2 for the annealed Ag/ZnO back reflector, with values at a reverse bias of −1 V to ensure complete collection. The currents were obtained using a top ITO contact that had an area of 0.125 cm2, typical for laboratory scale cells. Analogous studies[6,199] on superstrate n-i-p solar cells, using textured ZnO, also found plasmonic back contacts to have slightly higher

www.manaraa.com

short-circuit current and EQE than the randomly textured back contact, providing complementary support to the results here. The reasons underlying these enhanced EQE and current results are the highly beneficial diffraction from the periodic texture, resulting in densely spaced waveguide modes, where light propagates parallel to the interface. Such modes cannot be realized with randomly textured back reflectors. Furthermore the propagating surface plasmons in the periodic photonic–plasmonic back reflectors are highly beneficial in enhancing absorption, with large light concentration near the back reflector.

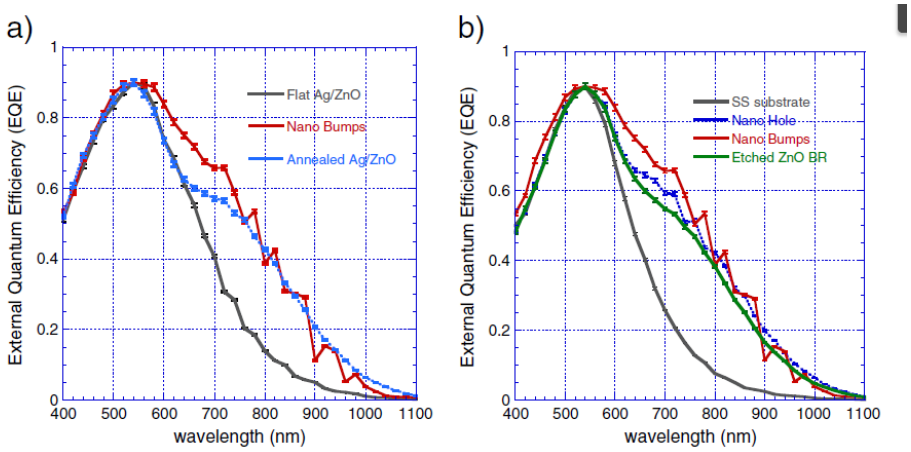

Figure A.6 : (a) Measured external quantum efficiency as a function of wavelength for nc-Si solar cells on the flat Ag/ZnO, randomly roughened Ag/ZnO and the nanobump photonic– plasmonic substrate. (b) Measured external quantum efficiency as a function of wavelength for nc-Si solar cells on the stainless steel substrate, nano-hole array randomly etched ZnO, and the nanobump substrate. The error bars are shown.

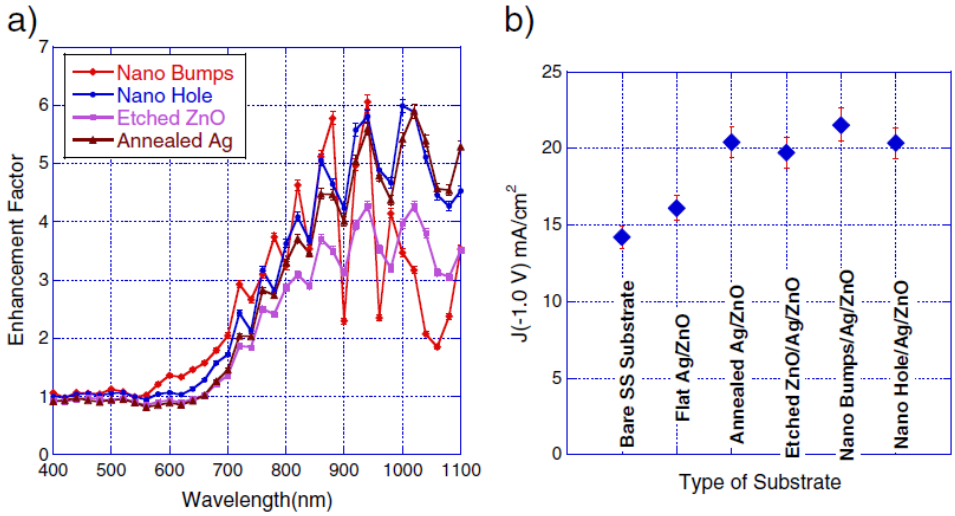

Figure 1.7: (a) Enhancement factor of quantum efficiency relative to flat silver, (b) Measured photo-current J(−1.0 V) for solar cells with different back-reflectors (with error bars).

www.manaraa.com

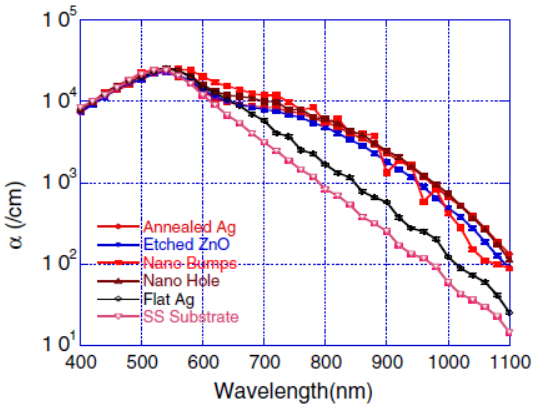

Figure 1.8: Calculated absorption corrected for thickness and reflection loss for the nc-Si devices on the different substrates (with error bars).

Conclusion

In conclusion The EQE for the photonic plasmonic BR exceeds that of the etched ZnO and annealed Ag BRs over a wide range (580–800 nm). Significantly the photo-current Jsc for the photonic plasmonic substrate is the highest (21.5 mA/cm2), exceeding that of the randomly roughened annealed Ag BR, the etched ZnO/Ag, by comfortable margins much greater than the experimental uncertainties. For maximum plasmonic enhancement the back nþ layer should be very thin so that the reradiated photons from the plasmonic effect are not absorbed directly into it. Our devices had relatively thick back nþ layers, 0.25 μm to avoid shorts. Calculations show the best effects when the n+ layer thickness is <100 nm. We chose absorber layer thickness of 1 lm, typical for micro-morph cells. These conclusions should be observed for other thicknesses. Although surface plasmons can cause losses in random BRs, a substantial fraction of light coupled into localized plasmonic modes at the Ag/ZnO interface may be re-radiated in optimized textured back reflectors,[193] and dynamical effects need further understanding. The randomly textured BRs were chosen to have very high diffuse reflectance. The periodic BR of photonic plasmonic nano-structures outperforms the best annealed silver randomly textured back reflector,

www.manaraa.com

illustrating the viability of the photonic plasmonic structure for advanced photon harvesting. A very interesting direction is to combine our plasmonic structure with random texture which will be addressed by the thesis work of another graduate student.

www.manaraa.com

APPENDIX B : ESTIMATION OF CAPTURE CROSS SECTION

Capture cross-section is an important parameter in the disordered semiconductor that has direct correlation with trap assisted recombination. Estimation of capture cross section is important for the fact that, it determines several important parameters related to the charge transport in a solar cell. Capture cross-section is firstly related to the attempt to escape frequency that we repeatedly used in our work to plot the distribution of defect states at the interface of donor and acceptor interface. We started our defect analysis with preliminary assumption of ν_o (attempt to escape frequency) to be 10^{12}/sec[170]. For our DOS plot, we used the following equation to predict the x- axis in terms of energy.

$$E\omega = E - E_{homo} = (k_bT)*\ln(\omega_o/\omega)$$

$$\omega_o = 2\pi\,\nu_o \quad \text{and} \quad \omega = 2\pi\,\nu$$

ν is the input frequency of perturbation and ν_o is the attempt to escape frequency. It was discussed in the literature,[179] about the freeze-out frequency where traps stop responding to the input signal and all capacitance response is essentially from the charge carrier in the band itself. Such is the condition when demarcation energy level is aligned with the Fermi level.

$$E_f - E_{homo} = K_bT\,Ln(N_v/p) = E_w = (k_bT)*\ln(\omega_o/\omega)$$

From the above equation we can estimate the value of ν_o which is roughly in the range of (5-8)E10 /sec. In all our experiment(from chapter 6 onwards) we have used 5E10/sec for DOS measurement except in chapter 5 where we have used initial assumption of 1E12 /sec. It's also mentioned in the seminal paper of T Walter et al[169] that ν_o is related to capture cross-section by the following equation.

$$\nu_o = 2*Cp*Nv$$

www.manaraa.com

Estimated capture cross section from the above equation was found to be 4-5E-11. Now here comes a contradiction. We know for SRH recombination, carrier life time can be calculated from the following equation.[200]

$$\tau = \frac{1}{Nt*Vth*\sigma}$$

With the fair assumption of N_t to be between (1-5E15/cm3) with thermal velocity of the charge carrier to be 1E7 cm/sec,[98] we estimate the lifetime to be 5E-13 sec. with a general assumption of carrier mobility to be 1-2E-4 cm2/v-sec[201-206], the $\mu\tau$ product will become roughly 1E-16 cm2/v, which is roughly 6 order of magnitude lower than the extracted value of $\mu\tau$ from the photo current vs bias experiment. This apparent deviation in the estimation of $\mu\tau$ product can be explained by the consideration of the nature of traps. For our estimation, we used the equation defined for SRH recombination theory in bulk where trap density is defined as purely as a bulk density in a unit per volume. However in our bulk hetero junction theory it is well proven that majority of recombination, whether trap assisted or bi-molecular are strictly happening at the vicinity of interface. This assumption is pretty good because, interface between donor acceptor is the place which account for the maximum amount of opposite charge carrier at any given time. So in the place of bulk defect density, our calculation must include an interface defect density. So we used a very simple technique as used by street et al[147] to change the bulk defect density estimation to an interface density expression.

We calculated the volume to area ratio for any given position inside the active layer.

The multiplication factor $= \frac{volume}{area} = \frac{(\frac{4}{3}\pi r^3)}{(4\pi r^2)}$=r/3

Assuming r= 10 nm (domain size), we get multiplication factor to be roughly 1E-6.

www.manaraa.com

So the apparent anomaly gets resolved when we use this multiplication factor to multiply total effective recombination centers at the interface. This gives a pretty smaller value of defect states per unit area(1E9-1E10/cm2).[147] This estimation of interface states can actually match the life time value and in turn $\mu\tau$ product pretty well to the experimentally extracted value as well as reported value elsewhere[147]. In all of our work, we plotted the bulk DOS. When interpreting the results, we must multiply the factor as described in this appendix to estimate the interface DOS.

www.manaraa.com

APPENDIX C : TECHNIQUE OF ESTIMATION OF FLAT BAND VOLTAGE

Flat band voltage is an important parameter repeatedly used in many semiconductor related device calculation. In our study, estimation of flat band voltage is important because of the measurement of density of states where the proposed equation can only be used with a known value of flat band voltage. In the section we will briefly see, how can we estimate flat band voltage in the organic thin film devices.

Flat band voltage is the forward voltage (externally applied) at which the forward bias dark current cancels all the photo generated current in the diode. In other words, flat band voltage is the voltage at which all the band bending in the thermal equilibrium (due to band alignment) are cancelled by an external applied bias. In a normal p-n junction diode, flat band voltage is the external bias that is equal to the built in voltage generated at p-n junction interface. This is based on the assumption that there is no voltage drop in the quasi neutral region at the either side of the junction.

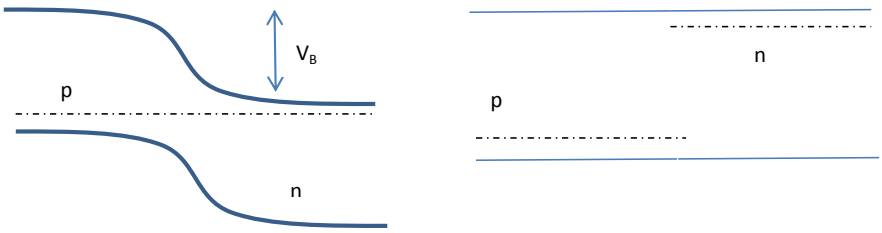

Figure C-1(a/b) : (a) energy band diagram of a p-n junction diode at thermal equilibrium showing built-in voltage, (b) Energy band diagram of same diode under flat band condition

There is numerous way of calculating the flat band voltage of a solar cell. One way is to measure capacitance as a function of voltage.(see figure C-2)

www.manaraa.com

$$\left(\frac{\mathrm{A}}{\mathrm{C}}\right)^{2} = \left(\frac{2\,(\mathrm{V}bi - V)}{\mathrm{q} \in 0 \in \mathrm{r\ Na}}\right)$$

From the above equation, at $V=V_{bi}$ measured capacitance should be infinite or conversely $[A/C]^2$ term should be zero. The intercept of the $(A/C)^2$ curve with voltage axis should help us to obtain the flat band voltage.

Secondly flat band voltage can be extracted from the photo current measurement as a function of external bias using lock in amplifier. This should give us a direct estimation of flat band voltage as photo current should be zero at the flat band voltage condition.

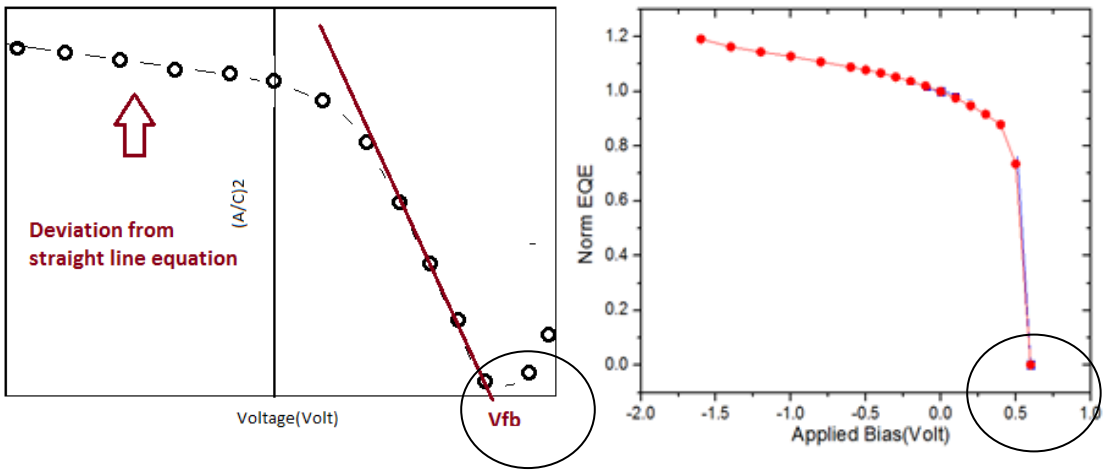

Figure C-2(a/b) : (a) Mott-Schottky plot of $(1/C)^2$ as a function of voltage with intercept of the plot with voltage axis showing V_{fb}, (b) Normalized EQE –Bias plot showing direct estimation of V_{fb}

By definition Voc plotted as a function of intensity can also help us to estimate flat band voltage in a solar cell. As we know open circuit voltage is the difference between the two separated quasi Fermi levels.

$$Voc = (\,E_{fn}\text{-}E_{fp})/q$$

If we increase the intensity (which will increase the generation rate as well as photo generated charge carrier) resulting in the band-ward shift of respective quasi Fermi level. This will

www.manaraa.com

lead to the increase in Voc upon increased light intensity. There will be an intensity beyond which change in intensity cannot move the Fermi level further as they have touched the band edge. Such voltage will represent the maximum separation in quasi Fermi level, thus flat band voltage of a solar cell. Experimentally such method is complex because of increasing the intensity of sun spectrum is difficult.

From the dark current, we can also estimate the flat band voltage.

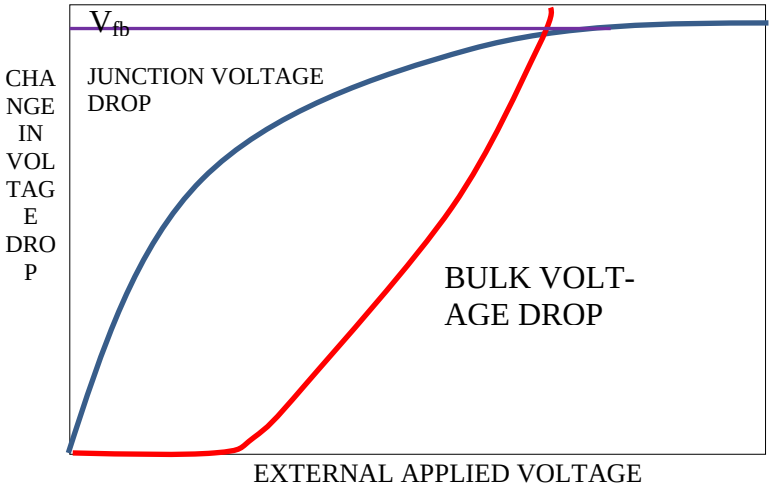

Figure C-3: Schematic of change in junction voltage and bulk voltage as a function of applied voltage. Saturation in junction voltage drop indicates the flat band voltage.

We know the well know equation for forward current in a diode as follow.

$$I = Io * \exp\left(q\frac{V-Vb}{nKT}\right) \qquad \ldots\ldots\ldots\ldots\ldots\ldots (1)$$

Where $Vb = I(V) * Rs$ [bulk voltage drop] and V is the external applied bias and Rs is the total resistance in series including bulk resistance and contact resistance. We extract the value of Io as well as n in the low and medium forward bias region to estimate the amount and type of recombination taking place at the interface. However higher voltage regime data remained un-used in most of the analysis. In the higher voltage of diode dark current, current is mostly following a

www.manaraa.com

summation of a linear (depending of series resistance and quadratic function (because of SCLC region due to high level injection at higher forward bias).

$$I = B * Vb + C * Vb^2 \quad (2)$$

$$Where \quad B = \frac{1}{Rs} \quad and \; C = \frac{9}{8} * \frac{\in o \in r * \mu o}{d^3} \quad (3)$$

Here d is thickness of entire charge transport layer, εo and εr are absolute and relative permittivity and μo is the zero field mobility of the active layer charge transport material. V_b is the voltage drop in the bulk while Vj is the voltage drop across the junction. At the flat band condition Vj will saturate and become parallel to Vapp (x-axis) while V_b will shoot up as can be seen in the figure C-3. As can be seen, equation 2 is a quadratic equation which can be solved with two possible roots. The equation can be rearranged as follow.

$$C * Vb^2 + B * Vb - I = 0 \quad (4)$$

$$Vb = \frac{-B \pm \sqrt{B^2 - 4C*I}}{2C} \quad (5)$$

First root of the above equation is $Vb1 = \frac{-B+\sqrt{B^2-4C*I}}{2C}$, second root $Vb1 = \frac{-B-\sqrt{B^2-4C*I}}{2C}$. Considering only the positive root we get,

$$Vb = \frac{-B+\sqrt{B^2-4C*I}}{2C} \quad (6)$$

Or

$$Vb = \frac{B}{2C} * [\sqrt{1 + \frac{4C*I}{B}} \text{ -1}] \quad (7)$$

As we know C is a constant and is inversely proportional to d^3 (thickness). Thus value of C is very high. If we assume $\sqrt{1 + \frac{4C*I}{B}}$ >> 1, then we end up with following equation.

$$Vb = \frac{B}{2C} * [\sqrt{\frac{4C*I}{B}}]$$

www.manaraa.com

Or $$Vb = [\sqrt{\frac{4B*I}{C}}\,] \quad (9)$$

Bulk voltage drop is proportional to current as with by square root with $\sqrt{\frac{4B}{C}}$ as proportionality constant.

Now we know $$Vj = V - V_b \quad (10)$$

Or $$Vj = V-[\sqrt{\frac{4B*I}{C}}\,] \quad (11)$$

$$\frac{dVj}{dV} = 0 \quad \text{at } V \geq V_{fb} \quad (12)$$

$$\frac{d\sqrt{I}}{dV} = \sqrt{C/B} \quad (13)$$

$$\frac{d^2\sqrt{I}}{dV^2} = 0 \quad (14)$$

From experimental dark current vs voltage graph we can estimate flat band voltage with the assistance of some assumptions as mentioned. Following figures show the derivative curve of dark current as we derived above. Finally flat band voltage can also be measured from the following equation in similar way we described only photo current measurement using lock in amplifier.

$$I_{ph} = I_{total} - I_{dark}$$

Flat band voltage estimated from CV technique always gave us a flat band voltage between 0.5 to 0.55 volt for regular P3HT: PCBM cells, while the open circuit voltages of our devices were 0.58-0.6 V. This lead to a confusion because flat band voltage should always be higher than the open circuit voltage. However both photo current vs bias plot and (light IV –Dark IV) gave us flat band voltage between 0.65-0.7 volt which is higher compared to the open circuit voltage. Dark current voltage analysis also indicated to a possible value of flat band voltage of around 0.6-0.62 volt which is in good agreement with other measurement results.

www.manaraa.com

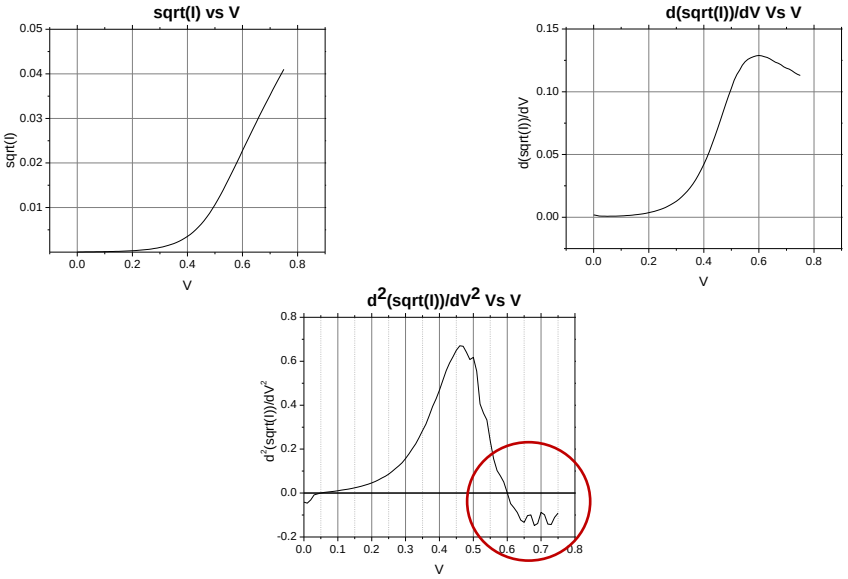

Figure C-3(a/b/c): (a) change in $\sqrt{I}$ as a function of external applied bias, (b) First derivative of curve plotted in figure (a), (c) Second derivative of curve plotted in figure (a). The voltage at which the curve touches zero can be considered as flat band voltage.

All the measurement technique assumes a diode with a single depletion region. However in organic bulk hetero junction, we get as much as three depletion region in the entire device as will be discussed later in appendix H. That makes the voltage drop analysis critical and complex. When measuring capacitance, we are not sure, which capacitance (which particular depletion region) or (charging and discharging of traps) is/are contributing to the capacitance measured by LCR meter. This ambiguity leads to faulty conclusion about the flat band voltage. For example we can have depletion region between (1) PEDOT:PSS –PCBM interface[$C_{d\text{-}pedot}$], (2) P3HT-PCBM interface[$C_{d\text{-}int}$], and (3) P3HT-Ca interface[$C_{d\text{-}Ca}$].

$$\frac{1}{[\mathrm{Ctotal}]} = \frac{1}{[\mathrm{Cd-pedot}]} + \frac{1}{[\mathrm{Cd-int}],} + \frac{1}{[\mathrm{Cd-Ca}],}$$

If we assume all the three capacitance are in series, Then what we get is [$C_{d\text{-}Ca}$], because other two are negligible because of very small depletion width (yet another assumption) as mentioned elsewhere[179]. This might explain why V_{fb} (CV) is always smaller than V_{fb} (measured by other technique and real V_{fb}). The flat band condition seen in C-V technique could be the flat

www.manaraa.com

band condition achieved in a particular interface (P3HT-PCBM) which is lower than the total band bending in the entire device. Some further study is required to determine the true nature of capacitance measured by LCR meter and its interpretation for bulk hetero junction organic solar cells.

www.manaraa.com

APPENDIX-D
EFFECT OF DIFFERENT HOLE TRANSPORT LAYER (HTL) ON PHOTO DEGRADATION OF POLYMER SOLAR CELLS

Introduction

In the chapter 5, we have observed that increase in the mid gap defect states can be correlated to the degradation of the polymer solar cells. However it is not found conclusively, what causes the mid-gap states to increase which increases trap assisted recombination in solar cells. In this appendix, we will investigate the role of hole transport layers(HTL) on the photo degradation of entire device performance because in such a multi-layer solar cell each layer could play a critical role in terms of stability of solar cells.

The role of hole transport layer was widely investigated for the ambient atmosphere related degradation in organic solar cell[49,207] for both standard and inverted architectures. However not much were reported on their role on the photo degradation phenomena of organic solar cells. In 2011 Ecker et al[208] reported that, HTL- active layer interface is responsible for the source of interface states which can affect the recombination dynamics and in-turn can affect the photovoltaic performances of the solar cell . In this appendix, we will investigate two widely used hole transport layer MoO_x and PEDOT:PSS as a hole transport layer and tried different baking/annealing condition before depositing the active layer film. We wanted to see if the degradation dynamics and the change in the fundamental device properties of the solar cell remain same with the photo degradation for different hole transport layers (HTL).

www.manaraa.com

Device fabrication

We followed the standard cleaning procedure to clean the commercially available ITO coated glass substrate. The substrates are first sonicated for 15 minutes in soap water filled petri-dish followed by cleaning them subsequently in de-ionized water in 3 separate cycle for 10 minutes each. This step is followed by a cleaning cycle by isopropanol-acetone-isopropanol separately for 10 minutes each. Finally before depositing the hole transport layer (HTL) the substrates are plasma treated in the plasma cleaner for 10 minutes. We deposited PEDOT:PSS as a hole transport layer outside the glove box(in air) at a spin rate of 5000 rpm for 40 second. While MoOx films were deposited by thermal evaporation inside the glove-box under high vacuum. All hole transport layers were baked at different temperature to see their effect on device performances as well as on their photo stability. In our experiment matrix, we used three treatment condition for baking our hole transport layer. Firstly un-annealed, annealed at 150^{o}C and annealed at 200^{o}C. In the next step we deposited P3HT:PC_{60}BM bulk hetero junction having a concentration of (17mg/ml) and mixed at a ratio of 1:1 by weight. The bulk hetero-junction was kept on hotplate constantly stirred at 65C for 24 hours before spin coating. The solution was spin coated at 600 rpm for 40 second. After deposition, the films were kept for drying under petri-dishes for roughly 20-30 minutes depending on the time solvents trapped inside the films get evaporated. Once the films are dried visibly(can be identified by the change in color), they are transferred to the hot plate inside the glove box and thermally annealed at 160C for 2 minutes followed by 110C for 10 minutes. The two-step annealing is done in order to get rid of the trapped solvent inside the polymer matrix as well as to crystallize the polymer domain. Finally the devices are transferred to thermal evaporator, where we have deposited cathode layer (Ca/Al).

www.manaraa.com

Pristine device performances

The fabricated devices were first measured under simulated AM1.5 solar spectrum (from ELH lamp). The figure D.1 describes the device performance as measured in the pristine condition. It should be noted that the short circuit current are observed to be lower for MoOx base device compared to PEDOT:PSS based device. The performances of the devices were summarized in the table D.1.

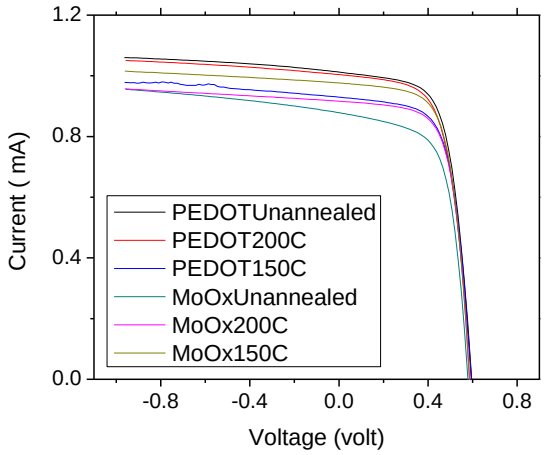

Figure D.1 Light IV measured of P3HT:PCBM blend cell measured under 100 mW/cm^2 ELH lamp –made on differently treated hole transport layer. (contact are -0.106 cm^2)

DEVICE/CONTACT	Voc	Isc	FF	PCE	HTL	TREATMENT
S161A-CT2	0.596	1.01	67.4	3.83	PEDOT:PSS	NO ANNEAL
S161B-CT2	0.595	1	65.4	3.67	PEDOT:PSS	200 C
S161C-CT1	0.595	0.929	67.9	3.54	PEDOT:PSS	150 C
S161D-CT4	0.58	0.875	66.4	3.18	MoOx	NO ANNEAL
S161E-CT6	0.586	0.914	69.2	3.50	MoOx	200 C
S161F-CT2	0.587	0.974	68.5	3.69	MoOx	150 C

Table D.1: pristine device performance comparison for devices made on different heat treated htl

Since the devices with different HTL are not identical, the percentage of change in the device performance and several other fundamental device parameters over photo exposure could be a way for overall comparison. In this set of experiment we have only varied the thermal treat-

www.manaraa.com

ment condition of the hole transport layer while left other experimental parameter constant. We exposed each of the solar cells to 2x intensity (ABET solar simulator) for 24 hours under continuous flow of nitrogen. The inside chamber temperature were kept constant to room temperature by a fan running during the light exposure. Except the device with un-annealed MoOx – rest of the device shows almost similar device performances. To understand further, we measured density of states by capacitance spectroscopy as described in the section 4.2.6. Estimated DOS of different devices show that defect states located at the interface of the donor and acceptor is highest for the device with MoOx without annealing. This again corroborates that higher trap assisted recombination could be a dominant source of loss and might have reduced solar cell performance as observed before.

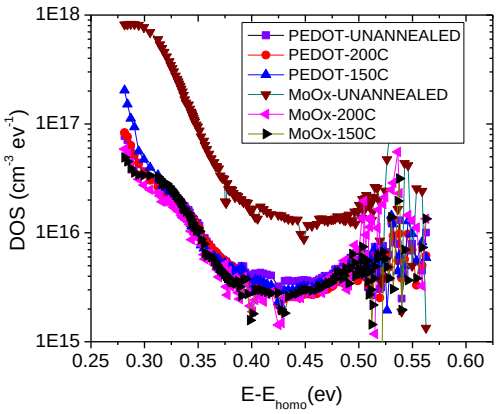

Figure D.2 DOS measured on pristine device made on different HTL (different heat treated)

The DOS data was found to be very noisy closer to mid-gap because of raw capacitance measured at very low frequency. Nevertheless, the DOS shows uniformity for almost all the devices except the un-annealed MoOx based device. This explains almost uniform open circuit voltage for the entire device as summarized in the previous table. It is not yet clear why trap density for un-annealed device higher than the rest.

www.manaraa.com

Photo degradation – in-situ drop

To understand, if underlying layer has any role to play in the photo degradation process, we exposed the entire batch of samples one by one to the exposure condition as described in the previous section. The following set of figures (D.3) show the percentage of drop of different solar cell parameters for same exposure condition. In addition to the percentage drop,

Unlike the general perception about the MoOx based device as being more air stable, it was found that PEDOT :PSS based devices recorded higher photo stability in comparison to MoOx based devices. Secondly it can be observed from the figure D.3 that un-annealed MoOx device recorded highest photo instability with the drop of efficiency of about 37% within first 24 hrs. Thermal treatment of MoOx layer improves the condition and reduces the percentage of drop in solar cell performance. Since all HTL forms the seed layer for subsequent active layer blend film, the surface roughness of the bottom layer could be a driving force for the determination of active layer morphology. In addition to that, another interesting observation can be made. The drop in open circuit voltage is almost similar with 1-2% deviation in their percentage of drop.

The short circuit current as well as fill factor drop follows a different pattern suggesting two different photo degradation dynamics going simultaneously in the device. It could be because of the fact that, open circuit voltage is a logarithmic function of short circuit current. So the change in open circuit voltage will be smaller as compared to short circuit current. However If trap assisted recombination is the only source of loss mechanism originating in the solar cells due to prolonged light soaking, the effect would be similar for all the devices because active layer films were deposited by following the same recipe. This is not the case that we observed experimentally. It is further substantiated by repeating the same experiment in a subsequent batch to reproduce the pattern. The data follow exactly the patter of the previous batch. In a later appendix

www.manaraa.com

(while discussing about the effect of active layer morphology on the photo degradation of organic solar cell), the phenomena was observed repeatedly which strongly indicate a second loss mechanism involved in the solar cell which is a function of active layer morphology.

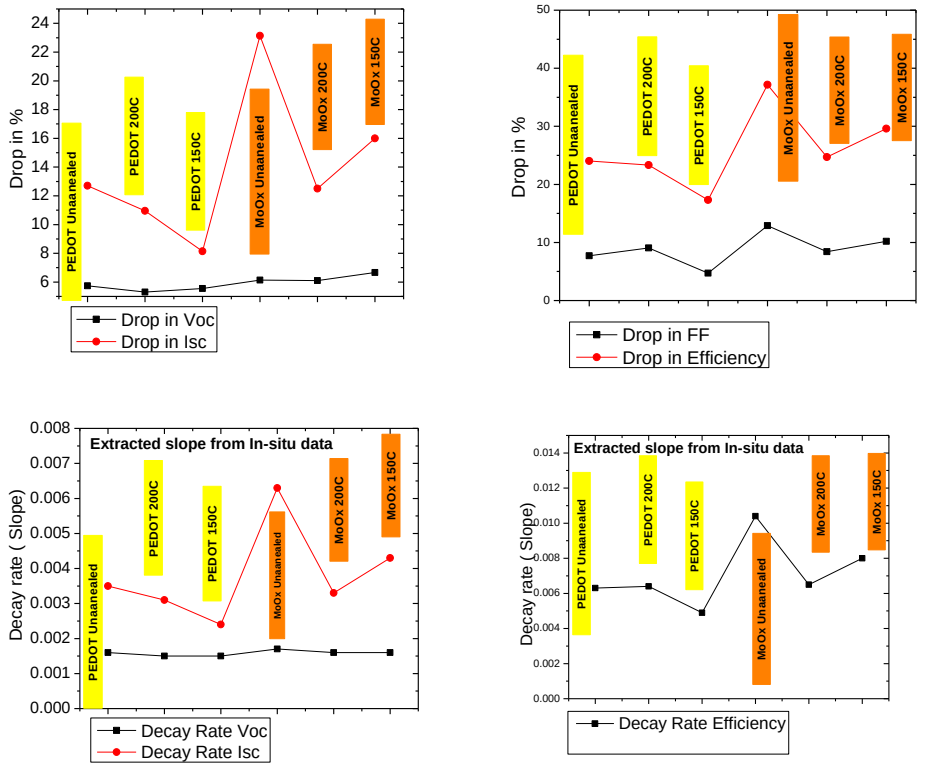

Figure D.3 % of drop recorded after exposure) for different devices in (a) Voc and Isc, (b) in FF and Efficiency (c) Decay rate measured for different device of Isc and Voc (d) decay rate in efficiency

To investigate the morphology of the active layers on different substrate, we measured the surface roughness of all the devices after the photo degradation experiment was completed on them. Following figure D.4 shows the variation of surface roughness with different hole transport layer used in the experiment. It is interesting to note that the surface roughness measured by AFM(atomic force microscopy) is showing a strong correlation between the drop in photo current after 24 hours light exposure. The device with highest surface roughness recorded

www.manaraa.com

highest photo degradation while the device with lowest active layer roughness (150 C PEDOT) showed lowest drop in photo current.

We also measured the surface roughness of the substrate coated with 10 nm MoOx treated with same temperature as in the above experiment to see if that changes the surface roughness property of the substrate in any way. The summary of surface roughness suggests that it's true that thermal annealing reduces the surface roughness but in very small in magnitude (nanometer scale even within the 2% error bar). How such small change in substrate roughness is leading to a bigger deviation in the surface roughness of the active layer above the HTL is yet to be under-stood.

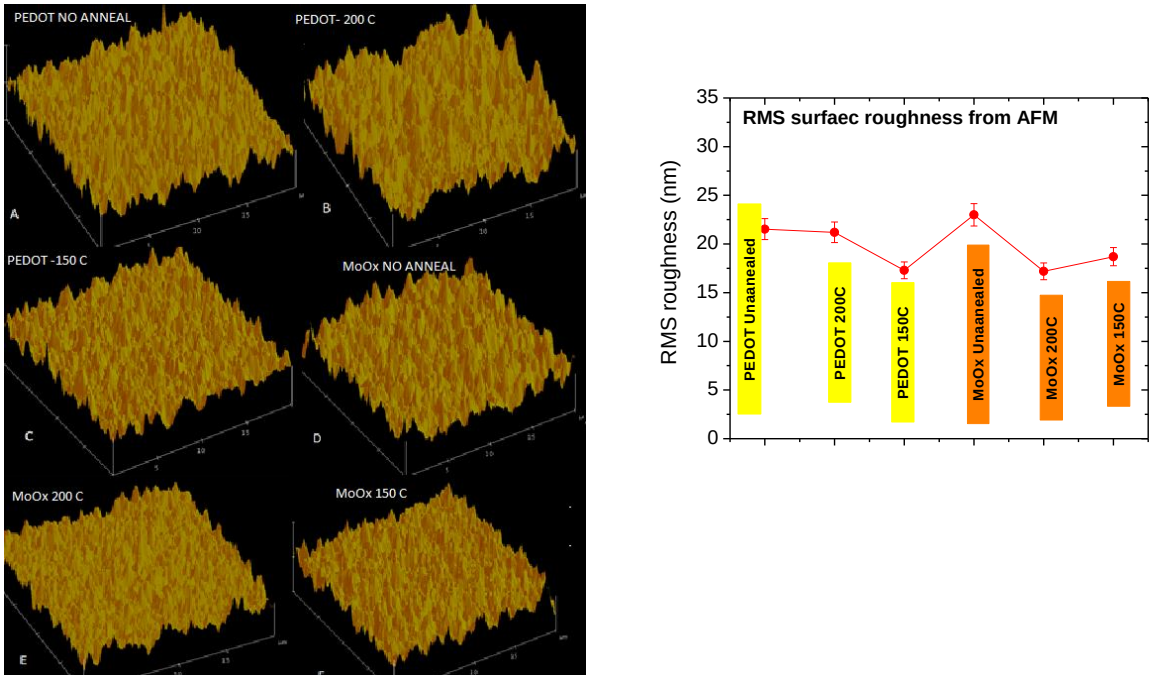

Figure D.4 (a) AFM images of sample surface made on different heat treated substrate.(b) RMS roughness variation for different P3HT:PCBM blend device made on differently treated substrates.

www.manaraa.com

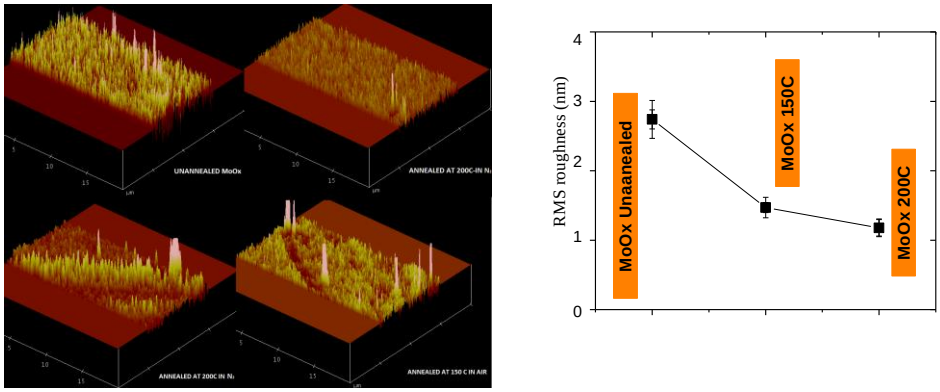

Figure D.5 (a) AFM images of substrates only coated with MoOx (10 nm) with different heat treatment (b) RMS roughness variation for MoOx coated substrates (10 nm) with different heat treatment.

Quantum efficiency

We further studied the quantum efficiency of the devices exposed to 2x sun spectrum and calculated the drop ratio for every device. The drop ratio is the ratio of QE taken before to QE taken after the exposure. The EQE ratio can be directly correlated to the drop in photo current after degradation. It also shows that certain wavelengths have higher drop in quantum efficiency compared to others. We yet to find a reason behind the wavelength dependence of photo current drop in bulk hetero junction.

(b)

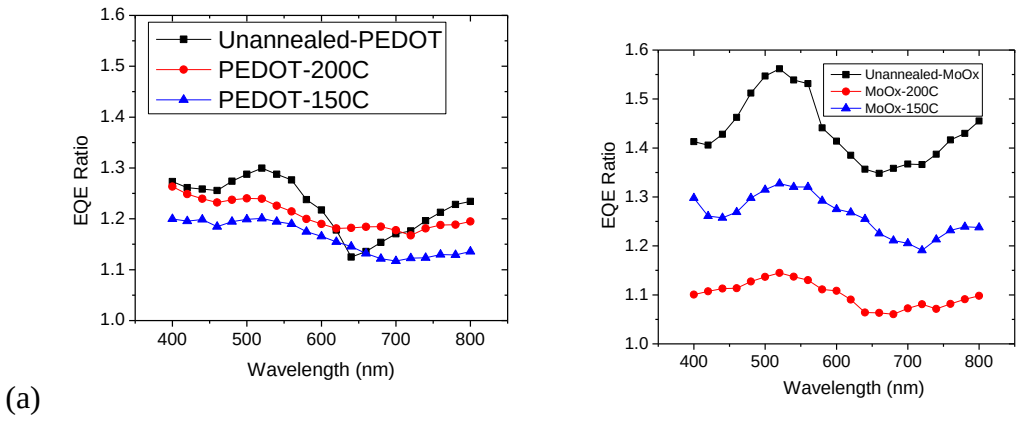

(a)

Figure D.6 (a) EQE drop ration (Non degraded /Degraded) as a function of wavelength for different PEDOT:PSS based device (b) EQE drop for different MoOx based device

www.manaraa.com

In case of SRH recombination at the D-A interface, the rate of recombination should precisely be a function independent or weakly dependent of photon wavelength. So recombination based loss should be wavelength independent or at least marginally dependent for small signal measurement condition. However such dependence of the drop in the absolute EQE with photon wavelength is again suggesting a second dynamics for the loss in photo. A better way to check the wavelength dependence of trap assisted recombination is to check the variation in $\mu\tau$ as a function of different wavelength. To check the wavelength dependence of $\mu\tau$, we measured photo current of a standard P3HT:PCBM sample from -1 volt to 0.6 volt range at different wavelength ranging from 400 nm to 700 nm. This wavelength range includes photon taken broadly from the in band absorption to sub-band-gap absorption. The photo current was then normalized with respect to the photo current at the short circuit condition for respective wavelength for the purpose of comparison. Later the same numerical expression[145] was used to extract mobility – lifetime product as discussed in the section 4.2.11 previously. As can be seen in the figure D.7, The normalized photo current Vs bias shows very small dependence on the wavelength. It's true that for 400 nm (in purple) shows less bias dependence compared to other wavelength. It could be due to the fact that at 400 nm number of generated charge carrier is low in comparison to other wavelength which lead to less separation in quasi Fermi level and less mid gap trap which can work as an effective recombination center. However such small variation in bias dependence is only for the small signal condition where light intensity is significantly smaller (which is used for all quantum efficiency measurement).

www.manaraa.com

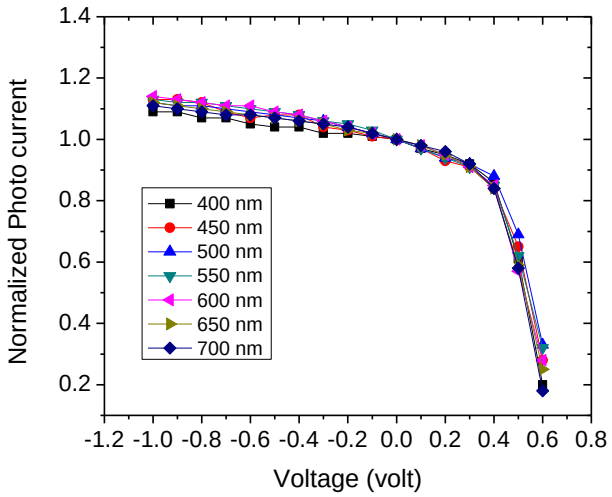

Figure D.7 Normalized photo current as a function of voltage for standard P3HT:PCBM solar cell measured at different wavelength to estimate mobility-lifetime product.

The extracted value of μτ was calculated to approximately 9E-10 cm^2-v. That number remains quite similar over the range of wavelengths of interest. As we know, μτ product is an important benchmark parameter for any disordered material and strongly depends on the rate of trap assisted recombination; we can conclude that in organic solar cell amount of trap assisted recombination do not vary over the range of wavelength available in the spectrum. This shows that, any drop in photo-current due to the increase in trap assisted recombination should be uniform across the spectrum. Such non-uniformity observed in the figure D.6 could be because of any second dynamics or it could be simply a scaling issue while plotting the experimental data.

Dark iv measurement

Now we want to see if we can explain the drop in open circuit voltage as well by dark current measurement. To understand the changes in open circuit voltage as mentioned in the previous section, we measured dark current before and after the degradation and compared to the enhancement in both the Io/n.

www.manaraa.com

Io and n were extracted from the measured dark IV and summarized in the figure D.8 which shows both Io and n extracted before and after the light exposure. The enhancement factors for both Io and n are also plotted in figure D.8.C. Interestingly the increase in Io is roughly 6-7 times the pristine value and also can be correlated with the open circuit voltage measured before and after the photo degradation.

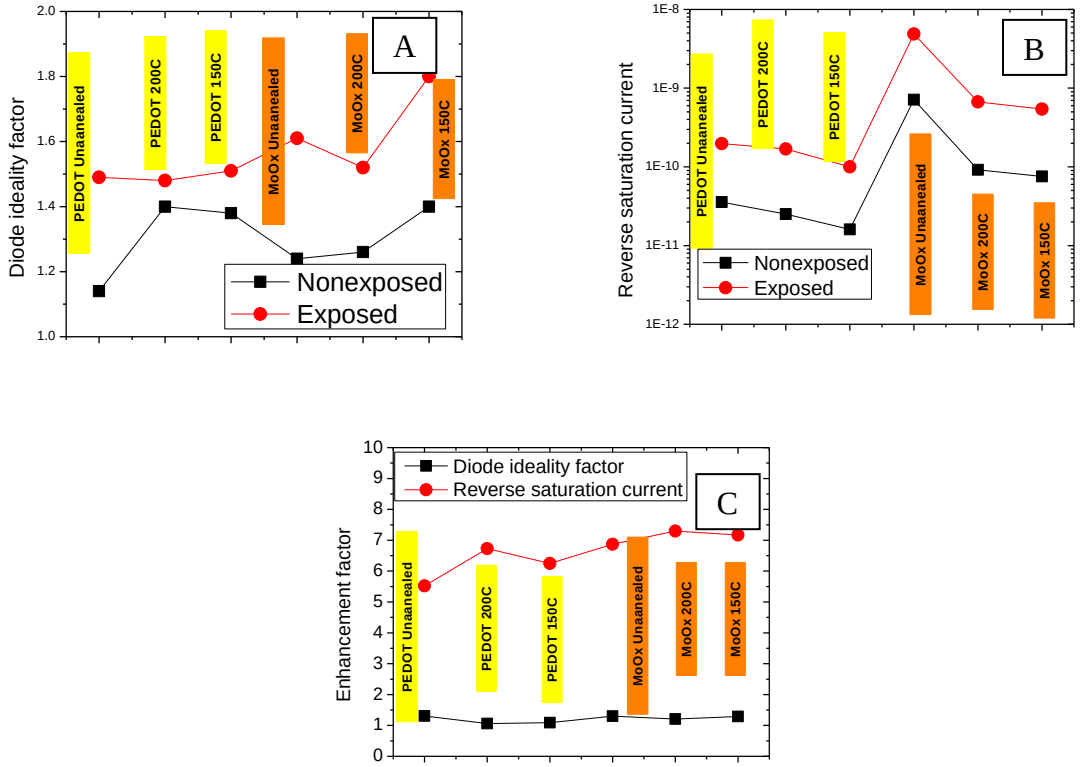

Figure D.8 (A-B) variation in diode ideality factor / reverse saturation current for different device made on different HTL. (Enhancement factor plotted for different devices made on different HTL after 24 hrs -2X light exposure.

Mobility measurement

We also wanted to see if the intrinsic polymer mobility of polymer changes with time of exposure. For that we made a same set of sample with similar hole transport layer and respective treatment. We deposited P3HT polymer on different substrate by spin coating and treated the

www.manaraa.com

films in exactly similar way as the blend based devices. We deposited an electron blocking layer (MoOx) on top of the film to make the device a resister which can only transport holes. Then we exposed the samples to light of 2x intensity (same spectrum) for 24 hours. During the light exposure, we measured hole mobility of polymer at different time by space charge limited current technique. The measured mobility and extracted resident charge carrier concentration shows no sign of reduction during the time of exposure. In fact for some devices (eg. PEDOT -150C annealed or MoOx -150C), it shows increase in hole mobility, which is apparently counter intuitive. Increasing mobility might be indicating to the growing domain size of polymer or at-least reduction in disorder in the polymer domain itself. Increasing domain might result in lesser number of successful charge separations leading to fewer separated charge carrier which can explain in increase in photoluminescence after light exposure observed in chapter 5.

Resident charge carrier could be used as a doping density in the organic semiconductor. There are several reports that suggest that photo exposure leads to the oxidation which increases the dopant density in the polymer and make it predominantly p-type. The extracted hole mobility and resident charge carrier concentrations are plotted in the figure D.9. It shows that, there is no change in mobility as well as resident charge carrier concentrations during the light exposure. This suggests that no such change in doping density is actually taking place in the polymer during the photo exposure. Since we have already experimentally shown that the creation of new defect states at the interface that might have effective role in the trap assisted recombination, It can be concluded that extra states that are getting created is not because of photo-oxidation incorporation of more dopant in the polymer itself. Also it can be said that interface states created due to light soaking are not affecting the bulk mobility of the polymer domain.

www.manaraa.com

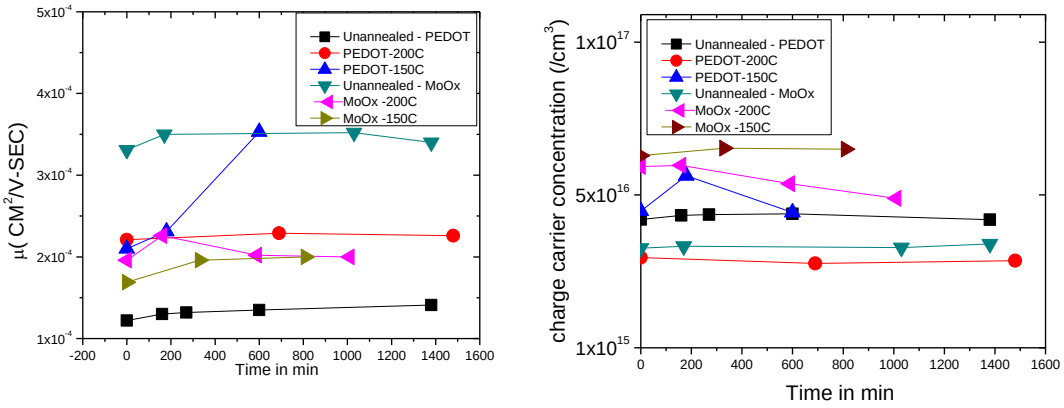

Figure D.9 Change in mobility over time for different device under same illumination, (b) Change in carrier concentration over same exposure time –same intensity of exposure for different P3HT only sample on different HTL.

XPS measurement on different thermal treated MoO_x substrates

It was repeatedly observed in this batch of experiment that thermal treatment on MoO_x (thermally evaporated) film can enhance not only the device performance over its un-annealed counterpart, but also helps in making much more photo-stable solar cells. What happens to MoO_x film chemically or better to say in terms of stoichiometry of the film?

In order to find the answer, we performed XPS(X-ray photo electron spectroscopy) on four different MoO_x films coated with thermally evaporated MoO_x on top of standard ITO coated glass substrate. Three films were thermally treated in the similar way we used them for the devices. The measured XPS in the figure D.10 shows two dominant peaks at the binding energy of 233 ev and 235.5 eV for MoO_3 . For un-annealed MoO_x these two peaks are only visible. When we increased the annealing temperature, we observed an increase in the shoulder of both the peak. When we de-convoluted the shoulder, we found the peaks to be located at 231 ev and roughly at 234 ev. The intensity of the two peaks was increasing with increasing annealing temperature. It's already experimentally shown[205] that these peaks are signature of MoO_2 oxidation states. It's already known that MoO_2 state are more conductive compared to MoO_3 states.

www.manaraa.com

Scanlon et al experimentally showed that MoO_2 behaves more metallic compared to MoO_3[209]. This explains why FF of the Thermal annealed MoO_x cell are higher compared to it un-annealed counterpart.

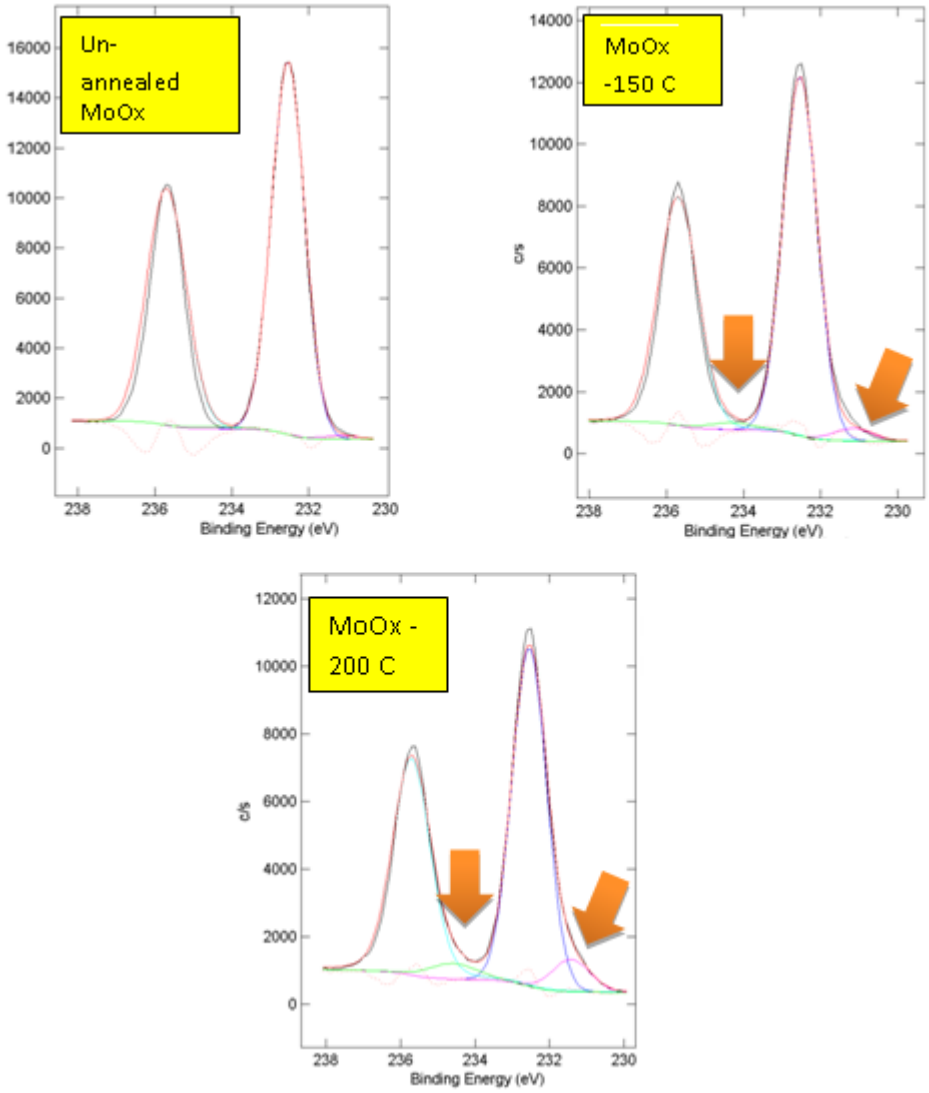

Figure D.10 Change in MoO_x XPS spectra for different temperature treated MoO_x film (10 nm)

The change in the chemical property of MoO_x can affect the series resistance of the HTL resulting in higher fill factor for the solar cells with MoO_x HTL. However it's not yet clear, what makes the solar cell more photo-stable when MoO_x are treated thermally. More detail investigation are required to address this question.

www.manaraa.com

Conclusion

In this appendix we have tried to understand the role of hole transport layers on the device performance and photo stability of organic solar cell. We observed that, for same intensity of light exposure, drop in open circuit voltage is almost similar for all the devices irrespective of their type of HTL. However short circuit current drop is different. The similar drop in Voc can be correlated to roughly same amount of increase in Io(reverse saturation current which is directly related to mid-gap state density. Although not clearly understood, we found that underlying HTL can affect the active layer film morphology and also has a direct correlation between the drop in photo current. We measured in-situ mobility and resident charge carrier concentration in polymer only devices and their change upon light illumination and found that, prolonged light exposure do not increase free carrier concentration which eliminates the possibility of photo-oxidation. We also studied, why fill factor of annealed MoO_x HTL improves upon thermal treatment. With increasing annealing temperature, MoO_2 oxidation state increases which increases conductivity of HTL film. However we do not know yet, what happens to MoO_x thin film under prolonged light exposure alone, which could a separate study altogether.

www.manaraa.com

APPENDIX-E
EFFECT OF DIFFERENT ACTIVE LAYER MORPHOLOGY ON PHOTO-DEGRADATION

Introduction Anode inter-layers were shown to have an impact on the photo degradation of bulk hetero-junction solar cells in the appendix D. In this appendix we are going to study, how different active layer morphology can affects the photo degradation kinetics. In order to see the effect of different active layer morphologies on photo-degradation, we carefully planned a set of experiments. Firstly, we made a batch of cells with different pre-production annealing temperature ranging from non-annealed to180^{o}C annealing for same time (10 min). We kept other experimental parameters constant in-order to make a meaningful comparison. Other experimental condition include, polymer fullerene blend ratio, concentration, HTL coating recipe, spin rate and time for active layer and cathode materials etc. In the second set, we made solar cells from different blend concentrations. Concentration is an important parameter and can control the internal morphology as well as thickness of bulk hetero-junction active layer films.

Device with different annealing condition

It is well known that thermal annealing helps in changing the internal morphology of bulk hetero-junction solar cells[95,128,210-215]. Sole purpose of using thermal annealing after active layer deposition by spin coating, is firstly to remove the residual solvent trapped in the thin film active layer made from the blend solution. Secondly, it was also found that thermal annealing improves the crystallinity of polymer domain by the re-organization and improved packing.[125,128,216] It is also found that thermal annealing improves the hole mobility with increasing annealing time and temperature[217], which is also an indication of improving charge transport in the polymer domain.

www.manaraa.com

In this set of experiment we made five devices with five different thermal annealing conditions. We used PEDOT:PSS (PH4083) spin coated at 5000rpm for 40 second followed by a baking at air in 150^{o} C for 20 minutes. Then the samples were transferred to glove-box and active layer blend was spin coated at 400 rom for 40 sec. The active layer blend was made from (1:1) P3HT (Solaris-chem) and PCBM (Nano C) material. Once the films were prepared, they were dried first by covering a glass petri-dish to remove the residual solvents. Later the devices were annealed on hot-plate at different temperature ranging from 90^{o}C- 180^{o}C. Finally calcium (25 nm) were thermally evaporated as a cathode interface layer followed by a thermal evaporation of 120 nm of aluminum as top metal contact.

Initial device performance comparison

In this section we will first see how solar cell performance changes with changing annealing temperature. The light IV in the figure E.1 shows some non-uniformity in Voc/Isc and FF for different annealing temperature. The values of different parameters were summarized in the following three figures.

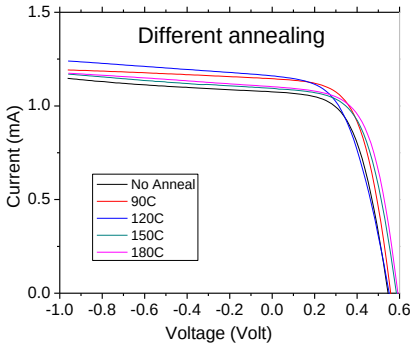

Figure E.1 light IV measured for devices (active layer annealed at different temperature.

First observation from the figure E.2 is that, with increasing annealing temperature open-circuit voltage increases and varies from 0.55 volt to 0.59 volt approximately. Secondly short

www.manaraa.com

circuit current attains a maximum value at around 120^{o} C and then drops further with increasing annealing temperature. Further FF also shows continuous increase with increasing temperature.

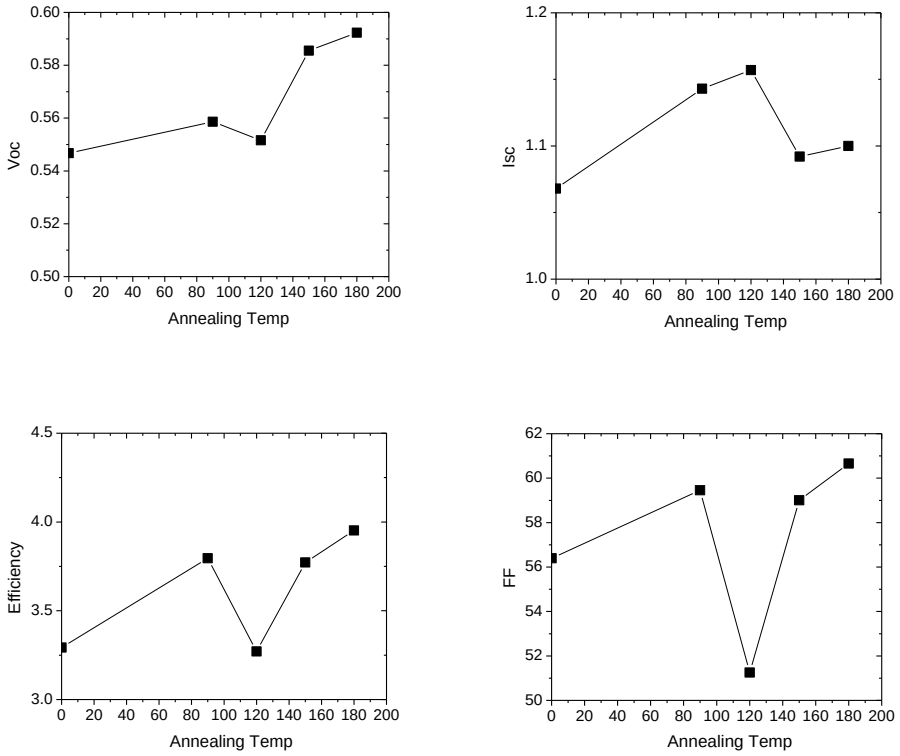

Figure E.2 Variation of Pristine Isc, Voc, FF and Efficiency for different annealed device

We have also measured dark current and defect density to see what changes are taking place to both interface defect states as well as reverse saturation current which is also a parameter strongly dependent on interface of donor- acceptor. It can observed from the figure E.3 that the entire defect distribution is going down with increasing annealing temperature until 150^{o}C and then at 180^{o}C, DOS starts increasing further from the DOS value estimated for 150^{o}C condition. Extracted Io shows drop with increasing annealing temperature from approximately 4E-10 Amps to 4E-11 Amps (an order of magnitude). This reduction in interface defect states can actually be

www.manaraa.com

well correlated to the change in open circuit voltage which is a direct function of Io which we extracted from dark current measurement.

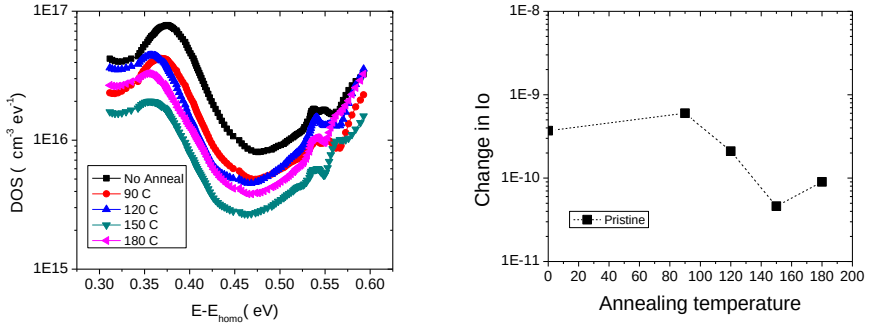

Figure E.3 Change in DOS –PRISTINE DEVICE, (b) Change in Io for –PRISTINE DEVICE

We also measured EQE vs external bias experiment to see, how different thermal treatment can affect the charge collections from the interface. This EQE vs Bias experiment is also important to extracted mobility –life time product which is an important indicator of device performance from the bias dependent charge collection perspective.

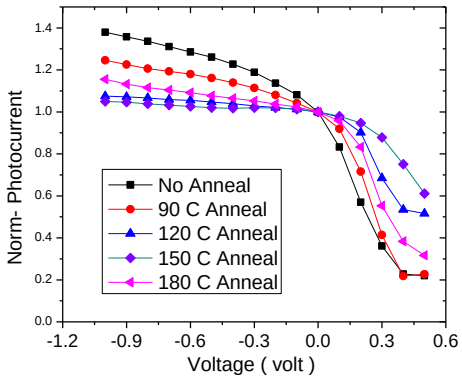

Figure E.4 Change photocurrent- voltage for different thermally annealed device

Clearly it can be seen from the above figure E.4 that un-annealed device shows very high bias dependence compared to other annealed device. The bias dependence is reduced with increasing annealing temperature which is again in good agreement with the previously shown re-

www.manaraa.com

sult of defect state distribution as well as reverse saturation current in the figure E.3, where we have seen the reduction in the defect states with increasing annealing temperature. Best device (flat reverse bias photo current) was obtained for 150^{o} C annealed device which also shows lowest defect density as well as lowest Io as previously shown (figure E.3). The extracted mobility – lifetime products were plotted as a function of annealing temperature. The figure E.5 shows a clear trend of increasing mobility life time with increasing annealing temperature. The observed sudden drop at 150^{o}C could be an outlier in the experiment. Nevertheless this shows a good agreement with the change in defect states where DOS drops with increasing temperature. This experiment helped us to explain the change in the device performances with different annealing temperature. In addition to these electrical experiments, we also did AFM to see if this thermal treatment of active layer has any effect on the surface property (mainly the roughness) of active layer films. The figure E.6 shows how surface roughness changes with different annealing conditions. It can be seen that the surface roughness are actually decreasing with increasing annealing temperature.

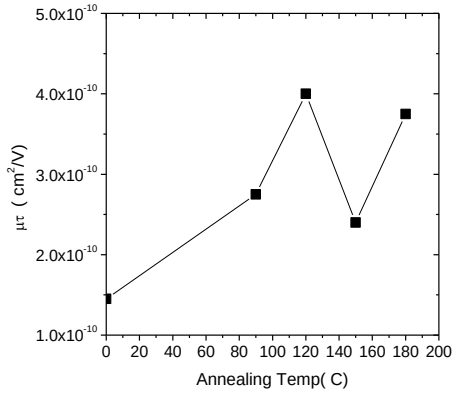

Figure E.5 Change in mobility –lifetime product for different annealed devices

www.manaraa.com

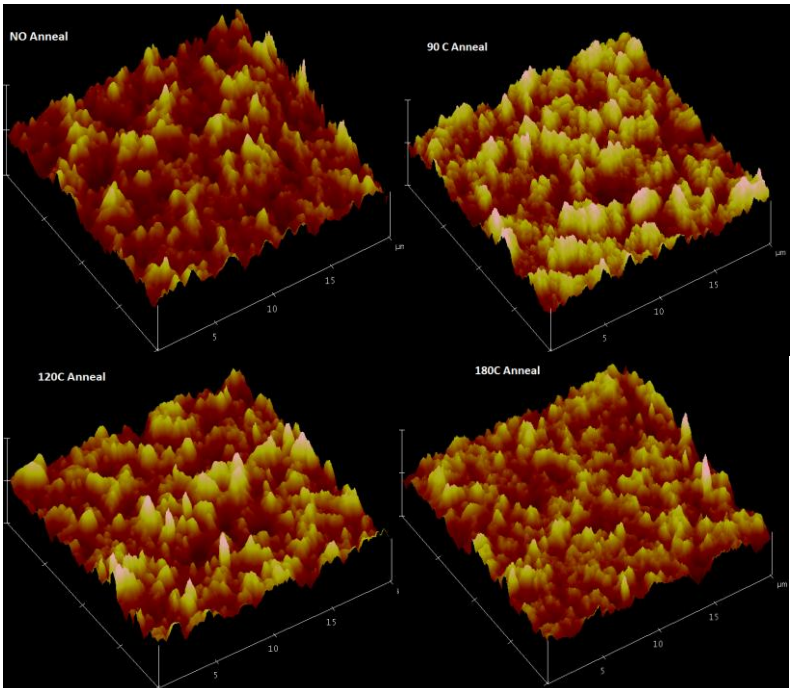

Figure E.6 3d surface image from AFM for different annealed (active layer) devices

Photo-degradation of different annealed devices

In this section, we will discuss about the effect of photo degradation on devices whose active layers were annealed at different temperature. A dot from each device was exposed to light spectrum of 2x intensity for 24 hours. Then electrical properties were measured and compared to the property of a non-exposed dot. The following figure E.7 shows how different parameters of solar cells have changed after the light exposure. It can be observed that the drops in Voc, for the entire batch of device are ranging between 4.5% to 6%. However short circuit current drop varied between 20% (max) to 7%(min).

www.manaraa.com

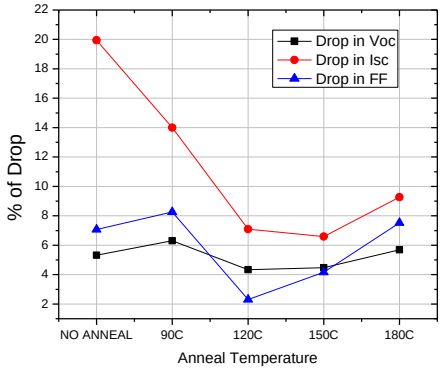

Figure E.7: Percentage of drop in Isc/Voc and FF for different annealed sample upon photo exposure(2x-24 Hrs)

An initial observation suggests that device without anneal shows maximum drop in current while device annealed at 150 C presents minimum photo degradation in short circuit current. The following figure shows in-situ drop in Isc/Voc for different device. The figures also show that un-annealed device recorded a maximum drop in Isc while annealed at 180^{o}C recorded lowest drop. It is interesting to note that, the drop in Voc is almost same for all the devices as observed previously.

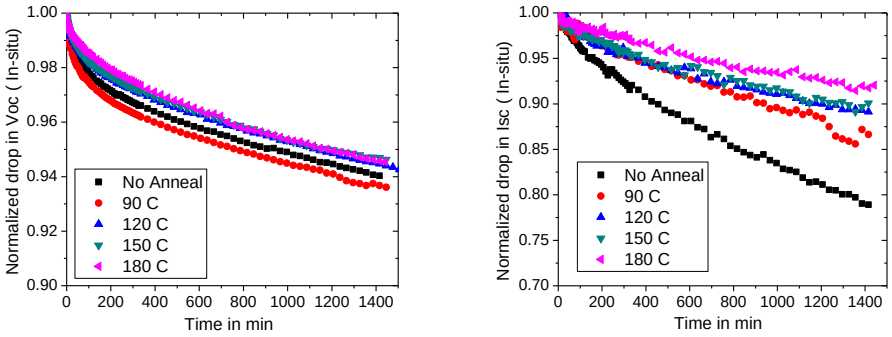

Figure E.8 In-situ drop recorded for different annealed sample

www.manaraa.com

Next we wanted to measure dark current and see how drop in Voc/Isc can be explained by the change in extracted Io (reverse saturation current). Figure E.9 shows how reverse saturation

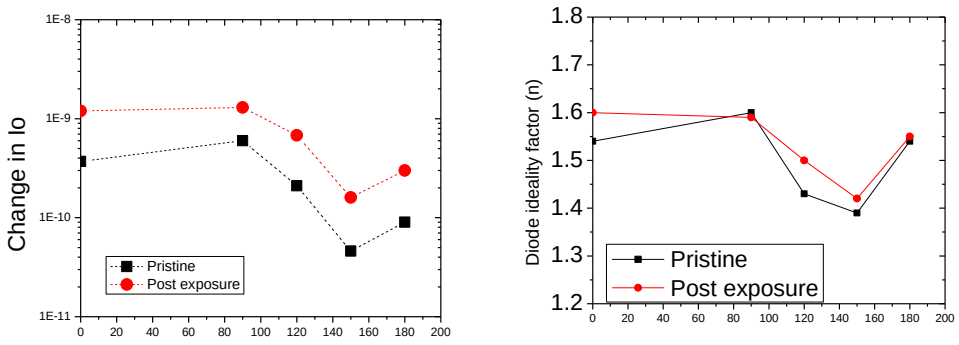

Figure E.9(a) Change in Io(reverse saturation current) for different devices, (b) Change in n(ideality factor) upon exposure to light (2x- 24 Hrs)

current and diode ideality factor have changed after light exposure for different sample. Interesting thing to notice here is the increase in Io is almost similar for all the device of different annealing condition. When we summarized the enhancement factor for Io in figure E.10, it can be observed that on an average Io changed around 3-3.25 times over its pristine value. However ideality factor didn't seem to change much from its pristine value.

The change in Io/n is well correlated with the change in Voc. It can be said that the amount of trap assisted recombination is almost similar for the entire device irrespective of annealing condition. It's only the drop in photo current that finally reduced the solar cell efficiency drastically. We also measured DOS for different devices and calculated the factor by which DOS increased after photo exposure (see figure E.10). It can be seen that the recorded increase in DOS is between 2-3 times between 0.5 ev to 0.6 ev. At the same time the enhancement factor for different annealed sample remained same. This resembles the change in Io closely and again sub-

www.manaraa.com

stantiate the fact that drop in V_{oc} is strongly correlated to the amount of change in Io and DOS. Further we plotted the drop factor of mobility-lifetime product extracted from EQE vs bias experiment. The drop factors obtained are in good agreement with enhancement factor in Io and DOS.

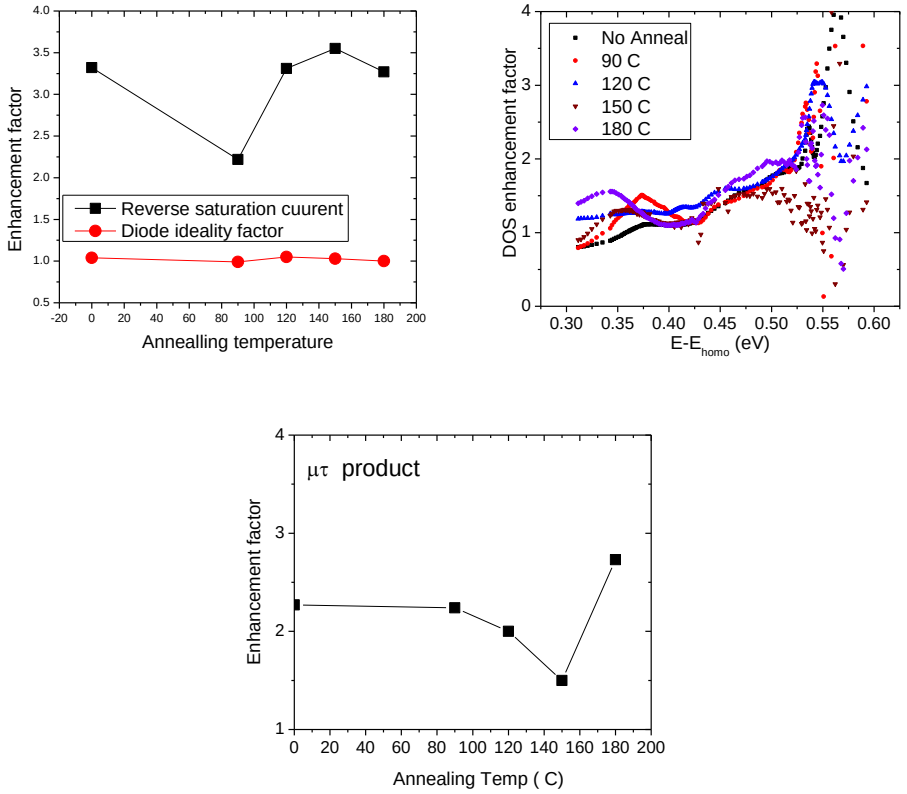

Figure E.10 (a-c) Enhancement factor for Io, n , DOS , mobility lifetime product for different sample upon light illumination

Further we measured absolute EQE and calculated the drop ratio for all the devices (see figure E.11). It was found that, un-annealed device show greater drop in comparison to rest of the device. Higher annealed device showed lesser drop in photo-current, have much flatter and uniform drop across all wavelengths.

www.manaraa.com

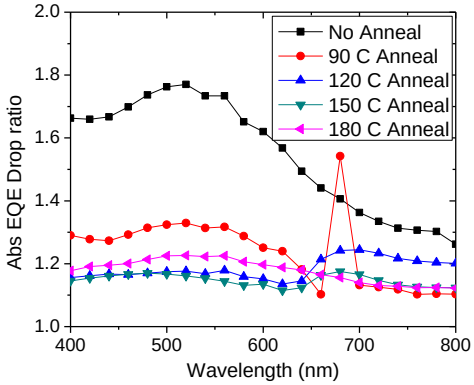

Figure E.11 EQE drop ratio plotted as a function of wavelength for different annealing temperature.

Device with different concentration

In this subsection we have changed the internal morphology and thickness by changing the concentration of polymer in the blend solutions.[214,218-220] We used PEDOT:PSS (PH4083) as HTL and spin coated at 5000rpm for 40 second followed by a baking step in air at 150 C for 20 minutes. Then the samples were transferred to glove-box and active layer blend was spin coated at 400 rom for 40 sec. The active layer blend was made from (1:1) P3HT (solaris-chem) and PCBM (Nano C) material of two different concentration (10 mg/ ml and 15 mg/ ml). Once the films were prepared, they were dried first by covering a glass petri-dish to remove the solvent slowly for improving crystallinity. Later the devices were annealed on hot-plate at 160^{o}C for 2 min and then 110^{o}C for 10 min. Finally calcium (25 nm) were thermally evaporated as a cathode interface layer followed by an thermal evaporation of 120 nm of aluminum as top metal contact.

Initial device performance comparison

In this subsection we will analyze the differences between the devices made from different concentration. For obvious reason device with lower concentration are expected to show less

www.manaraa.com

photo current because of thinner film and lesser optical absorption. At the same time the polymer domain are expected to show less crystallinity with fullerene molecule tend to make better percolation to improve the charge separation. This is expected to increase the overall fill factor (FF) of the device. The following light IV (figure E.12a) shows expected behavior from the pristine device with different concentrations. For concentration of 10 mg/ml, short circuit current is almost 21 % lower compared to 15 mg/ml device. We also measured EQE and compared in the figure E.12b. It can be observed that The EQE for 15mg/ml device is not only higher than its counterpart but also shifted towards red wavelength. This result is expected, because for 15mg/ml device the crystallinity of the polymer domain improves, resulting in lower band gap of the polymer. As polymer band gap is reduced, more and more band edge photon can be harvested resulting in better EQE at a wavelength beyond 600 nm. Further the vibronic peaks that are generally considered as the signature of crystallinity (conjugation length). These vibronic peaks seem to grow prominent compared to 10mg/ml device. That is also an indication of improved crystallinity in the solar cell active layer.

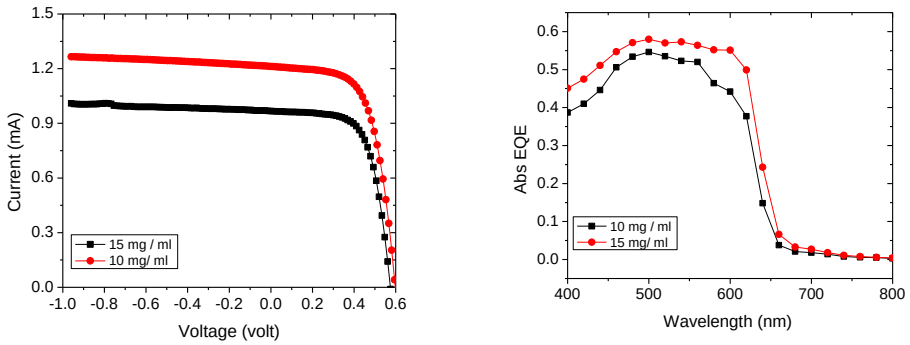

Figure E.12 (a) Light IV for different concentration measured under 1sun spectrum of ELH lamp, (b) Absolute EQE measured for different sample with different active layer (blend) concentration

www.manaraa.com

Measurement of DOS shows (see figure E.13) not much difference between the devices which is corroborated by dark IV measurement. Io was estimated to be roughly 2-3E-10 Amps.

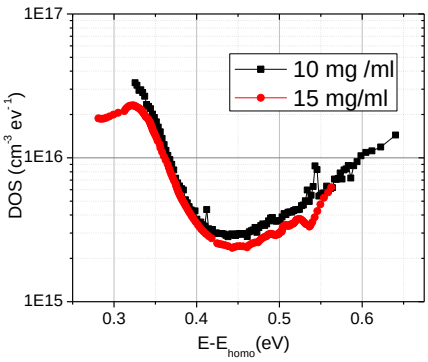

Figure E.13 DOS plotted for two devices with two different concentration

Photo-degradation of different concentration devices

In this section we will compare the drop in performance between two devices which underwent same light exposure of 2x intensity for 24 hours approximately. As before, entire device is covered by aluminum foil to protect other contacts. Different electrical measurements were conducted to understand the changes in the device property. Figure E14 (a-d) compared the light IV and EQE change in solar cells with different concentrations after 24 hours light exposure. The drop in 15mg/ml solution is higher as in comparison to 10 mg/ml device.

Device with higher concentration lost 11% of the initial photo current while it lost around 3.5 % of open circuit voltage. While the device with lower concentration suffer only minor drop (around 5.5%) in photo current and almost same amount of drop in open circuit voltage as can measured for higher concentration device.

www.manaraa.com

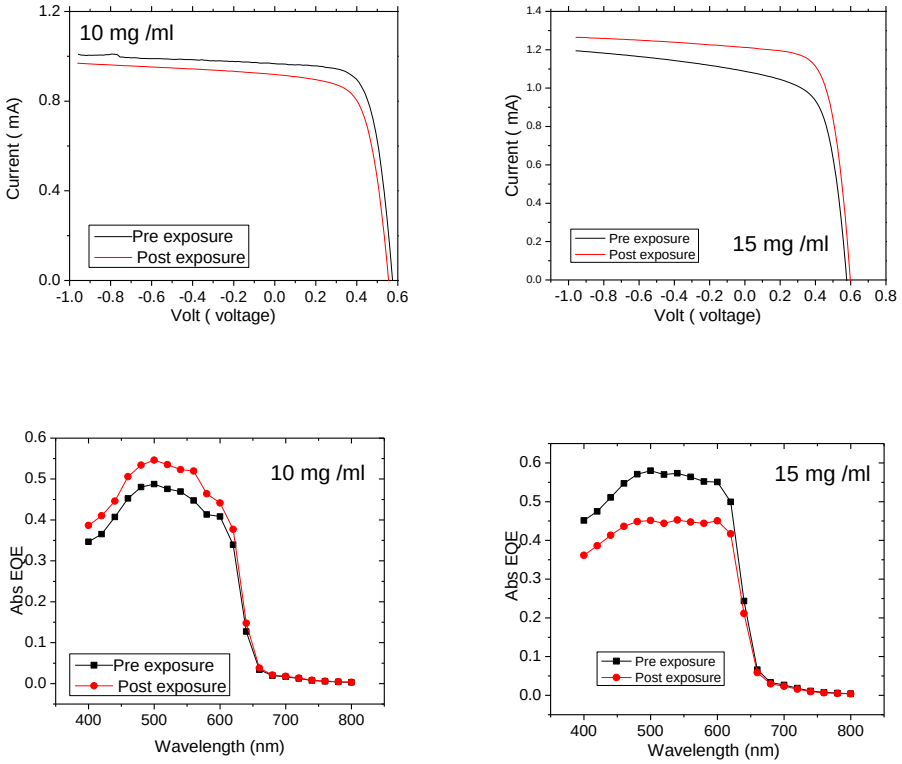

Figure E.14(a-d) Drop in Light IV and EQE upon exposure to 2x-24HRS(ABET SIMULATOR)

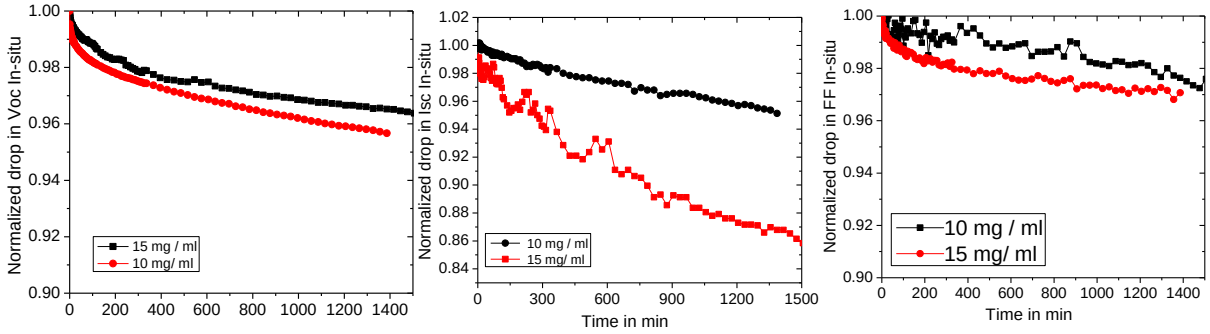

Figure E.15(a-c) Drop in Voc /Isc and FF(measured in-situ) compared for two different active layer concentration.

Figure E.15 (a-c) summarized the in-situ measured changes in Isc/Voc and FF with exposure time. As expected it follows exactly same trend as already summarized. Voc and FF for both the

www.manaraa.com

devices almost dropped equally while change in short circuit current is almost double for the high concentration device compared to the low concentration device.

We also calculated the drop ratio of EQE measured for exposed and non-exposed contact. The drop ratio was plotted for the devices made of three different concentrations. It can be seen in the figure E.16 that for the device with lowest concentration the drop ratio is almost flat and lying around 1.1. As we are increasing the concentration of the blend solution, drop ratio is going further up which is consistent with general observation in previous appendix D. The device with lowest drop in photo current shows flatter drop ratio, when plotted as a function of wavelength.

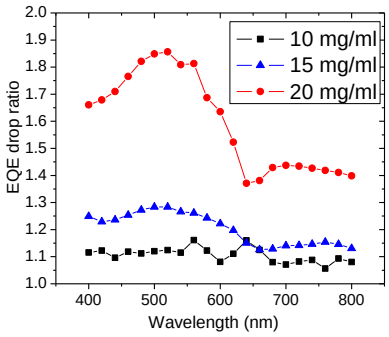

Figure E.16 Change in EQE ratio for different concentration as a function of wavelength

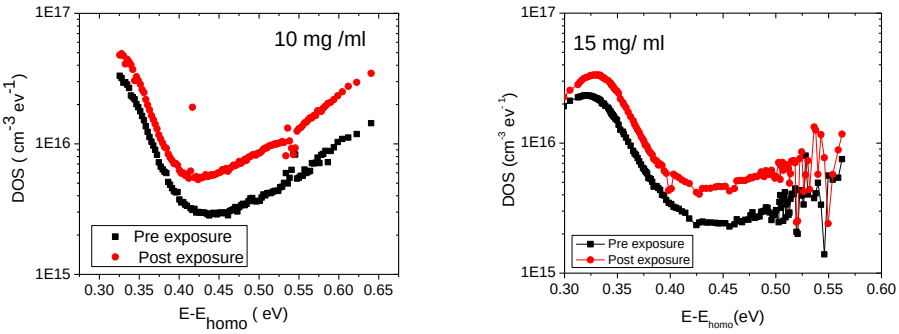

Figure E.17 Change in DOS upon photo exposure-(a) 10 mg/ml , (b) 15 mg/ml

www.manaraa.com

We also plotted the DOS measured by capacitance spectroscopy technique in figure E.17. We calculated the enhancement factor from the measured DOS before/after the exposure and compared them with two different devices with two different concentrations.

Firstly the shape of the DOS distributions might look different. This is because the DOS for 10mg/ml was measured by HIOKI LCR meter that can measure capacitance only in the range o f 1 Hz to 200Kz. While the DOS measured for 15 mg/ml was measured by Quadtech LCR analyzer whose measurement range is restricted between 20 Hz and 1 MHz. So for 15mg/ml device DOS was extended to much shallower energy level while for lower concentration, it can extend to deeper energy level from the valence band of polymer. The figure E.18 compares the overall enhancement factors for different concentrations. This shows the increase in DOS is almost same for both the device after same amount of light exposure. Here the increase in DOS is almost same (approximately 2-2.5 times) over its pristine value. Further we measured dark current voltage characteristics in order to extract Io which can help us to explain the drop in Voc. The following table summarizes the parameters extracted from the dark current measurement. It is interesting to note that Io increased for both the device by roughly around 3 times the pristine value.

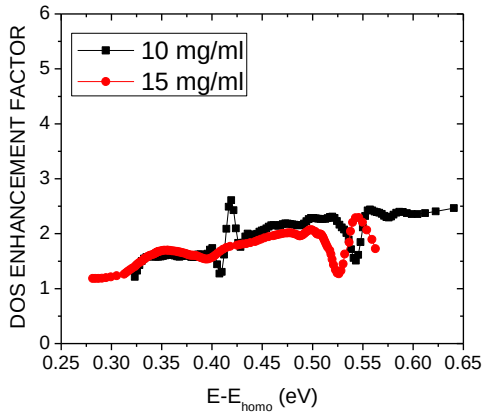

Figure E.18 DOS enhancement factor as a function of energy

www.manaraa.com

Type	Exp	Increase in Io	Io	n	Voc(cal)	Voc(exp)
10 mg/ml	After	2.95	5.90E-10	1.5	0.556	0.555
	Before		2.00E-10	1.44	0.576	0.578
15 mg/ml	After	3.08	8.50E-10	1.58	0.578	0.578
	Before		2.76E-10	1.5	0.597	0.593

Table E.1 Summary of Io and n for different concentration device.

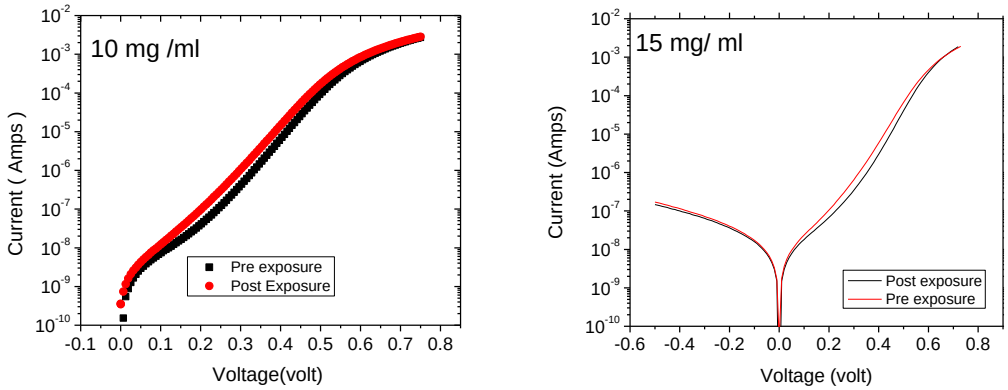

Figure E.19 Change in dark IV for different concentration device upon 2x- exposure

Thicknesses of the films were found to be 80nm and 190 nm respectively for 10mg/ml and 15mg/ml device. With thicker device, effective electric field inside is lesser compared to thinner (low concentration) devices. This might explain why drop in photo current is less for low concentration device because of more sweeping of charge carriers under higher effective electric field.

Conclusion

In this appendix, we have experimentally shown that photo-degradation of organic solar cells depends on the active layer morphology. In either of the cases (differing concentration and differing annealing temperature), we found that the increase in defects as an extra source of recombination is inevitable. We also found that thickness of the film plays a critical role in determining the built-in electric field strength that can change the drop in photo-current due to prolonged light soaking.

www.manaraa.com

APPENDIX-F
EFFECT OF CATHODE INTERLAYER ON PHOTO DEGRADATION OF POLYMER SOLAR CELL

Introduction In appendix D and E, we have discussed about the effect of hole transport layer as well as active layer morphology on photo stability of polymer solar cells. We observed that light induced creation of mid-gap defect states increases the trap assisted recombination resulting in the drop of both photo voltage and current. It was postulated that prolonged photo exposure creates mid-gap defect states because of the cession of C-H bond abundant in the polymer side chain.[47] Several report indicated that morphological change in the polymer structure as well as back bone can result in meta-stable mid-gap states which can induce defects at the polymer interface.[47] Cathode layer are generally deposited at the very last step of device fabrication. It has very little contribution to the internal device physics and morphology of active layer. The only purpose of this layer is to get an Ohmic contact at metal organic (active layer) interface. The choice of metal electrode becomes easier as it no longer requires having a material with matching work function with the organic semiconductor for efficient charge transfer. Cathode interlayer pins the Fermi level at the interface and makes a contact for efficient charge transfer in both direction. In this appendix, we are trying to investigate the effect of different cathode layer on the photo-stability of organic solar cells. If light induced degradation is only an active layer related effect, then the photo stability must be independent of cathode material we use. In next few sections we are going to see the effect of light soaking on solar cells with identical active as well as hole transport layer but different cathode layer.

www.manaraa.com

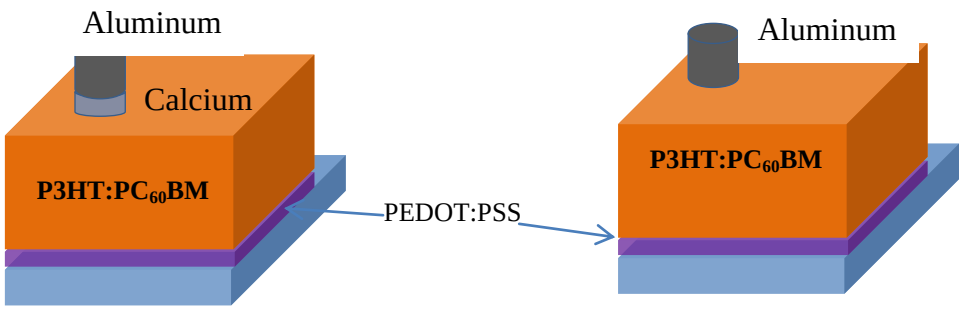

Figure F.1 Schematic diagram for device architecture

Intuitively, an equal drop was expected from two samples because of their similarity in all fabrication steps and recipe. We will firstly study briefly-why do we need a cathode inter-layer in organic solar cells. In the later subsections, we will compare the device parameters of a standard cell with calcium as an inter-layer and a device without any inter layer as shown in the above schematic (figure F.1). Finally we will compare their photo stability and the change in electrical property after photo degradation.

In this set of experiment we have tried to use magnesium as a cathode interlayer because of its low work function. However all the device made from magnesium cathode degraded very rapidly once we took them out of the thermal evaporator because magnesium is highly reactive in air and react with both ambient oxygen and moisture resulting in barrier formation and lowering of photo current in the process. So we have less number of variables for this experiment (because we have very few elements which have a low work function in the range of 2-3 ev). For our experiment we have used calcium as a standard cathode interlayer which is reasonably stable in air. We compared the result with a device where calcium is not used and aluminum was deposed directly instead. The devices are fabricated similarly as described in appendix E. Only difference in device fabrication is the use of calcium as ETL (electron transport layer) before aluminum deposition in one device while in other device, aluminum deposited directly without calcium.

www.manaraa.com

Why cathode inter layer?

Different cathode inter-layers are widely used for efficient charge collection from organic bulk hetero-junction solar cells.[141,221-229] Why do we need for such extra layer in the device architecture? – This questions are addressed in many previous work[141,221,222]. The figure F.2 describes the band alignment between HTL, active layer and cathode layer. The maximum open circuit voltage that can be attained is the difference between the HOMO level polymer and LUMO level of acceptor. If the work function of the HTL is lower than the Fermi level of polymer or in other way, work function of cathode interface layer is placed higher than the acceptor Fermi level, we are going to have a ΔHOMO or ΔLUMO at the respective interface. This extra loss due to the energy misalignment will reduce the maximum attainable photo voltage in the device.

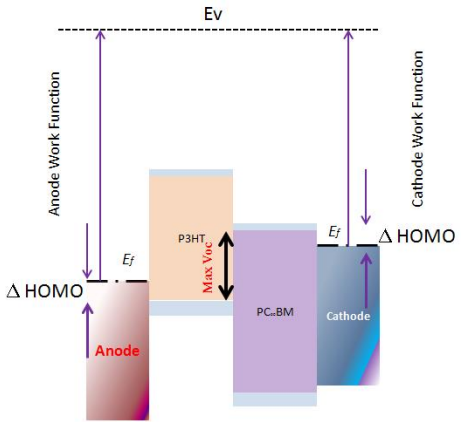

Figure F.2 Possible origin voltage loss due to misalignment of work function

Figure F.3 shows how the energy band of the device can bend at the metal semiconductor interfaces. The figure in the left shows, how the Schottky barrier might have generated due to the work function mismatch. Such a barrier at the metal interface can produce a band offset which can reduce the open circuit voltage and short circuit current as well.

www.manaraa.com

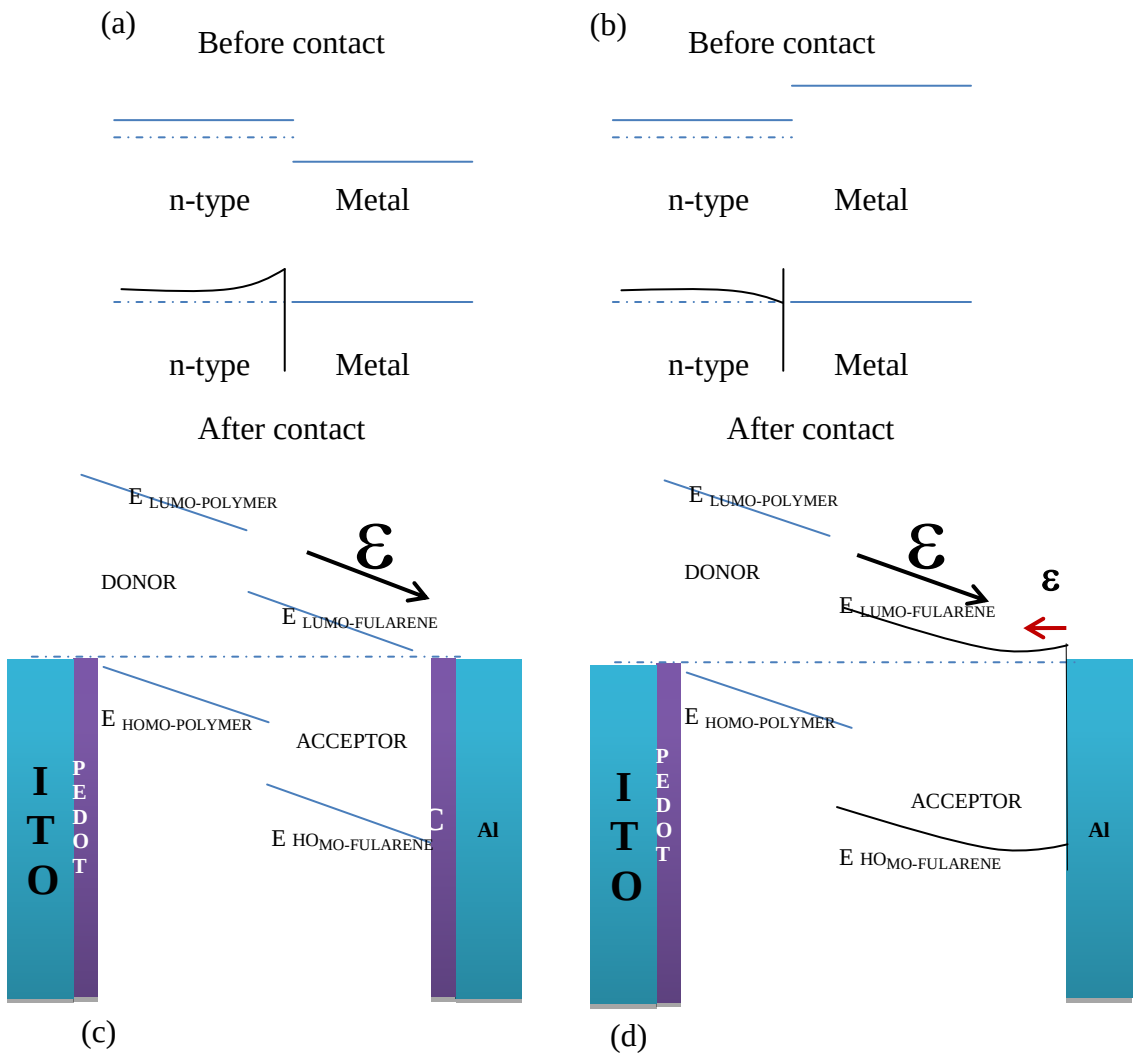

Figure F.3 (a) Metal semiconductor junction with schottky barrier,(b) Ohmic junction, (c)Band-alignment at thermal equilibrium (band diagram shown of possible charge transport path that contributes photo current), (d) Presence of barrier at metal interface- reduced flat band voltage.

Above band diagram (figure F.3) is depicting the possible band bending at the metal – organic interface due to the absence of cathode inter-layer. The bigger symbol epsilon (Ɛ) represents the built-in electric field due to Fermi-level alignment at thermal equilibrium. The smaller epsilon (ε) with red colored arrow shows the possible presence of extra –electric field due to the Schottky barrier at the metal interface. This small barrier will not only reduce the electron collec-

www.manaraa.com

tion at the cathode but also will reduce the photo voltage, since now at forward bias we need less voltage (less injected charge carrier) to counter the photo-current generated at the interface.

Pristine device performances

The discussion starts with the comparison of pristine device performance of device with and without a cathode layer. The figure F.4 shows light IV & EQE of two devices in comparison.

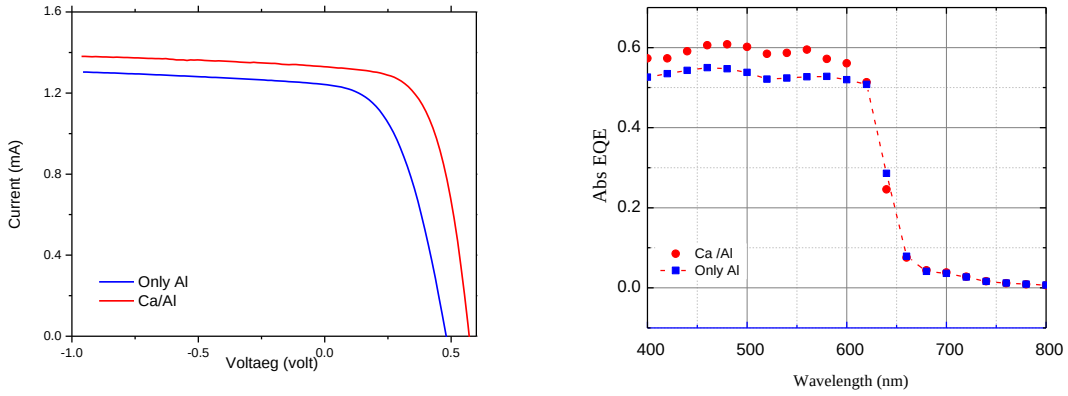

Figure F.4 Light IV and Absolute EQE comparison of devices with two different

First observation that we can make is -both short circuit current and open circuit voltage dropped from the control device with calcium as a cathode inter layer. The drop in Voc is almost 80-90 mV from its control value of 580 mV approximately which accounts for roughly 14%. Similarly drop in current is roughly around 6%. In order to investigate further we measured dark current for both the devices. The reverse saturation current (Io) can be a very good indicator of open circuit voltage. For repetition of the results, we made two identical device with name A and B for aluminum only device. The plot with maroon and red colored line in figure F.5 corresponds to aluminum only device while the blue curve depicts Ca/Al device. The dark IV curve shows identical behavior for both aluminum only devices. Extracted Io and n (ideality factor) from ex-

www.manaraa.com

ponential region of mid forward bias dark current region was found to be 3E-10 Amps and 1.2 approximately. We calculated the V_{oc} using the following equation where I_{sc} is 1.24 mA.

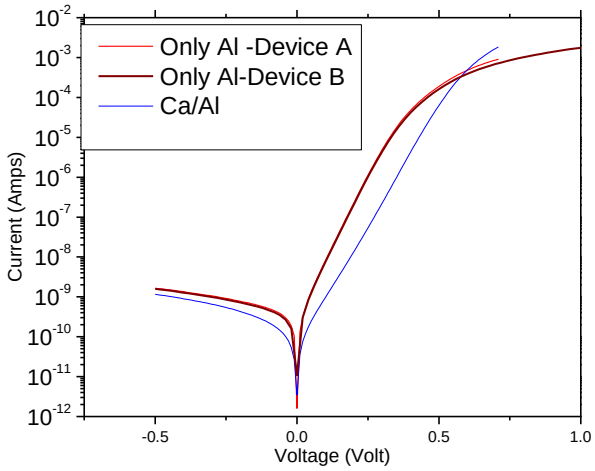

Figure F.5 Comparing dark iv measurement of devices with two different cathode.

$$Voc = \left(\frac{KT}{q}\right) * \ Ln\left(\frac{Isc}{Io}\right)$$

Our calculated Voc(473 mV) matches closely to the experimentally pristine value (480 mV) with a deviation of 1.5%. The dark current thus found to explain the lower Voc in aluminum only device. The Io extracted from Ca/Al device was found to be slightly lower compared to the Al only device. Io was estimated to be 5.6E-11 Amps with n is around 1.28. We also calculated the Voc from the above equation which happened to be in good agreement with the measured Voc of Ca/Al device. It is apparently not in agreement with the theory we predicted in the previous section. It implies that an extra amount of recombination is taking place in the device with only aluminum. Such an anomaly is not clearly understood. Is this extra recombination is due to the small band bending at the metal-organic interface? Its well-known that such trap assisted recombination are dominant form of recombination at the interface of donor and acceptor which contains both type of charge carrier. If that is the case, then there must be some defect states are

www.manaraa.com

evolving during the direct deposition of aluminum by thermal evaporation. So we measured DOS for both Ca/Al based device as well as Al based device. The DOS curve is smoothened further by FFT tool in ORIGIN 8.0 software. We also integrated the total defect states between 0.4 ev to 0.65 ev to see if it shows any difference.

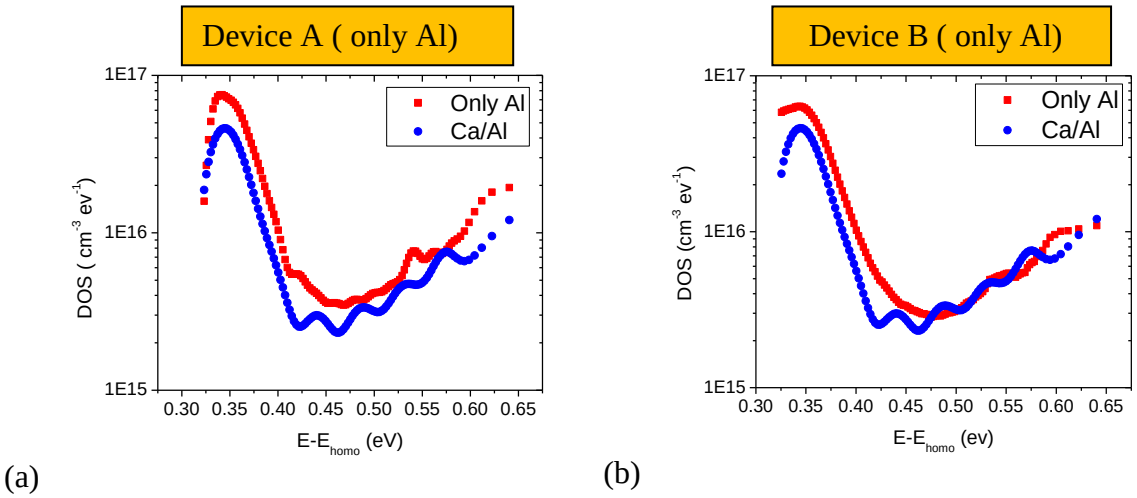

Figure F.6 Comparing DOS measurement of devices with two different cathodes.(Blue marker- Ca/Al cathode – Red marker – (a/b) Only aluminum based two different solar cells

The integrated DOS was found to be 1.03E15 /cm^3 between 0.45ev to 0.65 ev for Ca/Al based device while that for only aluminum device was found to be 1.57E15/cm^3. When DOS was measured for the second device named B (only aluminum) and compared to the Ca/Al based device, it shows uniform overlapping of DOS of both the devices roughly between 0.45ev to 0.65 ev. The integrated DOS for aluminum only device is roughly 1.5 times (device A) and almost 1 times (for device B) the integrated DOS calculated for Ca/Al based device. The increase in Io is roughly 5.4 times for aluminum based device over its counterpart. Measurement of density of defect states does not agree with the measured value of Io from dark IV technique. If DOS is same for both type of device, then what is increasing the Io for aluminum only device over Ca/Al based device? One explanation could be that, effective built-in electric field is lower in only

www.manaraa.com

aluminum device which will give more time for the free charge carrier to recombine at the interface as we have already seen in appendix E.

We also measured photocurrent vs external bias to extract mobility lifetime product using numerical expression as discussed elsewhere.[135, 145] The photocurrent shows less bias dependence for Ca/Al based device while compared to both aluminum based device in reverse bias. Also an interesting point to note that, the flat band voltage dropped for aluminum based device compared to Ca/Al based device which is again point to the theory of reduced built-in field due to the presence of a schottky barrier at metal organic interface. $\mu\tau$ product are summarized in the following table.

Type of Cathode	$\mu\tau$ (cm^2 /V)
Only Al(Device-A)	3.05E-10
Ca/Al	3.4E-10

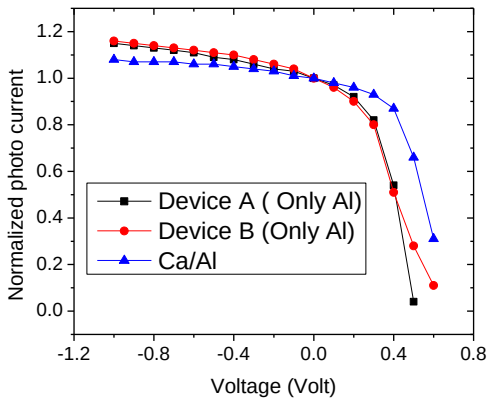

Figure F.7 Comparing photocurrent vs bias measurement of devices with two different cathode.

The tabulated value of mobility-lifetime indicates that there is hardly any difference between the two pristine devices so far as interface properties are concerned. This is in good

www.manaraa.com

agreement with the DOS data mentioned before but not in agreement with the reverse saturation current extracted from forward bias dark current.

Finally we can conclude that distribution of traps at donor-acceptor interface remains roughly same for both devices. However an extra source of recombination is added to the dominant trap assisted recombination that is reducing the open circuit voltage and short circuit current in only aluminum based device which could be because of lower built-in field. The reduction in flat band voltage is substantiating the theory of lowered built-in potential.

Photo degradation results

In previous appendix we have discussed about the nature and possible reason of photo degradation of organic solar cells with different HTL as well as active layer. In this section we are going to compare the photo-degradation process in cells with different cathode inter-layer. Figure F.8 show the light IV measured before and after the photo-degradation under 2x sun intensity for 24 hours. It can be seen that in both the devices short circuit current dropped significantly. Interestingly open circuit voltage dropped significantly for aluminum only device compared to Ca/Al device. The percentage of drop in Isc and Voc is roughly 14 % and 3.5 % for Ca/Al based device while percentage of drop for aluminum based device recorded 26% and 30 % drop respectively. Such huge drops in Isc as well as Voc were never observed before for standard Ca/Al based devices.

www.manaraa.com

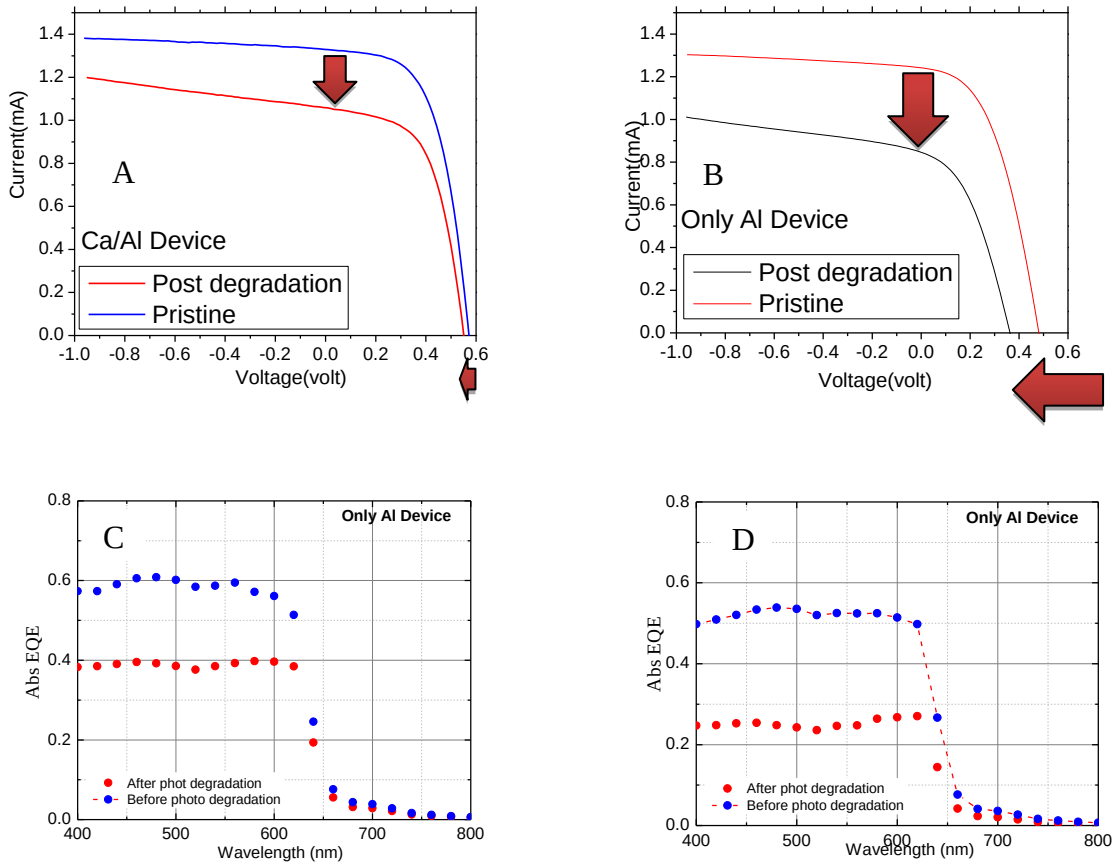

Figure F.8 The effect of photo degradation – (A) Light IV of only Al device , (B) Light IV of Ca/Al device (C) Abs EQE drop of Al only device, (D) Abs EQE drop of Ca/Al only device

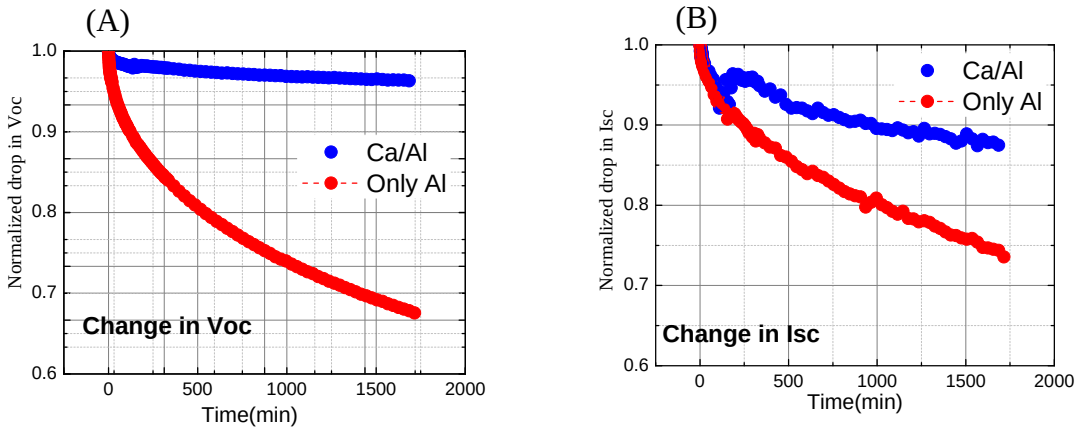

Figure F.9 (A) Comparison of In-Situ drop in Voc of devices with only Al cathode and Ca/Al Cathode, (B) Comparison of In-Situ drop in Isc of devices with only Al cathode and Ca/Al Cathode (2x-24 Hours)

.

www.manaraa.com

Figure F.9(A-B) show the in-situ recorded drops in Isc and Voc which are matching exactly to the drop measured outside the degradation chamber. Another observation can be made is – both the device show significant bias dependence after light exposure consistent with our initial observation as reported in chapter 5. The absolute EQE measurements of both the devices before and after photo degradation are quite consistent with the amount of drop observed in light IV measurement. In order to gather further understanding about the loss of Voc, we measured dark current (see figure F.10) and DOS (see figure F.11) to see if there is any correlation between them. We extracted Io from all the measured dark current at forward bias. It can be easily seen that overall dark current of the device with only aluminum increased significantly in comparison to Ca/Al based device. The extracted Io for aluminum based device increased from 3.05E-10 Amps (Pristine) to 4.7E-9 Amps (after photo-exposure) which is almost more than an order of magnitude. For Ca/Al based device Io increased from 5.6E-11 Amps to 1.33E-10 Amp which is an increase by roughly 2.4 times the pristine value. The measured DOS shows enhancement for (only aluminum) based device compared to the standard Ca/Al device. The plotted enhancement factor shows that in the region between 0.45 ev to 0.6 ev, only aluminum device shows increased amount of defect states compared to Ca/Al based device.

This could be the reason of extra drop in photo current and open circuit voltage in the cells with only aluminum as cathode. However the enhancement in the only aluminum devices recorded is only 3 times the pristine value of defect states around mid-gap of donor and acceptor interface. The recorded increase in Io is around 15 times the pristine value which is not at all consistent with the DOS measurement. Another interesting point to notice is that, for Ca/Al device n (ideality factor) increased from 1.28 to 1.34 after 24 hours of photo degradation. While in (only aluminum devices) the ideality factor dropped from 1.2 to 1.17 which could an indication

www.manaraa.com

of a possible bi-molecular recombination mechanism already present in the device due to the direct deposition of aluminum as cathode.

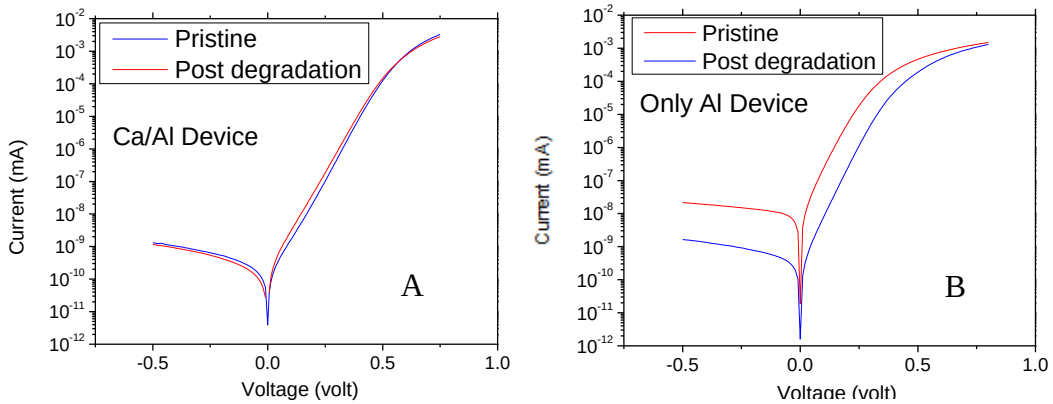

Figure F. 10 (A)Comparison of dark iv measurement of Al only device after exposure, (B) Comparison of dark iv measurement of Ca/Al standard device after exposure(2x-24 Hours)

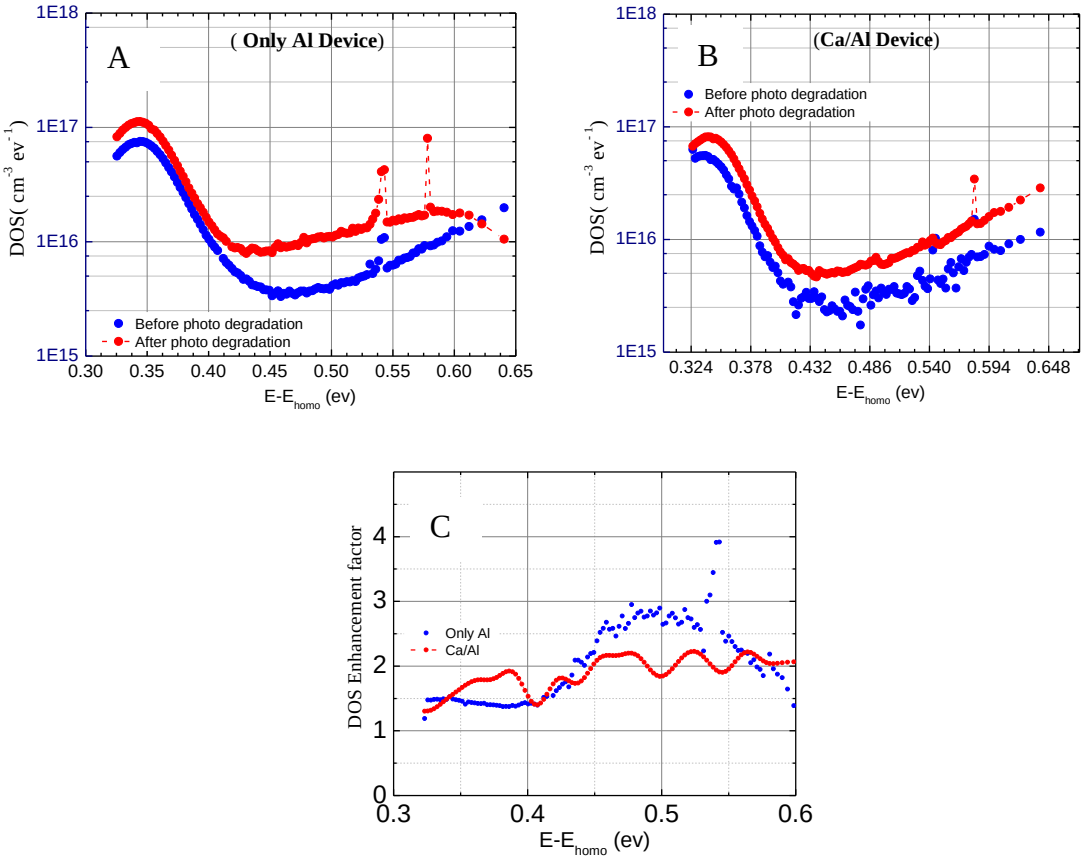

Figure F.11 (A) DOS comparison for Al only device after light exposure, (B) DOS comparison for standard Ca/Al based device, (C) DOS enhancement factor(Degraded DOS/Non Degraded) comparison for two different device

www.manaraa.com

Quite interestingly it should also be noted that, the observation made in this experiment is in contrary to the understanding we gathered in the previous chapter. It was previously thought that active layer contribute significantly to the photo degradation and formation of defects under prolonged light exposure is an intrinsic property of active layer material as proposed elsewhere.[53] If that argument is to be true, then we should have noticed same amount of photo degradation in both the device because of same active layer recipe that we used during fabrication. This result suggests that defect creation can be enhanced if we deposit aluminum directly on top of active layer. The photo-current bias measurement shows higher bias dependence of photo-current for aluminum only device compared to Ca/Al based standard device. μτ were extracted for both the device after light exposure from the figure F.12. It was found that the μτ dropped from 3E-10 cm2/v to 9.5E-11 cm2/V for aluminum based device while μτ that of Ca/Al based device dropped from 3.4E-10 cm2/v to 1.4E-10 cm2/v which is roughly two times.

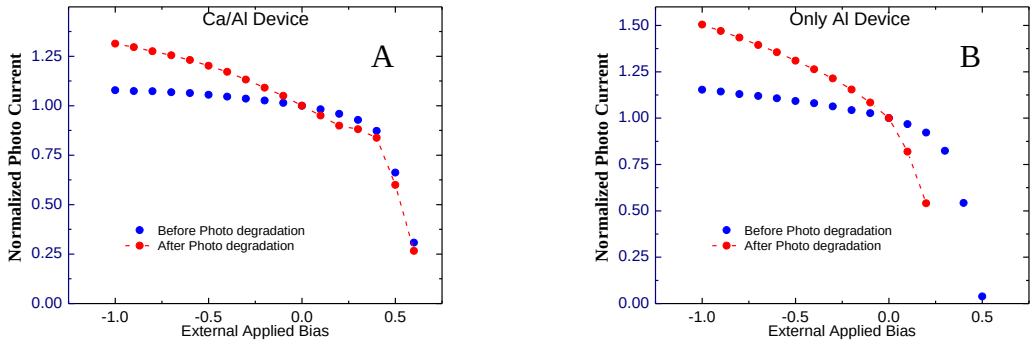

Figure F.11(A) Comparison of photo current vs bias for standard Ca/Al device, (B) Photo current Vs bias device for only Al device

The drop in μτ is exactly matching with the increase in defect states measured for both devices. For aluminum only device mid gap states increased roughly 3 times between 0.45 ev to 0.6 ev which can be correlated to the drop in lifetime roughly 3 times. Similarly increase in defects

www.manaraa.com

for standard cell in the same range is roughly 2 times the pristine value which is exactly matching with the drop in lifetime by a factor of two.

Conclusion

In conclusion, we presented the experimental data on the photo-degradation of organic solar cells with different electron transport layer to study the effect of light soaking on defect evolution at the interface of donor-acceptor. We showed that nature of cathode layer can have significant impact on not only the performance but also the photo stability of organic solar cells. We observed that the amount of defect created (which is responsible to the charge carrier recombination through SRH method) is different and higher for aluminum only device. One possibility could be the metal ion diffusion into active layer which can create trap states near interfaces. But such speculation must be supported by structural characterizations such as depth profiling of device from metal side and layer by layer compositional analysis using SIMS or Auger electron microscopy. This can help to correlate the increase in defect states to any structural or chemical change in the active layer material due to direct introduction of metal ion into active layer.

www.manaraa.com

APPENDIX-G
ZNO: AL BASED INVERTED SOLAR CELLS

Introduction

There are several motivation for using ZnO:Al as a transparent conductive cathode. Indium based TCO's are widely used as transparent conductive electrode for solar cell as well as LED application since long time. However Indium is a rare earth material and not available in abundance in the earth crust.[230-232] In addition, ITO has environment concern as mentioned in some literature.[233] ZnO:Al, on the contrary is widely available material and very much cost effective in comparison to conventional ITO based TCO.[234] Next ZnO:Al can be easily deposited by RF magnetron sputtering with optimized electrical and optical property.[235-239] Finally ZnO:Al can be etched easily by diluted HCL to obtain random roughened structure which can be used as both front and back end reflector that can scatter the incoming light resulting in increasing the light path inside the active medium of solar cell.[2,5] In this batch of experiment, we would first optimize the ZnO:Al film. Secondly we will see some device result comparison that are made on optimized ZnO:Al substrate. Later we will compare the photo stability of ZnO:Al based inverted solar cells.

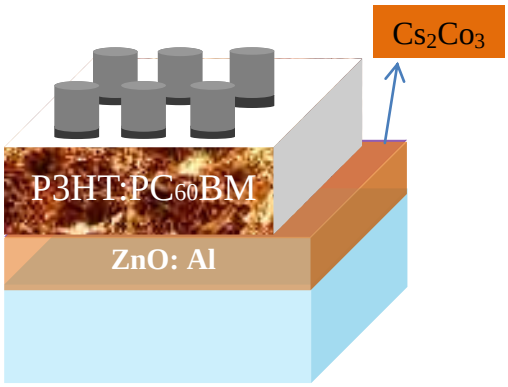

Fig G.1: Schematic layer wise structure of an inverted solar cell on ZnO:Al substrate.

www.manaraa.com

The ZnO:Al coated substrates were prepared by RF magnetron sputtering on the standard microscopic glass slides. Different recipe of sputtering was used to optimize the sheet resistance and transmission. In our experiment we kept the pressure constant to 2.5 mTorr and temperature to 150C. We varied the RF power from 80 W to 120 W to choose the substrate with optimum transmission and sheet resistance. The inverted device architecture is shown in figure G.1

ZnO:Al film optimization and device fabrication

The first goal of this work was to produce optimum ZnO:Al film by RF Magnetron sputtering. For that, we varied RF power while keeping the chamber pressure and substrate temperature constant to 2.5 mT and 150 C. The table G.1 summarizes the sheet resistance of the ZnO: Al film produced by RF sputtering. All the films were deposited for 10 min 30 sec time duration. It was quite clear from the following table that with increasing RF power the rate of deposition increases which increases the thickness of the ZnO:AL film also.

However with higher power, we could achieve lower sheet resistance which could help in reducing the series resistance of the solar cell and thus improve the fill factor. However that reduction in sheet resistance comes at the cost of drop in transmission through the ZnO: Al film with significant drop in the blue region of the solar spectrum. With increasing RF power, we tend to lose more photon compared to standard ITO coated substrate as can be seen in the figure G.2. Here we have compared the transmission of different ZnO: Al substrate with standard ITO substrate. Initially we made solar cells directly on top of the ZnO directly without applying any electron transport layer (such as Cs_2Co_3) on ZnO: Al film. Figure G.3 shows the light IV curve of devices on ZnO:Al with a control device spin coated on (ITO+ Cs_2CO_3) substrate as well as (ZnO: Al + Cs_2CO_3) substrate. The efficiency of the device on bare ZnO: Al is limited because

www.manaraa.com

of lower open circuit voltage and fill factor. The lower Voc can be explained by the argument given in the previous appendix F.

Run No	Power (watt)	Time (min)	Rs (Ω/□)	Thickness (nm)
7923	80	10.5	19	370
7929	110	10.5	13.1	540
7941	120	10.5	10.55	650
7942	120	10.5	11.78	640

Table: G.1 Summary of ZnO:Al film (electrical property)

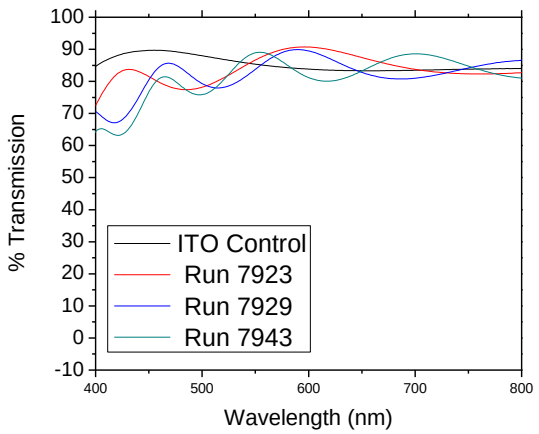

Fig-G.2 Transmission of ZnO:Al Film

As shown in the figure G.3, the control device maintains high Voc because of better alignment of work function with the LUMO of acceptor due to the presence of intermediate thin layer of Cs_2CO_3 as a work function modifier. Direct deposition of active layer on ZnO:Al results in ΔLUMO at the ZnO:Al and PC60BM interface that reduces the Voc.

Device performance

We deposited Cs_2CO_3 (3.06 ev) as an electron transport layer[240,241] because of their lower work function to see if we can further improve the open circuit voltage. Using Cs_2Co_3 improved the Voc and the efficiency (3.8%) improved significantly from its initial value (1.69%) for cell on bare ZnO:Al. In that way we achieved best efficiency of 4.1% for ZnO :Al based cathode while similar recipe gave 4.3 % for ITO based cathode. Finally we successfully fabricated devices with comparable efficiency on ZnO:Al substrate using Cs2Co3 as an precursor layer for modifying the work function of under laying electrode.

www.manaraa.com

In the next part, we investigated the effect of thickness of the ZnO:Al layer on the performances of solar cells. In order to vary the thickness of the ZnO layer, we changed the deposition time of the ZnO:Al layer. The table G.2 summarizes the sheet resistance of the ZnO:Al layer. With increasing the thickness we started losing more photon in the blue region. In the range of wavelength where P3HT absorbs, ITO remains the best transparent electrode. However 10.5 min deposition time of ZnO:Al gave us the optimized performance so far as the sheet resistance and transmission is concerned. The device made on those substrates mentioned in the table G.3 follow a definite pattern.

Run No	Time (Min)	Rs (Ω/□)	Thick-ness(nm)
7964	20	6.44	1253
7965	15	10.05	933
7942	10.5	11.78	640
7967	5	43.67	312

Table G.2 Summary of different different run time for ZnO: Al film

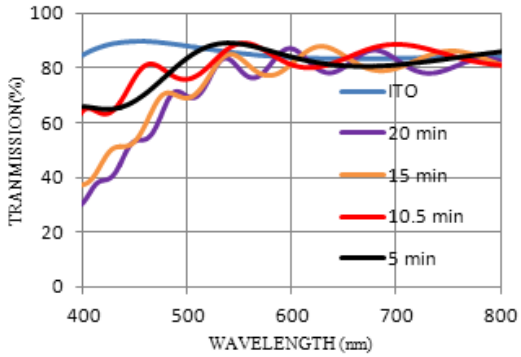

Figure: G.3 Transmission of ZnO: Al for thickness

Device/Substrate Description	Voc	Isc	FF	Rs	Run Time(min)	Efficiency
219 B- Run 7964- Rs-6.44	0.56	1.188	60.64097	65.41557	20	4.025
219 C- Run 7965- Rs-10.05	0.563	1.205	58.57358	77.76396	15	3.98
211 D- Run 7946 -Rs- 13	0.554	1.249	54.72546	88.63461	10.5	3.79
219 D- Run 7967- Rs-43.67	0.564	1.269	43.50326	202.6324	5	3.12

Table G.3: Summary of solar cell performances on ZnO:Al cathode of different thickness

With thicker ZnO:Al film as shown in the table 3, Transmission drops significantly in the blue region while the sheet resistance improved. The Light IV and quantum efficiency both follow the same trend (see figure G.4) As we can see in the table 3, the current increases with de-

www.manaraa.com

creasing thickness of ZnO:Al while at the same time FF decreases because of increase in sheet resistance.

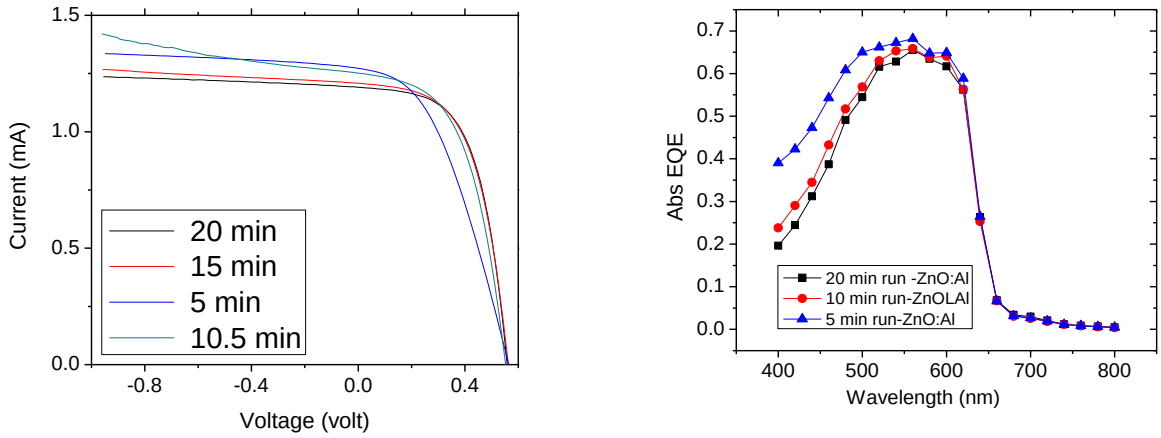

Fig G.4 Light IV Characteristics of OPV on different ZnO: Al thickness, EQE of OPV on different ZnO: Al thickness

However the best efficiency we obtain in the device with ZnO:Al (20 min) have lowest transmission in blue region. In spite of that the FF improved to 61 % which led to increase in device efficiency. So we maintained the device efficiency while cutting the blue photons.

Photo-stability of zno:al based inverted cells

Next we have studied the photo degradation in detail for the three different devices. One with 1250 nm ZnO:Al (20 min run) , with 640 nm ZnO:Al (10.5 min run) and a similar control device with standard ITO. The figure 10.16(A) and 10.16(B) are the comparison of photo induced drop in open circuit voltage and short circuit current measured in-situ shows that the results are in good agreement with the trend observed in the transmission data of figure G.3. We found that by changing the cathode thickness we can tune the number of photon that actually enters the photo active layer of polymer solar cell.

www.manaraa.com

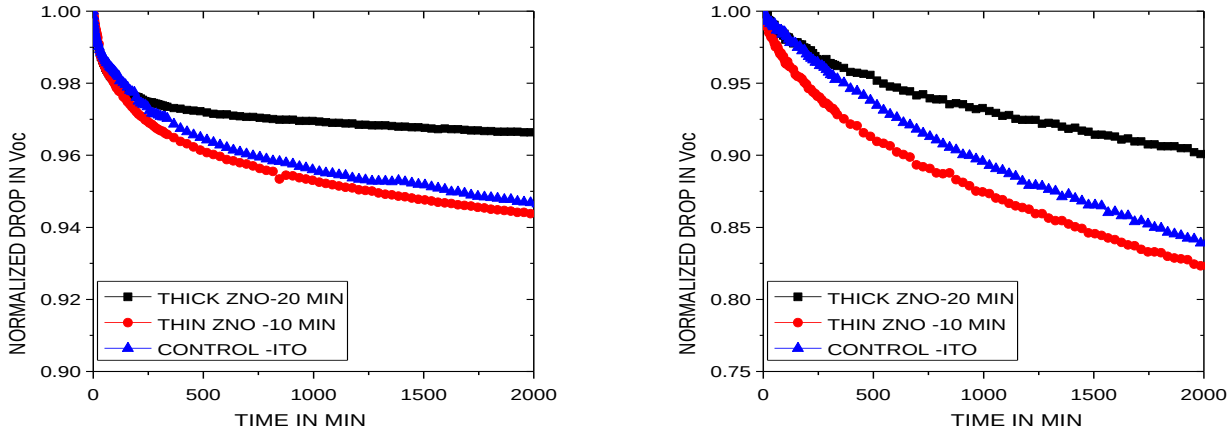

Fig G.5: In-situ drop recorded at 2x intensity for various device under test of light soaking. (A) –Drop in Voc, (B) Drop in Isc.

The results are also in good agreement with the result reported elsewhere.[42,53] This shows that higher energy photon contributes significantly to the photo degradation process of organic photo active layer.

In the figure G.6, a distinct feature of photo induced drop in FF can be noticed. It is recorded in-situ for all different devices. It was observed that in-stead of going down with time of exposure, its actually going up after certain time. Such behavior in the change of FF during photo degradation of inverted solar cell were seen repeatedly in all the other batches of light exposure experiments on inverted solar cells. The time axis of the figure G.6 is kept in logarithm to see the change (deflection) more clearly. It can be seen that the FF is fairly stable for thick ZnO:Al device. While for both thinner ZnO:Al based device as well as ITO based standard sample FF is actually increasing after initial 50-100 minutes of exposure. Before that FF dropped slightly for all type of device. One possible explanation of this could be the top hole transport layer (which is placed at the top of the device architecture). It is possible that prolonged light exposure can induce some chemical changes in the top HTL which improves the charge collection in the cells as described in appendix D. However such speculation requires substantial experimental evidence

www.manaraa.com

to be a proven fact. This observation suggests blue photon can induce chemical changes in MoO_x hole transport layer (HTL).

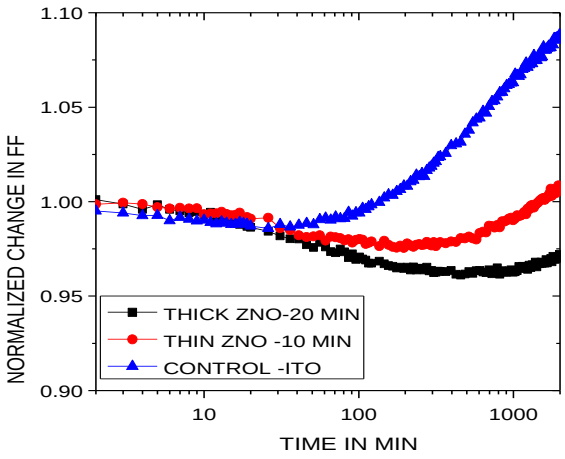

Fig G.6: In-situ drop in FF recorded at 2x intensity for various devices under test of light soaking.

We have also measured the absolute quantum efficiency of all (devices under Test), were made with the same recipe but on the different TCO as mentioned earlier. It can be seen that Thicker ZnO:Al coated substrate cuts most of the blue photon resulting in lower drop in photo current which can be seen in the figure G.7(A). With thinner ZnO:Al as well as ITO based control device drop in current is almost same which is also seen in the EQE figure G.7 respectively.

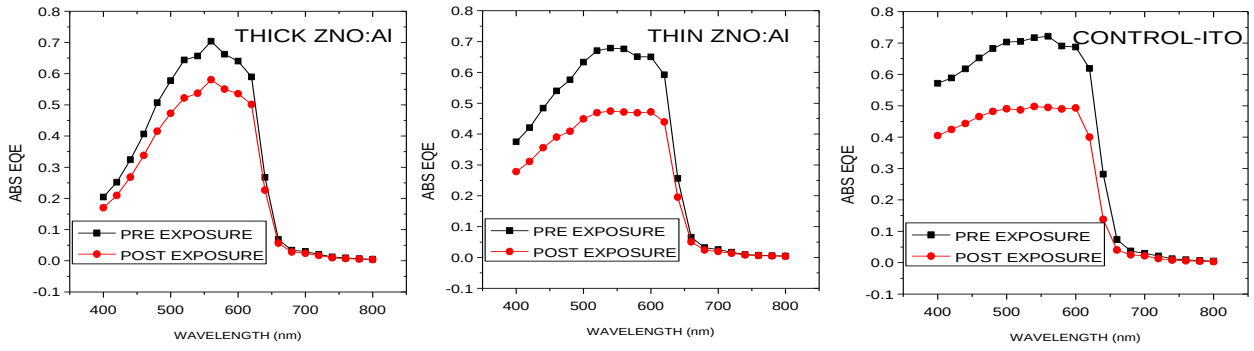

Fig G.7: Change in Absolute EQE after photo degradation for (A)(Thick –[2000 nm] ZnO:Al) based device. (B) (Thin –[1000 nm] ZnO:Al) based device. (C) ITO based control device

www.manaraa.com

Conclusion

In this appendix, we used sputtered ZnO: Al as a transparent conducting oxide (TCO) for making organic solar cells. We also optimized the TCO to get comparable power conversion efficiency (4%). Also we studied the effect of light soaking of the solar cells made on ZnO: Al TCO of different thicknesses. It was shown that, thicker ZnO: Al substrate can maintain efficiency of the solar cells while stopping blue photon to enter the active layer of the solar cells. This makes the organic solar cells more photo-stable compared to the conventional ITO based cells.

www.manaraa.com

APPENDIX H : NATURE OF TRAP STATES

We have already used capacitance measurement as a effective tool to identify the energetic defect states in the P3HT: PCBM bulk hetero junction solar cells. In all our work we have assumed that the traps are located at the interface as opposed to the general trend of calling these traps as a bulk polymer traps[167,168,170,171,179]. If the traps are bulk polymer traps, then these traps should not have any correspondence to the interface state recombination[147] which are the dominant sources of loss mechanism in organic solar cells. Further, capacitance vs voltage technique gives us unusual flat band voltage[134,170] which is lower than open circuit voltage. In a paper by Kirchartz et al [166,240,242], it was proposed that it's the P3HT-cathode interface which has a Schottky junction leading to an apparent resolution of the lower flat band voltage problem (see figure H.1).

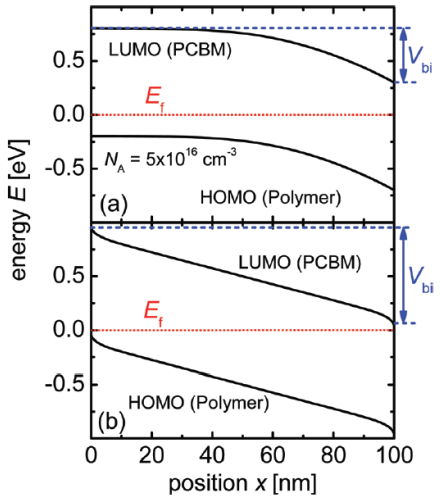

Figure- H-1: top figure shows the band bending in the depletion region created at P3HT-cathode interface while the bottom figure shows the total band bending in the device[166]

www.manaraa.com

Again this did not explain why such estimation of defect states can be correlated to the amount of recombination in bulk hetero junction devices.

In this appendix, we will try to investigate the nature of traps we are looking at by the capacitance measurement (Mott-Schottky technique and admittance spectroscopy technique).[169] Let us determine what are the possible depletion region and band bending present in the device.

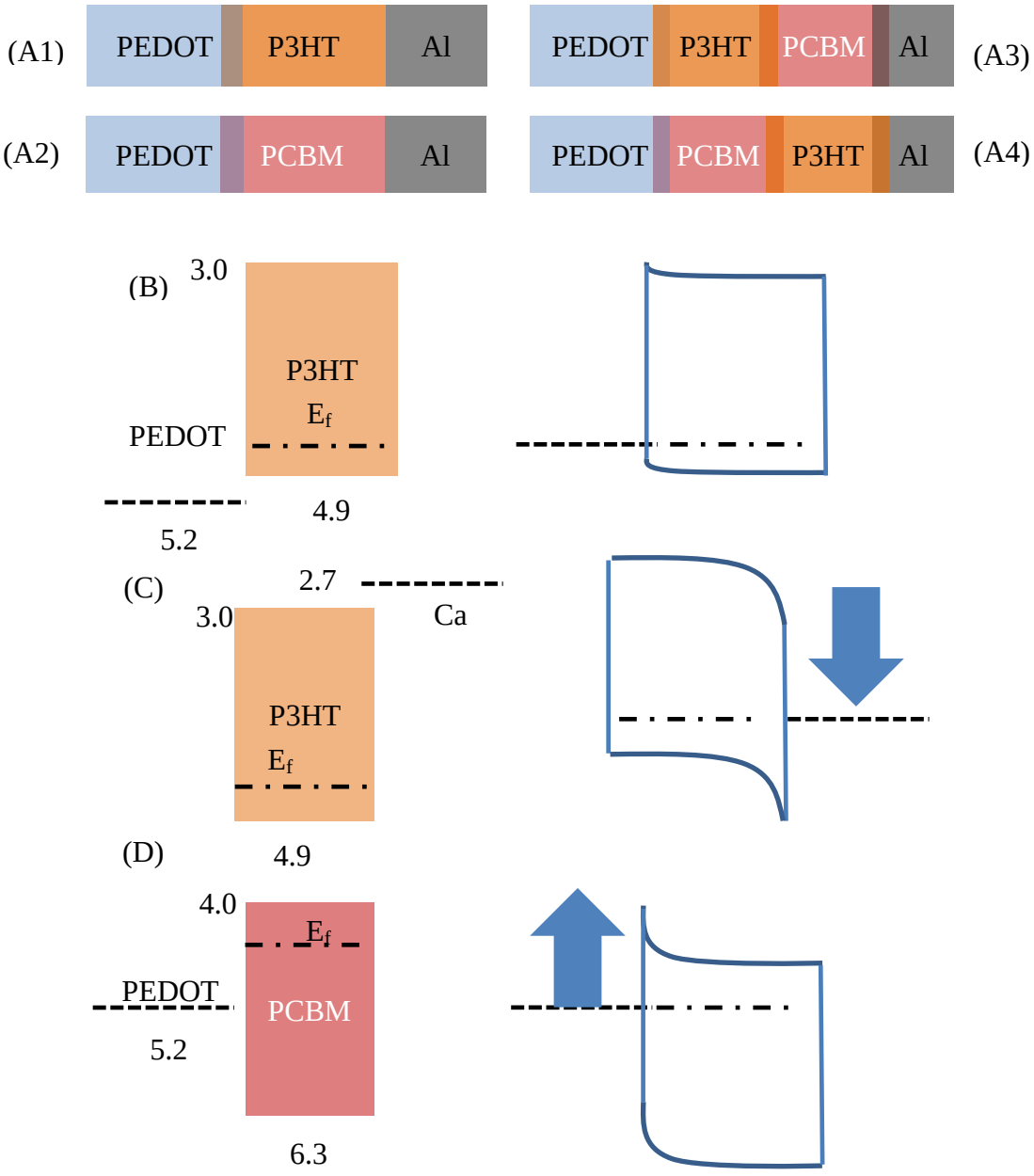

www.manaraa.com

Figure H-2 continued

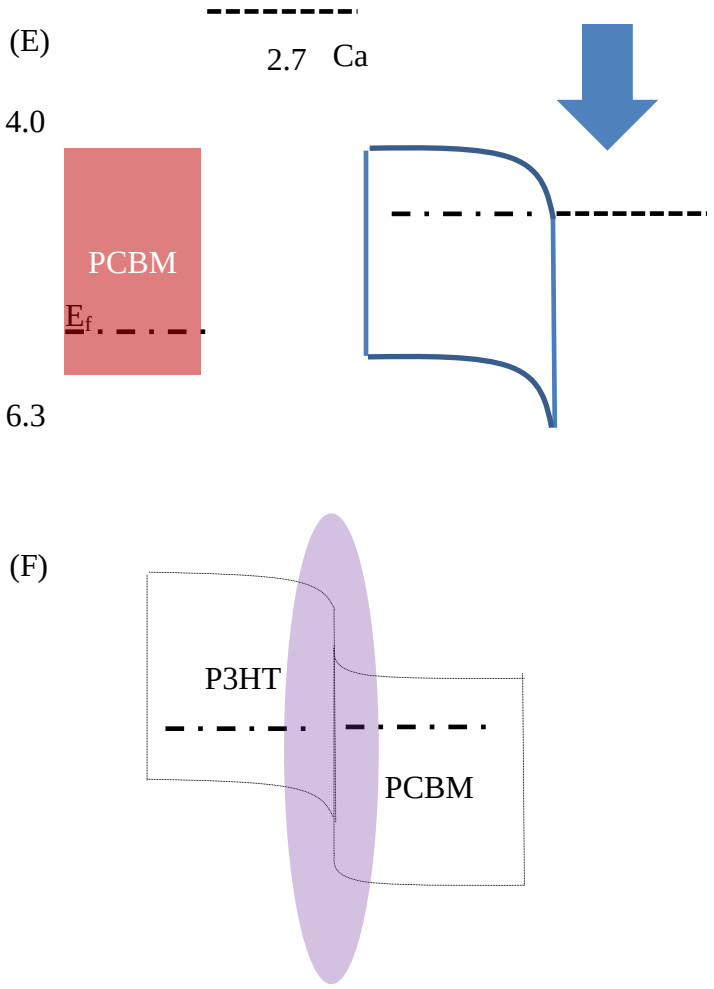

Figure- H-2: A(1-4) different possible interfaces in the blend device, (B) Band diagram for P3HT-PEDOT interface at anode side, (C) Band diagram of P3HT –Ca interface at anode side.(D) Band diagram for PCBM-PEDOT interface at anode side, (E) Band diagram of PCBM –Ca interface at anode side.(F) Band diagram showing band bending at donor-acceptor interface.

Above figure depicts several possible band bending and the presence of depletion region at the various interfaces of our devices. Out of all interfaces, PEDOT:PSS makes Ohmic contact with P3HT while calcium makes Ohmic contact with PCBM. PEDOT: PSS makes a Schottky barrier with PCBM and calcium makes a Schottky barrier with P3HT. So at anode interface, we should have a depletion region (Schottky barrier) between PEDOT: PSS and PCBM while at cathode side, we should have another depletion region between calcium and P3HT. In addition to

www.manaraa.com

that depletion region, we have a third possible depletion region at donor-acceptor interface as shown in figure H2-F. This is because electron in the PCBM may find lower energetic states in the P3HT and can have quantum mechanically possible transitions, resulting in the depletion of some of the free electrons near interface while some free holes in the polymer, leading to such band bending. Amount of band bending in either side of the interface is not yet known accurately because we don't know precisely the number of free charge carriers.

The presence of three possible depletion regions can lead to three depletion capacitances as measured (parallel capacitance model) using LCR meter. J Carr et al[167] assumed that the depletion regions at the anode interface between PEDOT and PCBM as well as the depletion region at donor-acceptor interface are very small because of large number of free electron and hole respectively in the range of 1E16/cm^3- 1E17/cm^3 [167,179]. At the same time they assumed that all the depletion capacitance are in series as can be seen in the following equation. Following are the capacitances related to different depletion region.

PEDOT:PSS –PCBM interface[$C_{d\text{-}pedot}$], P3HT-PCBM interface[$C_{d\text{-}int}$], P3HT-Ca interface[$C_{d\text{-}Ca}$].

$$\frac{1}{[\mathrm{Ctotal}]} = \frac{1}{[\mathrm{Cd-pedot}]} + \frac{1}{[\mathrm{Cd-int}],} + \frac{1}{[\mathrm{Cd-Ca}],}$$

$C_{d\text{-}pedot}$ and $C_{d\text{-}int}$ are very high because of their small depletion region width, which eliminates their contribution to the total capacitance.

$$\frac{1}{[\mathrm{Ctotal}]} = \frac{1}{[\mathrm{Cd-Ca}],}$$

Authors[177]concluded that total capacitance measured by LCR meter is the capacitance measured at the P3HT-Ca interface[179]. Finally the author concluded that all the traps probed by capacitance measurement are actually traps located in P3HT itself. But author fails to explain how and

www.manaraa.com

why changes in such trap states have a close correlation with the photovoltaic properties of the devices as can be seen in chapter 5.

Let us now see if this assumption is correct or not? What if both interface depletion capacitance and P3HT-Ca depletion capacitance are in parallel to each other. In that case total measured capacitance will be the summation both capacitances.

$$C_{total} = C_{d\text{-}int} + C_{d\text{-}ca}$$

We conducted a careful experiment to show that both the depletion capacitances are indeed in parallel, which makes perfect sense from device point of view. We made two devices- one with P3HT:PCBM blend (mixed at 1:1) weight ratio with 10mg/ml concentration. Other device was made from only P3HT solution (1:0) of 10mg/ml concentration. The blend and only P3Ht solution were spin coated on standard ITO coated glass substrate with further coating of usual hole transport layer (PEDOT-PSS). After spin coating of the solutions on PEDOT:PSS coated substrate, the films were annealed on hot plate at 160^{o}C for 2 min and 110^{o}C for 10 min respectively. Finally 25 nm of calcium was deposited by thermal evaporation followed by thermal evaporation of aluminum (100 nm). On these devices (P3HT:PCBM blend and only P3HT) we measured Light IV, dark IV , Cp-f and Cp-V for further comparison.

Firstly we measured light IV for two devices as can be seen in figure H-3. As for obvious reasons, P3HT only device didn't show any current in normal scale when compared to standard bulk hetero junction device. The inset figure shows the light IV characteristics of P3HT only device. The blend device showed normal parameters (Voc-0.59 volt /Isc- 0.8 mA(~8mA/cm2) and FF-70.5%), while P3HT only device shows (Voc-0.85 volt with /Isc in micro amps and FF - 28%). This proves the efficacy of acceptor in successful exciton dissociation. However one in-

www.manaraa.com

teresting point to note is that, the open circuit voltage for P3HT only device is around 0.85 volt, which is quite high in comparison to blend device. This also proves that Voc in P3HT only device is determined by the band bending of P3HT at calcium interface.

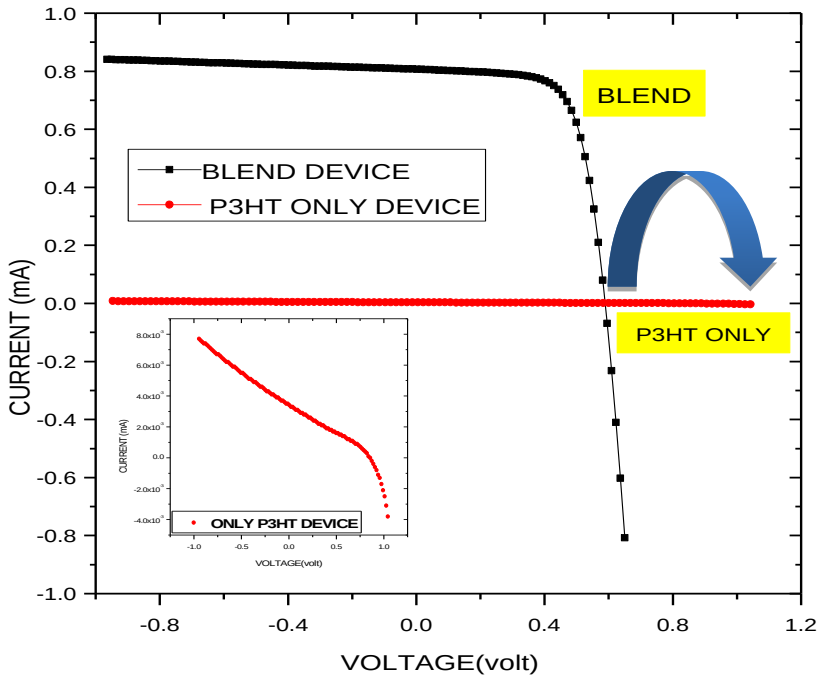

Figure- H-3: Light IV characteristics of Blend device as well as P3HT device, Inset- P3HT only device with expanded scale.

We have also measured and compared dark current for both the devices to see what happens to dark current when we remove PCBM from the bulk hetero-junction matrix. The intention of this measurement is to see how differently two device with two different depletion region would respond to the external applied bias. P3HT:PCBM blend device shows standard dark current as we have seen in chapter 5. For P3HT only device, we observed that the series resistance increased significantly along with reduction in dark current at both bias. If both P3HT-Ca depletion region and P3HT-PCBM interface are in series then we would expect similar current. But if

www.manaraa.com

these two junctions are in parallel, we would expect total diode current to be the linear summation of current contribution from both junctions.

$$I_{total} = I_{d\text{-}Ca} + I_{d\text{-}int}$$

The dark current in P3HT only device is almost 2-3 order of magnitude smaller than the blend device which says that the total current we measure for blend device also include the contribution of P3HT-Ca junction. However their contribution is small and hence does not influence the Io/n estimation (which are purely for D-A interface characteristics).

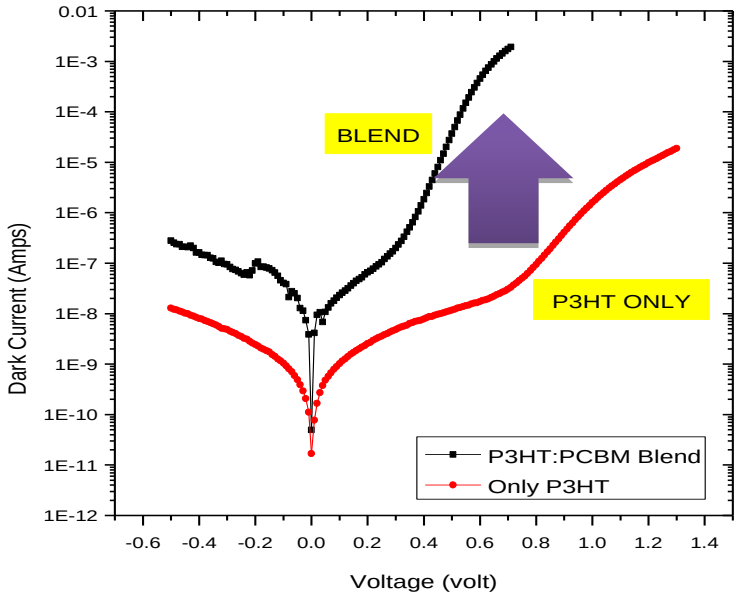

Figure- H-4: Dark IV characteristics of Blend device as well as P3HT device

The dark current measurement indicates that the increase in dark current in blend device which is purely because of interface recombination over P3HT only device(which is purely because of Schottky junction). This again substantiates the presence of interface junction with energetic states at D-A interface resulting in increased dark current.

www.manaraa.com

Further we measured parallel capacitance using HIOKI LCR meter from 1Hz frequency to 200 KHz frequency at zero bias condition. We used 0.101 volt as small signal ac amplitude. We also measured capacitance (parallel) as a function of external bias. The capacitance –frequency spectrum was plotted in the figure D-5A where we can see the parallel capacitance in increasing the moment we add acceptor. This again strengthens the theory of two junction capacitance working in parallel. Cp measured for only P3HT device is way lower in the entire frequency spectrum compared to P3HT:PCBM device . Capacitance measured as a function of voltage also shows very important differences. The Cp-V were measured at 100KHz to exclude the contribution of most deeper trap states.

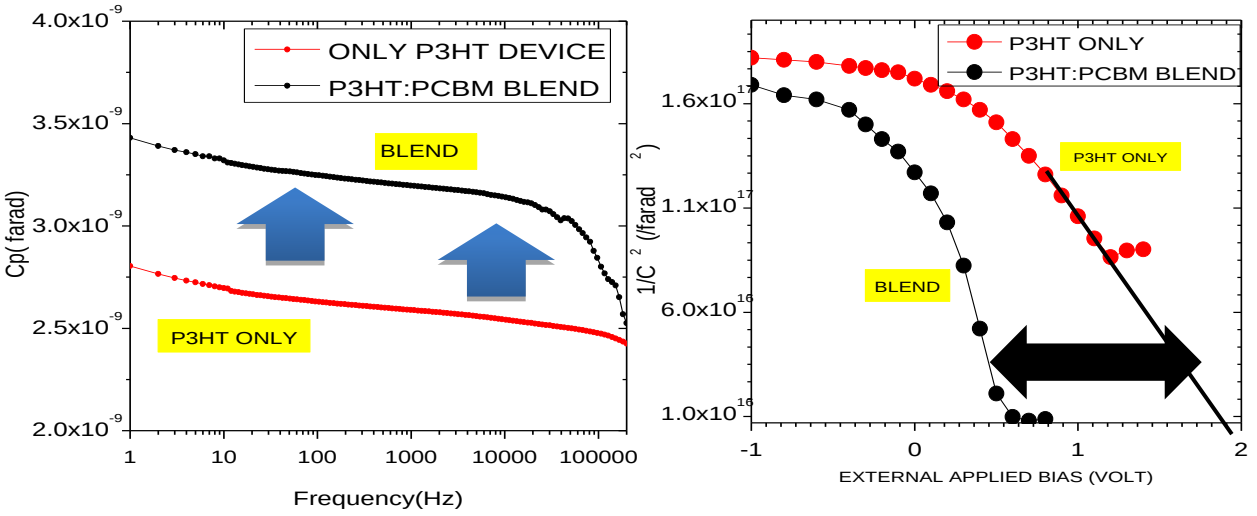

Figure- H-5: (A) Capacitance (parallel) measured as a function of frequency for P3HT only device and P3HT-PCBM blend device. (B) Cp-V measurement for P3HT only device and P3HT-PCBM blend device

Firstly it can be seen that, the capacitance for blend device at zero bias is higher than the P3HT only device which made ($1/C^2$) smaller for P3HT: PCBM blend device. Next the flat band voltage (intersection of $1/C^2$ curve with voltage axis in forward bias) can be seen to increases from ~0.5volt approximately (for blend device) to 1.8-1.9volt (for P3HT only device). This says – in the absence of any acceptor material in the device, the only depletion region active in the

www.manaraa.com

device is P3HT-Ca interface which is responsible for both dark IV and capacitance, which we measured. Very high flat band voltage (1.8-1.9 volt) is another indication of the nature of depletion region governing the measurement. For P3HT only device the band bending is almost close to the band gap of the P3HT resulting in such a high external bias required to flatten the bending of band at the cathode. With the introduction of acceptor, we introduced another junction at D-A interface which is dominating the dark current and capacitance measurement. This lowered flat band voltage (0.5 volt) in the blend device can also be explained by the fact that, the capacitance (by trapping-de-trapping of electronic states at D-A interface) in the blend device is depending on the depletion region and hence the band bending at the interface of D-A. The band bending at interface must be smaller than the band bending in the entire device (because of dissimilarities in metal work function) in the thermal equilibrium. Now we can explain why flat band voltage in any P3HT-PCBM blend device is always lower than open circuit voltage of the device. Also we have seen in our previous work on photo degradation (chapter-5) of P3HT-PCBM blend standard cell that, change in photo voltaic property can be directly correlated to the change in C-F measurement as well as change in DOS and dark current measurement.

In conclusion we have shown that the trap distribution measured by capacitance measurement as well as the Io estimated from dark IV measurement is purely depending on the density of traps located at the interface of donor and acceptor. There are defect states both in the polymer as well as in the polymer-fullerene interface. We see only the effect of interface states because that dominate the contribution of polymer (bulk) states as can be seen in forward bias dark current and capacitance measurements.

www.manaraa.com

APPENDIX I: PHOTO OXIDATION

It was proposed in many literatures[36,51,52,57,58,61] that degradation of organic solar cells under light is mainly because of the presence of either molecular oxygen in ambient or trace amount of oxygen present in the fullerene itself. In this appendix we conducted a simple experiment to distinguish two completely different nature of photo degradation. We made a bulk hetero junction film of (P3HT:PCBM) of (1:1) weight ratio and 18mg/ml concentration as used in our device fabrication. We deliberately deposited the blend on ITO coated glass without any hole transport layer and top metal electrode. We used 300 mw/cm^2 intensity for this experiment for accelerating the photo degradation. Unlike all other previous experiments, (where we exposed all our film/device under nitrogen atmosphere) we exposed the film in ambient condition. We measured absorbance at various time of exposure and finally after 90 hours of exposure, we thermally annealed the film at 110C for 1 hour. In chapter 6 we observed that, photo degradation under inert atmosphere are completely reversible process. In review section as discussed in chapter 2, we have seen that photo oxidation tend to reduce the optical absorbance of polymer only as well as bulk hetero-junction film. We wanted to see if photo oxidation process is reversible as we have seen in chapter 6. This could support the claim that oxygen is indeed a significant contributor to the degradation of organic solar cells under light but their dynamics of reversibility is different from the only light induced degradation under inert atmosphere.

It can be seen in the fig-I.1 that, absorbance of the BHJ film is going down with significant drop in the vibronic peaks at 550, 600 nm. These are widely recorded phenomena and can be explained by the theory of photo-oxidation or in other words, photo bleaching. It is interesting to note that after an exposure of 90 hours at 3x intensity , the film lost its absorbance significantly as expected. So we annealed the sample for 110C for 1 hour and measured absorbance. After

www.manaraa.com

thermal treatment inside nitrogen filled glove-box, we barely recovered the film absorbance. This experiment clearly shows photo-oxidation is an irreversible process unlike the photo degradation under nitrogen atmosphere.

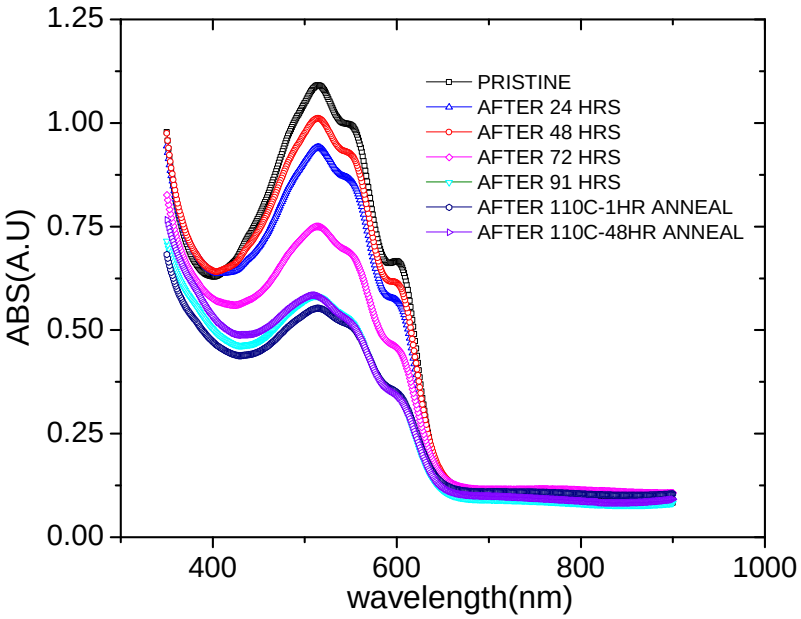

Fig- I.1 Change in Absorbance of P3HT: PCBM bulk hetero-junction film(1:1 wt ratio)under ambient air exposure(3x Sun intensity)

We conducted the experiment under ambient atmosphere and assumed that the atmospheric moisture has not affected the active layer. The study separates photo-oxidation from photo degradation under nitrogen atmosphere. Further thermal annealing for 48 hours was performed to see the change in absorbance. Interestingly absorbance remained roughly same after 48 hours of annealing at 110^{o}C inside nitrogen filled glove-box. It can be concluded that the damage caused by oxygen under light is permanent and cannot be reversed by thermal annealing.

www.manaraa.com

REFERENCES

1 Wilson, Greg. "Latest Solar Cell Efficiency Chart." NREL: Home Page. National Renewable Energy Laboratory, 1 Aug. 2013. Web. 21 Aug. 2013. <http://www.nrel.gov/ncpv/images/efficiency_chart.jpg>.

2 Bhattacharya, J. *et al.* A photonic-plasmonic structure for enhancing light absorption in thin film solar cells. *Applied Physics Letters* **99**, doi:10.1063/1.3641469 (2011).

3 Biswas, R. & Xu, C. Nano-crystalline silicon solar cell architecture with absorption at the classical 4n(2) limit. *Optics Express* **19**, A664-A672 (2011).

4 Biswas, R. *et al.* Enhancement of solar cells with photonic and plasmonic crystals - overcoming the Lambertian limit. *Journal of Materials Research* **28**, 1021-1030, doi:10.1557/jmr.2013.41 (2013).

5 Bhattacharya, J. *et al.* Comparison of optical properties of periodic photonic-plasmonic and randomly textured back reflectors for nc-Si solar cells. *Journal of Non-Crystalline Solids* **358**, 2313-2318, doi:10.1016/j.jnoncrysol.2011.12.108 (2012).

6 Paetzold, U. W. *et al.* Plasmonic reflection grating back contacts for microcrystalline silicon solar cells. *Applied Physics Letters* **99**, doi:10.1063/1.3657513 (2011).

7 Ferry, V. E. *et al.* in *35th Ieee Photovoltaic Specialists Conference IEEE Photovoltaic Specialists Conference* 760-765 (2010).

8 Haug, F. J., Soederstroem, T., Cubero, O., Terrazzoni-Daudrix, V. & Ballif, C. Plasmonic absorption in textured silver back reflectors of thin film solar cells. *Journal of Applied Physics* **104**, doi:10.1063/1.2981194 (2008).

9 Schiff, E. A. Thermodynamic limit to photonic-plasmonic light-trapping in thin films on metals. *Journal of Applied Physics* **110**, doi:10.1063/1.3658848 (2011).

10 Yue, G. *et al.* Optimization of back reflector for high efficiency hydrogenated nanocrystalline silicon solar cells. *Applied Physics Letters* **95**, doi:10.1063/1.3279143 (2009).

11 "Cadmium Telluride." Wikipedia. Wikimedia Foundation, 11 July 2013. Web. 24 July 2013.

12 Li, G., Zhu, R. & Yang, Y. Polymer solar cells. *Nature Photonics* **6**, 153-161, doi:10.1038/nphoton.2012.11 (2012).

13 Sariciftci, N. S., Smilowitz, L., Heeger, A. J. & Wudl, F. PHOTOINDUCED ELECTRON-TRANSFER FROM A CONDUCTING POLYMER TO BUCKMINSTERFULLERENE. *Science* **258**, 1474-1476, doi:10.1126/science.258.5087.1474 (1992).

14 Aernouts, T., Aleksandrov, T., Girotto, C., Genoe, J. & Poortmans, J. Polymer based organic solar cells using ink-jet printed active layers. *Applied Physics Letters* **92**, doi:10.1063/1.2833185 (2008).

15 Girotto, C., Moia, D., Rand, B. P. & Heremans, P. High-Performance Organic Solar Cells with Spray-Coated Hole-Transport and Active Layers. *Advanced Functional Materials* **21**, 64-72, doi:10.1002/adfm.201001562 (2011).

16 Lange, A. *et al.* A new approach to the solvent system for inkjet-printed P3HT:PCBM solar cells and its use in devices with printed passive and active layers. *Solar Energy Materials and Solar Cells* **94**, 1816-1821, doi:10.1016/j.solmat.2010.05.054 (2010).

www.manaraa.com

17 Hoth, C. N., Choulis, S. A., Schilinsky, P. & Brabec, C. J. High photovoltaic performance of inkjet printed polymer: Fullerene blends. *Advanced Materials* **19**, 3973-+, doi:10.1002/adma.200700911 (2007).

18 Pudas, M., Halonen, N., Granat, P. & Vahakangas, J. Gravure printing of conductive particulate polymer inks on flexible substrates. *Progress in Organic Coatings* **54**, 310-316, doi:10.1016/j.porgcoat.2005.07.008 (2005).

19 Krebs, F. C., Spanggard, H., Kjaer, T., Biancardo, M. & Alstrup, J. Large area plastic solar cell modules. *Materials Science and Engineering B-Solid State Materials for Advanced Technology* **138**, 106-111, doi:10.1016/j.mseb.2006.06.008 (2007).

20 Chen, L.-M. *et al.* Multi-Source/Component Spray Coating for Polymer Solar Cells. *Acs Nano* **4**, 4744-4752, doi:10.1021/nn901758p (2010).

21 Ding, J. M., Vornbrock, A. d. l. F., Ting, C. & Subramanian, V. Patternable polymer bulk heterojunction photovoltaic cells on plastic by rotogravure printing. *Solar Energy Materials and Solar Cells* **93**, 459-464, doi:10.1016/j.solmat.2008.12.003 (2009).

22 Huang, J., Li, G. & Yang, Y. A semi-transparent plastic solar cell fabricated by a lamination process. *Advanced Materials* **20**, 415-+, doi:10.1002/adma.200701101 (2008).

23 Shaheen, S. E., Radspinner, R., Peyghambarian, N. & Jabbour, G. E. Fabrication of bulk heterojunction plastic solar cells by screen printing. *Applied Physics Letters* **79**, 2996-2998, doi:10.1063/1.1413501 (2001).

24 Girotto, C. *et al.* in *35th Ieee Photovoltaic Specialists Conference IEEE Photovoltaic Specialists Conference* 1068-1072 (2010).

25 Steirer, K. X. *et al.* Ultrasonic spray deposition for production of organic solar cells. *Solar Energy Materials and Solar Cells* **93**, 447-453, doi:10.1016/j.solmat.2008.10.026 (2009).

26 Krebs, F. C. Fabrication and processing of polymer solar cells: A review of printing and coating techniques. *Solar Energy Materials and Solar Cells* **93**, 394-412, doi:10.1016/j.solmat.2008.10.004 (2009).

27 Krebs, F. C. Polymer solar cell modules prepared using roll-to-roll methods: Knife-over-edge coating, slot-die coating and screen printing. *Solar Energy Materials and Solar Cells* **93**, 465-475, doi:10.1016/j.solmat.2008.12.012 (2009).

28 Krebs, F. C. Pad printing as a film forming technique for polymer solar cells. *Solar Energy Materials and Solar Cells* **93**, 484-490, doi:10.1016/j.solmat.2008.09.003 (2009).

29 Krebs, F. C. *et al.* A complete process for production of flexible large area polymer solar cells entirely using screen printing-First public demonstration. *Solar Energy Materials and Solar Cells* **93**, 422-441, doi:10.1016/j.solmat.2008.12.001 (2009).

30 Krebs, F. C., Gevorgyan, S. A. & Alstrup, J. A roll-to-roll process to flexible polymer solar cells: model studies, manufacture and operational stability studies. *Journal of Materials Chemistry* **19**, 5442-5451, doi:10.1039/b823001c (2009).

31 Li, G. *et al.* High-efficiency solution processable polymer photovoltaic cells by self-organization of polymer blends. *Nature Materials* **4**, 864-868, doi:10.1038/nmat1500 (2005).

32 Blom, P. W. M., Mihailetchi, V. D., Koster, L. J. A. & Markov, D. E. Device physics of polymer : fullerene bulk heterojunction solar cells. *Advanced Materials* **19**, 1551-1566, doi:10.1002/adma.200601093 (2007).

33 Chen, H.-Y. *et al.* Polymer solar cells with enhanced open-circuit voltage and efficiency. *Nature Photonics* **3**, 649-653, doi:10.1038/nphoton.2009.192 (2009).

www.manaraa.com

34 Dennler, G., Scharber, M. C. & Brabec, C. J. Polymer-Fullerene Bulk-Heterojunction Solar Cells. *Advanced Materials* **21**, 1323-1338, doi:10.1002/adma.200801283 (2009).

35 Tong, M. *et al.* Charge carrier photogeneration and decay dynamics in the poly(2,7-carbazole) copolymer PCDTBT and in bulk heterojunction composites with PC70BM. *Physical Review B* **81**, doi:10.1103/PhysRevB.81.125210 (2010).

36 Peters, C. H. *et al.* High Efficiency Polymer Solar Cells with Long Operating Lifetimes. *Advanced Energy Materials* **1**, 491-494, doi:10.1002/aenm.201100138 (2011).

37 Banerji, N., Cowan, S., Leclerc, M., Vauthey, E. & Heeger, A. J. Exciton Formation, Relaxation, and Decay in PCDTBT. *Journal of the American Chemical Society* **132**, 17459-17470, doi:10.1021/ja105290e (2010).

38 Seo, J. H. *et al.* Improved High-Efficiency Organic Solar Cells via Incorporation of a Conjugated Polyelectrolyte Interlayer. *Journal of the American Chemical Society* **133**, 8416-8419, doi:10.1021/ja2037673 (2011).

39 Liang, Y. *et al.* For the Bright Future-Bulk Heterojunction Polymer Solar Cells with Power Conversion Efficiency of 7.4%. *Advanced Materials* **22**, E135-+, doi:10.1002/adma.200903528 (2010).

40 He, Z. *et al.* Enhanced power-conversion efficiency in polymer solar cells using an inverted device structure. *Nature Photonics* **6**, 591-595, doi:10.1038/nphoton.2012.190 (2012).

41 Sista, S. *et al.* Highly Efficient Tandem Polymer Photovoltaic Cells. *Advanced Materials* **22**, 380-+, doi:10.1002/adma.200901624 (2010).

42 Pattnaik, S., Xiao, T., Shinar, R., Shinar, J. & Dalal, V. L. Novel Hybrid Amorphous/Organic Tandem Junction Solar Cell. *Ieee Journal of Photovoltaics* **3**, 295-299, doi:10.1109/jphotov.2012.2212700 (2013).

43 Dou, L. *et al.* Tandem polymer solar cells featuring a spectrally matched low-bandgap polymer. *Nature Photonics* **6**, 180-185, doi:10.1038/nphoton.2011.356 (2012).

44 You, J. *et al.* A polymer tandem solar cell with 10.6% power conversion efficiency. *Nature Communications* **4**, doi:10.1038/ncomms2411 (2013).

45 Rohr, Steffanie. "Heliatek Consolidates Its Technology Leadership by Establishing a New World Record for Organic Solar Technology with a Cell Efficiency of 12%." Heliatek. Heliatek GmbH, 16 Jan. 2013. Web. 14 Apr. 2013.

46 Krebs, F. C. & Norrman, K. Analysis of the failure mechanism for a stable organic photovoltaic during 10000 h of testing. *Progress in Photovoltaics* **15**, 697-712, doi:10.1002/pip.794 (2007).

47 Seemann, A., Egelhaaf, H. J., Brabec, C. J. & Hauch, J. A. Influence of oxygen on semi-transparent organic solar cells with gas permeable electrodes. *Organic Electronics* **10**, 1424-1428, doi:10.1016/j.orgel.2009.08.001 (2009).

48 Jorgensen, M., Norrman, K. & Krebs, F. C. Stability/degradation of polymer solar cells. *Solar Energy Materials and Solar Cells* **92**, 686-714, doi:10.1016/j.solmat.2008.01.005 (2008).

49 Kawano, K. *et al.* Degradation of organic solar cells due to air exposure. *Solar Energy Materials and Solar Cells* **90**, 3520-3530, doi:10.1016/j.solmat.2006.06.041 (2006).

50 Kawano, K. & Adachi, C. Reduced initial degradation of bulk heterojunction organic solar cells by incorporation of stacked fullerene and lithium fluoride interlayers. *Applied Physics Letters* **96**, doi:10.1063/1.3297876 (2010).

www.manaraa.com

51 Peters, C. H. *et al.* The Mechanism of Burn-in Loss in a High Efficiency Polymer Solar Cell. *Advanced Materials* **24**, 663-+, doi:10.1002/adma.201103010 (2012).

52 Reese, M. O. *et al.* Photoinduced Degradation of Polymer and Polymer-Fullerene Active Layers: Experiment and Theory. *Advanced Functional Materials* **20**, 3476-3483, doi:10.1002/adfm.201001079 (2010).

53 Street, R. A., Northrup, J. E. & Krusor, B. S. Radiation induced recombination centers in organic solar cells. *Physical Review B* **85**, doi:10.1103/PhysRevB.85.205211 (2012).

54 Street, R. A., Krakaris, A. & Cowan, S. R. Recombination Through Different Types of Localized States in Organic Solar Cells. *Advanced Functional Materials* **22**, 4608-4619, doi:10.1002/adfm.201200031 (2012).

55 Hoke, E. T. *et al.* The Role of Electron Affinity in Determining Whether Fullerenes Catalyze or Inhibit Photooxidation of Polymers for Solar Cells. *Advanced Energy Materials* **2**, 1351-1357, doi:10.1002/aenm.201200169 (2012).

56 Norrman, K., Gevorgyan, S. A. & Krebs, F. C. Water-Induced Degradation of Polymer Solar Cells Studied by (H2O)-O-18 Labeling. *Acs Applied Materials & Interfaces* **1**, 102-112, doi:10.1021/am800039w (2009).

57 Manceau, M. *et al.* Effects of long-term UV-visible light irradiation in the absence of oxygen on P3HT and P3HT:PCBM blend. *Solar Energy Materials and Solar Cells* **94**, 1572-1577, doi:10.1016/j.solmat.2010.03.012 (2010).

58 Rivaton, A. *et al.* Light-induced degradation of the active layer of polymer-based solar cells. *Polymer Degradation and Stability* **95**, 278-284, doi:10.1016/j.polymdegradstab.2009.11.021 (2010).

59 Reese, M. O. *et al.* Pathways for the degradation of organic photovoltaic P3HT : PCBM based devices. *Solar Energy Materials and Solar Cells* **92**, 746-752, doi:10.1016/j.solmat.2008.01.020 (2008).

60 Wang, M. *et al.* Degradation mechanism of organic solar cells with aluminum cathode. *Solar Energy Materials and Solar Cells* **95**, 3303-3310, doi:10.1016/j.solmat.2011.07.020 (2011).

61 Guerrero, A. *et al.* Oxygen doping-induced photogeneration loss in P3HT:PCBM solar cells. *Solar Energy Materials and Solar Cells* **100**, 185-191, doi:10.1016/j.solmat.2012.01.012 (2012).

62 Krebs, F. C. Air stable polymer photovoltaics based on a process free from vacuum steps and fullerenes. *Solar Energy Materials and Solar Cells* **92**, 715-726, doi:10.1016/j.solmat.2008.01.013 (2008).

63 Krebs, F. C. Stability, degradation, and operational lifetimes of fully solution R2R processed flexible polymer solar cells. *Abstracts of Papers of the American Chemical Society* **238** (2009).

64 Krebs, F. C. Degradation and stability of polymer and organic solar cells. *Solar Energy Materials and Solar Cells* **92**, 685-685, doi:10.1016/j.solmat.2008.01.016 (2008).

65 Gevorgyan, S. A., Jorgensen, M. & Krebs, F. C. A setup for studying stability and degradation of polymer solar cells. *Solar Energy Materials and Solar Cells* **92**, 736-745, doi:10.1016/j.solmat.2008.02.008 (2008).

66 Lu, X. & Winnik, M. A. Luminescence quenching in polymer/filler nanocomposite films used in oxygen sensors. *Chemistry of Materials* **13**, 3449-3463, doi:10.1021/cm011029k (2001).

www.manaraa.com

67 Norrman, K., Larsen, N. B. & Krebs, F. C. Lifetimes of organic photovoltaics: Combining chemical and physical characterisation techniques to study degradation mechanisms. *Solar Energy Materials and Solar Cells* **90**, 2793-2814, doi:10.1016/j.solmat.2006.04.009 (2006).

68 Holger,H., Egelhaaf H J., Luer L, Hauch J, Peisert H, and Chasse T. "Photo-degradation of P3HT-A Systematic Study of Environmental Factors. *Chemistry of Materials* **23**, 145-54, doi:10.1021/cm102373k (2011).

69 Schafferhans, J., Baumann, A., Wagenpfahl, A., Deibel, C. & Dyakonov, V. Oxygen doping of P3HT:PCBM blends: Influence on trap states, charge carrier mobility and solar cell performance. *Organic Electronics* **11**, 1693-1700, doi:10.1016/j.orgel.2010.07.016 (2010).

70 Staebler, D. L. & Wronski, C. R. Optically induced conductivity changes in discharge-produced hydrogenated amorphous-silicon. *Journal of Applied Physics* **51**, 3262-3268, doi:10.1063/1.328084 (1980).

71 Kounavis, P. Changes in the trapping and recombination process of hydrogenated amorphous-silicon in the staebler-wronski effect. *Journal of Applied Physics* **77**, 3872-3878, doi:10.1063/1.358565 (1995).

72 Su, T., Taylor, P. C., Ganguly, G. & Carlson, D. E. Direct role of hydrogen in the Staebler-Wronski effect in hydrogenated amorphous silicon. *Physical Review Letters* **89**, doi:10.1103/PhysRevLett.89.015502 (2002).

73 Wyrsch, N. & Shah, A. Drift mobility and staebler-wronski effect in hydrogenated amorphous-silicon. *Solid State Communications* **80**, 807-809, doi:10.1016/0038-1098(91)90512-t (1991).

74 Bautista, L. B., Enomoto, H. & Ozaki, H. Field-effect study of the staebler-wronski effect in hydrogenated amorphous-silicon. *Japanese Journal of Applied Physics Part 1-Regular Papers Short Notes & Review Papers* **28**, 153-159 (1989).

75 Su, T., Taylor, P. C., Ganguly, G. & Carlson, D. E. A hydrogen-related defect and the Staebler-Wronski effect in hydrogenated amorphous silicon. *Journal of Non-Crystalline Solids* **338**, 357-360, doi:10.1016/j.jnoncrysol.2004.02.073 (2004).

76 Belich, T. J. & Kakalios, J. Long-range disorder and the Staebler-Wronski effect in N-type amorphous silicon. *Physical Review B* **66**, doi:10.1103/PhysRevB.66.195212 (2002).

77 Costea, S., Kherani, N. P. & Zukotynski, S. Metastable defect creation in tritiated hydrogenated amorphous silicon and the Staebler-Wronski effect. *Journal of Materials Science-Materials in Electronics* **18**, S175-S182, doi:10.1007/s10854-007-9184-x (2007).

78 Fritzsche, H. Photoinduced structural-changes associated with the staebler-wronski effect in hydrogenated amorphous-silicon. *Solid State Communications* **94**, 953-955, doi:10.1016/0038-1098(95)00220-0 (1995).

79 Pinarbasi, M., Abelson, J. R. & Kushner, M. J. Reduced staebler-wronski effect in reactively sputtered hydrogenated amorphous-silicon thin-films. *Applied Physics Letters* **56**, 1685-1687, doi:10.1063/1.103117 (1990).

80 Qin, G. G. & Kong, G. L. Silicon-hydrogen bonds and microvoids in hydrogenated amorphous-silicon and staebler-wronski effect. *Solid State Communications* **71**, 41-43, doi:10.1016/0038-1098(89)90168-3 (1989).

81 Dawson, R. M. A. & Fortmann, C. M. The Staebler-Wronski effect and the thermal equilibration of defect and free carrier concentrations. *Journal of Applied Physics* **79**, 3075-3081, doi:10.1063/1.361249 (1996).

www.manaraa.com

82 Prasad, R. & Shenoy, S. R. Staebler-Wronski effect in hydrogenated amorphous silicon. *Physics Letters A* **218**, 85-90, doi:10.1016/0375-9601(96)00389-1 (1996).

83 Sheng, S. R., Sacher, E. & Yelon, A. Structural changes in amorphous silicon studied by X-ray photoemission spectroscopy: a phenomenon independent of the Staebler-Wronski effect? *Journal of Non-Crystalline Solids* **282**, 165-172, doi:10.1016/s0022-3093(01)00339-8 (2001).

84 Du, M. H. & Zhang, S. B. Topological defects and the Staebler-Wronski effect in hydrogenated amorphous silicon. *Applied Physics Letters* **87**, doi:10.1063/1.2130381 (2005).

85 "Staebler–Wronski Effect." Wikipedia. Wikimedia Foundation, 23 May 2013. Web. 21 Aug. 2013. <http://en.wikipedia.org/wiki/Staebler–Wronski_effect>.

86 Branz, H. M. Hydrogen collision model: Quantitative description of metastability in amorphous silicon. *Physical Review B* **59**, 5498-5512, doi:10.1103/PhysRevB.59.5498 (1999).

87 Biswas, R., Pan, B. C. & Ye, Y. Y. Metastability of amorphous silicon from silicon network rebonding. *Physical Review Letters* **88**, doi:10.1103/PhysRevLett.88.205502 (2002).

88 Kumar, A. *et al.* Origin of Radiation-Induced Degradation in Polymer Solar Cells. *Advanced Functional Materials* **20**, 2729-2736, doi:10.1002/adfm.201000374 (2010).

89 Devine, R. A. B., Mayberry, C., Kumar, A. & Yang, Y. Origin of Radiation Induced Damage in Organic P3HT:PCBM Based Photocells. *Ieee Transactions on Nuclear Science* **57**, 3109-3113, doi:10.1109/tns.2010.2068577 (2010).

90 Logdlund, M. & Bredas, J. L. Theoretical-studies of the interaction between aluminum and poly(p-phenylenevinylene) and derivatives. *Journal of Chemical Physics* **101**, 4357-4364 (1994).

91 Schaefer, S. *et al.* Influence of the indium tin oxide/organic interface on open-circuit voltage, recombination, and cell degradation in organic small-molecule solar cells. *Physical Review B* **83**, doi:10.1103/PhysRevB.83.165311 (2011).

92 Krebs, F. C. All solution roll-to-roll processed polymer solar cells free from indium-tin-oxide and vacuum coating steps. *Organic Electronics* **10**, 761-768, doi:10.1016/j.orgel.2009.03.009 (2009).

93 Bertho, S. *et al.* Effect of temperature on the morphological and photovoltaic stability of bulk heterojunction polymer: fullerene solar cells. *Solar Energy Materials and Solar Cells* **92**, 753-760, doi:10.1016/j.solmat.2008.01.006 (2008).

94 Bertho, S. *et al.* Influence of thermal ageing on the stability of polymer bulk heterojunction solar cells. *Solar Energy Materials and Solar Cells* **91**, 385-389, doi:10.1016/j.solmat.2006.10.008 (2007).

95 Chambon, S. *et al.* MoO3 Thickness, Thermal Annealing and Solvent Annealing Effects on Inverted and Direct Polymer Photovoltaic Solar Cells. *Materials* **5**, 2521-2536, doi:10.3390/ma5122521 (2012).

96 Ma, W. L., Yang, C. Y., Gong, X., Lee, K. & Heeger, A. J. Thermally stable, efficient polymer solar cells with nanoscale control of the interpenetrating network morphology. *Advanced Functional Materials* **15**, 1617-1622, doi:10.1002/adfm.200500211 (2005).

97 "Albert Einstein - Facts." Albert Einstein - Facts. Nobel Media AB, 21 Aug. 2013. Web. 21 Aug. 2013.

98 Ben Streetman, S. B. *Solid State Electronic Devices*. (2005).

www.manaraa.com

99 Lisensky, George. "PN Junction." PN Junction for LED. Beloit College, n.d. Web. 14 Apr. 2013.

100 Pierret R, F. Semiconductor Device Fundamentals.

101 Zhang, Y. L., Liu, X. J., Sun, Z. & An, Z. Dynamics of exciton transfer in coupled polymer chains. *The Journal of chemical physics* **138**, 174906-174906, doi:10.1063/1.4803163 (2013).

102 Liang, W. Y. Exciton. *IOPSCIENCE* **5** (1970).

103 Honsberg, Christiana, and Stuart Bowden. "PVCDrom." Photovoltaic Education Network | Pveducation.org. N.p., n.d. Web. 21 Aug. 2013.

104 Chynoweth, A. G. & Schneider, W. G. The photoconductivity of anthracene .1. *Journal of Chemical Physics* **22**, 1021-1028 (1954).

105 Tang, C. W. 2-LAYER ORGANIC PHOTOVOLTAIC CELL. *Applied Physics Letters* **48**, 183-185, doi:10.1063/1.96937 (1986).

106 Potscavage, W. J., Jr., Sharma, A. & Kippelen, B. Critical Interfaces in Organic Solar Cells and Their Influence on the Open-Circuit Voltage. *Accounts of Chemical Research* **42**, 1758-1767, doi:10.1021/ar900139v (2009).

107 Kumar, P., Jain, S. C., Kumar, H., Chand, S. & Kumar, V. Effect of illumination intensity and temperature on open circuit voltage in organic solar cells. *Applied Physics Letters* **94**, doi:10.1063/1.3129194 (2009).

108 Huang, J., Yu, J., Qi, Y. & Jiang, Y. in *Proceedings of International Conference on Smart Grid and Clean Energy Technologies* Vol. 12 *Energy Procedia* (eds Q. Huang & J. Z. Kang) (2011).

109 Yamamoto, S., Orimo, A., Ohkita, H., Benten, H. & Ito, S. Molecular Understanding of the Open-Circuit Voltage of Polymer:Fullerene Solar Cells. *Advanced Energy Materials* **2**, 229-237, doi:10.1002/aenm.201100549 (2012).

110 Kulshreshtha, C. *et al.* Open-circuit voltage dependency on hole-extraction layers in planar heterojunction organic solar cells. *Applied Physics Letters* **99**, doi:10.1063/1.3610962 (2011).

111 Qi, B. & Wang, J. Open-circuit voltage in organic solar cells. *Journal of Materials Chemistry* **22**, 24315-24325, doi:10.1039/c2jm33719c (2012).

112 Garcia-Belmonte, G. & Bisquert, J. Open-circuit voltage limit caused by recombination through tail states in bulk heterojunction polymer-fullerene solar cells. *Applied Physics Letters* **96**, doi:10.1063/1.3358121 (2010).

113 Brabec, C. J. *et al.* Origin of the open circuit voltage of plastic solar cells. *Advanced Functional Materials* **11**, 374-380, doi:10.1002/1616-3028(200110)11:5<374::aid-adfm374>3.0.co;2-w (2001).

114 Potscavage, W. J., Yoo, S. & Kippelen, B. Origin of the open-circuit voltage in multilayer heterojunction organic solar cells. *Applied Physics Letters* **93**, doi:10.1063/1.3027061 (2008).

115 Xue, J., Rand, B. P. & Forrest, S. R. in *Organic Photovoltaics VII* Vol. 6334 *Proceedings of the Society of Photo-Optical Instrumentation Engineers (Spie)* (eds Z. H. Kafafi & P. A. Lane) U71-U80 (2006).

116 Street, R. A., Davies, D., Khlyabich, P. P., Burkhart, B. & Thompson, B. C. Origin of the Tunable Open-Circuit Voltage in Ternary Blend Bulk Heterojunction Organic Solar Cells. *Journal of the American Chemical Society* **135**, 986-989, doi:10.1021/ja3112143 (2013).

www.manaraa.com

117 Maurano, A. *et al.* Recombination Dynamics as a Key Determinant of Open Circuit Voltage in Organic Bulk Heterojunction Solar Cells: A Comparison of Four Different Donor Polymers. *Advanced Materials* **22**, 4987-+, doi:10.1002/adma.201002360 (2010).

118 Rauh, D., Wagenpfahl, A., Deibel, C. & Dyakonov, V. Relation of open circuit voltage to charge carrier density in organic bulk heterojunction solar cells. *Applied Physics Letters* **98**, doi:10.1063/1.3566979 (2011).

119 Blakesley, J. C. & Neher, D. Relationship between energetic disorder and open-circuit voltage in bulk heterojunction organic solar cells. *Physical Review B* **84**, doi:10.1103/PhysRevB.84.075210 (2011).

120 Cowan, S. R., Banerji, N., Leong, W. L. & Heeger, A. J. Charge Formation, Recombination, and Sweep-Out Dynamics in Organic Solar Cells. *Advanced Functional Materials* **22**, 1116-1128, doi:10.1002/adfm.201101632 (2012).

121 Cowan, S. R., Leong, W. L., Banerji, N., Dennler, G. & Heeger, A. J. Identifying a Threshold Impurity Level for Organic Solar Cells: Enhanced First-Order Recombination Via Well-Defined PC84BM Traps in Organic Bulk Heterojunction Solar Cells. *Advanced Functional Materials* **21**, 3083-3092, doi:10.1002/adfm.201100514 (2011).

122 Ratcliff, E. L. *et al.* Investigating the Influence of Interfacial Contact Properties on Open Circuit Voltages in Organic Photovoltaic Performance: Work Function Versus Selectivity. *Advanced Energy Materials* **3**, 647-656, doi:10.1002/aenm.201200669 (2013).

123 Cowan, S. R., Roy, A. & Heeger, A. J. Recombination in polymer-fullerene bulk heterojunction solar cells. *Physical Review B* **82**, doi:10.1103/PhysRevB.82.245207 (2010).

124 Koster, L. J. A., Mihailetchi, V. D., Xie, H. & Blom, P. W. M. Origin of the light intensity dependence of the short-circuit current of polymer/fullerene solar cells. *Applied Physics Letters* **87**, doi:10.1063/1.2130396 (2005).

125 Lilliu, S. *et al.* Dynamics of Crystallization and Disorder during Annealing of P3HT/PCBM Bulk Heterojunctions. *Macromolecules* **44**, 2725-2734, doi:10.1021/ma102817z (2011).

126 Bansal, N. *et al.* Influence of Crystallinity and Energetics on Charge Separation in Polymer-Inorganic Nanocomposite Films for Solar Cells. *Scientific Reports* **3**, doi:10.1038/srep01531 (2013).

127 Tsoi, W. C. *et al.* The Nature of In-Plane Skeleton Raman Modes of P3HT and Their Correlation to the Degree of Molecular Order in P3HT:PCBM Blend Thin Films. *Journal of the American Chemical Society* **133**, 9834-9843, doi:10.1021/ja2013104 (2011).

128 Agostinelli, T. *et al.* Real-Time Investigation of Crystallization and Phase-Segregation Dynamics in P3HT:PCBM Solar Cells During Thermal Annealing. *Advanced Functional Materials* **21**, 1701-1708, doi:10.1002/adfm.201002076 (2011).

129 Dibb, G. F. A., Jamieson, F. C., Maurano, A., Nelson, J. & Durrant, J. R. Limits on the Fill Factor in Organic Photovoltaics: Distinguishing Nongeminate and Geminate Recombination Mechanisms. *Journal of Physical Chemistry Letters* **4**, 803-808, doi:10.1021/jz400140p (2013).

130 Pal, S. K. *et al.* Geminate Charge Recombination in Polymer/Fullerene Bulk Heterojunction Films and Implications for Solar Cell Function. *Journal of the American Chemical Society* **132**, 12440-12451, doi:10.1021/ja104786x (2010).

www.manaraa.com

131 Kirchartz, T., Pieters, B. E., Kirkpatrick, J., Rau, U. & Nelson, J. Recombination via tail states in polythiophene: fullerene solar cells. *Physical Review B* **83**, doi:10.1103/PhysRevB.83.115209 (2011).
132 Koster, L. J. A., Mihailetchi, V. D. & Blom, P. W. M. Bimolecular recombination in polymer/fullerene bulk heterojunction solar cells. *Applied Physics Letters* **88**, doi:10.1063/1.2170424 (2006).
133 Shuttle, C. G. *et al.* Bimolecular recombination losses in polythiophene: Fullerene solar cells. *Physical Review B* **78**, doi:10.1103/PhysRevB.78.113201 (2008).
134 Garcia-Belmonte, G. Carrier recombination flux in bulk heterojunction polymer:fullerene solar cells: Effect of energy disorder on ideality factor. *Solid-State Electronics* **79**, 201-205, doi:10.1016/j.sse.2012.07.018 (2013).
135 Street, R. A. in *Physical Chemistry of Interfaces and Nanomaterials X* Vol. 8098 *Proceedings of SPIE* (ed C. Silva) (2011).
136 Zhou, S., Sun, J., Zhou, C. & Deng, Z. Comparison of recombination models in organic bulk heterojunction solar cells. *Physica B-Condensed Matter* **415**, 28-33, doi:10.1016/j.physb.2013.01.030 (2013).
137 Tress, W., Leo, K. & Riede, M. Dominating recombination mechanisms in organic solar cells based on ZnPc and C-60. *Applied Physics Letters* **102**, doi:10.1063/1.4802276 (2013).
138 Armin, A. *et al.* Doping-Induced Screening of the Built-in-Field in Organic Solar Cells: Effect on Charge Transport and Recombination. *Advanced Energy Materials* **3**, 321-327, doi:10.1002/aenm.201200581 (2013).
139 Zhang, T. *et al.* The effect of built-in field on the interface exciton recombination and dissociation in N-N type organic solar cells. *Solar Energy Materials and Solar Cells* **112**, 73-77, doi:10.1016/j.solmat.2013.01.009 (2013).
140 Szmytkowski, J. Four-body recombination in organic bulk heterojunction solar cells: an alternative interpretation. *Semiconductor Science and Technology* **28**, doi:10.1088/0268-1242/28/5/052002 (2013).
141 Verreet, B. *et al.* Improved cathode buffer layer to decrease exciton recombination in organic planar heterojunction solar cells. *Applied Physics Letters* **102**, doi:10.1063/1.4789852 (2013).
142 Cowan, S. R. *et al.* Intensity and wavelength dependence of bimolecular recombination in P3HT:PCBM solar cells: A white-light biased external quantum efficiency study. *Journal of Applied Physics* **113**, doi:10.1063/1.4801920 (2013).
143 Pivrikas, A., Sariciftci, N. S., Juska, G. & Osterbacka, R. A review of charge transport and recombination in polymer/fullerene organic solar cells. *Progress in Photovoltaics* **15**, 677-696, doi:10.1002/pip.791 (2007).
144 Li, L., Kwon, J. H. & Jang, J. Tail states recombination limit of the open circuit voltage in bulk heterojunction organic solar cells. *Organic Electronics* **13**, 230-234, doi:10.1016/j.orgel.2011.11.006 (2012).
145 Garcia-Belmonte, G. Temperature dependence of open-circuit voltage in organic solar cells from generation-recombination kinetic balance. *Solar Energy Materials and Solar Cells* **94**, 2166-2169, doi:10.1016/j.solmat.2010.07.006 (2010).
146 Cowan, S. R., Street, R. A., Cho, S. & Heeger, A. J. Transient photoconductivity in polymer bulk heterojunction solar cells: Competition between sweep-out and recombination. *Physical Review B* **83**, doi:10.1103/PhysRevB.83.035205 (2011).

www.manaraa.com

147 Street, R. A. & Schoendorf, M. Interface state recombination in organic solar cells. *Physical Review B* **81**, doi:10.1103/PhysRevB.81.205307 (2010).
148 Street, R. A. Localized state distribution and its effect on recombination in organic solar cells. *Physical Review B* **84**, doi:10.1103/PhysRevB.84.075208 (2011).
149 Conings, B. *et al.* Generalized approach to the description of recombination kinetics in bulk heterojunction solar cells-extending from fully organic to hybrid solar cells. *Applied Physics Letters* **100**, doi:10.1063/1.4714902 (2012).
150 Vandewal, K., Tvingstedt, K., Manca, J. V. & Inganas, O. Charge-Transfer States and Upper Limit of the Open-Circuit Voltage in Polymer: Fullerene Organic Solar Cells. *Ieee Journal of Selected Topics in Quantum Electronics* **16**, 1676-1684, doi:10.1109/jstqe.2010.2043061 (2010).
151 Mingebach, M., Walter, S., Dyakonov, V. & Deibel, C. Direct and charge transfer state mediated photogeneration in polymer-fullerene bulk heterojunction solar cells. *Applied Physics Letters* **100**, doi:10.1063/1.4711849 (2012).
152 Faist, M. A. *et al.* Competition between the Charge Transfer State and the Singlet States of Donor or Acceptor Limiting the Efficiency in Polymer:Fullerene Solar Cells. *Journal of the American Chemical Society* **134**, 685-692, doi:10.1021/ja210029w (2012).
153 Wiemer, M., Nenashev, A. V., Jansson, F. & Baranovskii, S. D. On the efficiency of exciton dissociation at the interface between a conjugated polymer and an electron acceptor. *Applied Physics Letters* **99**, doi:10.1063/1.3607481 (2011).
154 Nenashev, A. V., Wiemer, M., Jansson, F. & Baranovskii, S. D. Theory to exciton dissociation at the interface between a conjugated polymer and an electron acceptor. *Journal of Non-Crystalline Solids* **358**, 2508-2511, doi:10.1016/j.jnoncrysol.2011.12.036 (2012).
155 Zhu, X. Y., Yang, Q. & Muntwiler, M. Charge-Transfer Excitons at Organic Semiconductor Surfaces and Interfaces. *Accounts of Chemical Research* **42**, 1779-1787, doi:10.1021/ar800269u (2009).
156 Muntwiler, M., Yang, Q., Tisdale, W. A. & Zhu, X. Y. Coulomb Barrier for Charge Separation at an Organic Semiconductor Interface. *Physical Review Letters* **101**, doi:10.1103/PhysRevLett.101.196403 (2008).
157 Muntwiler, M., Yang, Q. & Zhu, X. Y. Exciton dynamics at interfaces of organic semiconductors. *Journal of Electron Spectroscopy and Related Phenomena* **174**, 116-124, doi:10.1016/j.elspec.2009.02.016 (2009).
158 Onsager, L. Initial recombination of ions. *Physical Review* **54**, 554-557, doi:10.1103/PhysRev.54.554 (1938).
159 Braun, C. L. Electric-field assisted dissociation of charge-transfer states as a mechanism of photocarrier production. *Journal of Chemical Physics* **80**, 4157-4161, doi:10.1063/1.447243 (1984).
160 Simmons, J. G. & Taylor, G. W. Nonequilibrium steady-state statistics and associated effects for insulators and semiconductors containing an arbitraty distribution of traps. *Physical Review B-Solid State* **4**, 502-&, doi:10.1103/PhysRevB.4.502 (1971).
161 Shockley, W. & Queisser, H. J. Detailed balance limit of efficiency of p-n junction solar cells. *Journal of Applied Physics* **32**, 510-&, doi:10.1063/1.1736034 (1961).
162 Street, R. A., Song, K. W., Northrup, J. E. & Cowan, S. Photoconductivity measurements of the electronic structure of organic solar cells. *Physical Review B* **83**, doi:10.1103/PhysRevB.83.165207 (2011).

www.manaraa.com

163 Kimerlin.Lc. Influence of deep traps on measurement of free-carrier distributions in semiconductors by junction capacitance techniques. *Journal of Applied Physics* **45**, 1839-1845, doi:10.1063/1.1663500 (1974).

164 Hegedus, S. S. & Fagen, E. A. Midgap states in a-si-h and a-sige-h p-i-n solar-cells and schottky junctions by capacitance techniques. *Journal of Applied Physics* **71**, 5941-5951, doi:10.1063/1.350444 (1992).

165 Bhattacharya, J., Mayer, R. W., Samiee, M. & Dalal, V. L. Photo-induced changes in fundamental properties of organic solar cells. *Applied Physics Letters* **100**, doi:10.1063/1.4711806 (2012).

166 Kirchartz, T. *et al.* Sensitivity of the Mott-Schottky Analysis in Organic Solar Cells. *Journal of Physical Chemistry C* **116**, 7672-7680, doi:10.1021/jp300397f (2012).

167 Carr, J. A. & Chaudhary, S. On accurate capacitance characterization of organic photovoltaic cells. *Applied Physics Letters* **100**, doi:10.1063/1.4720403 (2012).

168 Sharma, A., Kumar, P., Singh, B., Chaudhuri, S. R. & Ghosh, S. Capacitance-voltage characteristics of organic Schottky diode with and without deep traps. *Applied Physics Letters* **99**, doi:10.1063/1.3607955 (2011).

169 Walter, T., Herberholz, R., Muller, C. & Schock, H. W. Determination of defect distributions from admittance measurements and application to Cu(In,Ga)Se-2 based heterojunctions. *Journal of Applied Physics* **80**, 4411-4420, doi:10.1063/1.363401 (1996).

170 Boix, P. P. *et al.* Determination of gap defect states in organic bulk heterojunction solar cells from capacitance measurements. *Applied Physics Letters* **95**, doi:10.1063/1.3270105 (2009).

171 Nalwa, K. S., Mahadevapuram, R. C. & Chaudhary, S. Growth rate dependent trap density in polythiophene-fullerene solar cells and its implications. *Applied Physics Letters* **98**, doi:10.1063/1.3560483 (2011).

172 Lampert, M. A. CITATION CLASSIC - Simplified theory of space-charge-limited currents in an insulator with traps. *Current Contents/Physical Chemical & Earth Sciences*, 24-24 (1982).

173 Lampert, M. A. Simplified theory of space-charge-limited currents in an insulator with traps. *Physical Review* **103**, 1648-1656, doi:10.1103/PhysRev.103.1648 (1956).

174 Wong, •Diana. "Electronic Spectroscopy: Theory - ChemWiki." Electronic Spectroscopy: Theory - ChemWiki. University of California, Davis, 6 May 2013. Web. 21 June 2013.

175 Street, R. A., Song, K. W. & Cowan, S. Influence of series resistance on the photocurrent analysis of organic solar cells. *Organic Electronics* **12**, 244-248, doi:10.1016/j.orgel.2010.11.012 (2011).

176 Chang, Y.-M., Su, W.-F. & Wang, L. Influence of photo-induced degradation on the optoelectronic properties of regioregular poly(3-hexylthiophene). *Solar Energy Materials and Solar Cells* **92**, 761-765, doi:10.1016/j.solmat.2008.01.002 (2008).

177 Paci, B. *et al.* Photo-degradation and stabilization effects in operating organic photovoltaic devices by joint photo-current and morphological monitoring. *Solar Energy Materials and Solar Cells* **92**, 799-804, doi:10.1016/j.solmat.2008.02.019 (2008).

178 Williams, G., Wang, Q. & Aziz, H. The Photo-Stability of Polymer Solar Cells: Contact Photo-Degradation and the Benefits of Interfacial Layers. *Advanced Functional Materials* **23**, 2239-2247, doi:10.1002/adfm.201202567 (2013).

www.manaraa.com

179 Carr, J. A. & Chaudhary, S. *On the identification of deeper defect levels in organic photovoltaic devices.Journal of Applied Physics* **114**, 064509, dx.doi.org/10.1063/1.4818324. (2013)

180 Tabata, A., Kuroda, M., Mori, M., Mizutani, T. & Suzuoki, Y. Band gap control of hydrogenated amorphous silicon carbide films prepared by hot-wire chemical vapor deposition. *Journal of Non-Crystalline Solids* **338**, 521-524, doi:10.1016/j.jnoncrysol.2004.03.033 (2004).

181 Tabata, A., Kuno, Y., Suzuoki, Y. & Mizutani, T. Properties of hydrogenated amorphous silicon carbide films prepared by a separately excited plasma CVD method. *Journal of Physics D-Applied Physics* **30**, 194-201, doi:10.1088/0022-3727/30/2/006 (1997).

182 Vanecek, M. *et al.* Nanostructured three-dimensional thin film silicon solar cells with very high efficiency potential. *Applied Physics Letters* **98**, doi:10.1063/1.3583377 (2011).

183 Yang, J., Yan, B. J., Yue, G. Z. & Guha, S. in *Amorphous and Polycrystalline Thin Film Silicon Science and Technology - 2009, Vol 1153* Vol. 1153 *Materials Research Society Symposium Proceedings* (eds A. Flewitt *et al.*) (2009).

184 Biswas, R., Bhattacharya, J., Lewis, B., Chakravarty, N. & Dalal, V. Enhanced nanocrystalline silicon solar cell with a photonic crystal back-reflector. *Solar Energy Materials and Solar Cells* **94**, 2337-2342, doi:10.1016/j.solmat.2010.08.007 (2010).

185 Yan, B. J., Yue, G. Z., Yang, J., Banerjee, A. & Guha, S. in *Amorphous and Nanocrystalline Silicon-Based Films-2003* Vol. 762 *Materials Research Society Symposium Proceedings* (eds J. R. Abelson *et al.*) 309-320 (2003).

186 Ferry, V. E. *et al.* Light trapping in ultrathin plasmonic solar cells. *Optics Express* **18**, A237-A245 (2010).

187 Zhou, D. & Biswas, R. Photonic crystal enhanced light-trapping in thin film solar cells. *Journal of Applied Physics* **103**, doi:10.1063/1.2908212 (2008).

188 Tiedje, T., Yablonovitch, E., Cody, G. D. & Brooks, B. G. Limiting efficiency of silicon solar-cells. *Ieee Transactions on Electron Devices* **31**, 711-716, doi:10.1109/t-ed.1984.21594 (1984).

189 Yablonovitch, E. Statistical ray optics. *Journal of the Optical Society of America* **72**, 899-907, doi:10.1364/josa.72.000899 (1982).

190 Rana Biswas, E. T. *Nano-photonic light trapping near the Lambertian limit in organic solar cell architectures* (Optics Express, 2013).

191 Springer, J. *et al.* Absorption loss at nanorough silver back reflector of thin-film silicon solar cells. *Journal of Applied Physics* **95**, 1427-1429, doi:10.1063/1.1633652 (2004).

192 Zhao, H. *et al.* Plasmonic Light-trapping and Quantum Efficiency Measurements On Nanocrystalline Silicon Solar Cells and Silicon-On-Insulator Devices. *MRS Online Proceedings Library* **1245**, null-null, doi:doi:10.1557/PROC-1245-A03-02 (2010).

193 Dahal, L. R., Sainju, D., Podraza, N. J., Marsillac, S. & Collins, R. W. Real time spectroscopic ellipsometry of Ag/ZnO and Al/ZnO interfaces for back-reflectors in thin film Si:H photovoltaics. *Thin Solid Films* **519**, 2682-2687, doi:10.1016/j.tsf.2010.11.093 (2011).

194 Morgan, R. M. & Lynch, D. W. Optical properties of dilute ag-in alloys. *Bulletin of the American Physical Society* **13**, 124-& (1968).

195 Yan, B., Yue, G., Yang, J., Banerjee, A. & Guha, S. Hydrogenated Microcrystalline Silicon Single-Junction and Multi-Junction Solar Cells. *MRS Online Proceedings Library* **762**, null-null, doi:doi:10.1557/PROC-762-A4.1 (2003).

www.manaraa.com

196 Yue, G. Z., Yan, B. J., Owens, J. M., Yang, J. & Guha, S. in *Amorphous and Nanocrystalline Silicon Science and Technology- 2004* Vol. 808 *Materials Research Society Symposium Proceedings* (eds G. Ganguly *et al.*) 593-598 (2004).

197 Haase, C., Knipp, D. & Stiebig, H. in *Nanoengineering: Fabrication, Properties, Optics, and Devices IV* Vol. 6645 *Proceedings of the Society of Photo-Optical Instrumentation Engineers (Spie)* (eds E. A. Dobisz & L. A. Eldada) W6450-W6450 (2007).

198 Sai, H., Fujiwara, H. & Kondo, M. Back surface reflectors with periodic textures fabricated by self-ordering process for light trapping in thin-film microcrystalline silicon solar cells. *Solar Energy Materials and Solar Cells* **93**, 1087-1090, doi:10.1016/j.solmat.2008.12.030 (2009).

199 Moulin, E. *et al.* Thin-film silicon solar cells applying optically decoupled back reflectors. *Materials Science and Engineering B-Advanced Functional Solid-State Materials* **178**, 645-650, doi:10.1016/j.mseb.2012.10.016 (2013).

200 Zeghbroeck, D. B. V. *Semiconductor Fundamentals*. (Web, 1996-1997).

201 Dennler, G. *et al.* Charge carrier mobility and lifetime versus composition of conjugated polymer/fullerene bulk-heterojunction solar cells. *Organic Electronics* **7**, 229-234, doi:10.1016/j.orgel.2006.02.004 (2006).

202 Zhou, M., Aryal, M., Mielczarek, K., Zakhidov, A. & Hu, W. Hole mobility enhancement by chain alignment in nanoimprinted poly(3-hexylthiophene) nanogratings for organic electronics. *Journal of Vacuum Science & Technology B* **28**, C6M63-C66M67, doi:10.1116/1.3501343 (2010).

203 Chen, M.-C. *et al.* Improving the efficiency of an organic solar cell by a polymer additive to optimize the charge carriers mobility. *Applied Physics Letters* **99**, doi:10.1063/1.3664127 (2011).

204 von Hauff, E., Dyakonov, V. & Parisi, R. Study of field effect mobility in PCBM films and P3HT : PCBM blends. *Solar Energy Materials and Solar Cells* **87**, 149-156, doi:10.1016/j.solmat.2004.06.014 (2005).

205 Mozer, A. J. *et al.* Time-dependent mobility and recombination of the photoinduced charge carriers in conjugated polymer/fullerene bulk heterojunction solar cells. *Physical Review B* **72**, doi:10.1103/PhysRevB.72.035217 (2005).

206 Ballantyne, A. M. *et al.* in *Organic Photovoltaics VII* Vol. 6334 *Proceedings of the Society of Photo-Optical Instrumentation Engineers (Spie)* (eds Z. H. Kafafi & P. A. Lane) U21-U31 (2006).

207 Girtan, M. & Rusu, M. Role of ITO and PEDOT:PSS in stability/degradation of polymer: fullerene bulk heterojunctions solar cells. *Solar Energy Materials and Solar Cells* **94**, 446-450, doi:10.1016/j.solmat.2009.10.026 (2010).

208 Ecker, B. *et al.* Degradation Effects Related to the Hole Transport Layer in Organic Solar Cells. *Advanced Functional Materials* **21**, 2705-2711, doi:10.1002/adfm.201100429 (2011).

209 Scanlon, D. O. *et al.* Theoretical and Experimental Study of the Electronic Structures of MoO3 and MoO2. *Journal of Physical Chemistry C* **114**, 4636-4645, doi:10.1021/jp9093172 (2010).

210 Verploegen, E. *et al.* Effects of Thermal Annealing Upon the Morphology of Polymer-Fullerene Blends. *Advanced Functional Materials* **20**, 3519-3529, doi:10.1002/adfm.201000975 (2010).

www.manaraa.com

211 Karagiannidis, P. G., Kassavetis, S., Pitsalidis, C. & Logothetidis, S. Thermal annealing effect on the nanomechanical properties and structure of P3HT: PCBM thin films. *Thin Solid Films* **519**, 4105-4109, doi:10.1016/j.tsf.2011.01.196 (2011).

212 Zhokhavets, U., Erb, T., Hoppe, H., Gobsch, G. & Sariciftci, N. S. Effect of annealing of poly(3-hexylthiophene)/fullerene bulk heterojunction composites on structural and optical properties. *Thin Solid Films* **496**, 679-682, doi:10.1016/j.tsf.2005.09.093 (2006).

213 Kim, H., Shin, M., Park, J. & Kim, Y. Effect of Long Time Annealing and Incident Light Intensity on the Performance of Polymer: Fullerene Solar Cells. *Ieee Transactions on Nanotechnology* **9**, 400-406, doi:10.1109/tnano.2009.2027120 (2010).

214 Ho, C.-S. *et al.* Effects of Annealing on Polymer Solar Cells with High Polythiophene-Fullerene Concentrations. *Japanese Journal of Applied Physics* **50**, doi:10.1143/jjap.50.04dk21 (2011).

215 Li, G., Shrotriya, V., Yao, Y. & Yang, Y. Investigation of annealing effects and film thickness dependence of polymer solar cells based on poly(3-hexylthiophene). *Journal of Applied Physics* **98**, doi:10.1063/1.2008386 (2005).

216 Tsoi, W. C. *et al.* Effect of Crystallization on the Electronic Energy Levels and Thin Film Morphology of P3HT:PCBM Blends. *Macromolecules* **44**, 2944-2952, doi:10.1021/ma102841e (2011).

217 Mihailetchi, V. D., Xie, H. X., de Boer, B., Koster, L. J. A. & Blom, P. W. M. Charge transport and photocurrent generation in poly (3-hexylthiophene): Methanofullerene bulk-heterojunction solar cells. *Advanced Functional Materials* **16**, 699-708, doi:10.1002/adfm.200500420 (2006).

218 Han, X. G., Zhang, X. F., Ma, Y. H., Zhang, C. X. & Guan, Y. B. Effects of polymer concentration and chain length on aggregation in physically associating polymer solutions. *Condensed Matter Physics* **14**, doi:10.5488/cmp.14.43601 (2011).

219 Radbeh, R. *et al.* Nanoscale control of the network morphology of high efficiency polymer fullerene solar cells by the use of high material concentration in the liquid phase. *Nanotechnology* **21**, doi:10.1088/0957-4484/21/3/035201 (2010).

220 Hu, Z. & Gesquiere, A. J. PCBM concentration dependent morphology of P3HT in composite P3HT/PCBM nanoparticles. *Chemical Physics Letters* **476**, 51-55, doi:10.1016/j.cplett.2009.05.066 (2009).

221 Mihailetchi, V. D., Blom, P. W. M., Hummelen, J. C. & Rispens, M. T. Cathode dependence of the open-circuit voltage of polymer : fullerene bulk heterojunction solar cells. *Journal of Applied Physics* **94**, 6849-6854, doi:10.1063/1.1620683 (2003).

222 Oida, T. & Harafuji, K. Cathode Work Function Dependence of Electron Transport Efficiency through Buffer Layer in Organic Solar Cells. *Japanese Journal of Applied Physics* **51**, doi:10.1143/jjap.51.091601 (2012).

223 Yang, L., Xu, H., Tian, H., Yin, S. & Zhang, F. Effect of cathode buffer layer on the stability of polymer bulk heterojunction solar cells. *Solar Energy Materials and Solar Cells* **94**, 1831-1834, doi:10.1016/j.solmat.2010.05.043 (2010).

224 Chang, C.-C. *et al.* Effects of cathode buffer layers on the efficiency of bulk-heterojunction solar cells. *Applied Physics Letters* **96**, doi:10.1063/1.3456530 (2010).

225 Wang, Y. *et al.* Enhanced performance and stability in polymer photovoltaic cells using lithium benzoate as cathode interfacial layer. *Solar Energy Materials and Solar Cells* **95**, 1243-1247, doi:10.1016/j.solmat.2011.01.012 (2011).

www.manaraa.com

226 Kageyama, H., Kajii, H., Ohmori, Y. & Shirota, Y. MoO3 as a Cathode Buffer Layer Material for the Improvement of Planar pn-Heterojunction Organic Solar Cell Performance. *Applied Physics Express* **4**, doi:10.1143/apex.4.032301 (2011).

227 Park, S. H. *et al.* Bulk heterojunction solar cells with internal quantum efficiency approaching 100%. *Nature Photonics* **3**, 297-U295, doi:10.1038/nphoton.2009.69 (2009).

228 Lee, J. H., Cho, S., Roy, A., Jung, H.-T. & Heeger, A. J. Enhanced diode characteristics of organic solar cells using titanium suboxide electron transport layer. *Applied Physics Letters* **96**, doi:10.1063/1.3409116 (2010).

229 Gupta, V. *et al.* Barium: An Efficient Cathode Layer for Bulk-heterojunction Solar Cells. *Scientific Reports* **3**, doi:10.1038/srep01965 (2013).

230 Cattin, L., Bernede, J. C. & Morsli, M. Toward indium-free optoelectronic devices: Dielectric/metal/dielectric alternative transparent conductive electrode in organic photovoltaic cells. *Physica Status Solidi a-Applications and Materials Science* **210**, 1047-1061, doi:10.1002/pssa.201228089 (2013).

231 Ghosh, D. S. *et al.* High figure-of-merit Ag/Al:ZnO nano-thick transparent electrodes for indium-free flexible photovoltaics. *Solar Energy Materials and Solar Cells* **107**, 338-343, doi:10.1016/j.solmat.2012.07.009 (2012).

232 Koo, B., Kim, S. & Lee, J.-L. Indium-tin-oxide free transparent electrodes using a plasmon frequency conversion layer. *Journal of Materials Chemistry C* **1**, 246-252, doi:10.1039/c2tc00049k (2013).

233 Nagano, K. *et al.* Inhalation Carcinogenicity and Chronic Toxicity of Indium-tin Oxide in Rats and Mice. *Journal of Occupational Health* **53**, 175-187 (2011).

234 Meyer, J. *et al.* Indium-free transparent organic light emitting diodes with Al doped ZnO electrodes grown by atomic layer and pulsed laser deposition. *Applied Physics Letters* **93**, doi:10.1063/1.2975176 (2008).

235 Daniel, G. P. *et al.* Effect of annealing temperature on the structural and optical properties of ZnO thin films prepared by RF magnetron sputtering. *Physica B-Condensed Matter* **405**, 1782-1786, doi:10.1016/j.physb.2010.01.039 (2010).

236 Lee, K.-H., Cho, N.-I., Nam, H. G. & Yun, E.-J. Effects of H2O Introduction during ZnO Deposition by rf Magnetron Sputtering. *Journal of the Korean Physical Society* **53**, 3273-3277 (2008).

237 Lee, Y. E., Kim, Y. J. & Kim, H. J. Thickness dependence of microstructural evolution of ZnO films deposited by rf magnetron sputtering. *Journal of Materials Research* **13**, 1260-1265, doi:10.1557/jmr.1998.0180 (1998).

238 Liao, Y.-P. *et al.* Structural evolution of ZnO films deposited by rf magnetron sputtering on glass substrate. *Physica Status Solidi a-Applications and Materials Science* **207**, 1850-1853, doi:10.1002/pssa.200925131 (2010).

239 Rosa, A. M. *et al.* in *14th Latin American Workshop on Plasma Physics* Vol. 370 *Journal of Physics Conference Series* (eds L. Bilbao, F. Minotti, & H. Kelly) (2012).

240 Li, G., Chu, C. W., Shrotriya, V., Huang, J. & Yang, Y. Efficient inverted polymer solar cells. *Applied Physics Letters* **88**, doi:10.1063/1.2212270 (2006).

241 Liao, H.-H., Chen, L.-M., Xu, Z., Li, G. & Yang, Y. Highly efficient inverted polymer solar cell by low temperature annealing of Cs(2)CO(3) interlayer. *Applied Physics Letters* **92**, doi:10.1063/1.2918983 (2008).

www.manaraa.com

242 Mingebach, M., Deibel, C. & Dyakonov, V. Built-in potential and validity of the Mott-Schottky analysis in organic bulk heterojunction solar cells. *Physical Review B* **84**, doi:10.1103/PhysRevB.84.153201 (2011).

www.manaraa.com